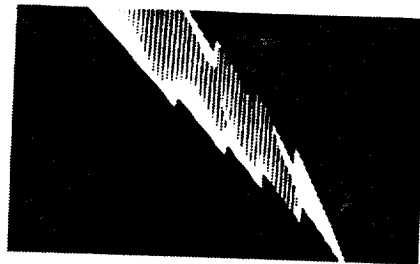


NAS8-36300  
SA41/Cory Rutland



# **Lightning Tests & Analyses of Tunnel Bond Straps & Shielded Cables on the Space Shuttle Solid Rocket Booster**

**Final Report  
SI-93-2679**

**November 1993**

*Prepared By:  
William M. Druen  
Senior Project Engineer*



N94-24801

Unclass

G3/16 0206786

(NASA-CR-193921) LIGHTNING TESTS  
AND ANALYSES OF TUNNEL BOND STRAPS  
AND SHIELDED CABLES ON THE SPACE  
SHUTTLE SOLID ROCKET BOOSTER Final  
Report (United Technologies Corp.)  
157 p

***Lightning Tests & Analyses  
of Tunnel Bond Straps &  
Shielded Cables on the  
Space Shuttle Solid  
Rocket Booster***

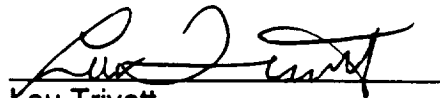
SI-93-2679

November 1993

*Prepared By:*

  
William M. Druen  
Senior Project Engineer

*Approved By:*

  
Lou Trivett  
Manager, Systems Integration

## Table of Contents

### Chapter

1	Introduction and Background.....	1
2	Configuration of the Test Article.....	8
3	Test and Measurement Methods .....	17
4	Summary of the Data .....	21
5	Comparison of Cable Coupling Before and After Changes .....	34
6	Coupling to Operational Flight Cables .....	38
7	Bond Strap Survivability Tests .....	60
8	Selection of an Adequate Tunnel Bond Strap Design .....	63
9	Conclusions .....	64
10	Recommendations .....	68
Appendix A Calculated Differential Mode Voltages .....		A-1
Appendix B Common Mode to Differential Voltage as a Band Pass Filter.....		B-1
Appendix C References .....		C-1

### List of Illustrations

1-1	Systems Tunnel Floor Plate Assembly Ground Strap .....	3
1-2	Tunnel Bond Strap No. 1 (External Location) .....	4
1-3	Location of Four Cover-to-Cover Flat Aluminum Bond Straps, the No. 7 Cover-to-Case Bond Strap, and the AWG 12 Cover-to-ETA Ring Bond Straps .....	5
1-4	Electrical Bonding of GEI Cables to Motor Case and Tunnel Floor Plate.....	6
2-1	Assembled Test Article .....	9
2-2	Test Article, Peaking Capacitor, and Locations of Four current Injection Points .....	9
2-3	Location of Three OF Cables in Test Article Forward Tunnel .....	11
2-4	Configuration of OF Test Cables .....	11
2-5	Aluminum Test Article Box Simulation of Aft IEA .....	12
2-6	Circuit Schematic, Breakout Box .....	13
2-7	Location of Three OF Cables and GEI Cables in the Forward Tunnel.....	13
2-8	OF Test Cables Located in the Tunnel for Worst Case Magnetic Field Coupling .....	14
2-9	Location of External GEI Cables on Test Article .....	15
2-10	Foil Between Aft BOB and Last Tunnel Cover .....	16
3-1	Measured CW Short Circuit Current, Cable 6, Injection Point 1, Relative to Injected Current .....	18
3-2	Measured Marx Injection Current Waveform .....	18
3-3	Measured Continuing Current Bank (CCB) Injection Current Waveform .....	19
4-1	Measured CW Injection Current (1 kHz to 2 MHz) .....	24
4-2	Measured CW Injection Current (1 MHz to 10 MHz) .....	24
4-3	Measured Instrumentation Noise Level in Forward Breakout Box, Relative to Current Injected at Forward Tunnel Cover .....	25
4-4	Measured Instrumentation Noise Level in Aft Breakout Box, Relative to Current Injected at Forward Tunnel Cover .....	25
4-5	Measured Cable 6 Short Circuit Current with Marx Current Injected at Point 3 .....	27
4-6	Measured Cable 12 Open Circuit Voltage with Marx Injected Current at Point 3 .....	27
4-7	Measured Cable 6 Open Circuit Voltage with Marx Current Injected at Point 2 .....	30
4-8	Measured High Current Bank (HCB) Injection Current .....	31
4-9	Measured Cable 6 Short Circuit Current with HCB Current Injected at Point 1 .....	31

**List of Illustrations (Contd)**

4-10	Measured Cable 11 Open Circuit Voltage with HCB Current Injected at Point 1 .....	31
6-1	Electrical Connections of the Test Article Structural Elements .....	39
6-2	Electrical Equivalent of Forward Tunnel of Figure 6-1 .....	42
6-3	Calculated, CW, and Pulse Data, $I_{sc}/I_i$ (in dB), versus Frequency .....	44
6-4	Calculated, CW, and Pulse Data, $V_{oc}/I_i$ (in dB) Versus Frequency .....	44
6-5	Transfer Impedances ( $Z_t$ ) of Shielded Cables .....	45
6-6	Decrease in $I_{sc}/I_i$ at 20 dB/decade and 40 dB/decade .....	46
6-7	Calculated $I_{sc}/I_i$ and $V_{oc}/I_i$ as Functions of Frequency .....	47
6-8	Aft Skirt Cable Transfer Impedance Approximation .....	49
6-9	Ground Loop Coupling Model and Variables .....	51

### List of Tables

1-1	Four Types of Current Injection Tests .....	2
2-1	Description of New Cover-To-Case Bond Straps .....	10
2-2	Description of OF Test Cables .....	12
4-1	Measured DC Resistances Prior to Tests .....	22
4-2	New Bond Strap Resistance Measurements .....	23
4-3	Induced Peak Common Mode Short Circuit Currents, Marx Test .....	28
4-3	Induced Peak Common Mode Short Circuit Currents, Marx Test (contd) .....	29
4-4	Induced Peak Common Mode Open Circuit Voltages, Marx Test (130 kHz Comp.) .....	29
4-5	Induced Peak Common Mode Open Circuit Voltages, Marx Test (1 MHz Comp.) .....	29
4-6	Induced Peak Common Mode Short Circuit Currents, HCB Test .....	32
4-6	Induced Peak Common Mode Short Circuit Currents, HCB Test (Contd) .....	33
4-7	Induced Peak Common Mode Open Circuit Voltages, HCB Test .....	33
5-1	Scaled Common Mode Short Circuit Currents and Open Circuit Voltages from the Prior Test, Injection Point 3 (Motor Case) .....	34
5-2	Scaled Common Mode Short Circuit Currents and Open Circuit Voltages from the Retest, Worst Case Tunnel Injection Points .....	35
6-1	Resistance of Core Conductors within Test Cables .....	46
6-2	Calculated Common Mode Voltages on Aft Cables Due to Component A of Lightning Current .....	50
6-3	Peak VDM (in millivolts) caused by Component A Coupling through Tunnel Covers and GEI Cables. C2B = 22.5 pf .....	54
6-4	Peak VDM (in millivolts) caused by the first part of Coupling by Component A to Aft Skirt Cables. C2B = 22.5 pf .....	54
6-5	Peak VDM (in millivolts) caused by Component A Narrow Pulse Waveform Coupling. C2B = 22.5 pf .....	55
6-6	Peak VDM (in millivolts) caused by Component H Coupling through the Aft Tunnel and the GEI Cables .....	57
6-7	Peak VDM (in millivolts) caused by the first part of Component H Coupling through Aft Skirt Cables .....	57
6-8	Peak VDM ( in millivolts) caused by the second part of VCM <sub>2</sub> . .....	57
6-9	Peak VDM (in millivolts) on Forward and Aft Cables Due to Tunnel, GEI Cables, and Aft Skirt Cables and all Components of a Lightning Current Specified by reference 2 .....	58
7-1	Results of Bond Strap Survivability Retest .....	61

## **Chapter 1 Introduction and Background**

The purposes of the tests and analyses described in this report are to:

- Determine the lightning current survivability of five alternative changed designs of the bond straps which electrically bond the solid rocket booster (SRB) systems tunnel to the solid rocket motor (SRM) case.
- Determine the amount of reduction in induced voltages on operational flight (OF) tunnel cables obtained by a modified design of tunnel bond straps (both tunnel cover-to-cover and cover-to-motor case).
- Determine the contribution of coupling to the OF tunnel cables by ground electrical and instrumentation (GEI) cables which enter the systems tunnel from unshielded areas on the surfaces of the motor case.
- Develop a model (based on test data) and calculate the voltage levels at electronic "black boxes" connected to the OF cables that run in the systems tunnel.

A prior simulated lightning test (reference 1) had demonstrated that the tunnel-to-case bond straps currently used on the SRB will debond from the case if criterion lightning currents (reference 2) attach directly to the tunnel covers. Although a lightning strike is much more likely to attach to other locations on the STS (reference 2), an attachment to the tunnel covers cannot be ruled out because the tunnel is located on the outer surface of the SRB at 180 degrees from the attachment points to the external tank.

This prior test had also indicated that transient voltage levels of several hundred volts would be induced in tunnel cables by lightning strikes that attach to the systems tunnel.

The tests described in this report were conducted at the Wendover, Utah, lightning test site which was operated and maintained by Thiokol Corporation under contract to NASA/MSFC. The lightning test equipment is modular and mounted on trailers which may be relocated relatively easily. The modules are made up of arrays of capacitors, charging and switching circuits, and pressurized gas control devices. In these tests, the Marx bank module was used to obtain high currents with high rates of current rise. The high current bank (HCB) module was used to obtain high currents with high action integrals, and the continuing current bank (CCB) was used to obtain currents with a high total charge transfer. The low-level continuous wave (CW) current injection tests were performed with a rented network analyzer to obtain transfer function data over the frequency range of interest.

The lightning simulator, including the capacitor storage banks, the high voltage control and switching circuits, and the instrumentation and data acquisition system was designed, installed and operated by Electromagnetic Applications, Inc. (EMA) under subcontract to Thiokol Corporation. The USBI tests described in this report

were planned by USBI and conducted by a team of USBI, Thiokol, and EMA engineers. All technician and facility support was provided by Thiokol Corporation. Some of the assembly procedures and test operations were witnessed by NASA/MSFC representatives. The interpretation and analyses of the data as documented in this report were completed solely by USBI engineers. A separate report that includes all of the test data was prepared by Thiokol Corporation and submitted to MSFC (reference 3). After the completion of the planned USBI tests, Thiokol engineers returned the test article to its "flight" configuration and obtained measurements of a few OF cable short circuit currents while injecting currents from the Marx pulser. The data from these latter tests are included in this report. For reference, these test events are numbered 109 through 114 in table 4-3.

Table 1-1 summarizes the four types of tests conducted. All of the current injection points used during these tests were located on the tunnel covers, the GEI cables, the heater cable connector, or at a single point on the case next to the forward most tunnel cover on the forward motor segment. These injection points were selected because they are the worst case locations for coupling to tunnel cables.

**Table 1-1 Four Types of Current Injection Tests**

Test Name	Purpose	Injection Current Levels	No. of Injection Pts	No. of Cables Meas.
CW Current Injection (CI)	Measure Cable Responses across Lightning Frequency Band (1 kHz-10 MHz)	9 amps	6	6
Marx CI	Measure cable responses with high level pulse currents with fast risetimes. 1 kA = 1,000 amps	20 kA to 30 kA	6	6
High Current Bank CI	Measure cable responses with high level currents and high action integrals	60 kA to 133 kA	14	6
Bond Strap Survivability	Determine levels of current and action integral at which bond straps (new designs) debond from motor case. 1M = $10^6$ amp <sup>2</sup> seconds	70 kA to 133 kA 1M-4.6M action integral	14	2

During the prior cable coupling test (reference 1) simulated lightning currents were injected onto the tunnel covers (and other locations), and OF cable responses (transient voltages and currents) were measured on cables that ran in the aft tunnel and the shortened forward tunnel. The test article was made up of an aft SRB segment and the forward-most SRB segment in both that test and the tests described in this report. Flight-configured SRBs have two additional forward segments between these two.



The test article forward tunnel, therefore, was about one-third of the length of the operational flight forward tunnel. In reference 1, the measured cable voltage responses were scaled for several factors (including length of test article, peak injected current, rate of rise of the injected current and coupling mode) to derive the peak common-mode open circuit voltage on each type of tunnel OF cable. For forward tunnel cables, the peak scaled open circuit common mode voltages from the prior tests were between 87 and 316 volts. For OF cables located in the aft tunnel, the peak scaled open circuit voltages were between 20 and 64 volts. These levels are referenced to a lightning peak current of 200,000 amps, which is the level specified by NSTS 07636F (reference 2). The reference 1 report stated that "when lightning induced voltages from the SRB/orbiter interface cables are added, the levels become 439 volts and 156 volts respectively. Several SRB criticality 1 and 1R circuits (power transorbs, solid state switches, SRM chamber pressure sensor, and APU speed control) fail in the 60 to 140 volt range." It was recommended to NASA that the SRB test article at the Wendover test site be reconfigured with proposed systems tunnel design changes and another coupling test be performed. This recommendation was accepted, and the SRB tunnel coupling retest was conducted. The following changes were made to the test article prior to the retest:

1. The bond straps between the tunnel and the SRM case were moved from the internal location to an external location, and the footprint of the conductive epoxy bond was increased from 2.5 square inches to 8.0 square inches. The internal location had these straps bolted to the middle of the tunnel floor plates (figure 1-1). The external location had them bolted to one side of each tunnel cover (figure 1-2). Several alternative designs were used for these external bond straps and these were tested for their survivability to lightning currents after the tunnel coupling tests were completed. The results of these survivability tests are described in chapter 7 of this report.

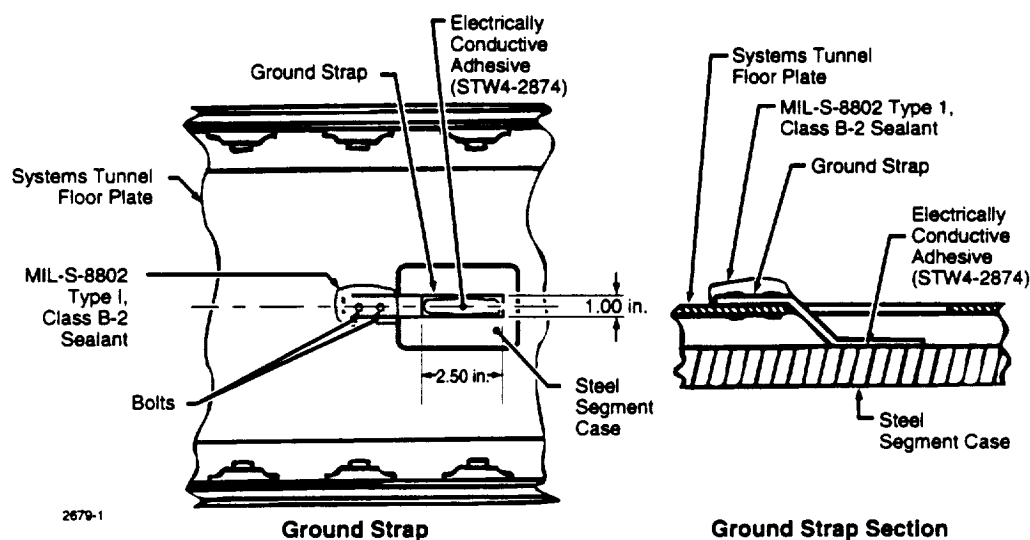


Figure 1-1 Systems Tunnel Floor Plate Assembly Ground Strap



**Figure 1-2 Tunnel Bond Strap No. 1 (External Location)**

2. The two AWG No. 12 wire bond straps across each tunnel cover gap were replaced by four flat aluminum straps in order to reduce the resistance and inductance across each gap (figure 1-3). Two of the flat straps were 0.75 inches wide and were connected to the covers by the same bolts that are used to connect the No. 12 wire straps. The other two flat straps were 1.25 inches wide and were fitted in length to the first cover-to-angle-bracket bolts on each side of the gap and on each of the two sides of the covers. The unmodified No. 12 wire bond straps were used between the ETA ring structure and the first tunnel cover on each side of the ring (figure 1-3).



**Figure 1-3 Location of Four Cover-to-Cover Flat Aluminum Bond Straps, the No. 7 Cover-to-Case Bond Strap, and the AWG 12 Cover-to-ETA Ring Bond Straps**

3. All of the external GEI cables that penetrate the tunnel envelope were enclosed within cable shields, and these shields were electrically bonded to the case at intervals of approximately 18 inches around the motor case circumference and at the points where they entered the tunnel (figure 1-4). In order to determine the contribution of these cables to the measured signals on the OF cables, one phase of the coupling test was conducted with all of the external GEI cables disconnected from the internal mating GEI cables at their points of entry into the tunnel.
4. Developmental flight instrumentation (DFI) cables in the tunnel (installed for the prior tests) were removed, reducing from 15 to 10 the total number of tunnel cables. Identical sets of three OF cables were installed in the forward and aft tunnels and configured to allow measurements of their core conductors' open circuit voltages and short circuit currents on one end. The other end of each cable was connected to a simulated aft integrated electronics assembly (IEA) and the core conductors were shorted to chassis ground inside the simulated IEA. In all cases, the core conductors of each cable were shorted together on both ends to form a single bundle. There was one bundle of GEI cables in the forward tunnel and two bundles in the aft tunnel. The GEI cable shields were terminated to the outside of the aft breakout box. The conductors inside the GEI cables were not extended into the breakout box. There were two simulated SRM joint heater power cables in the aft tunnel.



**Figure 1-4 Electrical Bonding of GEI Cables to Motor Case and Tunnel Floor Plate**

5. The breakout box at the aft end of the test article was electrically bonded with bolts directly to the SRM case. The prior test was conducted with the aft breakout box grounded to the SRM case only through the tunnel floor plates and the tunnel-to-case bond straps. The forward breakout box was electrically bonded with bolts directly to the case in both tests.

It is important to understand that the measured voltages and currents on the simulated OF cables cannot be used directly as the levels that would be seen by circuits that are connected to these cables in a flight configuration. These test measurements are used to support the calculation of the common mode voltage waveforms on the core conductors for the specified lightning criteria waveforms. A coupling model is developed in chapter 6 and the appendices and the model is used to calculate the differential mode waveforms at circuit interfaces. Common mode voltages are those developed across the total length of the cables. Differential mode voltages are those developed between twisted pairs of conductors within the cable. There were no actual or simulated cable interface electronic circuits included in these tests. It is also important to note that the tests described in this report do not account for coupling to SRB cables that cross the interface with the external tank. A calculation in chapter 6 accounts for coupling due to magnetic fields in the aft skirt area caused by lightning currents flowing from the SRM case to the SRM nozzle through the twelve nozzle bond straps. Before a complete assessment of the SRB can be made the following additional sources must be evaluated:

1. Cable shield currents on cables that cross the SRB/ET interface through the upper strut. These currents induce voltages on cable core conductors within

those cables. For those core conductors that are hard-wired through the aft IEA, these voltages can be added directly to those developed in this report for coupling through the tunnel, the GEI cables, and the aft skirt cables.

2. Cable shield currents on the aft BSM ordnance cables due to lightning attachments directly to the aft booster separation motors (BSMs) or their mounting frame.
3. Cable shield currents on cables that pass through the forward separation ring which is located between the forward skirt and the frustum. These cables include those that run to the altitude barometric sensors, the nose cap separation initiators, and the forward BSM initiators.

The remainder of this report describes the configuration of the updated test article (chapter 2), the test and measurement methods (chapter 3), summary of the data (chapter 4), comparison of cable coupling before and after tunnel bond strap changes (chapter 5), the development of coupling models and the extrapolation of the data to the specified threat (chapter 6), the results of the bond strap survivability tests (chapter 7), an analysis to select an adequate bond strap design (chapter 8), conclusions (chapter 9), recommendations (chapter 10), and three appendices.

## **Chapter 2 Configuration of the Test Article**

The test article included an inert (no propellant) SRM forward segment mated to an inert aft segment at a field joint (figures 2-1, 2-2). A nozzle (but no aft skirt) was installed on the aft segment. The forward segment included one factory joint, while the aft segment had two factory joints and three stiffener rings. The ETA ring was installed on the aft segment. System tunnel floor plate sections were previously installed on each segment with vulcanized EPDM rubber. The "flight" floor plate-to-case electrical bond straps were not connected for these tests. These straps were replaced with a set of external bond straps which had a larger case footprint (8 square inches versus the internal straps' 2.5 square inches). There was one external strap for each tunnel cover; table 2-1 summarizes the characteristics of each external bond strap. The cable coupling tests were completed prior to the start of the bond strap survivability tests. A set of three USBI operational flight cables was installed in the forward tunnel, and an equivalent set was installed in the aft tunnel (figures 2-3 and 2-4). These six cables represent all of the types of USBI OF cables used in the forward and aft tunnels of flight boosters and are described in table 2-2. The connectors on both ends of each of these shielded cables were terminated at bulkhead mating connectors which were mounted on shielded enclosures (called breakout boxes) with the core conductors and internal shields continuing into the enclosures. The enclosure at the ETA ring end of the cables was a sheet metal box which simulated the aft IEA (figure 2-5). The breakout box at the forward end simulated a forward skirt and the breakout box on the aft end simulated the termination of the cables at the aft skirt "rooster tail." At the aft IEA end of the cables, the core conductors were shorted directly to chassis ground inside the breakout box. At the other end of the cables (forward or aft breakout box), the core conductors were connected to a rotary switch in such a manner that the core bundle could be shorted to chassis ground for short circuit current measurements, or connected to chassis ground through a 340-ohm resistor for open circuit voltage measurements (figure 2-6). The 340-ohm value was chosen to be much larger than the impedance of the core conductor bundles so that the voltage drop measured across the 340 ohms would be nearly equal to the lightning induced voltage across the length of the cables. The open circuit voltage values were obtained as the product of 340 ohms multiplied by the measured current through the 340-ohm resistor. The OF cables were grouped within the angle brackets of the floor plates as they are in the flight configuration. Of course, in the flight configuration there are many more cables in the tunnels than the six that were installed for the lightning test. The pyro cables (numbers 6 and 12) were grouped on one side with the cables (numbers 8 and 10) that have twisted pairs with an overall shield. Two other cables (numbers 7 and 11) were placed on the other side of the tunnel floor with the bundle made up of the cables which connect to external sensors (figure 2-7). These two cables are similar to cables 8 and 10 but they have additional internal shields on sets of twisted signal conductors. These sets carry the lower level operating signal voltages. The OF cables were tie-wrapped to the inside bracket of the floor plates so that they were located at the largest feasible distance above the floor plate (figure 2-8). This was done to intentionally maximize the magnetic field-induced currents in the cable shields. Prior to the connection of the OF cables, the bulkhead connectors were removed from the breakout boxes and the simulated aft IEA and their contact areas and the mating contact surfaces on the boxes were sandpapered to remove the aluminum oxide that had developed since prior lightning tests.

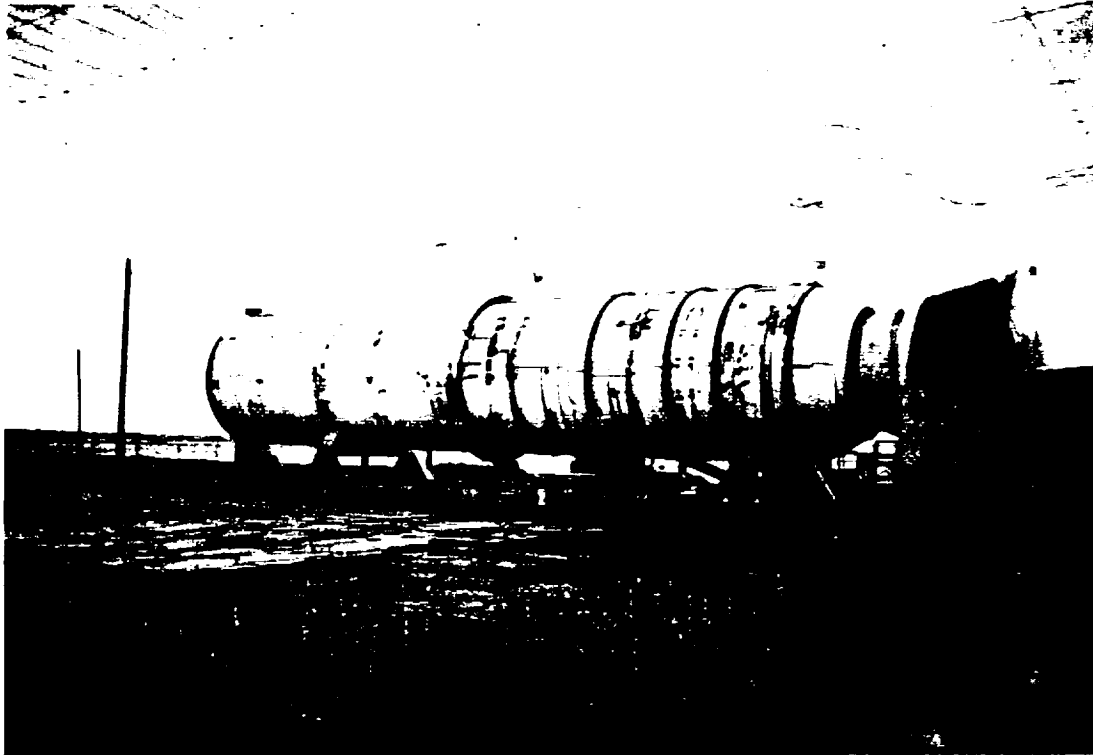
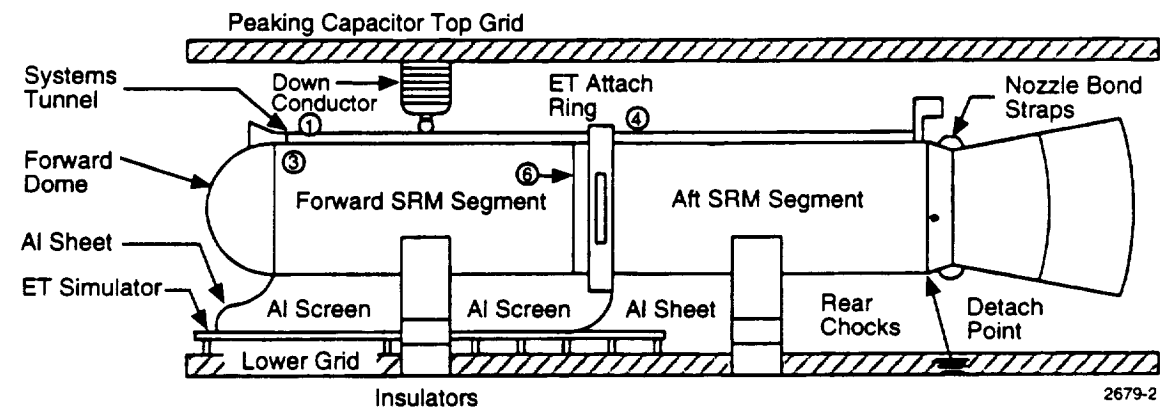


**Figure 2-1 Assembled Test Article**



Injection Point	Description
1	First tunnel cover on forward segment
3	Motor case approximately 1 foot from tunnel
4	First tunnel cover aft of ETA ring
6	Heater cable connector at the ETA ring

**Figure 2-2 Test Article, Peaking Capacitor, and Locations of Four Current Injection Points**

Table 2-1 Description of New Cover-To-Case Bond Straps

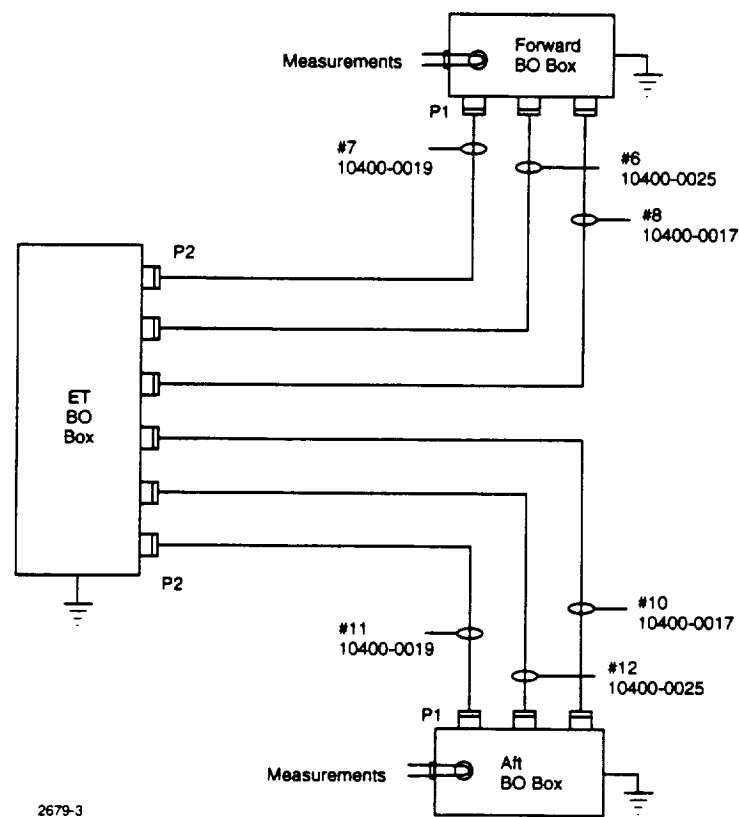
Sequence of Tunnel Parts	Bond Strap No.	Strap Type <sup>1</sup>	Conductive Epoxy <sup>2</sup>	Footprint R(milliohms)
<b>FWD BOB<sup>4</sup></b>				
Cover 1	1	4" holes	Traduct	0.041
Cover 2	2	4" notched	Traduct	0.180
Cover 3	3	4" notched	None <sup>3</sup>	Open
Cover 4	4	3" woven	None	0.360
Cover 5	5	3" woven	Traduct	0.110
Cover 6	6	3" woven	Ecco	0.092
Cover 7	7	2" woven	Traduct	0.160
<b>ETA Ring</b>				
Cover 8	8	4" notched	Traduct	1.000
Cover 9	9	3" woven	Ecco	0.128
Cover 10	10	4" notched	Ecco	5.720
Cover 11	11	4" notched	None	Open
<b>Stiff. Ring</b>				
Cover 12	12	4" holes	Traduct	1.130
Cover 13	13	2" woven	Ecco	0.397
Cover 14	14	3" woven	None	1.700
Cover 15	15	3" woven	Ecco	0.840
<b>Stiff. Ring</b>				
Cover 16	16	4" solid	Traduct	0.140
Cover 17	17	4" solid	None	25.00
<b>Stiff. Ring</b>				
Cover 18	18	4" solid	Ecco	0.806
Cover 19	19	3" woven	Traduct	0.110

1. Woven straps are tinned-copper strands Alpha part Nos. 1242 and 1242/4. Other straps are 4-inch width solid aluminum of .063-inch thickness. Straps with holes have .063 inches diameter, 30 holes in footprint area. Straps with notches have .375-inches width, 10 notches around footprint edges.
2. Traduct refers to Traduct 2902, a product of Tra-con, Inc., Medford, Mass. Ecco refers to Ecco Bond 56C, a product of Emerson & Cuming, Woburn, Mass.
3. "None" means the case was cleaned to bare metal for contact and the strap is held down with the thermal protection material designated as K5NA.
4. BOB—Breakout Box





**Figure 2-3 Location of Three OF Cables in Test Article Forward Tunnel**



2679-3

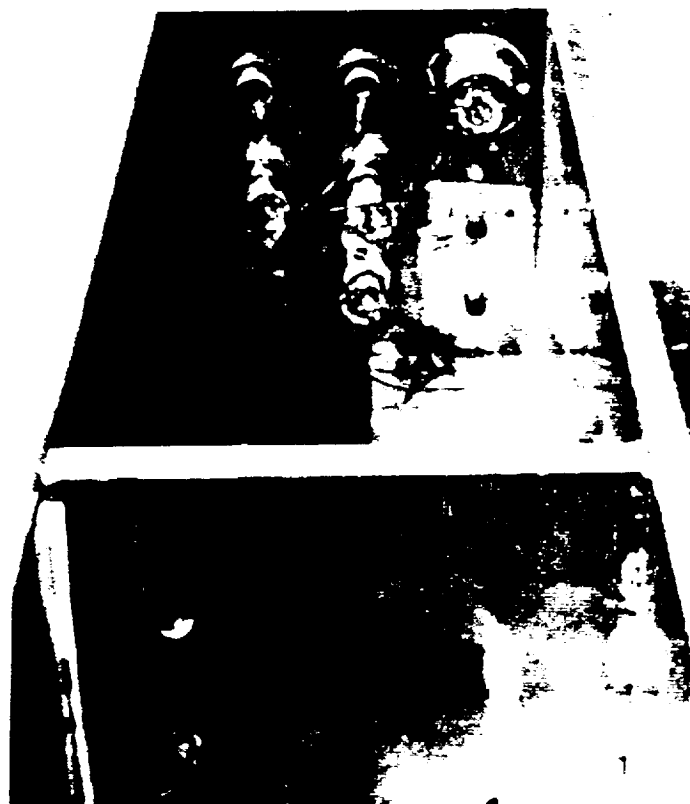
**Figure 2-4 Configuration of OF Test Cables**

**Table 2-2 Description of OF Test Cables**

Cable No	Drawing No	Test Article Location	Dia. of Shield	Overall Shield Thickness	Approx. Length	Description	No. of Cond	Conductor Sizes (AWG)
6	10400-0025	Fwd	.220"	.0050"	39 ft.	Pyro (TWS)*	2	#12
7	10400-0019	Fwd	.650"	.0063"	39 ft	TWDS	49	#22 & #24
8	10400-0017	Fwd	.520"	.0063"	39 ft	TWS	41	#20 & #22
10	10400-0017	Aft	.520"	.0063"	39 ft	TWS	41	#20 & #22
11	10400-0019	Aft	.650"	.0063"	39 ft.	TWDS	49	#22 & #24
12	10400-0025	Aft	.220"	.0050"	39 ft.	Pyro (TWS)	2	#12

\*TWS Twisted pairs with overall shield

\*TWDS Twisted sets of conductors enclosed by internal EMI shields. Cables 7 and 11 each had 17 EMI shields.


**Figure 2-5 Aluminum Test Article Box Simulation of Aft IEA**

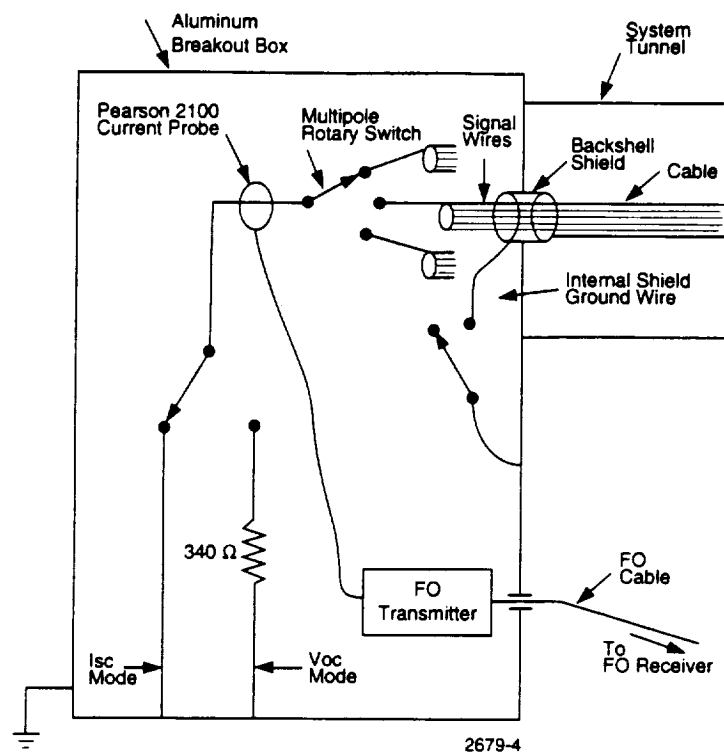


**Figure 2-6 Circuit Schematic, Breakout Box**

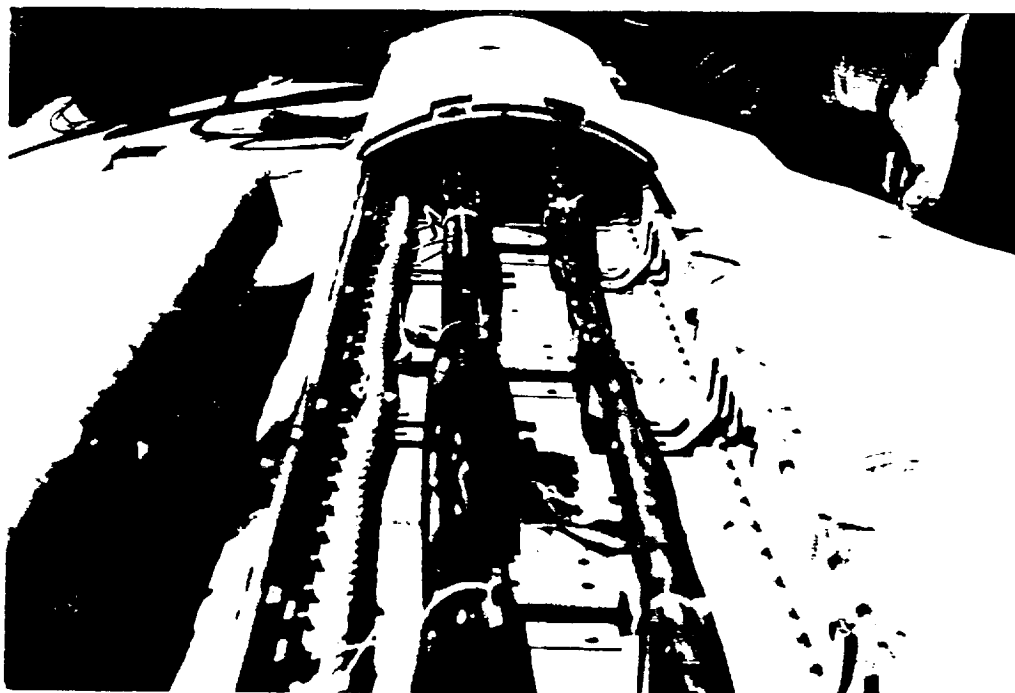


**Figure 2-7 Location of Three OF Cables and GEI Cables in the Forward Tunnel**

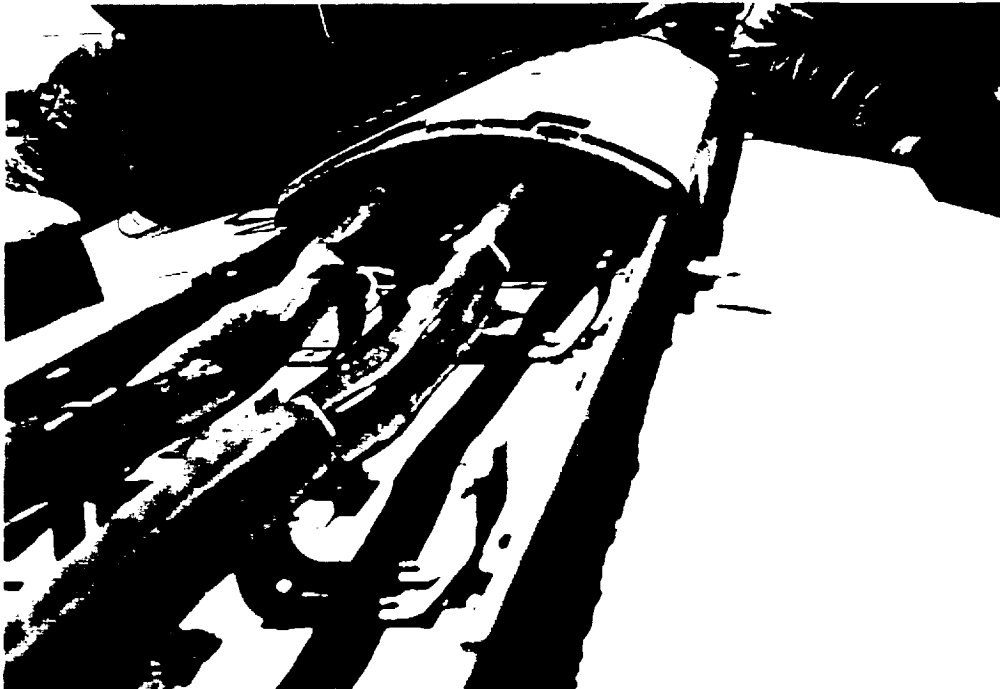


**Figure 2-8 OF Test Cables Located in the Tunnel for Worst Case Magnetic Field Coupling**

The simulated aft IEA aluminum box was bolted to the ETA ring mounts and was enclosed by a sheet metal cover to simulate the aft IEA covers. The simulated aft IEA cover was clamped to the ETA ring cap in several places to provide electrical continuity between the cover and the ETA ring.

The external GEI sensor cables were installed near stations 539, 703, 1504, 1701, 1751 and 1829 (figures 1-4 and 2-9). Each external sensor cable had a twisted pair inside a shield. The twisted pair terminated across a 50-ohm resistor to simulate the sensor. Each simulated sensor was located at the appropriate location around the circumference of the motor case and was electrically bonded to the motor case approximately at 18-inch intervals where the cables enter the systems tunnel. The footprint of the bonding material was 1.0 square inches at each of the case interval points.

The Thiokol Corporation test engineers chose to install two sets of external cables at each of the above listed stations. One set was electrically bonded to the case with the conductive epoxy designated as Ecco-Bond 56C. The other set was bonded with the conductive epoxy designated as Traduct 2902.

The Ecco-Bond 56C is the epoxy that has been used by Thiokol to bond the GEI cables and the internal bond straps to the motor case and the Traduct 2902 is a candidate epoxy for future use in bonding any strap or cable to the case. Only one set of GEI cables was connected at a time to the cables inside the tunnel during the coupling tests (that included the external cables). During one phase of the coupling tests, all external cables were disconnected at their tunnel entry points in order to obtain the data needed to assess the contribution of these cables to the coupling of lightning energy to the OF cables.

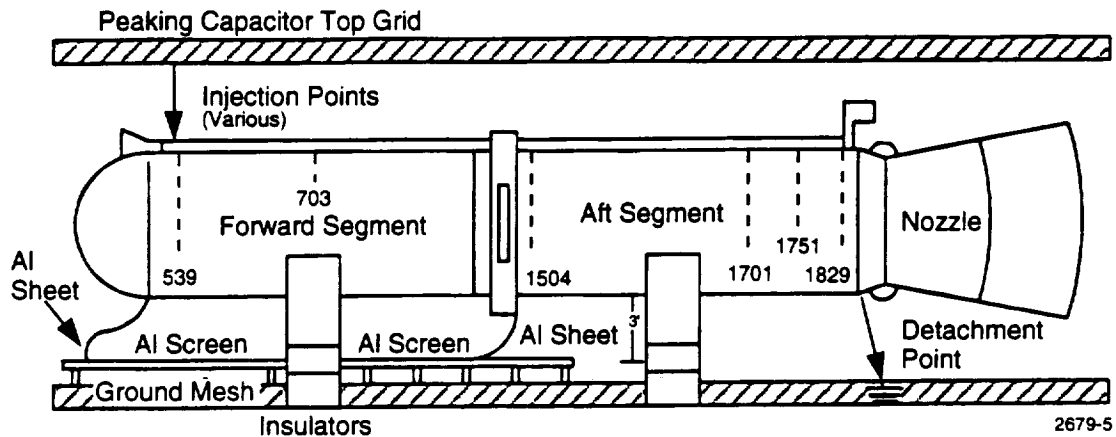


**Figure 2-9 Location of External GEI Cables on Test Article**

After the OF and GEI cables were satisfactorily installed, the tunnel covers were installed along with the new cover-to-cover bond straps. The DC resistance between each tunnel cover and its corresponding floor plate was measured prior to the installation of the new cover-to-case external straps. The case ends of the new cover-to-case straps were installed and the conductive epoxies allowed to cure for two days during warm weather (65-70° F) prior to the beginning of the CW transfer function tests. The manufacturers' recommended a room temperature cure time of 24 hours. The resistance between each new bond strap and the motor case was measured after the epoxy had cured for 9 days. The 9-day delay was selected to allow the CW tests to begin sooner. The tunnel on the forward segment had seven covers and eight floor plate sections. The ends of the floor plate sections coincided with the end of the covers at eight cover gaps (reference USBI drawing number 90001-0050). On the forward end of the forward tunnel and the aft end of the aft tunnel there were gaps of approximately 3 inches between the BOBs and the first tunnel cover. There are no equivalent gaps on flight hardware. These gaps were covered as well as feasible with aluminum foil (figure 2-10). On the aft end of the forward tunnel and the forward end of the aft tunnel there were smaller gaps of about one inch to the ETA ring (figure 1-3). These smaller gaps are representative of flight hardware. The aft tunnel had 12 tunnel covers and 12 floor plate segments. USBI drawing number 90001-0050 contains additional information on the test article configuration details related to tunnel covers, tunnel floor plates, bond straps, and assembly procedures. Thiokol drawing number 7U77268 has additional information on the details of the installation of the external sensor cables. Thiokol drawings number 7U76546, 7U76787, and 7U76947 have additional information on the fabrication and installation of the breakout boxes.

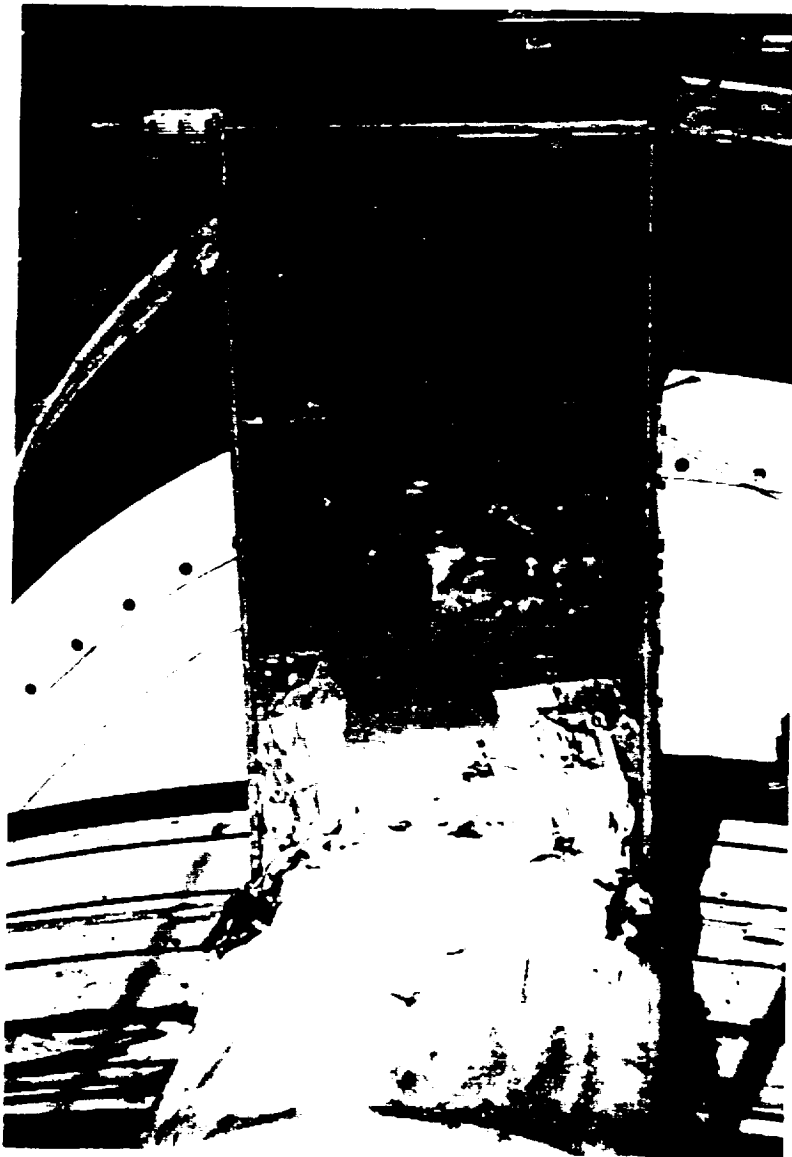


**Figure 2-10 Foil Between Aft BOB and Last Tunnel Cover**

The assembled test article was placed between a ground plane and an upper grid of wires (figure 2-2) and the energy stored in banks of capacitors was delivered to the strike attachment points as described in the prior lightning test report (reference 1).

### **Chapter 3 Test and Measurement Methods**

In general, the test and measurement methods used during this test were similar to those that have been successfully used on many prior lightning tests on commercial and military aircraft. The lightning current injection points were selected to be on and near the systems tunnel based on the prior test (reference 1) and the fact that the worst case attachment points for the tunnel cables are on the tunnel covers. One current exit point at the bottom (180 degrees around the motor case from the tunnel) of the aft segment was used for all of the tests. This simulated an exit through the nozzle and plume area.

The current injection sources used during the tests included a swept CW generator (CW is short for continuous wave, i.e., a steady-state single frequency), a Marx high rate of current rise capacitor bank, a high current capacitor bank, and a "continuing" current capacitor bank. The term "continuing" refers to a component of the lightning current that has a time duration of about 0.5 seconds. The swept CW generator was used first because the results were used to plan the setting of gains and attenuations in the fiber optic instrumentation channels for the pulse tests. The output of the swept CW source was connected directly to the injection points. The CW source delivered low current levels (approximately 9 amps) as it automatically stepped through discrete frequencies over the range of 1 kilohertz (kHz) to 10 megahertz (MHz). The short circuit current was measured with a shielded current probe placed around a conductor inside the shielded breakout boxes as shown in figure 2-6. The open circuit voltage was obtained by the measurement of the current flowing through a 340-ohm resistor connected between the cable core conductors and the inside of the breakout box (chassis ground). The voltage outputs of the shielded current probes were passed to the input of a fiber optic transmitter. The transmitter amplified or attenuated (as selected by the operator) the signal and then converted it to an optical output. This output was transferred through a fiber optic cable to a receiver located inside a well-shielded instrumentation room. The receiver converted the signal back to an electrical voltage. This voltage was returned to the CW network analyzer which automatically measured the ratio of this voltage to the injected current level at each frequency step. The network analyzer output drove an X-Y plotter and produced plots of the ratio versus frequency (figure 3-1). When the pulse tests were conducted, the output voltage of the fiber optic receiver was an input to a transient digitizer located in the shielded room which was set up (programmed) to sample the input voltage at preselected time intervals and to convert the result to a digital format which was stored in memory under the control of a mini-computer. The stored data was scaled for gain and attenuation settings and then plotted on an X-Y plotter to produce transient waveforms (figure 3-2). Prior to the beginning of the tests, the frequency responses of the current probes, the fiber optic links, and the transient digitizers were checked to assure that the bandwidths were sufficient and the responses flat enough to measure the pulse waveforms without unacceptable distortion.

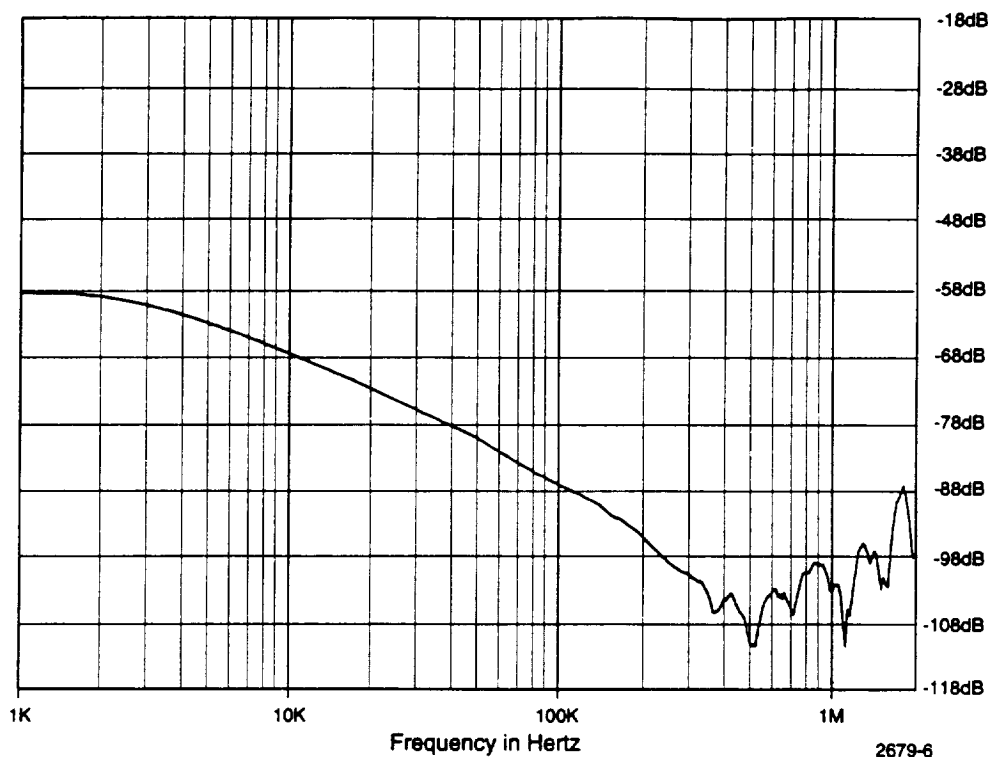


**Figure 3-1 Measured CW Short Circuit Current, Cable 6, Inject. Point 1, Relative to Injected Current**

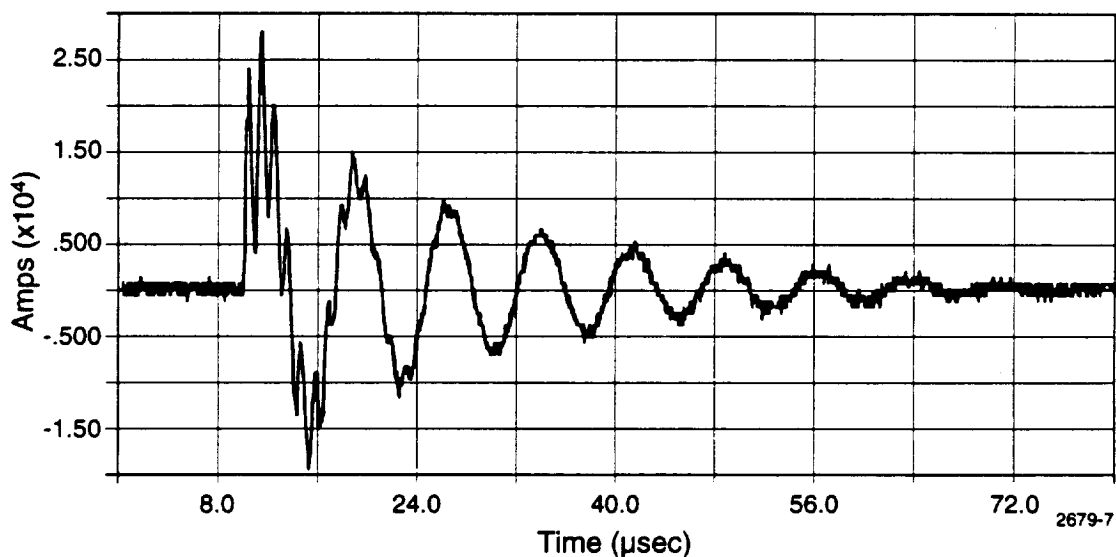


**Figure 3-2 Measured Marx Injection Current Waveform**

The fiber optic links were used for two reasons. The first, and most important, is that the very high electromagnetic fields created by the injected currents would have generated "noise" in electrical instrumentation cables. The second is that the connection of electrical instrumentation cables to the test article would produce "unnatural" current paths which would obscure the natural response of the coupling



to the test article. The Marx capacitor bank consisted of twenty 1.8 microfarad capacitors which were charged in unison to a selected voltage level of up to 50 kV each. They were then discharged in series, by an arrangement of spark gaps, into the top plate of grid wires. The top plate was pulse charged, as a peaking capacitor, to the maximum output voltage of the Marx bank (approximately 20 times 50 kV, or 1.0 million volts). A down conductor from the top plate had an adjustable length steel rod which was set at the appropriate distance from the test article injection point to allow the voltage to build up nearly to the maximum possible and then to form an arc from the rod to the test article. After the arc formed, the electrical charge that had been stored in the capacitors produced a high amplitude pulse of current through the test article. The risetime of this waveform was determined by the inductance of the test article and the inductance of the current path through the capacitor bank. The frequency of the decaying sine wave was determined primarily by the capacitance of the generator and the inductance of the total current loop through the upper grid of wires, the test article, and the lower grid of wires.

The high current capacitor bank (HCB) was a set of 144 1.8 microfarad capacitors which were charged in parallel up to 50 kV each and discharged in a parallel-series arrangement to produce pulsed currents of up to 250 kA through the test article. The output of the HCB was also connected through the top grid of wires.

The continuing current bank (CCB) was designed to deliver up to 200 coulombs and consisted of a set of 180 capacitors (3500 microfarad) which were discharged through an inductance of 4.5 millihenries to the test article. The inductance served to spread the current pulse over a longer period of time. As shown in figure 3-3, the pulse width was approximately 0.6 seconds at the half-maximum amplitude.

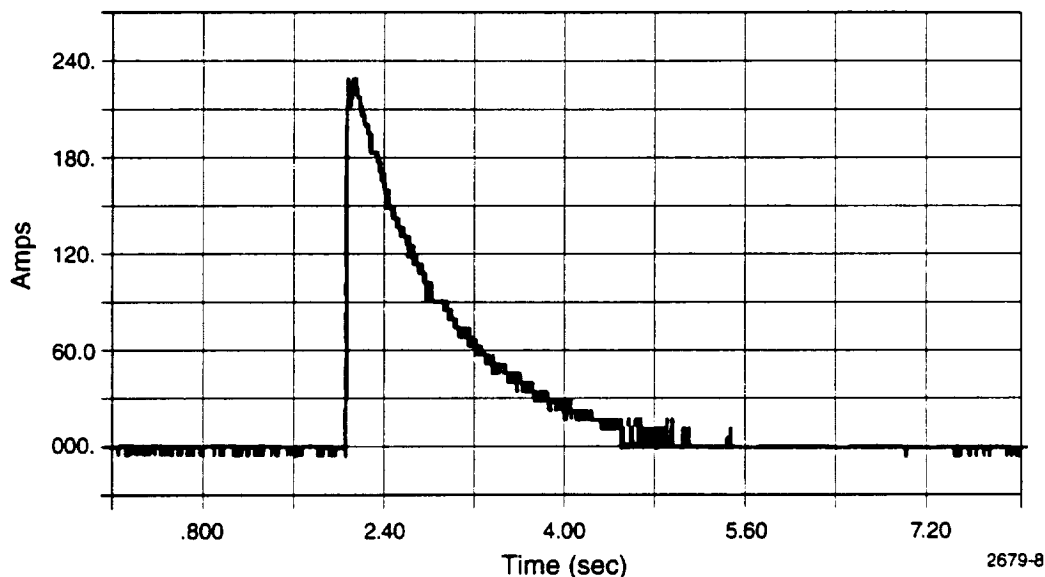


**Figure 3-3 Measured Continuing Current Bank (CCB) Injection Current Waveform**

At the beginning of the CW tests, noise measurements were made in order to establish the noise floor within each breakout box. These were done by measurement of the output of the instrumentation channels while the current

sensing probe was removed from the cable conductors in the breakout box and the CW current was driven through the test article. The resulting measurement was the noise level. In this case, noise is defined as the instrumentation response to the currents and fields with no input to the measuring device.

Many similar lightning coupling tests have been conducted on aircraft, rockets, and missiles where short circuit current and open circuit voltage data were used to develop coupling models and to find the coupling modes which are the primary drivers of the responses measured. As in the test reported here, it is usually not feasible to perform go/no-go type lightning tests on complex systems due to the number of injection points and the number of test article configurations that would be needed, the fear (or cost) of causing damage to operational subsystems, and the cost of providing lightning simulators which adequately simulate the waveforms required by the specifications. This means that the SRB must be *evaluated* against the specified waveforms because it cannot be *tested* against them.

During the external bond strap survivability tests, currents from the HCB (which had a primary frequency of 5 kHz) with high action integrals (up to 2.3 times the NASA specification) were injected into the tunnel covers. The energy deposited in a conductive epoxy footprint is proportional to the time integral of the current flowing through the epoxy. The failure level of the bond is dependent upon the heat added by this energy. The HCB produced the highest action integral current pulses and was used in all of the bond strap survivability tests. The CCB produced the highest total charge pulses and was used in the bond strap tests until it was damaged by unanticipated discharges of the HCB back through the charging and firing circuits of the CCB. Prior to this damage, the HCB and CCB were discharged simultaneously into the test article. The loss of the CCB had no effect on the test results because the energy content of the CCB current pulse in the epoxy footprints was much less than the energy from the HCB.

## **Chapter 4 Summary of the Data**

In this chapter, the test data are summarized. The interpretation and analysis of these data are found in later chapters.

The following is a list of the important steps, in chronological sequence, that were followed after the assembly of the test article:

1. Tunnel cover-to-cover and cover-to-floor plate DC resistances measured
2. CW transfer functions measured (GEI cables connected)
3. External bond strap footprint resistances measured
4. Marx current injection tests (GEI cables connected)
5. Increased torque on cover-to-angle bracket bolts from about 60 or 70 inch-pounds to 120 inch-pounds (the torque specified for flight hardware). (Not expected to affect test results but listed here for completeness.)
6. HCB current injection tests (GEI cables connected)
7. HCB current injection tests (GEI cables disconnected)
8. Marx current injection tests (GEI cables disconnected)
9. Bond strap survivability tests
10. Marx current injection tests (test article bond straps changed to flight configuration with internal bond straps, AWG No. 12 wire cover-to-cover bond straps, and GEI cables reconnected).

Table 4-1 contains a list of the tunnel DC resistance measurements that were made after the covers and the new cover-to-cover bond straps were installed but before bolting of the new cover-to-case bond straps to the tunnel covers (step 1 above).

As the table demonstrates, all of the measured resistances between covers and between a cover and a ring (ETA or aft stiffeners) were lower than the 2.5 milliohms that has traditionally been used as a standard in the shuttle program. Some of the cover-to-floor plate resistances were higher than the 2.5 milliohms standard. However, it is unlikely that these cover-to-floor plate resistances affected the coupling to the cables with the new external bond straps installed between each of the covers and the motor case. Most of the external straps that were bonded to the motor case with conductive epoxies had resistances of less than one milliohm (table 4-2).

Table 4-1 Measured DC Resistances Prior to Tests

Sequence of Structure Parts	Cover-To-Floor Plate R (Milliohms)	Part-To-Part R(Milliohms)
<b>FWD BOB</b>		
Cover 1	0.27	1.02
Cover 2	0.22	.058
Cover 3	2.65	.066
Cover 4	0.83	.070
Cover 5	2.15	.064
Cover 6	0.58	.052
Cover 7	0.28	.073
<b>ETA Ring</b>		.390
Cover 8	6.60	.620
Cover 9	2.27	.023
Cover 10	0.47	.027
Cover 11	0.16	.030
<b>Stiff. Ring</b>		.116
Cover 12	2.17	Not measured
Cover 13	1.50	.024
Cover 14	1.13	.030
Cover 15	3.37	.021
<b>Stiff. Ring</b>		.112
Cover 16	0.47	Not measured
Cover 17	0.78	.028
<b>Stiff. Ring</b>		.119
Cover 18	3.90	Not measured
Cover 19	0.64	.024
<b>Aft BOB</b>		1.88

Table 4-2 lists the cover-to-case bond straps used on the test and the measured DC bonding resistance between each strap and the motor case (step 3 above). It should be noted that these measurements were made in a careful process to verify that each measured value was accurate:

1. A calibrated Biddle meter was used.
2. The tunnel end of each strap was mechanically separated from the tunnel and electrically isolated by the insertion of a nonconductive card.
3. Prior to each measurement, the contact probes of the Biddle meter were placed close together on the surface of one of the aluminum straps to ensure that the meter produced a very low reading.
4. Prior to each measurement, the contact probes of the Biddle meter were placed close together on a cleaned surface area of the motor case to obtain a very low reading to ensure that the probe contact with the case was acceptable.

**Table 4-2 New Bond Strap Resistance Measurements**

<b>Tunnel Cover No.</b>	<b>Bond Strap Type</b>	<b>Conductive Epoxy</b>	<b>Bonding Resistance (Milliohms)</b>
1	4" with holes	Traduct	.041
2	4" notched edge	Traduct	.180
3	4" notched edge	none	>60,000*
4	3" woven	none	.360
5	3" woven	Traduct	.110
6	3" woven	Ecco-Bond	.092
7	2" woven	Traduct	.160
8	4" notched edge	Traduct	1.00
9	3" woven	Ecco-Bond	0.128
10	4" notched edge	Ecco-Bond	5.72
11	4" notched edge	none	>60,000*
12	4" with holes	Traduct	1.13
13	2" woven	Ecco-Bond	.397
14	3" woven	none	1.70
15	3" woven	Ecco-Bond	.840
16	4" solid	Traduct	.140
17	4" solid	none	25.0
18	4" solid	Ecco-Bond	.806
19	3" woven	Traduct	.110

\* The Biddle meter highest range limit was 60 ohms. These two straps were not in direct contact with the motor case. There had to be a small air gap under their footprints.

The straps that had no conductive epoxy (number 3, 4, 11, 14, 17) were placed over a cleaned bare metal surface and held down with tape while K5NA TPS material was applied over the strap and allowed to cure. In two out of the five cases (number 4 and 14), this process produced a low footprint resistance. In two cases, the footprint resistance was higher than the maximum measuring range of the Biddle meter (60 ohms). It is important to note that the value of the footprint resistance depends more on the installation procedure than on which of the two conductive epoxies was used. For example, the lowest bonding resistance obtained was on strap number one which was the first one installed. This low value was the result of one of the installers standing on the strap for an extended period of time (30–45 minutes). Sand bags were used to maintain pressure on the other straps while the epoxy cured. The sand bags did not exert as much pressure on the other straps as this first one experienced.

At the beginning of the CW tests, the outputs of the two amplifiers which provided the CW injection currents for two frequency ranges were measured (see figures 4-1 and 4-2). One of the amplifiers covered the frequency range 1 kHz to 2 MHz and the other amplifier covered the range of 1 MHz to 10 MHz. The noise floor was measured in the forward BOB (breakout box) and the aft BOB with current injected at injection point number 1 (the forward tunnel cover). Figure 4-3 is the noise floor in the forward BOB and figure 4-4 is the noise floor in the aft BOB. From these plots, the noise floor in both BOBs is -90 dB at low frequency (less than 10 kHz), decreases to about -118 dB at 100 kHz, and then increases with frequency back to -90 dB at 2 MHz.

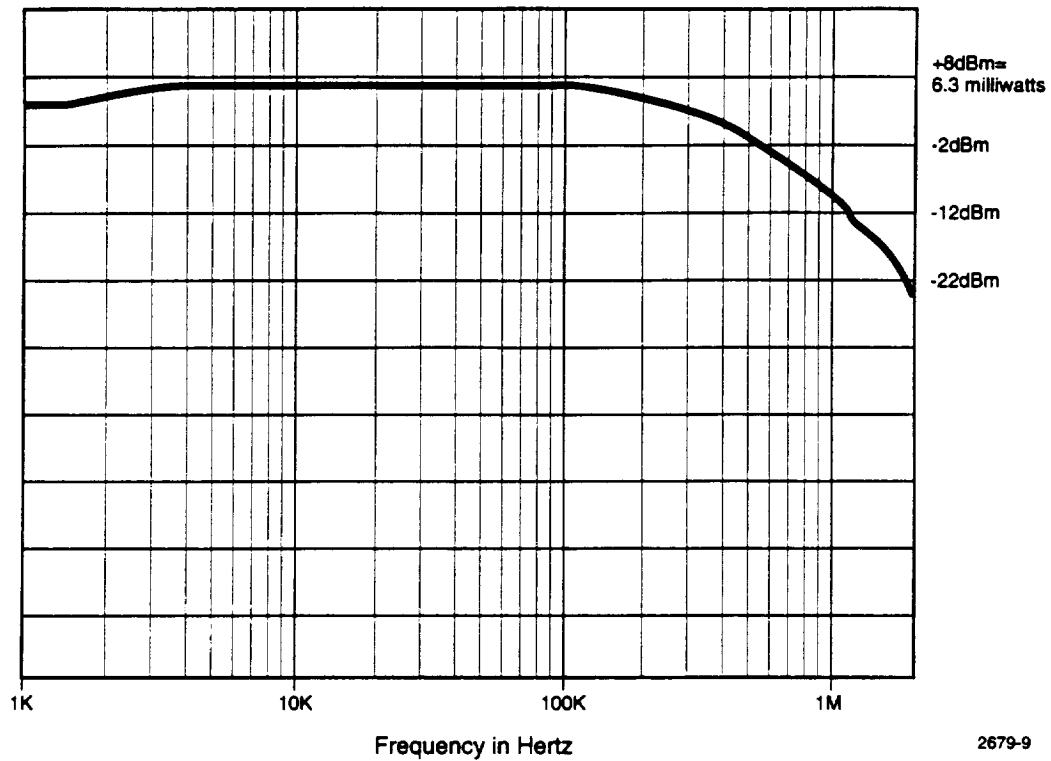


Figure 4-1 Measured CW Injection Current (1 kHz to 2 MHz)

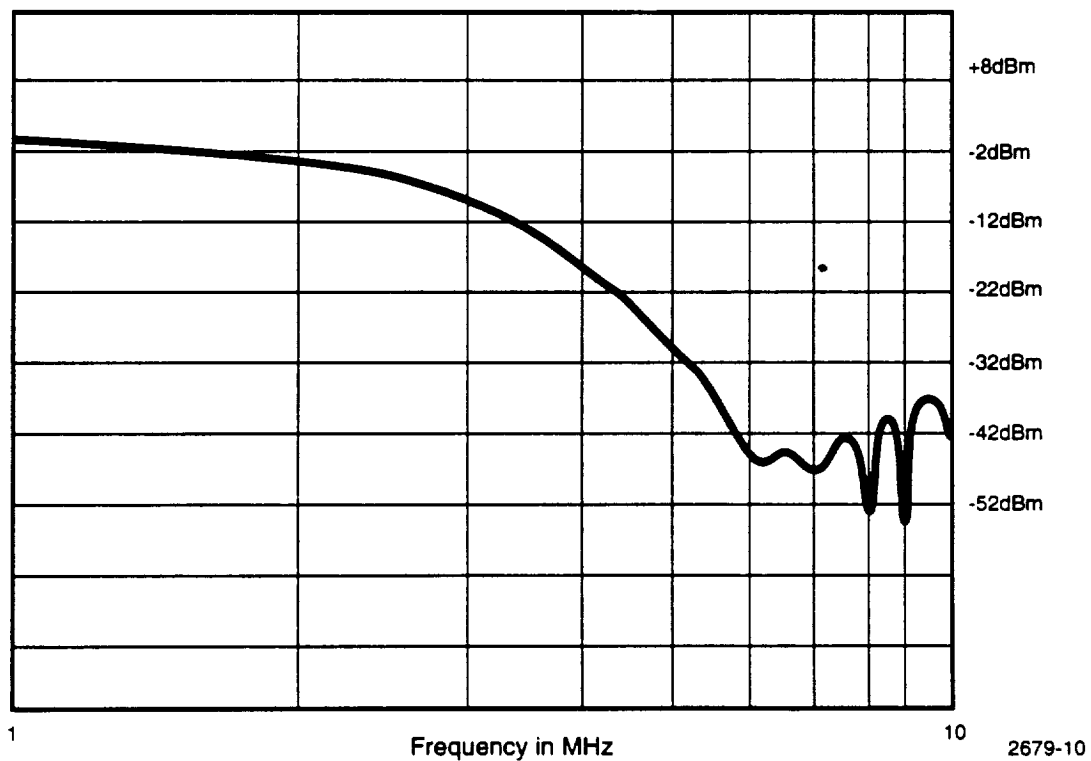
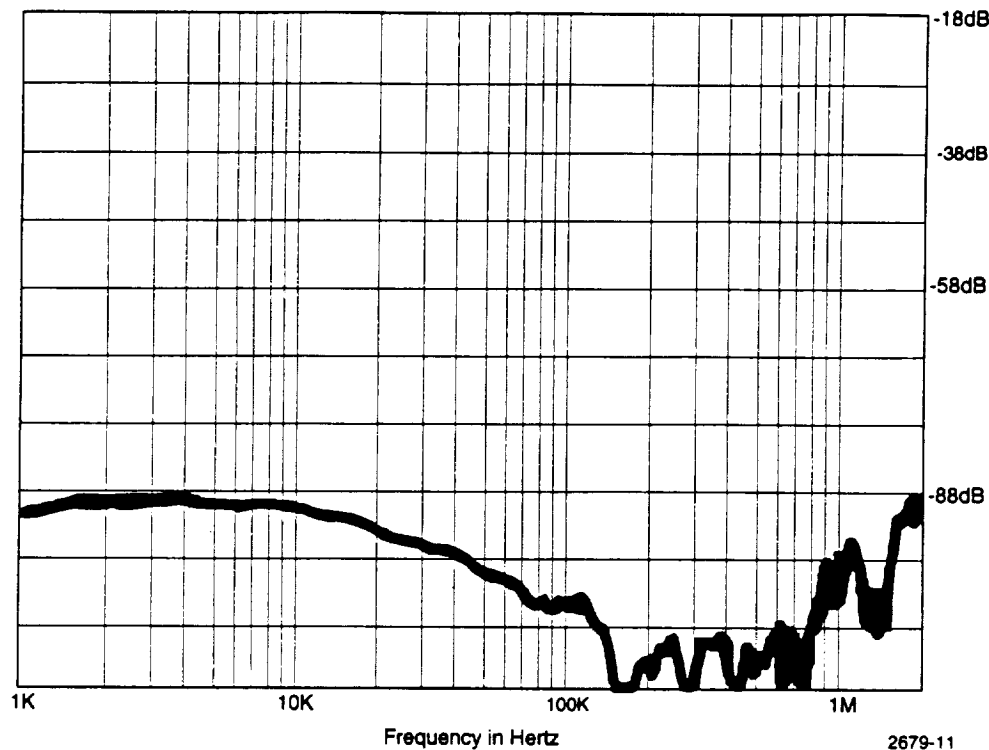
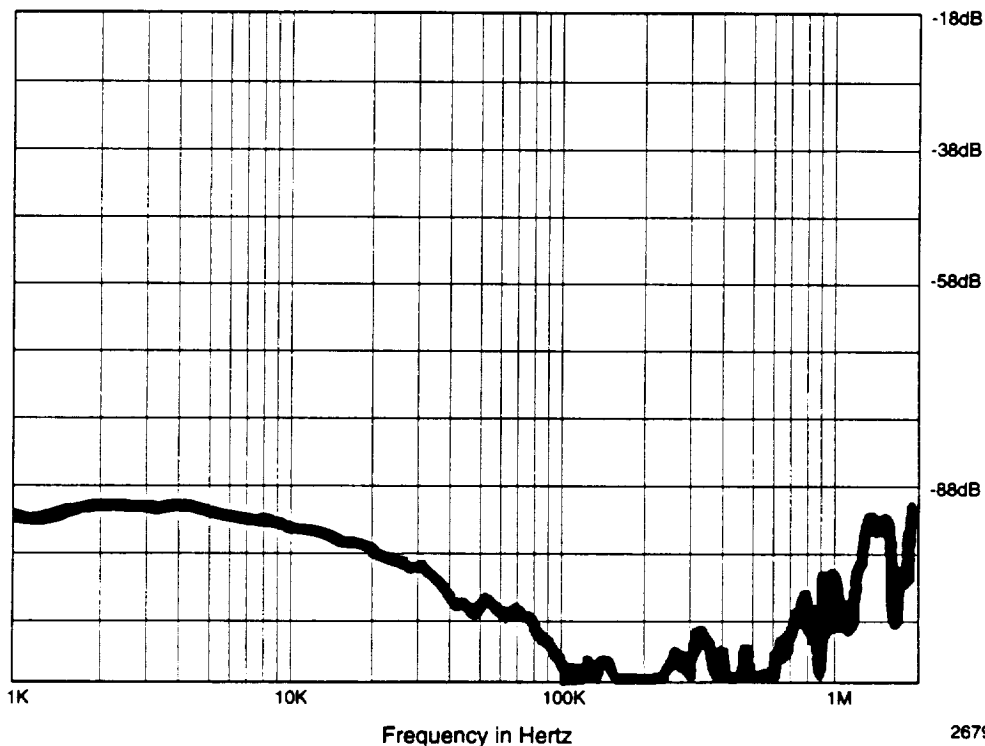


Figure 4-2 Measured CW Injection Current (1 MHz to 10 MHz)



**Figure 4-3 Measured Instrumentation Noise Level in Forward Breakout Box, Relative to Current Injected at Forward Tunnel Cover**



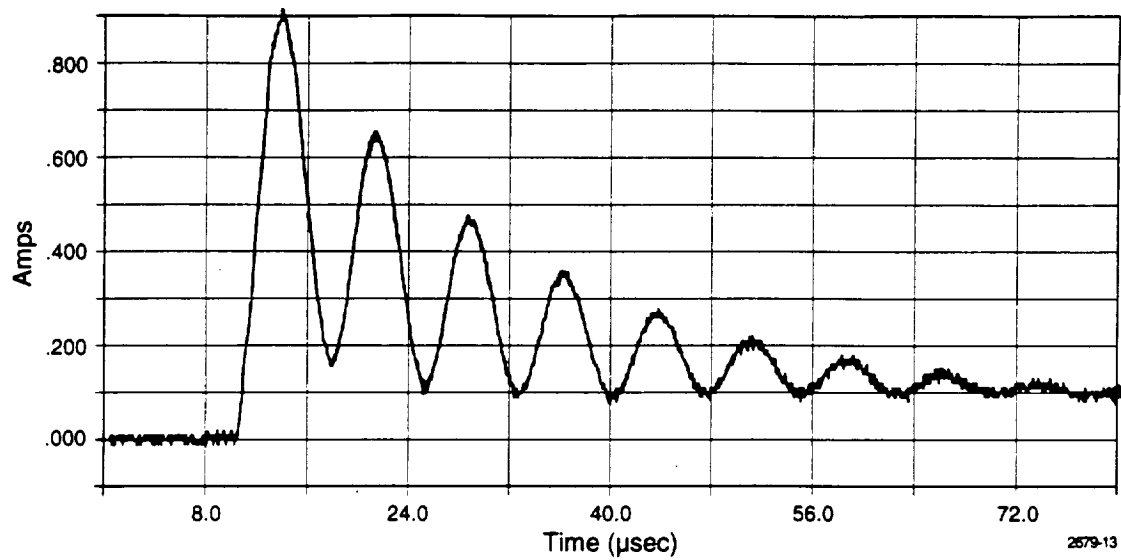
**Figure 4-4 Measured Instrumentation Noise Level in Aft Breakout Box, Relative to Current Injected at Forward Tunnel Cover**

After the noise floors were established, the CW short circuit currents and CW open circuit voltages were measured on the OF cables with current injection points located at injection points 1, 3 (the case next to tunnel cover number 1), 539, 703, 1701, 1751, and 1829. These last five injection points were the shields on the external GEI cables located at the station numbers as designated (figure 2-9). Some of these measurements were made with the EMI shields on cables 7 and 11 shorted to chassis ground and some with these shields open. Early in this series of CW measurements, it was determined that the noise floor was reached at frequencies between 100 kHz and 300 kHz. For this reason, the measurements with the higher frequency amplifier (1 MHz to 10 MHz) were discontinued because it was known that the results would be at the noise floor level. All of the CW cable response measurements had similar characteristics as a function of frequency. Examples of these CW measurements are provided in chapter 6 of this report.

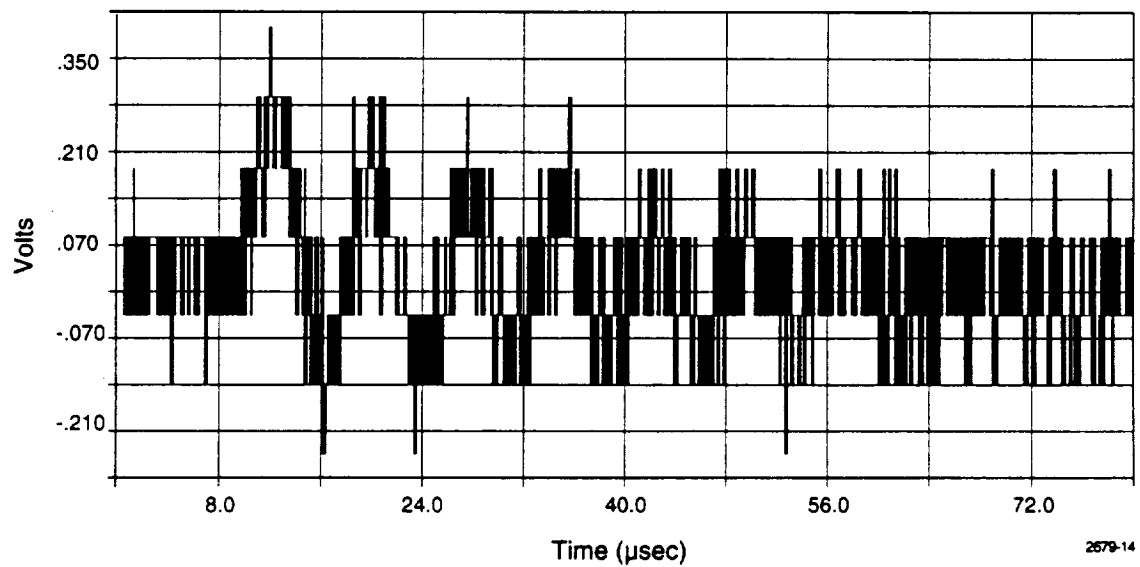
Figure 3-2 is a typical waveform of the Marx generator injected current. The primary frequency of this damped sine wave is 130 kHz. The frequency of the oscillations riding on the first two cycles is approximately 1 MHz. The steps up and down at times after 24  $\mu$ sec are not valid data. They are caused by the sampling and digitization process of the instrumentation.

Figure 4-5 is a typical measured short circuit current cable response and figure 4-6 is a typical measured open circuit voltage cable response from the Marx tests. The discrete step changes in figure 4-6 are caused by the digitization process and is not valid data. This data plot is interpreted as a 130 kHz damped sine wave with a peak value of 0.2 volts. Most of the open circuit voltage data from the Marx tests are of a similar quality because of the low signal levels produced. Tables 4-3, 4-4, and 4-5 contain listings of all of the valid short circuit current and open circuit voltage measurements obtained during the Marx current injection tests. A few test shots were omitted from table 4-3 and several test shots were omitted from table 4-4 and 4-5 because the data was considered to be at or near the noise floor level. Since the induced cable currents were greatly reduced by the 340-ohm terminations added for the open circuit voltage measurements, these measurements were closer to the noise floor than the short circuit current measurements. Tests numbered 9 through 63 were completed with the new bond straps installed and external GEI cables connected. Tests numbered 64 through 108 were completed with the new bond straps installed and the external GEI cables disconnected. Tests numbered 109 through 114 were completed after the test article was returned to the "flight configuration" (i.e., internal cover-to-case bond straps, AWG No. 12 wire straps between covers, and external cables connected).





**Figure 4-5 Measured Cable 6 Short Circuit Current with Marx Current Injected at Point 3**



**Figure 4-6 Measured Cable 12 Open Circuit Voltage with Marx Current Injected at Point 3**

**Table 4-3 Induced Peak Common Mode Short Circuit Currents, Marx Test**

Cable No.	Test No.	Injection Point No.	Peak Injection Current (kA)	Peak Cable Current (amps)	Cable Current + Injection Current (dB)
6	16	3	27.3	0.92	-89.4
6	24	4	21.7	0.04	-114.7
6	32	1701	23.3	0.05	-113.4
6	34	1701	22.3	0.07	-110.1
6	71	4	31.1	0.18	-104.7
6	72	1	25.6	1.44	-85.0
6	75	3	22.5	1.00	-87.0
6	76	6	21.0	0.22	-99.6
6	110	3	31.4	1.88	-84.5
6	113	1	31.9	3.72	-78.7
6	114	539	32.7	2.15	-83.6
7SS**	10	1	28.7	0.18	-104.0
7SS	10	4	27.4	0.11	-107.9
7SS	77	6	23.4	0.07	-110.6
7SS	111	3	30.7	1.52	-86.1
7SS	112	1	-	2.23	-
7SO*	35	4	28.5	0.11	-108.3
7SO	37	1	23.6	0.35	-96.6
7SO	40	539	23.8	0.41	-95.3
7SO	41	3	22.1	0.35	-96.0
8	9	1	31.0	0.20	-103.8
8	26	4	21.5	0.15	-103.1
10	9	1	31.0	0.28	-100.8
10	11	1	27.8	0.18	-103.8
10	18	3	27.5	0.17	-104.2
10	26	4	21.5	0.13	-104.4
10	22	539	22.4	0.30	-97.5
11SS	10	1	28.7	0.33	-98.8
11SS	17	3	27.5	0.31	-98.9
11SS	25	4	22.5	0.36	-95.9
11SS	70	4	27.4	1.20	-87.2
11SS	73	1	28.9	0.21	-102.8
11SS	74	3	21.2	0.14	-103.6
11SS	77	6	23.7	0.12	-105.9
11SS	111	3	30.7	0.62	-93.9
11SS	112	1	-	0.63	-
11SO	33	1701	23.5	0.21	-101.0
11SO	35	4	28.5	0.17	-104.5
11SO	37	1	23.6	0.27	-98.8
11SO	40	539	23.8	0.28	-98.6
11SO	41	3	22.1	0.35	-96.0

\* "SO" indicates that the internal shields were open

\*\* "SS" indicates that the internal shields were shorted to chassis ground inside the breakout box

**Table 4-3 Induced Peak Common Mode Short Circuit Currents, Marx Test (continued)**

Cable No.	Test No.	Injection Point No.	Peak Injection Current (kA)	Peak Cable Current (amps)	Cable Current + Injection Current (dB)
12	16	3	27.3	0.25	-100.8
12	24	4	21.7	1.12	-85.7
12	30	1701	23.4	0.41	-95.1
12	34	1701	22.3	0.32	-96.9
12	71	4	31.1	2.18	-83.1
12	72	1	25.6	0.26	-99.9
12	75	3	22.5	0.27	-98.4
12	76	6	21.0	0.60	-90.9
12	109	3	30.6	0.32	-99.6
12	110	3	31.4	0.26	-101.6
12	113	1	31.9	0.31	-100.2
12	114	539	32.7	0.30	-100.7

**Table 4-4 Induced Peak Common Mode Open Circuit Voltages, Marx Test (130 kHz Comp.)**

Cable No.	Test No.	Injection Point No.	Peak Injection Current (kA) at 130 kHz	Peak Cable Voltage (Volts) at 130 kHz	Cable Current + Injection Current (dB)
6	23	539	16	0.6	-87.3
11SS	14	1	16	0.2	-98.1
11SS	20	3	16	0.2	-98.1
11SO	38	1	14	0.2	-97.0
11SO	39	539	15	0.15	-100.0
11SO	42	3	14	0.2	-96.9
12	21	3	—	0.2	—
12	29	4	14	0.4	-90.9

**Table 4-5 Induced Peak Common Mode Open Circuit Voltages, Marx Test (1 MHz Comp.)**

Cable No.	Test No.	Injection Point No.	Peak Injection Current (kA) at 1 MHz	Peak Cable Voltage (Volts) at 1 MHz	Cable Current + Injection Current (dB)
6	23	539	8.3	0.4	-85.4
11SS	14	1	10.0	0.1	-100.0
11SS	20	3	—	NM*	NM
11SO	38	1	8.5	0.1	-98.6
11SO	39	539	7.8	0.15	-94.3
11SO	42	3	—	NM	NM
12	21	3	—	NM	NM
12	29	4	—	NM	NM
12	31	1701	—	NM	NM

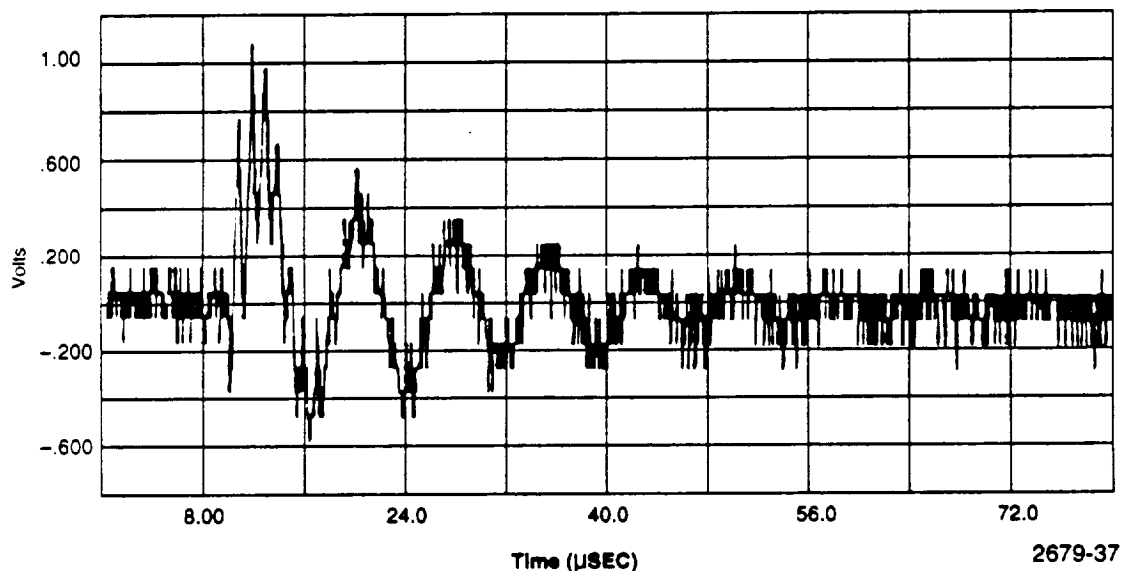
\* NM Not Measurable

Figure 4-7 is a plot of the largest open circuit voltage measured on any cable during the Marx injection tests. This response clearly shows both the 130 kHz and the 1 MHz components of the injected current waveform. In tables 4-4 and 4-5 the response data at these two frequencies are listed separately for ease of reference.

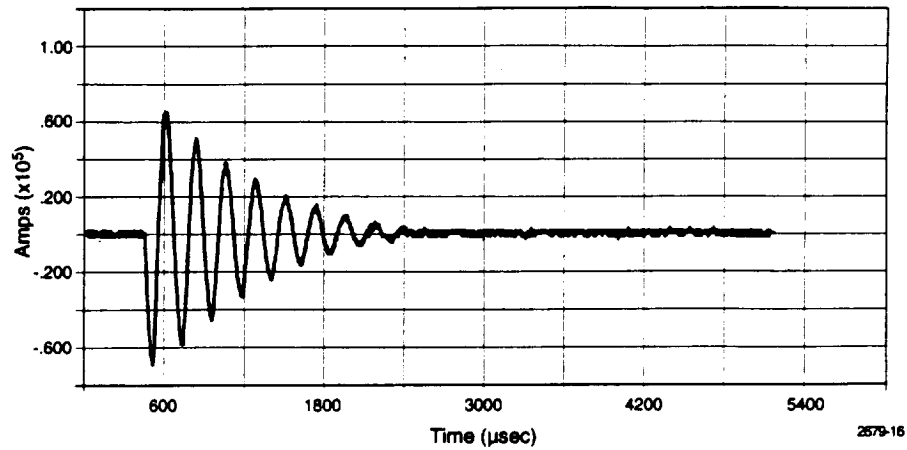
All of the cable coupling data has been compiled and summarized by Thiokol Corporation in reference 3.

Figure 4-8 is a typical waveform of the HCB injected current. The peak value of this waveform is 68.23 kiloamps. Nearly all of the energy in this current is concentrated at one frequency, which is 5 kHz. Figure 4-9 is a typical measured short circuit current cable response (peak value of 36.16 amps) and figure 4-10 is a typical open circuit voltage cable response (peak value of 1.48 volts) from the HCB tests. Tables 4-6 and 4-7 contain listings of the valid short circuit current and open circuit voltage measurements obtained during the HCB current injection tests. Tests 43 through 64 were completed with GEI cables connected. Tests 64 through 108 were completed with GEI cables disconnected. It should be noted that the cable response data summarized in these tables and in tables 4-3, 4-4, and 4-5 have not been scaled to specification levels. The interpretation of the data and the scaling of it to the specified criteria in NSTS 07636F is contained in chapter 6.

Table 7-1, in chapter 7, contains a summary of the results of the bond strap survivability tests.



**Figure 4-7 Measured Cable 6 Open Circuit Voltage with Marx Current Injected at Point 539**



**Figure 4-8 Measured High Current Bank (HCB) Injection Current**

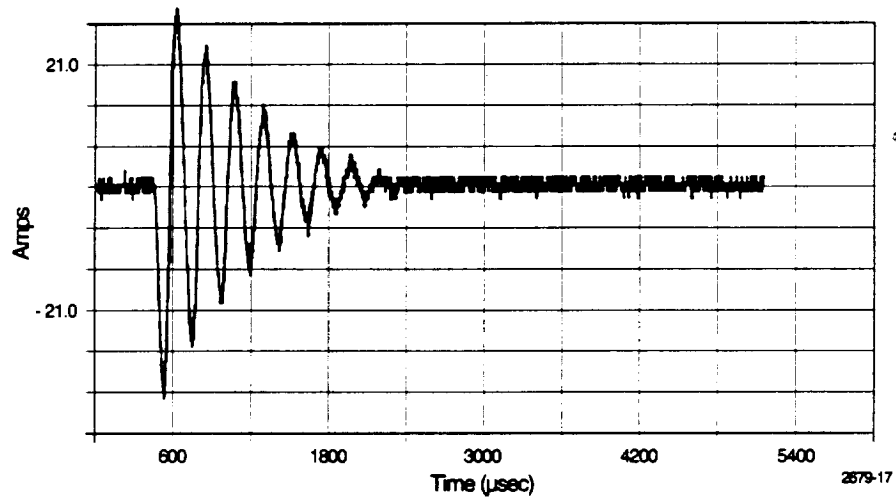


**Figure 4-9 Measured Cable 6 Short Circuit Current with HCB Current Injected at Point 1**

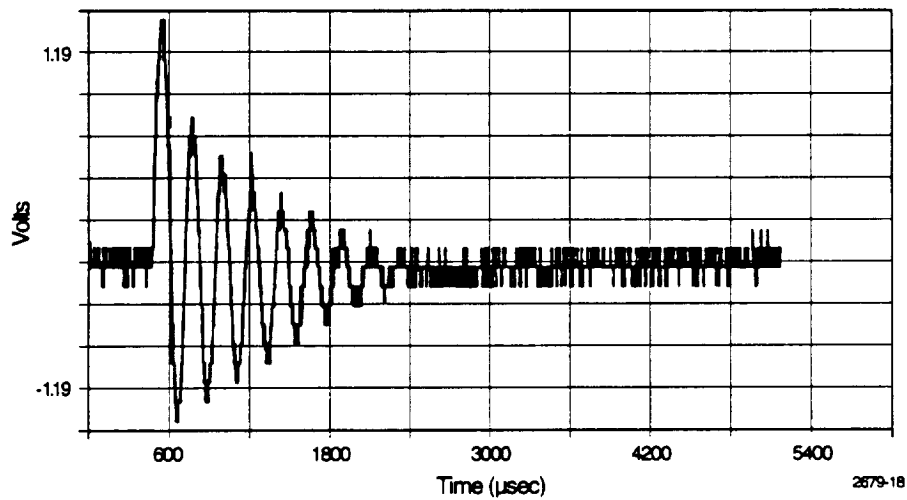


**Figure 4-10 Measured Cable 11 Open Circuit Voltage with HCB Current Injected at Point 1**

Table 4-6 Induced Peak Common Mode Short Circuit Currents, HCB Test

Cable No.	Test No.	Injection Point No.	Peak Injection Current (kA)	Peak Cable Current (amps)	Cable Current + Injection Current (dB)
6	43	3	77.90	34.9	-67.0
6	49	1	66.35	36.2	-65.3
6	55	539	64.52	33.2	-65.8
6	64	3	73.94	33.4	-67.0
6	67	1	75.71	35.0	-66.7
6	68	4	75.84	9.79	-77.8
6	78	3	74.33	10.	-77.4
6	79	*BS 1	72.92	32.7	-67.0
6	80	BS 2	84.39	34.9	-67.7
6	81	BS 2	73.31	24.5	-69.5
6	82	BS 2	100.9	18.9	-74.5
6	83	BS 4	85.37	25.5	-70.5
6	84	BS 4	99.39	25.8	-71.7
6	85	BS 5	91.88	31.7	-69.2
6	86	BS 6	98.53	49.0	-66.1
6	87	BS 7	96.04	57.0	-64.5
6	89	BS10	101.3	6.14	-90.2
6	90	BS12	-	2.87	-
6	91	BS13	107.6	3.05	-90.9
6	92	BS 4	85.5	24.3	-70.9
6	101	BS 9	121.0	8.67	-82.9
6	102	BS10	133.0	7.89	-84.5
6	103	BS11	84.47	5.60	-83.6
6	104	BS11	128.3	8.93	-83.1
6	105	BS 5	128.8	41.9	-69.8
6	106	BS 1	96.81	40.0	-67.7
6	107	BS 1	113.2	41.4	-68.7
6	108	BS 4	106.2	34.2	-69.8
7SS	45	3	79.90	24.7	-69.2
7SS	51	1	71.88	22.3	-70.2
7SS	56	539	63.87	22.7	-69.0
7SS	65	3	71.53	21.9	-70.3
7SS	66	1	74.50	13.4	-74.9
7SS	69	4	77.52	5.66	-82.7
7SO	60	4	75.72	6.04	-82.0
7SO	61	1701	65.61	2.89	-87.1
7SO	62	1	76.12	14.1	-74.6
7SO	63	3	70.47	24.4	-69.2
8	47	3	69.10	33.7	-66.2
8	53	1	71.66	31.7	-67.1
10	59	4	69.83	34.0	-66.3
11SS	51	1	71.88	15.8	-73.2
11SS	56	539	63.87	13.2	-73.7
11SS	58	4	77.31	37.8	-66.2
11SS	65	3	71.53	14.0	-74.2
11SS	66	1	74.50	12.8	-75.3
11SS	69	4	77.52	36.4	-66.6
11SO	60	4	75.72	68.5	-60.9

\*BS1 means injection into tunnel cover to which bond strap 1 is attached

**Table 4-6 Induced Peak Common Mode Short Circuit Currents, HCB Test (Contd)**

Cable No.	Test No.	Injection Point No.	Peak Injection Current (kA)	Peak Cable Current (amps)	Cable Current + Injection Current (dB)
11 SO	61	1701	65.61	4.82	-82.7
11 SO	62	1	76.12	22.3	-70.7
11 SO	63	3	70.47	26.9	-68.4
11 SO	66	3	71.53	14.0	-74.2
12	43	3	77.90	9.82	-78.0
12	49	1	66.35	7.70	-78.7
12	55	539	64.52	7.68	-78.5
12	57	4	77.69	29.2	-68.5
12	64	3	73.94	8.25	-79.0
12	67	1	75.71	7.09	-80.6
12	68	4	75.84	28.1	-68.6
12	78	3	74.33	8.86	-78.5
12	79	BS 1	72.92	6.53	-90.0
12	80	BS 2	84.39	8.14	-80.3
12	81	BS 2	73.31	7.16	-80.2
12	82	BS 2	100.9	7.32	-82.8
12	83	BS 4	85.37	5.59	-83.7
12	84	BS 4	99.39	7.54	-82.4
12	86	BS 5	91.88	7.31	-82.0
12	86	BS 6	98.53	9.07	-80.7
12	87	BS 7	96.04	10.4	-79.3
12	88	BS 9	105.0	10.2	-80.3
12	89	BS10	101.3	9.40	-80.6
12	91	BS13	107.6	2.41	-93.0
12	92	BS 4	85.50	9.35	-79.2
12	101	BS 9	121.0	12.4	-79.8
12	103	BS11	84.47	15.0	-75.0
12	104	BS11	128.3	22.3	-75.2
12	105	BS 5	128.8	14.1	-79.2
12	107	BS 1	113.2	58.9	-65.7
12	108	BS 4	106.2	6.77	-83.9

**Table 4-7 Induced Peak Common Mode Open Circuit Voltages, HCB Test**

Cable No.	Test No.	Injection Point No.	Peak Injection Current (kA) at 5 kHz	Peak Cable Voltage (Volts) at 5 kHz	Cable Current + Injection Current (dB)
6	50	1	72.48	7.06	-80.2
7SS	52	1	68.23	1.17	-95.3
8	54	1	77.68	3.07	-88.1
10	54	1	77.68	1.47	-94.5
11SS	52	1	68.23	1.48	-93.3
12	50	1	72.48	1.34	-94.7

## Chapter 5 Comparison of Cable Coupling Before and After Changes

The configuration of the tunnel and cables during the prior cable coupling tests simulated the presently used flight hardware. The configuration used during the retest simulated an improved design of the flight hardware (see chapter 2). The measured and scaled common mode short circuit currents and open circuit voltages from both tests are summarized in tables 5-1 (reference 1) and 5-2, respectively. The methodology for scaling the data in these two tables is the same as that used in reference 1. These two tables are included only for comparison of the data. The scaling methodology used in chapter 6 of this report is not the same as was used in reference 1.

The following observations are made from direct comparison of the data in the two tables and from knowledge of how the tables were developed:

- A. From rows F and G of the two tables, the short circuit currents are higher and the open circuit voltages are lower in the retest than in the prior test. The higher currents are partly the result of having used more injection points on the tunnel in the retest than in the prior test and that some of these produced higher cable currents than injection point 3, which was the reference injection point for the data in table 5-1.
- B. The short circuit currents in both tests (rows F and G) were determined primarily by the scaled HCB currents from row C. The Marx inductive and Marx resistive contributions were small.

**Table 5-1 Scaled Common Mode Short Circuit Currents and Open Circuit Voltages from the Prior Test, Injection Point 3 (Motor Case)**

		ISC (Amps)						VOC (Volts)					
Cable No.		6	7	8	10	11	12	6	7	8	10	11	12
A	Scaled Marx Inductive	2.5	0.29	2.3	0.125	0.67	0.1	68	14.6	61.4	1.3	18.2	3.7
B	Scaled Marx Resistive	13.5	2.7	14.2	6.4	2.8	2.4	34		27.3	3.3	14	4.9
C	Scaled HCB	81.0	30.1	90.6	22.9	7.8	13.6	26.7	13.2	16.8	9.4	9.5	6.4
D	Scaled Marx Inductive Plus Scaled Marx Resistive	16.0	3.0	16.5	6.5	3.5	2.5	102	15	89	4.6	32	8.6
E	Scaled Marx Inductive Plus Scaled HCB	83.0	30.0	93.0	23.0	8.5	14.0	95	28.	78	11	28	10
F	Test Peak Scaled	83	30	93	23	8.5	14	102	28	89	11	32	10
G	Flight	83	30	93	46	18	28	316	87	276	22	64	20



**Table 5-2 Scaled Common Mode Short Circuit Currents and Open Circuit Voltages from the Retest, Worst Case Tunnel Injection Points**

		ISC (Amps)						VOC (Volts)					
Cable No.		6	7	8	10	11	12	6	7	8	10	11	12
A	Scaled Marx Inductive	NM*	NM	NM	NM	NM	NM	NM	NM	NM	NM	NM	NM
B	Scaled Marx Resistive	11.3	3.44	1.40	1.30	8.75	10.3	NM	NM	NM	NM	2.86	5.72
C	Scaled HCB	118.7	69.7	88.5	98.1	180.9	75.2	19.5	3.43	7.90	3.78	4.34	3.70
F	Test Peak Scaled	118.7	69.7	88.5	98.1	180.9	75.2	19.5	3.43	7.90	3.78	4.34	5.72
G	Flight	118.7	69.7	88.5	196.2	361.8	150.4	60.5	10.6	25.0	7.56	8.68	11.5

- C. The open circuit voltage levels in rows F and G of table 5-1, in all cases, have a high percentage content determined by the entries in rows A and B. The better bond straps and the improved GEI external cable shields were designed for the retest to reduce the higher frequency coupling. The entries in rows A and B of table 5-2 demonstrate that the high frequency coupling was reduced.
- D. The open circuit voltages in rows C of the two tables are essentially at the same levels. This indicates that the low frequency (5 kHz) coupling was not affected by the bond strap changes as much as the higher frequency coupling. However, it should be kept in mind that all of the information in the two tables is based on tests where the cover-to-case bond straps had not been debonded by the lightning currents. As indicated in chapter 7, the present flight configuration of the floor plate-to-case bond straps are debonded by the high action integral of component A of the specification (reference 2).

It is important to note that the measured and scaled open circuit voltages are the common mode voltages discussed in chapter 6 and are not the voltages seen by circuits at the end of the cables.

It is also important to note that the measured short circuit currents are high because both ends of the cable core conductor bundles were shorted to chassis ground. Since there are no configurations where core conductors in the SRB tunnel cables are grounded to chassis on both ends, short circuit currents should not be viewed as indicative of the levels that would be seen on flight hardware electronic circuits.

As discussed in chapter 6, only differential mode voltages at the cable-to-circuit interfaces are important. The design requirements of SRB electrical systems require that only one end of a circuit function may be grounded to chassis and that signal grounds be provided by separate wires within the cable bundles. These factors result in large reductions in the translation of common mode voltages to differential mode voltages.

The last three test shots (106, 107, 108) of the bond strap survivability tests were conducted with cover-to-case straps numbered 2, 3, 5, 6 and 8 not connected. Short circuit currents were measured on cables 6 and 12 for comparison with the levels measured with all straps connected. From table 4-6, we see that the cable 6 HCB short circuit currents did not increase and cable 12 HCB short circuit currents increased by only about a factor of 1.4 (3 dB). This indicates that, for protection against low frequency coupling, it is not necessary to have an external cover-to-case bond strap on each tunnel cover.

After completion of all USBI planned tests at the Wendover test site, the Thiokol test crew removed the external cover-to-case bond straps and the "new design" cover-to-cover bond straps and installed the "old design" (internal straps and AWG No. 12 cover-to-cover straps). The external GEI cables were returned to the "flight" configuration with sock shields grounded to the case with conductive epoxy about every 18 inches. The OF cables and test instrumentation configurations remained the same (reference 3). Short circuit currents were then measured on cables 6 and 12 with Marx injected currents. The results are summarized in table 4-3 entries for tests 109, 110, 113, and 114. The cable 6 short circuit current increased by only 6.3 dB (85 dB minus 78.7 dB) for injection point 1 and remained about the same with other injection points (3 and 539) on and near the forward tunnel. The cable 12 short circuit current would also have likely increased if injection points on the aft tunnel had been used. The most important results of these last test shots are that the levels of the highest frequency component (1 MHz) remained very low compared to the prior coupling tests and the mid-range frequency component (130 kHz) increased by only 6.3 dB compared to the retest with the "new design" bond straps. The high open circuit voltages measured during the prior Marx tests (up to 72 volts) were probably caused by the shield configurations on some of the external cables and/or by the way the external cables were terminated at the breakout boxes.

This comparison of the coupling observed while the test article was in several different configurations during the test and the retest and the realization that the lower frequency components are greatly reduced in the translation from common mode to differential mode voltages suggests that a design with less protection capability than the retest configuration should be adequate. This adequate design should be based upon the following principles:

- A. The external GEI cables' sock shields should be electrically bonded to the case or the tunnel covers where these cables enter the tunnel. The test results demonstrate that the additional bonding of these shields to the case at 18-inch intervals is adequate. It is not clear whether this interval can be increased. It probably can be increased so long as the lightning energy deposited in the bond nearest the tunnel is kept low enough to prevent debonding. The number, spacing, and footprint resistances of these bonding points may be selected in a trade-off analysis.
- B. The tunnel-to-case bond straps should be designed to withstand a lightning attachment to any SRB outer surface without debonding. This may be achieved by *floor plate-to-case* bond straps or by *tunnel cover-to-case* bond straps. The number of straps required depends primarily on the current carrying capacity of

each footprint and the amount of current which flows through each footprint. The current carrying capacity, of course, depends upon footprint resistance and the amount of current that flows through the footprint. The footprint current depends upon how the cover-to-cover bond straps and the tunnel-to-case bond straps share the total lightning currents. The retest and the analyses and interpretation contained in this report demonstrate that footprint resistances of less than 0.5 milliohms are readily achievable with conductive epoxy applied in eight square inch footprints, that with the tested cover-to-cover bond straps on every tunnel cover gap the current sharing was such that most of the footprints did not debond, and that the spacing between tunnel-to-case bond straps could be about the same as the existing flight configuration if the footprint resistances are adjusted to handle the currents.

- C. The cover-to-cover bond strap design should be selected to both disperse the total current away from the injection point and to keep the coupling to the cables to acceptable levels.

## Chapter 6 Coupling to Operational Flight Cables

### I. Introduction

It is necessary to develop a coupling model based on theoretical principles and the experimental data in order to extrapolate the results of the test to a full length forward tunnel, to the criteria lightning current waveforms, and to translate from common mode voltages to differential mode voltages.

Common mode voltage is that voltage developed across the total length of a cable. It is equal to the voltage between the core conductors and the cable shield when it is measured across a high terminating impedance as in the tests and is called open circuit voltage. Differential mode voltage is that voltage which is developed between conductors within the core bundle. Within the SRB electronic systems, it is the differential mode voltage that appears across cable interface circuits. It is not sufficient to simply scale the measured open circuit cable voltages by the ratio of the criteria current to the test injected current because:

- A. The forward segment of the test article, the forward tunnel, and the cables in the forward tunnel were approximately one-third of the length of the flight configuration. The number of OF cables was less than the flight configuration.
- B. The test injected current waveforms did not (and could not) duplicate the criteria lightning current waveforms. To obtain the waveforms of the cable common mode voltage responses to criteria lightning currents, it is necessary to use the CW test responses and the pulse test responses to develop an estimate of the transfer function which, in turn, is used to calculate the correct response waveforms.
- C. The translation from cable common mode voltages to twisted pair differential mode voltages causes a large reduction. Interface circuits "see" only the differential mode voltage.

### II. Cable Coupling

The model for conversion from common mode to differential mode voltages was developed after completion of the tests described in this report. From this model, described in appendices A and B, we see that the high and low frequencies are greatly attenuated and the middle frequencies, in the range of 1 MHz to 10 MHz experience less attenuation. This means that, although most of the energy in lightning currents is confined to the lower frequencies (less than 1 MHz), it is more important in this specific case to determine the coupling in the middle frequency range. The internal design of the SRB electronic boxes (high isolation impedance and single point grounds) produces a large reduction in voltage in the translation from common mode to differential mode.

Figure 6-1 depicts the electrical connection of the structural elements of the test fixture. The impedances of the "new" cover-to-case bond straps are represented by  $R_s$  and  $L_s$  and the impedances of the "new" cover-to-cover bond straps are

represented by  $R_g$  and  $L_g$ .  $Z_{ie}$  (case) is the surface impedance of the motor case. The two aluminum cover-to-cover straps on the top of each tunnel gap were 1/16 inch thick and 7/8 inch wide. The aluminum cover-to-cover straps on the side of each tunnel gap were 1/16 inch thick and 1 1/4 inch wide. On the forward tunnel, the length of the top straps averaged about six inches and the length of the side straps averaged about 11 inches. With these lengths, the average calculated resistance of the four straps (in parallel) across each gap was 34 micro-ohms and the average inductance was .031 microhenrys. The resistance of each strap was calculated from:

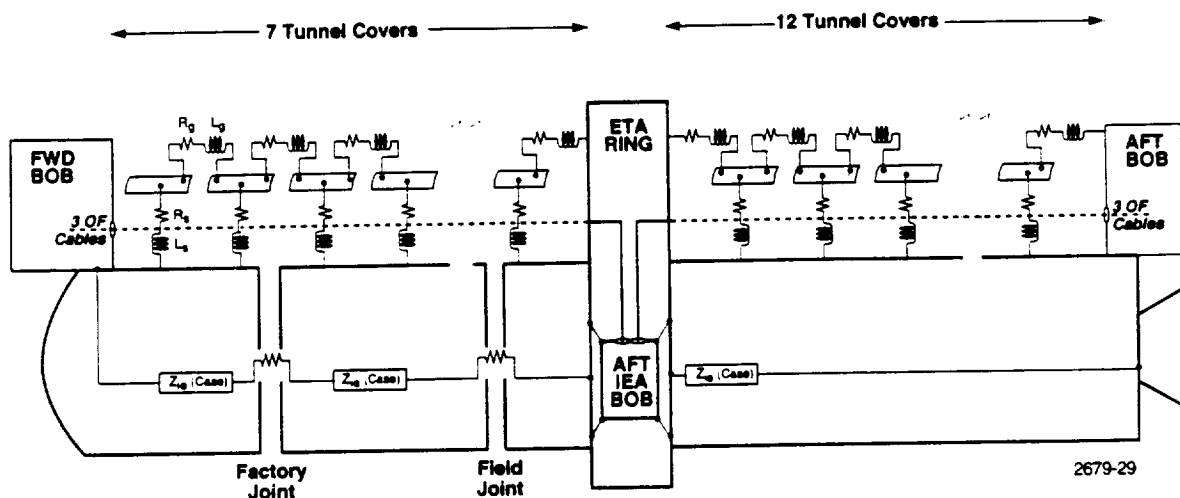


Figure 6-1 Electrical Connections of the Test Article Structural Elements

$$R = \frac{\rho \ell}{A} \text{ ohms}$$

where:  $\rho$  = resistivity of aluminum =  $2.8 \times 10^{-6}$  ohm - cm  
 $\ell$  = length of strap in cm  
 $A$  = area of cross section in  $\text{cm}^2$

The inductance of each strap was calculated by:

$$L = 2 \times 10^{-4} \ell \left[ \ln_e \frac{2\ell}{W+T} + 0.5 \right] \mu h$$

where:  $\ell$  = length in millimeters  
 $W$  = width in millimeters  
 $T$  = thickness in millimeters

The cover-to-cover resistance values were measured prior to the installation of the cover-to-case bond straps (see table 4-1). All of these values were slightly higher than the calculated 34 micro-ohms. These larger values were probably the result of

surface contact resistances between the straps and the covers. The resistance of the cover-to-case bond straps was taken to be the measured value because the resistance of the strap is negligible compared to the footprint resistance of the conductive epoxy. The inductance was estimated by assuming that the length of the current path was equal to the distance from the attachment bolt to the center of the footprint. This distance was about four inches. The widths were two, three, or four inches, and the calculated inductances are:

Width	Inductance
2 in.	.0377 $\mu$ h
3 in.	.0297 $\mu$ h
4 in.	.0239 $\mu$ h

At frequencies high enough that the electrical skin depth is less than the thickness of a conductive cylinder wall, the surface impedance of a cylinder is:

$$Z_{ie} = \frac{1+j}{2\pi\sigma\delta} \text{ when } \delta < T \text{ (reference 6 pg. 262).}$$

Where:  $r$  = radius of cylinder in meters  
 $\sigma$  = conductivity of material in mhos/meter  
 $\delta$  = electrical skin depth in meters  
 $T$  = thickness of cylinder wall in meters  
 $f$  = frequency  
 $\mu$  = magnetic permeability of material

$$\delta = \frac{1}{\sqrt{\pi f \mu \sigma}} \text{ (reference 6, pg. 248)}$$

These relations were used to calculate the surface impedance of the steel motor case and the aluminum forward tunnel covers. For these calculations the tunnel was assumed to be a solid cylinder with a radius of 4 inches and a thickness of 1/8 inch. The forward tunnel covers and all floor plates are 1/8 inch thick. The aft tunnel covers are 1/4 inch thick. The motor case has a radius of 73 inches and a thickness of 0.5 inch. The conductivity and permeability of the D6AC steel used in the motor case are not known precisely. By reference 7, page 116, reference 6, pages 121 and 247, and by comparison of the material characteristics with handbook materials, estimates of these constants were developed:

	D6AC Steel Case	Aluminum Tunnel Covers
Conductivity, $\sigma$	$1.4 \times 10^6$ to $1.2 \times 10^7$	$3.57 \times 10^7$ mhos/meter
Relative Permeability, $\mu_r$	100 to 500	1

where:  $\mu = \mu_r \mu_o$

$\mu_o = 4\pi \times 10^{-7}$  henry / meter = permeability of non-magnetic materials

The skin depths at 1 kHz are 0.105 inch in aluminum and 0.009 to 0.053 inch in steel. Since these depths are less than the thickness of the covers and case, the surface impedance expressions are valid for all frequencies above 1 kHz which are the frequencies of interest in this lightning analysis.

Substituting the equation for  $\delta$  into the equation for  $Z_{ie}$ , we obtain:

$$Z_{ie} = \left[ \frac{1+j}{2r} \right] \left[ \frac{\mu}{\pi\sigma} \right]^{1/2} (f)^{1/2}$$

$$[Z_{ie}(\text{case})]_{\min} = (1+j) (5.0 \times 10^{-7}) (f)^{1/2} \text{ ohms / meter}$$

$$[Z_{ie}(\text{case})]_{\max} = (1+j) (3.25 \times 10^{-6}) (f)^{1/2} \text{ ohms / meter}$$

$$[Z_{ie}(\text{tunnel})] = (1+j) (2.86 \times 10^{-8}) (f)^{1/2} \text{ ohms / meter}$$

The  $Z_{ie}(\text{case})$  impedance is in series with one factory joint and one field joint on the test article forward segment. Measurements have been made of the transfer impedance of an SRB field joint under three different loading conditions (reference 14). The results showed that the transfer impedance increased with the square root of frequency and had a worst case value of  $10^{-2}$  to  $10^{-3}$  ohm/meter at 100 kHz. For a surface current equally distributed around the motor case, the joint impedance is the measured transfer impedance divided by the circumference of the motor case (11.62 meters) or approximately  $10^{-4}$  to  $10^{-3}$  ohms at 100 kHz. Since the test article had one factory joint and one field joint on the forward segment, the total joint impedance was  $2 \times 10^{-4}$  to  $2 \times 10^{-3}$  ohms at 100 kHz. For a 10 meter long segment,  $Z_{ie}(\text{case})$  is approximately  $10^{-3}$  to  $10^{-2}$  ohms at 100 kHz. Both  $Z_{ie}(\text{case})$  and the total joint impedance increase with the square root of frequency. The sum of  $Z_{ie}(\text{case})$  and the total joint impedance is still equal to  $10^{-3}$  to  $10^{-2}$  ohms at 100 kHz. Therefore, the sum is equal to  $Z_{ie}(\text{case})$ .

Since  $Z_{ie}(\text{tunnel})$  is a factor of approximately 20 to 100 less than  $Z_{ie}(\text{case})$ , most of the lightning current injected into the tunnel would stay in the covers rather than flow into the case if the tunnel were a solid conduit and if there were no gaps. However, since there are gaps and these are bridged by straps which have resistance and inductance, the current distribution is affected by these straps as well as by the cover-to-case straps. The impedance of the straps across each gap is:

$$Z_g = R_g + j\omega L_g$$

where  $R_g$  is the calculated average of 34 micro-ohms for high level currents and  $L_g$  is .031 microhenrys. The inductive reactance,  $\omega L_g$ , is much larger than  $R_g$  and  $Z_{ie}(\text{tunnel})$  for all frequencies higher than 1 kHz.

On the test article, there were three OF cables in the forward tunnel and several small shielded sensor cables which entered the tunnel at stations 539 and 703. The resistance of one of the OF cable shields is approximately  $3.5 \times 10^{-3}$  ohms/meter or 43 milliohms for a 12 meter length. The resistance of the small sensor cables is much larger than the resistance of the OF cables based on their relative size and thickness of shields. Therefore, for calculation of the voltage between the ends of the OF cables, figure 6-2 is approximately the electrical equivalent of figure 6-1. Omitted from figure 6-2 is the impedance of the tunnel to case bond straps. These impedances certainly affect the flow of current from the tunnel to the case but they do not significantly affect the voltage across the length of the structure since the surface impedance of the motor case is much smaller than the other parallel current paths. Of course, if there were no tunnel-to-case bond straps, the injected current would be forced to stay on the tunnel and the voltage developed across the length of the tunnel would be much higher due to the flow of current through the cover-to-cover bond straps. The voltage across the length of the motor case and cables is approximately:

$$V(case) = Z_{ie}(case) \times I_i$$

when:  $Z_{sh} \gg Z_{ie}(case)$   
 $\omega L_g \gg R_g, \quad 7(\omega L_g) \gg Z_{ie}(case) \quad (\text{See Fig. 6-1})$

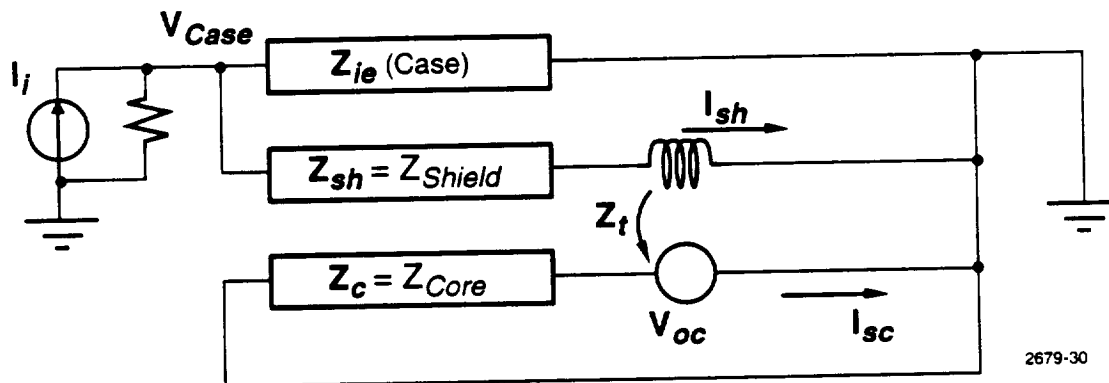


Figure 6-2 Electrical Equivalent of Forward Tunnel of Figure 6-1

The thickness of the aluminum breakout boxes was 0.125 inches. The frequency at which this thickness is one skin depth is 0.7 kHz. For higher frequencies, the depth of penetration of currents flowing on the breakout boxes is less than the box thickness. This "shielded" the current sense wires and the instrumentation inside the box from the fields created by the currents flowing on the outside of the box. Therefore, the only source of coupling to the core conductors inside each OF cable was from the current flowing in the shield of the cable and through the cable connectors which terminate the shield to the breakout boxes. The transfer



impedance of the OF cable shields is much larger than the impedance of the cable connectors (reference 7, page 173). The current in each cable shield is:

$$I_{sh} = V(case) + Z_{sh}$$

The open circuit voltage across the length of the core conductors is:

$$V_{oc} = I_{sh} \times Z_t$$

where  $Z_t$  is the transfer impedance of the cable shield (reference 7, page 162). The cable short circuit current is:

$$I_{sc} = V_{oc} + Z_c$$

where  $Z_c$  is the impedance of the core conductor bundle.  $V_{oc}/I_i$  and  $I_{sc}/I_i$  were measured on each of the six OF cables with both CW and pulse current sources and injection points at several locations. Figure 6-3 summarizes all of the  $I_{sc}/I_i$  data and figure 6-4 summarizes all of the  $V_{oc}/I_i$  data. The CW curve on figure 6-3 is one of the highest CW values measured. The pulse data at 5 kHz shows the range of values of all HCB tests conducted on all of the six OF cables. Each data point at 130 kHz represents the peak value of  $I_{sc}/I_i$  from the Marx tests. The CW curve on figure 6-4 is one of the highest  $V_{oc}/I_i$  CW values measured. Again, the data points at 5 kHz are from the HCB tests and the data points at 130 kHz are from the Marx tests. The data points at 1.0 MHz were also obtained from the Marx tests. By comparison of these two figures with the noise levels in figures 4-3 and 4-4, it is concluded that all of the CW data in figure 6-3 at frequencies higher than 250 kHz are at the noise level. Likewise, all of the CW data in figure 6-4 at frequencies higher than 20 kHz are at the noise level. The CW and pulse data are in good agreement at 5 kHz on both figures. All of the CW and pulse data are within reasonable agreement on figure 6-3. The largest differences between the CW and pulse data on figure 6-3 are due to the multiplicity of test conditions (injection points and new bond straps versus "flight" bond straps). For example, the highest three data points on cable 6 at 130 kHz were from tests on the "flight" configuration and the lowest four data points were from injection points on the aft segment (No. 4 and No. 1701). Similarly, the highest data points for cables 11 and 12 resulted from injection point 4. The primary conclusion from figure 6-3 is that the cable short circuit currents decreased rapidly with increasing frequency up to 250 kHz where the noise limit was reached. The data does not indicate whether or not  $I_{sc}$  increases or decreases for frequencies higher than 250 kHz because the signal is obscured by the noise. The  $V_{oc}$  pulse data at 130 kHz and 1 MHz on figure 6-4 are all significantly higher (up to 20 dB) than the CW data at the same frequencies. This indicates either that there were instrumentation problems with the  $V_{oc}$  CW measurements in this frequency range or there were non-linear sources of coupling (such as arcing) during the Marx tests. Since the  $I_{sc}$  data from the Marx tests agrees with the CW data and the coupling model, developed in following sections, agrees with the Marx  $V_{oc}$  data, we conclude that the higher frequency CW  $V_{oc}$  measurements are invalid. Since all of the test article structures are tied together with multiple low impedance current paths, it is unlikely that arcing caused the higher  $V_{oc}$  data.

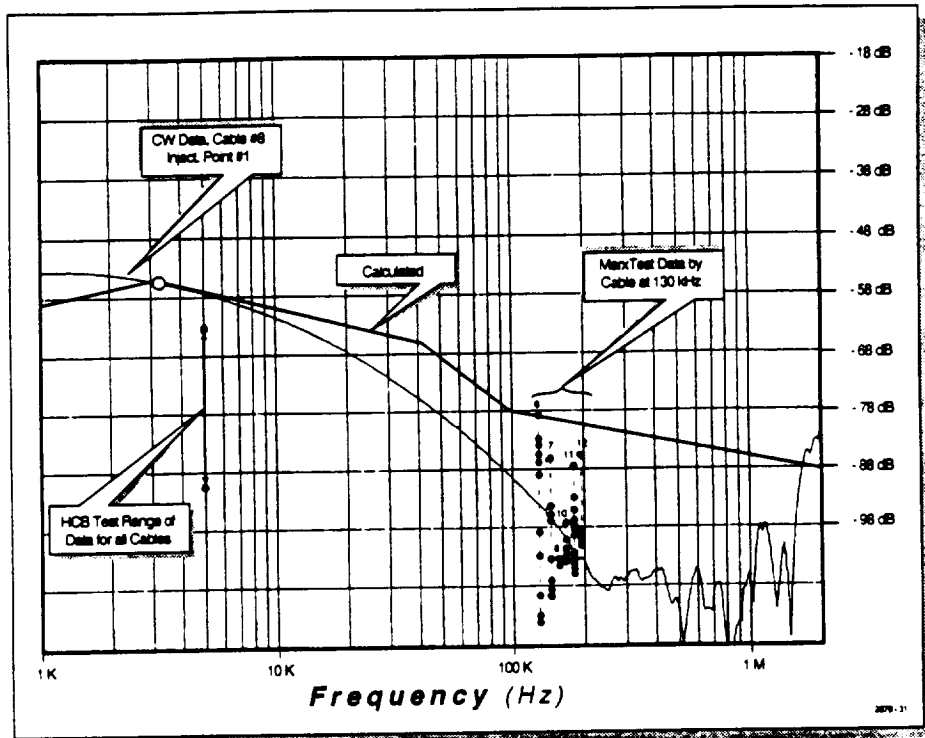


Figure 6-3 Calculated, CW, and Pulse Data,  $I_{sc}/I_i$  (in dB), Versus Frequency

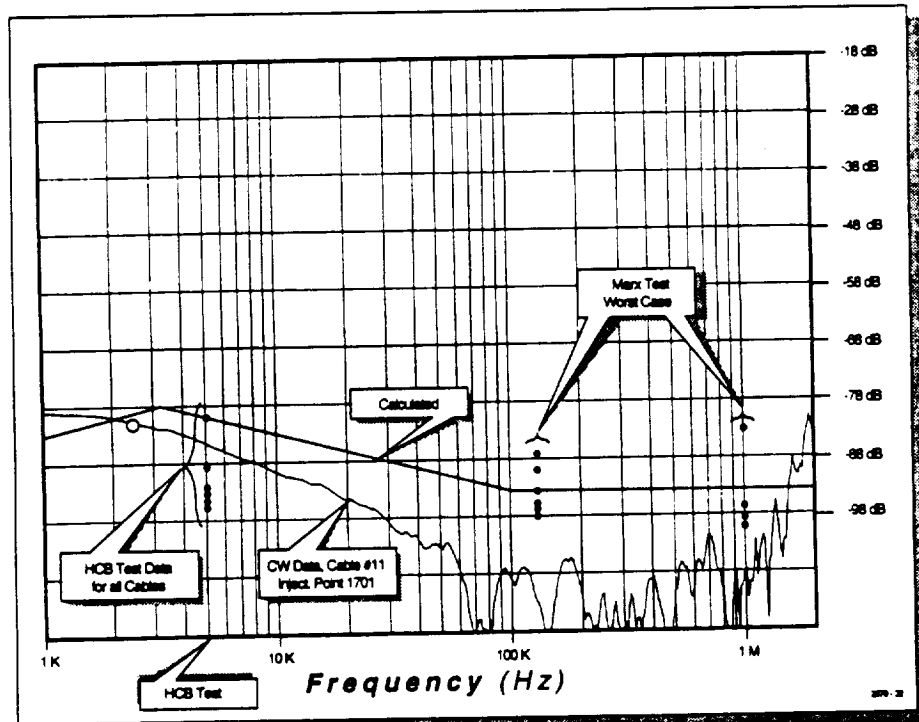


Figure 6-4 Calculated, CW, and Pulse Data,  $V_{oc}/I_i$  (in dB), Versus Frequency

Figure 6-5 shows how the transfer impedances,  $Z_t$ , of several cable shields vary with frequency (reference 9). Overlaid on figure 6-5 are the data points from the measurement of  $Z_t$  on a typical SRB cable (reference 8). From this figure, we see that  $Z_t$  is constant for frequencies up to approximately 100 kHz and increases with the square root of frequency up to at least 3 MHz. The affect of  $Z_t$  on  $I_{sc}$  and  $V_{oc}$  is embedded in the data of figures 6-3 and 6-4. The decrease in  $I_{sc}/I_i$  in figure 6-6 at a rate of 20 dB per decade between about 4 kHz and 40 kHz and at a rate of about 40 dB per decade between 40 kHz and 250 kHz suggests that there are two resistive-inductive effects also embedded in the CW data. Returning to the set of equations above, we find that:

$$\frac{I_{sc}}{I_i} = \frac{Z_{ie(case)} Z_t}{Z_{sh} Z_c}$$

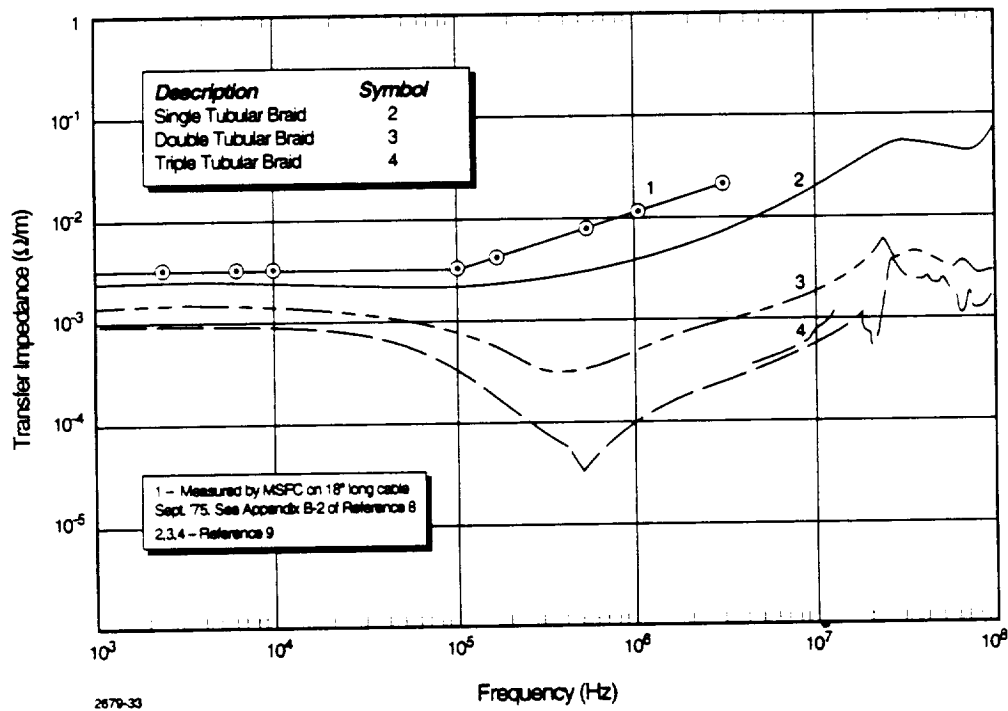


Figure 6-5 Transfer Impedances ( $Z_t$ ) of Shielded Cables

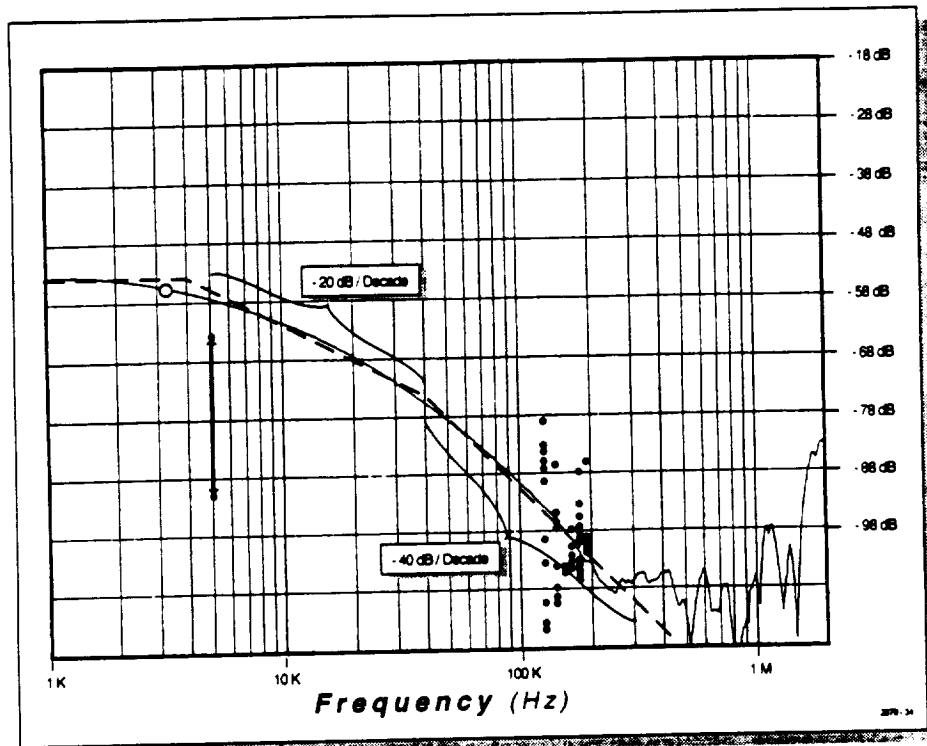


Figure 6-6 Decrease in  $I_{sc}/I_i$  at 20 dB/decade and 40 dB/decade

We know that  $Z_t$  is constant for frequencies below 100 kHz. Therefore, it is reasonable to suspect that both  $Z_{sh}$  and  $Z_c$  have a resistive-inductive effect. The resistances of the OF cables' core bundles were calculated (using reference 5, page D.2) and are listed in table 6-1. The external inductance of a center conductor within a coaxial structure is:

$$L_c = 2 \times 10^{-7} \ln \left( \frac{r_2}{r_1} \right) \text{ henry / meter (reference 6, pg 255)}$$

Table 6-1 Resistance of Core Conductors within Test Cables

Cable No.	No. of Core Conductors	Size of Each Conductor	Total Core Resistance
6 & 12	2	AWG 12	31.3 milliohms
7 & 11	49	AWG 20 & 22	15.7 milliohms
8 & 10	41	AWG 22 & 24	12.6 milliohms

The radius of the bundle of core conductors,  $r_1$ , is nearly equal to the inside radius of the shield,  $r_2$ . If we let  $r_2$  equal  $1.05 r_1$ , then

$$L_c = 1.17 \times 10^{-7} \text{ henry for } \ell = 12 \text{ meters}$$

For  $R_c=31.3$  milliohms (cables 6 and 12), the inductive reactance,  $\omega L_c$ , is equal to the resistance of the core bundle at a frequency of 42.6 kHz. The resistance of an OF cable shield is 3.5 milliohms per meter. For a cable length of 12 meters, the shield resistance is 42 milliohms. The inductance of a 12 meter length cable with 0.650 inch diameter within a coaxial structure of 8.0 inches diameter is 6.0 microhenry. The inductive reactance of this cable is equal to the resistance at a frequency of 1.1 kHz. This suggests that the first break frequency of figure 6-6 is due to the cable shield and the second break frequency is due to the core bundle.

In figure 6-7, the transfer functions that relate  $V_{oc}$  and  $I_{sc}$  to  $I_i$  are plotted as products of impedance functions. This type of plot is easy to construct because multiplication of functions becomes addition of their dB values. It is also informative because it clearly shows the effect of each function on the overall product.

$$\frac{I_{sc}}{I_i} = Z_{ie(case)} \times Z_t \times \frac{1}{Z_{sh}} \times \frac{1}{Z_c}$$

$$\frac{V_{oc}}{I_i} = Z_{ie(case)} \times Z_t \times \frac{1}{Z_{sh}}$$

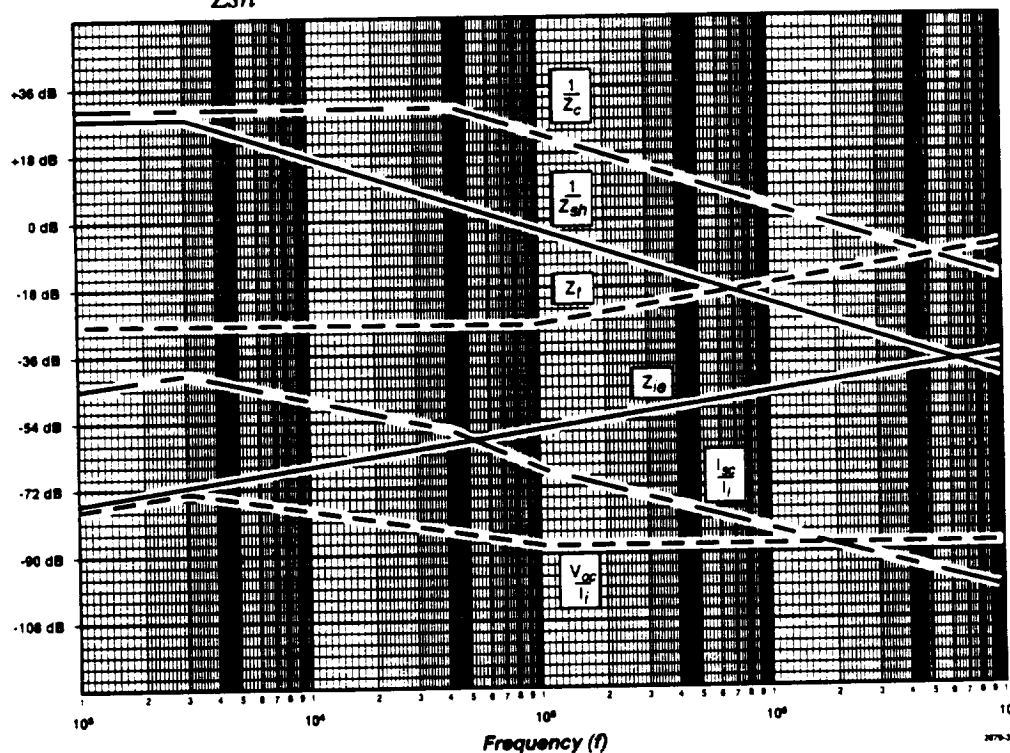


Figure 6-7 Calculated  $I_{sc}/I_i$  and  $V_{oc}/I_i$  as Functions of Frequency

From these figures, we see that calculated  $I_{sc}/I_i$  increase as  $f^{0.5}$  until the first corner frequency is reached at 3.0 kHz, then decreases as  $f^{-0.5}$  up to the second corner frequency (42 kHz) where it decreases as  $f^{-1.5}$  until  $Z_t$  starts to increase at 100 kHz and decreases as  $f^{-0.5}$  at frequencies higher than 100 kHz. We also see that

$V_{oc}/I_i$  increases as  $f^{0.5}$  up to 3.0 kHz, decreases as  $f^{-0.5}$  up to 100 kHz, and remains constant for frequencies higher than 100 kHz. These calculated curves are also shown on figure 6-3 and 6-4 for comparison with the measured CW and pulse data. For a worst-case estimate of the open circuit voltage, we may assume (from figure 6-4) that  $V_{oc}/I_i$  is "flat" with frequency at -79 dB for the test article conditions. The length of the longer forward tunnel is three times the length of the test article forward tunnel. Each of the four impedance terms in the  $I_{sc}/I_i$  equation is three times larger. Increases in the numerator are offset by increases in the denominator and  $I_{sc}/I_i$  remains unchanged. However,  $V_{oc}/I_i$  increases by a factor of three (9.5 dB); therefore, the  $V_{oc}/I_i$  level for the longer tunnel is at -69.5 dB. For an injected peak current of 200 kA, the peak value of  $V_{oc}$  is 69.5 dB lower, or 67 volts. The waveform of  $V_{oc}$  is the same as the waveform of  $I_i$ . It is important to note that this is the worst-case  $V_{oc}$  and includes coupling from injection points on the external GEI cables. If injection point 539 were removed from the data on figure 6-4,  $V_{oc}$  would be reduced by about 15 dB in the 1 MHz to 10 MHz frequency range. Since  $V_{oc}$  is directly proportional to the length of the motor case spanned by the cables and the aft cables span a length approximately one-third the length of the forward motor case,  $V_{oc}$  on the aft cables is approximately one-third of  $V_{oc}$  on the forward cables or 22.3 volts.

The scaled common mode voltages for cables in the aft tunnel must be adjusted upward for the additional coupling due to a source which was not included in the coupling tests. This source is caused by the fields generated in the aft skirt area which induce currents in the portions of the aft tunnel cables which extend into the aft skirt from the feed-through bulkhead located inside the "rooster tail." These currents were determined in a 1977 test and analysis effort conducted by MSFC and Mission Research Corporation (reference 8 page B5-39) to be 4.8 kiloamps, worst case, in the outer shields of the cables.

Since the cable shield currents in the aft skirt are driven directly by magnetic fields caused by currents flowing on the SRM motor case, the waveforms of the shield currents are the same as the injected current waveform. The transfer impedance of a cable with a single layer overall shield is shown in figure 6-8. For mathematical convenience and as a worst case approximation we represent the transfer impedance per unit length by the following function (which is plotted on figure 6-8 for comparison) in Laplace transform notation:

$$T(s) = 0.0035 + \frac{.06s}{s + a_3}$$

$$a_3 = 2\pi f_3 = (2\pi)(5 \text{ MHz}) = 3.14 \times 10^7$$

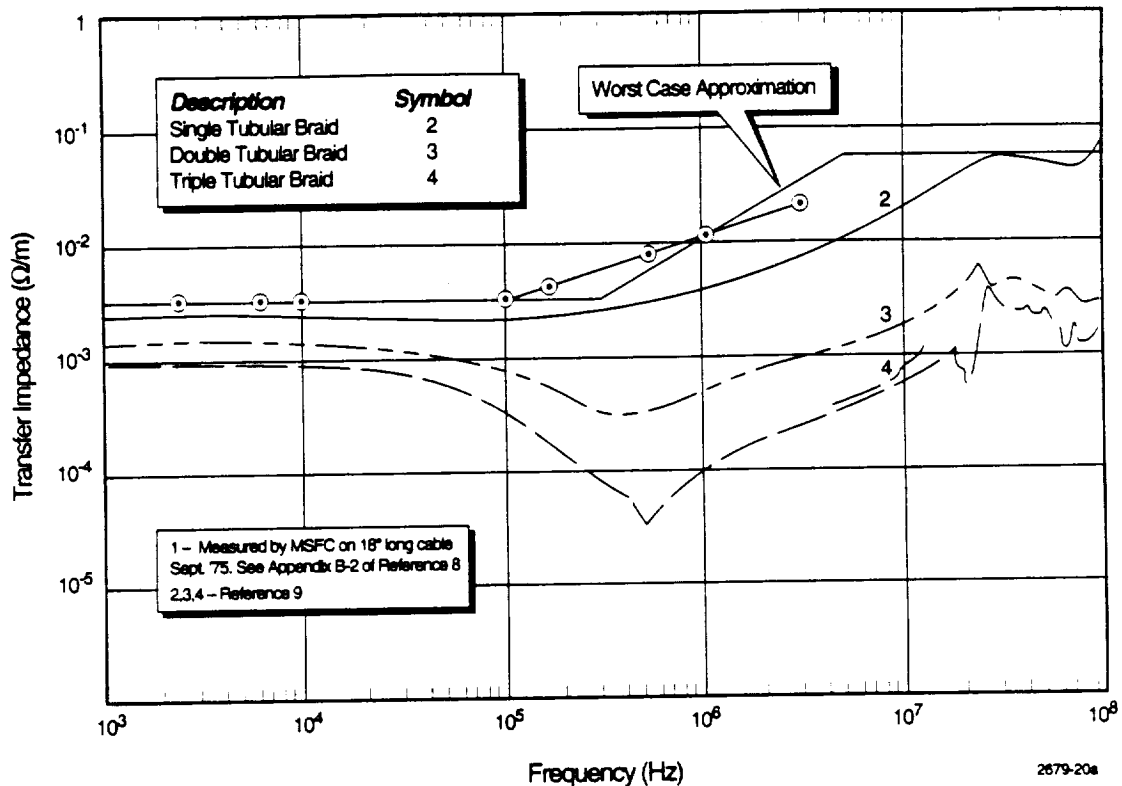


**Figure 6-8 Aft Skirt Cable Transfer Impedance Approximation**

This transfer impedance is multiplied by the length of the cables within the aft skirt (3.56 meters) to obtain:

$$T_3(s) = 0.01246 + \frac{0.2136s}{s + a_3}$$

The common mode open circuit voltage response,  $R_3(s)$ , due to the shield current flowing in the aft skirt area, is:

$$R_3(s) = I_{sh}(s) \times T_3(s)$$

where  $I_{sh}(s)$  is the Laplace transform of the cable shield current.

$$I_{sh}(t) = 5,250(e^{-\alpha t} - e^{-\beta t})$$

which has a peak value of 4.8 kiloamps.  $\alpha$  and  $\beta$  are the exponents of the criteria component A lightning current (reference 2).  $\alpha$  is equal to  $1.1354 \times 10^4$  and  $\beta$  is equal to  $6.47265 \times 10^5$ .

$$I_{sh}(s) = \frac{5,250}{s + \alpha} - \frac{5,250}{s + \beta}$$

After making some approximations to find the inverse Laplace transform of  $R_3(s)$ :

$$R_3(t) = 65.4(e^{-\alpha t} - e^{-\beta t}) + 23.1e^{-\beta t}$$

This common mode voltage response  $R_3(t)$ , is the sum of two waveforms. The first waveform is the same as the injected current and has a peak value of 59.8 volts. The second waveform is a narrow pulse which rises to 23.1 volts in zero time and decays to 10 percent of its peak value in less than four microseconds. In summary, the total common mode voltage on cables in the aft tunnel is the sum of the responses from three coupling sources as shown in table 6-2.

**Table 6-2 Calculated Common Mode Voltages on Aft Cables Due to Component A of Lightning Current**

Source	Waveform	Peak (volts)	Time to Peak (msec)
Tunnel and External GEI Cables	Same as injected current	22.3	6.4
Through Cable Segments Located in Aft Skirt	a. Injected current	59.8	6.4
	b. Narrow pulse	23.1	0.0

There is no coupling source for the forward cables that is equivalent to the aft skirt because the forward skirt is a highly shielded area. The translation of these common mode open circuit voltages to differential mode voltages is provided in the following section.

### III. Translation from Common Mode Voltages to Differential Mode Voltages

The common mode voltages derived in the prior paragraphs are the voltages developed across the total length of cable core conductors. If one end of the core is electrically connected to chassis ground and the other end has a high impedance to chassis ground, then it is also approximately the voltage across the high impedance. This was the test condition. In the flight configuration, SRB electrical systems meet the requirements for high DC isolation impedances between black box circuits and chassis ground (reference 10). Primary power circuits have at least 50K ohms isolation. Secondary power circuits and most signal circuits have at least two megohms isolation. The isolation specification for the multiplexer-demultiplexer (MDM) circuits located in the forward and aft IEAs is 130K ohms. Chassis ground is not used for power or signal return on any SRB electrical circuits. SRB power circuits are grounded at only a single point on the chassis or structure for safety requirements. The primary power busses from the orbiter have Transorbs installed between each power lead and chassis ground to protect SRB power systems from lightning transients that exceed common mode voltages of 100 volts.



In prior analyses of lightning coupling to SRB cables (reference 1), the differential mode voltages have been assumed to be 10 percent of the common mode voltages. A factor of 10 to 100 (20 dB to 40 dB) reduction has been the recommended prudent approach for *unshielded* cable bundles where magnetic field coupling to the loop area between conductors is the primary coupling mode (reference 2, page D-6). Based on lightning coupling tests of fighter aircraft with unshielded cable bundles (where the primary response frequencies were in the several MHz range), a reduction factor of from 10 to 200 was recommended (reference 6, page 377).

Section 6.4 and appendix D of reference 5 describe the development of a ground-loop coupling (GLC) model for use in the calculation of differential mode CW voltages for many conditions of cable lengths, source and load impedances, wire sizes, and most importantly, the parasitic capacitances between printed circuit boards and chassis ground. Appendix D of reference 5 includes 36 nomographs for use in finding the ratio of the differential mode voltage (VDM) to the common mode voltage (VCM) for CW signals at frequencies between 10 Hz and 10 GHz. Figure 6-9 depicts the model and the variables. C1C and C2C represent the parasitic capacitances between the electronic boxes and the reference ground plane (chassis ground). C1B and C2B represent the parasitic capacitances between the printed circuit boards and the inside of the electronic boxes. Rg1 and Rg2 represent the sending circuit output impedances and RL1 and RL2 represent the receiving circuit input impedances.  $C_i$  is the input circuit capacitance. Rw, Lw, and Cw represent the resistance, inductance, and capacitance of the wiring (through the cable) between the sending and receiving circuits.

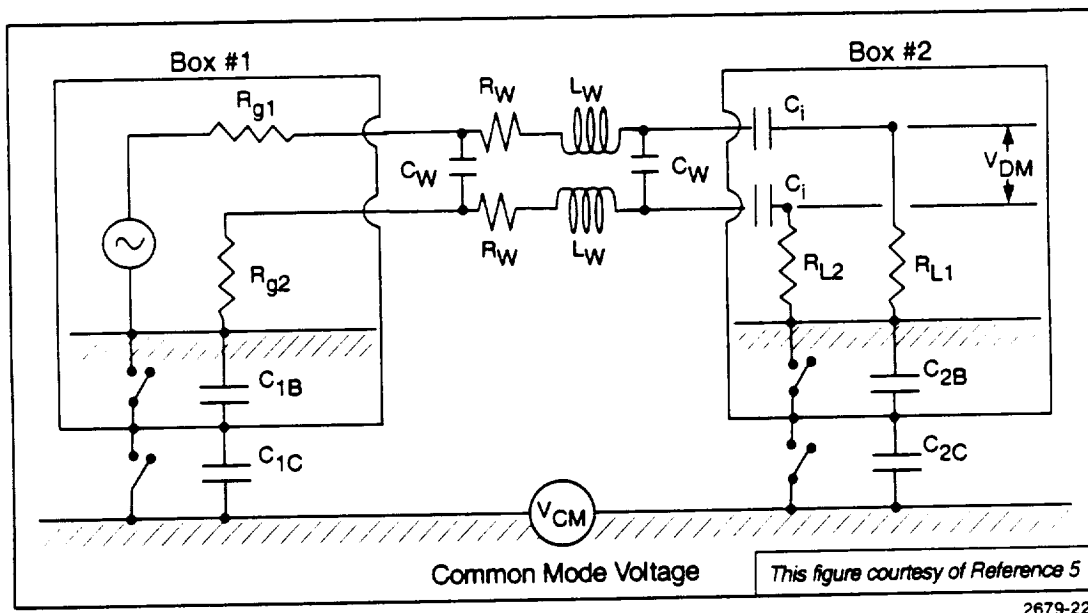


**Figure 6-9 Ground Loop Coupling Model and Variables**

Since the electronic boxes on the flight SRB are well-grounded to chassis' ground, and the forward and aft breakout boxes used in the test are well grounded to the test article motor case, the conceptual switches across C1C and C2C are closed.

The two boxes in figure 6-9 represent any set of two SRB electronic boxes connected together through tunnel cables. For example, the forward IEA and aft IEA are connected electrically through cables in the forward tunnel and the aft IEA is connected to circuits in the aft skirt by cables in the aft tunnel.

As shown in appendix B of this report and appendix D of reference 5, higher values of C2B cause an increase in VDM/VCM. This results because higher values of C2B produce lower values of capacitive reactance which causes less of the common mode voltage to be "dropped" across C2B. When the isolation resistance (2M or 50K ohms) is greater than the capacitive reactance of C2B, the effective impedance of the parallel combination of C2B and the isolation resistance is essentially determined by C2B. When the isolation resistance is less than the capacitive reactance of C2B, the calculation of VDM/VCM without the isolation resistance produces a higher value than would otherwise be obtained. For this reason and because most SRB circuits exceed the DC isolation resistance criteria, we have chosen to omit the isolation resistance from the calculation of VDM/VCM. For our nominal value of C2B (22.5 pf) and the most common value of isolation resistance (2 megohms), the isolation resistance has no effect on VDM/VCM for frequencies greater than about 3.5 kHz. Appendix D of reference 5 shows that the wiring values may be calculated as follows:

$$R_w = 2.19 \times 10^{-2} \ell / d^2 \text{ ohms}$$

$$C_w = \frac{13.9 \epsilon_r \ell}{\ln_e k} \quad \text{pf}$$

$$k = \left[ s / d + \sqrt{(s / d)^2 - 1} \right]$$

$$L_w = 0.2 \mu_r \ell \ln_e k \quad \mu\text{henry}$$

where:  $\ell$  = wire length in meters

$d$  = wire diameter in millimeters

$\epsilon_r$  = relative dielectric constant of wire insulation

$\mu_r$  = relative permeability of wire insulation

$s$  = center-to-center wire separation in millimeters

$\ln_e$  = natural logarithm

For AWG No. 22 copper wire, the diameter is 0.64 mm. The relative dielectric constant of the Teflon insulation is between 2.0 and 3.0, the insulation thickness is 0.23 mm (reference MSFC 40M39513),  $s$  is 1.097 mm,  $k$  is 3.1,  $\ln_e k$  is 1.13, and  $\mu_r$  is 1.0. The forward tunnel cables are approximately 30 meters long and the aft cables are approximately 10 meters long. The calculated wire values are:

	Rw (ohms)	Cw (pf)	Lw (μh)
Fwd Cables	1.602	738	6.78
Aft Cables	0.534	246	2.26

The parasitic capacitance between the printed circuit boards and chassis ground is:

$$C2B = \frac{\epsilon_0 A}{t}$$

where:  $\epsilon_0$  = dielectric constant of air  
 A = area of board  
 t = distance of the plane of the board from the inside surface of the electronic box.

The IEAs contain the largest-area printed circuit boards that are connected directly to tunnel cables. The printed circuit boards in the IEAs are 4.75 inches by 6.3 inches (12.06 cm by 16 cm) and the distance,  $t$ , of the end board closest to the chassis is 0.3 inches (0.762 cm). For circuits on these end boards  $C2B = 22.5$  pf. Since smaller values of  $C2B$  produce lower values of VDM and since the other boards will have lower parasitic capacitances, the circuits on the other boards will see lower values of VDM than the circuits on the end boards.

An automated circuit analysis code (PSpice) has been used to calculate the waveforms of VDM for several values of load impedance,  $RL1$ , for the two cable lengths and the input common mode voltage waveforms previously developed. These waveforms were calculated with a normalized VCM peak value as indicated in tables A-1 and A-2. Appendix A includes, for reference, all of the calculated normalized waveforms. The narrow pulse waveform is the second component caused by cables located in the aft skirt. It has a zero risetime and a decay time of less than four microseconds.

Using the results in appendix A and the common mode voltages calculated in this chapter, we can determine the total differential mode voltages on the forward and aft cables for many conditions. For example, the component A induced VDM on the *aft cables* (with  $C2B = 22.5$  pf and  $RL = 10^5$  ohms) from all coupling sources is the sum of:

1. Scaled voltage due to coupling of component A through tunnel covers and external GEI cables:

$$\begin{aligned} VDM1 &= \frac{22.3}{100} \times 100 \text{ millivolts (from table 6.2 and figure A-41)} \\ &= 22.3 \text{ millivolts (peak value)} \end{aligned}$$

2. Scaled voltage due to the first part of coupling by component A to aft skirt cables:

$$\text{VDM2} = \frac{59.8}{100} \times 100 \text{ millivolts} = 59.8 \text{ millivolts (peak value).}$$

3. Scaled narrow pulse waveform due to narrow pulse coupling through aft skirt cables:

$$\begin{aligned} \text{VDM3} &= \frac{23.1}{20} \times 1500 \text{ millivolts (from table 6.2 and figure A-46)} \\ &= 1,732 \text{ millivolts (peak value)} \end{aligned}$$

The waveform of the total VDM is the sum of these three response waveforms. Since the peak values may coincide in time, the worst case VDM is 1,814 millivolts.

Similarly, the worst case component A induced VDM on the forward cables (with  $C2B = 22.5$  pf and  $R_L = 10^5$  ohms) from all coupling sources is:

$$\begin{aligned} \text{VDM1} &= \frac{67.0}{100} \times 110 \text{ millivolts (from figure A-21)} \\ &= 74 \text{ millivolts} \end{aligned}$$

The VDM values in tables 6-3 through 6-9 were calculated by this process. It is important to note that the peak VDM of aft cables is influenced more by coupling through the cables inside the aft skirt than by coupling through the cables located inside the tunnel. This is the result of the higher frequency content of the fast risetime narrow pulse on the aft skirt cables. VDM on the forward cables is much lower than VDM on the aft cables.

**Table 6-3 Peak VDM (in millivolts) caused by Component A Coupling through Tunnel Covers and GEI Cables.  $C2B = 22.5$  pf**

	RL (ohms)				
	10	100	1,000	10,000	100,000
Fwd Cables	6.7	34.0	60.0	74.0	74.0
Aft Cables, VDM1	2.0	11.1	18.9	22.3	22.3

**Table 6-4 Peak VDM (in millivolts) caused by the first part of Coupling by Component A to Aft Skirt Cables.  $C2B = 22.5$  pf**

	RL (ohms)				
	10	100	1,000	10,000	100,000
Aft Cables, VDM2	5.38	29.9	50.8	59.8	59.8

**Table 6-5 Peak VDM (in millivolts) caused by Component A Narrow Pulse Waveform Coupling.  
C2B = 22.5 pf**

	RL (ohms)				
	10	100	1,000	10,000	100,000
Aft Cables, VDM3	404	1,386	1,732	1,732	1,732

As shown in appendix B, the transfer function that relates VDM to VCM for SRB circuits acts much like a band-pass filter that passes those frequencies near the resonant frequency of the cables and greatly attenuates higher and lower frequencies. The cable lengths on the SRB are resonant in the frequency range of a few MHz. Since most of the energy content of the lightning pulses is in the frequencies below 1 MHz, much of the energy is highly attenuated and does not contribute much to VDM.

#### IV. Cable Voltages Due to Other Components of the Lightning Specification

The cable voltages calculated in the prior paragraphs were obtained with component A of the lightning current. This section adjusts these results for the waveforms of the other components in the lightning specification.

Component B has a peak value of 4,350 amps, a risetime to peak of about 800 microseconds, and a decay time to 10 percent of peak of about 5 milliseconds (reference 2). Application of the transfer function of -79 dB produces a common mode voltage of 0.5 volts. Adjustments for cable lengths produce a peak voltage of 1.5 volts on the forward cables and 0.5 volts on the aft cables. Since the common mode to differential mode transfer function provides a very high attenuation of low frequencies, the differential voltages due to component B are much lower than those due to component A.

Component C has an average current of 400 amps and a duration of 500 milliseconds for a total charge of 200 coulombs (reference 2). Since component C is an even "slower" waveform than component B, the cable differential mode voltages are even lower than those due to component B.

Component D has a peak current of 100 kA, a peak rate of rise of  $1.4 \times 10^{11}$  amps/sec, a risetime to peak value of 3.18 microseconds, and a decay rate twice as fast as component A. It may be analytically represented by:

$$I_D(t) = K(e^{-\alpha_D t} - e^{-\beta_D t}) \text{ amps (reference 2)}$$

where:

$$K = 109,405 \text{ amps}$$

$$\alpha_D = 2.2708 \times 10^4$$

$$\beta_D = 1.29453 \times 10^6$$

Component D is a restrike component that may occur at the end of component C which means that it is separated in time from component A by at least 500 milliseconds. Since the fourier transform of component D is less than that of component A at all frequencies, the VCM and VDM responses to component D are less than or equal to the response to component A.

Component D/2 is a component D divided by two. It has the same waveform as component D and a peak current of 50 kA. The specification (reference 2) provides for a multiple stroke lightning flash made up of one component A followed by as many as 23 components D/2. The time spacings of the D/2 components are between 10 milliseconds and 200 milliseconds. Since the fourier transform of component D/2 is less than the transform of component D, the VDM response is less than or equal to the response to component A.

Component H has a peak current of 10 kA, a peak rate of rise of  $2 \times 10^{11}$  amp/sec, a rise time to peak value of 0.243  $\mu$ second and a decay time to 10 percent of peak value of about 12.3  $\mu$ second. It may be analytically represented by:

$$I_H(t) = K(e^{-\alpha_H t} - e^{-\beta_H t}) \text{ amps (reference 2)}$$

$$\begin{aligned} \text{where: } K &= 10,572 \\ \alpha_H &= 1.872 \times 10^5 \\ \beta_H &= 1.911 \times 10^7 \end{aligned}$$

The specification provides for up to 24 component H bursts distributed over a time period of up to two seconds with a time spacing between individual component H pulses of between 10  $\mu$ seconds and 50  $\mu$ seconds. Each of the 24 bursts has up to 20 individual component H pulses for a total of 480 component H pulses.

An examination of the VDM waveforms in appendix A reveals that all of the conditions which produce voltages higher than one millivolt also produce waveforms which decay to a small fraction of the peak value within 10  $\mu$ seconds. This means that the cable differential mode voltage responses do not overlap in time to a degree which would cause a peak voltage larger than the response to a single component H injected current.

The fourier transform of component H exceeds component A for all frequencies higher than about 300 kHz. The VCM-to-VDM transfer functions (appendix A) have peaks in the 1 MHz-to-20 MHz region. PSpice was used to calculate the VDM responses to the common mode voltages caused by component H. For coupling through the forward tunnel and the external GEI cables, VCM is the same waveform as component H and 69.5 dB lower, or:

$$VCM = 3.54(e^{-\alpha_H t} - e^{-\beta_H t}) \text{ volts}$$

For coupling through the aft tunnel and GEI cables VCM is a factor of three lower:

$$VCM_1 = 1.18(e^{-\alpha_H t} - e^{-\beta_H t}) \text{ volts}$$

Coupling to the cables in the aft skirt due to component H is :

$$VCM_2 = 3.46(e^{-\alpha_H t} - e^{-\beta_H t}) + 36.1e^{-\beta_H t} \text{ volts}$$

Appendix A provides the calculated VDM results with the above VCM input waveforms normalized to peak values of ten volts. Table 6-6 provides the peak VDM on the aft cables due to coupling through the aft tunnel and aft GEI cables. The appropriate waveforms are available in appendix A.

**Table 6-6 Peak VDM (in millivolts) caused by Component H Coupling through the Aft Tunnel and the GEI Cables**

	RL (ohms)				
	10	100	1,000	10,000	100,000
Aft Cables, VDM4	3.78	16.5	23.6	23.6	23.6

Table 6-7 provides the peak VDM on the aft cables due to the first part of  $VCM_2$ .

**Table 6-7 Peak VDM (in millivolts) caused by the first part of Component H Coupling through Aft Skirt Cables**

	RL (ohms)				
	10	100	1,000	10,000	100,000
Aft Cables, VDM5	1.26	5.5	7.87	7.87	7.87

Table 6-8 provides the peak VDM on the aft cables due to the second part of  $VCM_2$ .

**Table 6-8 Peak VDM ( in millivolts) caused by the second part of  $VCM_2$ .**

	RL (ohms)				
	10	100	1,000	10,000	100,000
Aft Cables, VDM6	632	2,166	2,707	2,707	2,707

The VDM responses on the forward cables due to component H were not calculated with PSpice. Instead, we estimate that the worst case values will be three times higher than the values listed in table 6-6.

Again, all of the VDM responses decay to low values within ten  $\mu$ seconds and the responses to multiple pulses of component H do not overlap in time. However, since component H pulses "have been found to occur randomly throughout a lightning

flash, being superimposed on or interspersed with the other current components" (reference 2, page A-5), the worst lightning flash VDM cable responses are the sum of the responses to component A and component H. Table 6-9 lists the peak values of these sums. From this table we see that the worst case VDM on the forward cables is 144.8 millivolts, the worst case VDM on the aft cables is 4,552 millivolts, and that the cause of the larger voltage on the aft cables is the coupling through the cables located in the aft skirt.

**Table 6-9 Peak VDM (in millivolts) on Forward and Aft Cables Due to Tunnel, GEI Cables, and Aft Skirt Cables and all Components of a Lightning Current Specified by reference 2**

	<b>R<sub>L</sub> Circuit Load Impedance in Ohms</b>				
	10	100	1,000	10,000	100,000
C2B = 22.5 pf RG2 = 10 ohms					
<b>Forward Cables</b>					
Thru Tunnel and GEI					
Component A	6.7	34.0	60.0	74.0	74.0
Component H	11.34	49.5	70.8	70.8	70.8
Total Forward	18.04	83.5	130.8	144.8	144.8
<b>Aft Cables</b>					
Thru Tunnel and GEI Cables					
Component A (VDM 1)	2.0	11.1	18.9	22.3	22.3
Component H (VDM 4)	3.78	16.5	23.6	23.6	23.6
Thru Aft Skirt Cables (Part 1)					
Component A (VDM 2)	5.38	29.9	50.8	59.8	59.8
Component H (VDM 5)	1.26	5.50	7.87	7.87	7.87
Thru Aft Skirt Cables (Part 2)					
Component A (VDM 3)	404	1,386	1,732	1,732	1,732
Component H (VDM 6)	632	2,166	2,707	2,707	2,707
Total Aft	1,048	3,615	4,540	4,552	4,552

The following summarizes the results of this chapter:

1. An analytical model was developed for the calculation of tunnel cable common mode short circuit currents and open circuit voltages. The model agrees reasonably well with the CW and pulse data obtained during the tunnel retest. The primary factor which determines these levels is the surface impedance,  $Z_{ie}$ , of the motor case. This surface impedance is much less than any of the parallel impedances (tunnel covers and cable shields) and, therefore, conducts nearly all of the injected current. The model is based upon an assumption that the tunnel-to-case bond straps survive the injected current.



2. Some of the common mode voltage pulse data exceeded the levels predicted by the model possibly due to coupling through the external GEI cables. For this reason, an intentionally conservative assumption was made that the  $V_{oc}/I_i$  response of the test article forward tunnel is "flat" with frequency at -79 dB (figure 6-4). This leads to a common mode voltage on the full length forward tunnel cables of 67 volts due to component A and 3.54 volts due to component H. This translates to a differential mode voltage of 74 millivolts due to component A and 70.8 millivolts due to component H when the circuit input impedance is  $10^5$  ohms and the printed circuit board capacitance is 22.5 pf (worst case values).
3. The common mode voltage on the aft tunnel cables due only to the tunnel and external GEI cables is 22.3 volts due to component A and 1.18 volts due to component H. However, when we account for coupling to the aft tunnel cables due to their extension into the aft skirt area, the common mode voltage increases by an additional 59.8 volts plus 23.1 volts for a total of 105.2 volts due to component A. This level is further increased by 3.46 volts plus 36.1 volts due to component H for a total of 144.7 volts. This translates to a differential mode voltage of 4.55 volts on the aft cables due primarily to the high frequency coupling of both component A and component H through the aft skirt cables. The differential mode voltage on the aft cables due only to coupling through the tunnel and external GEI cables is 46 millivolts.

## Chapter 7 Bond Strap Survivability Tests

During the linear shaped charge (LSC) portion of the lightning tests conducted at Wendover in the prior test, three simulated lightning injection current test events were run. One injection point on each of three separate tunnel covers was used. The three test events delivered injected currents from the HCB with the following characteristics:

Test Number	Maximum Current	Action Integral
1	105kA	1.764M
2	143.6kA	3.758M
3	143.6kA	3.685M

Disassembly of the systems tunnel after the three events revealed that each of the three internal bond straps had debonded and been pushed upward against the LSC with enough pressure that the straps were bent around the bottom of the LSC. It was not determined with certainty which test event was associated with each strap debond. The criterion action integral is two million amp<sup>2</sup>-sec (2M). The internal bond straps had been installed according to the procedures currently used during RSRM assembly. These internal straps were bolted to the tunnel floor plates and bonded to the motor case with a conductive epoxy (Ecco-Bond 56C) footprint which was 1-inch wide by 2.5 inches long. The DC resistance between the strap and the case is required to be less than 10 milliohms after the epoxy is fully cured. The DC resistances of the three bond strap footprints in the LSC test were measured prior to the tests and had values of approximately 1.0 milliohms (reference 13).

It was also reported that one internal bond strap debonded on the final shot of the prior HCB cable coupling test. On this shot, the peak current was 108 kA, the action integral was 2M, the injection point was on a tunnel cover four inches aft of station 611, and the damaged strap was located approximately at the same station. Adjacent bond straps were undamaged. Also, during the prior tests, an early version of the external bond straps used on the retest was tested. These external straps were solid aluminum with "four times the footprint area of the internal bond straps," or approximately 10 square inches. They were bonded to the case with Ecco-Bond 56C. Their footprint resistance was not reported. The results were summarized as follows: "Tests conducted with these external bond straps showed that they too fail at about the same level as for the original internal bond straps, presumably because the current is not equally distributed across the footprint area but concentrates along the edges. There were concerns that the epoxy for the external bond straps had not cured long enough before testing, but subsequent coupon tests conducted at the Wendover test site have precluded this concern" (reference 1).

Prior to the start of the coupling retest and bond strap survivability retest, one external bond strap was installed on each of the 19 tunnel covers as summarized in chapter 2. The results of the bond strap survivability retest are summarized in table 7-1. Due to retest failures in the control circuits of the continuing current bank, it was possible to test only a few of the straps with combined high action integral currents from the HCB and high total charge currents from the continuing current

bank. Due to retest time and schedule limitations, bond straps 3 and 14 through 19 could not be tested with high action integral or high total charge currents.

Significant observations regarding the results summarized in table 7-1 are as follows:

- A. Only 2 of the 13 tested straps debonded. One debonded at a level higher than the criterion of 2M. The one that debonded at less than criterion had survived a prior test at an action integral of 1.2M.
- B. Four of the tested straps did not debond at action integral currents of twice the criterion of 2M.
- C. None of the braided straps debonded. The range of values of footprint resistances of braided straps bonded with Ecco-Bond 56C was from 92 to 840 micro-ohms with an average of 353 micro-ohms. The range of values of footprint resistances of braided straps bonded with Traduct 2902 was from 110 to 397 micro-ohms with an average of 194 micro-ohms.
- D. The footprint resistances obtained in this field application of the bonding materials demonstrate that it is technically feasible to obtain values significantly lower than the present requirement of 10 milliohms and below 1.0 milliohms if necessary to preclude debonding of the straps.

**Table 7-1 Results of Bond Strap Survivability Retest**

Bond Strap Number	Strap Failure?	Highest AI/No Failure	Failure AI*
1	No	3.3	
2	Yes	1.2	2.2
3	Not Tested		
4	No	2.1	
5	No	4.5	
6	No	2.2	
7	No	2.0	
8	Yes		1.0
9	No	4.0	
10	No	4.6	
11	No	4.2	
12	No	2.2	
13	No	2.4	
14	Not Tested		
15	Not Tested		
16	Not Tested		
17	Not Tested		
18	Not Tested		
19	Not Tested		

\*AI is the injected current action integral in millions of amp<sup>2</sup>-seconds. When AI of the current flowing through a conductor is multiplied by the resistance (in ohms) of the conductor, the product is energy in joules.

There are two significant observations regarding the installation of the bond straps that are not reflected in the test data summarized above. The first is that the lowest footprint resistance (41 micro-ohms) was obtained on the bond strap which was kept under pressure by 170 pounds of weight for approximately 30-45 minutes after the application of the conductive epoxy. The other straps were kept under the pressure of approximately 25 pounds of weight for at least 24 hours. The second observation is that the degree of conformance of the shape of the solid straps to the curvature of the RSRM case may have affected the average thickness of the bonding material and, therefore, the footprint resistance and the action integral of the current at which these straps debonded.

Based on the experience obtained in these tests and the results of coupon tests (reference 11), the factors which have the most affect on footprint resistance are:

- A. The volume of the conductive epoxy between the strap and the case.
- B. The condition of the bond strap surface. It appears that the thin aluminum oxide that forms after the aluminum straps are cleaned increases the resistance between the strap and the conductive epoxy. It also appears that the tinned copper strands in the woven bond straps produce a lower contact resistance between the strap and the conductive epoxy.

Due to test schedule limitations and component failures in the CCB, bond straps numbered 14 through 19 were not tested with high action integral or high total charge currents injected at the tunnel covers to which these straps were attached. Based upon the test experience gained during these tests, the fact that bond straps 14 through 19 were much closer together than the bond straps on the forward tunnel, the methods used to install all of the bond straps, and the measured values of footprint resistances, it is likely that four of the untested bond straps would have survived tests up to 4.0 million action integral levels. One bond strap (number 17) which had a footprint resistance of 25 milliohms might have failed.

The results of these tests and the coupon tests conducted by Thiokol, when combined, should provide an adequate database for the selection of a bond strap design which will meet all of the requirements for lightning-survivable bond straps.

## Chapter 8 Selection of an Adequate Tunnel Bond Strap Design

In chapter 6, it was shown that the worst-case lightning-induced differential mode voltages are 144.8 millivolts on the forward cables and 4.55 volts on the aft cables when the tunnel is protected by the improved bond strap designs used in the coupling retest. These low levels of differential mode voltages and corresponding very large safety margins indicate that less protection than represented by the tested configuration may be acceptable. An increase in differential mode voltages *due to tunnel and GEI cable coupling* by a factor of 10 would increase these voltages only to 1.45 volts on the forward cables and 4.96 volts on the aft cables. A corresponding increase in common mode voltage by a factor of 10 would produce a peak level of about 700 volts. Most of the common mode voltage is developed across the parasitic capacitance between the printed circuit board and the inside of electronic boxes. With about 0.3 inches spacing between the boards and the boxes, the voltage breakdown level is about 23 kV in air (3.0 MV per meter). The dielectric strengths of the cable materials between the core conductors and the overall shields are at least 6.5 kV (reference 12, sheet 22). Since the voltages along the length of the shield and along the length of the core rise together, the 6.5 kV rating would not be exceeded.

A comparison of the entries on line D of table 5-1 and line B of table 5-2 demonstrate that the Marx test scaled peak voltages for the present flight configuration are less than ten times the scaled peak voltages for the improved design configuration. A similar comparison of the scaled HCB peak voltage levels on lines C of the two tables demonstrates that the low frequency coupling levels are essentially equal. This low frequency equality is expected since the low frequency voltage developed across the length of the cables is determined by the injected current flowing through the equivalent resistance of the case, tunnel, cable shields, and core conductors in parallel and the change in bond strap configurations has a small effect on this equivalent resistance. Therefore, the present bond strap design is adequate to protect the USBI operational flight cables located in the systems tunnel from lightning induced voltages *when the floor plate-to-case bond straps do not debond from the case*.

An optimized design of the tunnel bond straps to preclude debonding should be selected based on a trade-off analysis of larger footprints versus heavier cover-to-cover straps. It may be less costly to implement a satisfactory design if it can be shown that the presently used cover-to-cover straps are acceptable. To retain these straps, it may be necessary to enlarge the footprints of the tunnel-to-case straps to more than eight square inches. At this time, there is no data or evidence that the attachment of the tunnel-to-case bond straps to the tunnel covers is any better than their attachment to the tunnel floor plates.

## Chapter 9 Conclusions

At the time of the prior test and this retest, the NASA lightning specification was NSTS 07636, revision D. The inflight lightning criteria of the revision D first return stroke was 50,000 amps. The action integral of this stroke is  $0.125 \times 10^6$  amp<sup>2</sup>-seconds. The test results indicate that the tunnel bond straps presently used on the SRB meet this inflight criteria. The revision D criteria for equipment unprotected by facilities or other structures (i.e., the STS during rollout to the launch pads) was 200,000 amps and an action integral of  $2 \times 10^6$  amp<sup>2</sup>-seconds. The test results indicate that the presently used tunnel-to-case bond straps nearest the stroke attachment point would debond from the motor case at these higher current levels if the stroke attachment is located on the tunnel covers. If the attachment point is located anywhere else on the SRB, the tunnel straps would not debond.

Plans for the lightning retest anticipated that NASA would approve the draft of NSTS 07636, revision F, which increased the inflight criteria peak current to 200,000 amps and the action integral to  $2 \times 10^6$  amp<sup>2</sup>-seconds. Revision F has been baselined by the NASA Level II Program Requirements Change Board. The tunnel bond strap configuration was changed for the retest with the intent to obtain test data that would assist in the development of a suitable design to meet revision F. The changes included:

1. Enlargement of each conductive epoxy footprint where the cover-to-case bond straps are attached to the motor case from 2.5 square inches to 8 square inches.
2. A change of the attachment point of the cover-to-case bond straps from the tunnel floor plate to the tunnel covers.
3. Replacement of the two AWG 12 bond straps across each cover-to-cover gap with four aluminum straps that lowered both the inductance and resistance across the gaps.

Several alternative configurations of the cover-to-case bond straps were installed and tested. The alternatives included four-inch-wide solid aluminum straps with the footprint ends configured with either holes or notches, both three-inch and four-inch wide woven straps made up of tin-coated copper strands, and three alternative footprint attachment methods. These three methods were Ecco-Bond 56C conductive epoxy, Traduct 2902 conductive epoxy, and no epoxy (with straps held against the bare metal footprint on the case by cured K5NA, which is the thermal protective material used at several locations on the surfaces of the SRB). During the retest, currents with action integrals up to  $4.6 \times 10^6$  amp<sup>2</sup>-seconds were injected into tunnel covers at the location of the "new" cover-to-case bond straps. These were worst case locations for the bond strap nearest the injection point. One bond strap debonded at an action integral of  $1 \times 10^6$  amp<sup>2</sup>-seconds and another bond strap debonded at an action integral of  $2.2 \times 10^6$  amp<sup>2</sup>-seconds. Due to lightning simulator control circuit failures, not all of the 19 bond straps were tested. Of the 13 that were tested, 11 survived the revision F action integral criterion of  $2 \times 10^6$  amp<sup>2</sup>-seconds. Four of these eleven were tested at levels between  $4 \times 10^6$  and  $4.6 \times 10^6$  amp<sup>2</sup>-seconds. None of the four debonded.

The debond failure of tunnel-to-case bond straps is caused by the heating of the conductive epoxy footprint. The amount of heating depends upon the footprint resistance and the action integral of the current which flows through the footprint. The footprint resistance depends upon the area and the thickness of the epoxy and the contact resistance between the bond strap and the epoxy and between the epoxy and the motor case. There is substantial evidence that the bond line between the aluminum strap and the conductive epoxy fails first. This failure mechanism is most likely caused by the formation of a layer of aluminum oxide on the strap prior to contact with the epoxy. This theory is supported by the fact that none of the woven bond straps failed. The woven straps are made of strands of tin-plated copper and would not form a bond line equivalent to the aluminum oxide. The amount of current that flows through each tunnel-to-case bond strap depends upon how the total injected current divides and distributes among all of the bond straps. The impedance of the cover-to-cover bond straps affects this distribution. The lower impedance straps used in the retest allowed a higher percentage of the total current to be conducted away from the tunnel-to-case bond straps nearest the injection point.

The footprint resistances of all tunnel-to-case bond straps used in the retest were measured prior to the pulsed current injection tests. The resistances of the conductive epoxy footprints ranged from 0.041 milliohms to 5.72 milliohms. The average of all 14 conductive epoxy footprints was 0.775 milliohms. The average of all aluminum straps with conductive epoxy was 1.288 milliohms and the average of all woven straps with conductive epoxy was 0.262 milliohms. The average of the three woven straps bonded with the Traduct 2902 conductive epoxy was 0.127 milliohms and the average of the four woven straps bonded with the Ecco-Bond 56C conductive epoxy was 0.364 milliohms. Both of the bond straps that failed were aluminum straps bonded with Traduct 2902. The lowest failure level of  $1 \times 10^6$  amp<sup>2</sup>-seconds occurred on bond strap No. 8 which had a footprint resistance of 1.0 milliohm and was located just aft of the ETA ring. This location contributed to the lower failure level because of the higher impedance of the bond straps between the ETA ring and the No. 8 tunnel cover. The next lowest failure level of  $2.2 \times 10^6$  amp<sup>2</sup>-seconds occurred on bond strap No. 2 which had a footprint resistance of 0.180 milliohms and was located at the second tunnel cover. The reasons for this failure are unknown. The two adjacent tunnel-to-case bond straps (No. 1 and No. 3) had footprint resistances of 0.041 milliohms and greater than 60 ohms, respectively. The 60 ohms strap was one of the straps which had no conductive epoxy. For comparison, the criterion for the footprint resistance of the presently used tunnel-to-case bond straps is 10 milliohms. These presently used straps are made of solid aluminum and are bonded to the case with Ecco-Bond 56C with a 2.5 square inch footprint. Test data from the prior tests indicates that these straps would survive tunnel cover injected currents with  $0.125 \times 10^6$  amp<sup>2</sup>-seconds action integrals of the NSTS 07636 D inflight criteria. The final details of a modified design of the tunnel bond straps to meet the revised inflight criteria is beyond the scope of this report. Through the experience gained during the installation and test of the candidate designs and the analysis of the data obtained from the retest, the author believes that sufficient information is available to support an acceptable conceptual design for the SRB without additional tests.

The cable coupling data obtained during the retest was measured with the "new design" cover-to-cover and cover-to-case bond straps in place. Other significant changes from the test article configuration used in the prior test included (a) all DFI cables were removed from the tunnel, reducing from 15 to 6 the number of tunnel OF test cables; (b) all GEI cables that penetrate the tunnel envelope were enclosed within shields, and the shields were bonded to the motor case every 18 inches and at the point where they entered the tunnel (this change has been approved by an ECP and has already been incorporated into the flight SRM); (c) the aft breakout box was electrically bonded directly to the aft motor case instead of through the tunnel bond straps. The cable coupling data demonstrated a reduction, by a factor of 300, in the higher frequency ( $>100$  kHz) coupling to the operational flight cables.

The coupling data consisted of common mode short circuit currents and common mode open circuit voltages measured on the OF cable core bundles. This data was used to construct a coupling model from which the common mode open circuit voltage waveforms due to the specified revision F lightning components were calculated. The peak open circuit common mode voltages on the OF cables in the forward and aft tunnels due to coupling of lightning components A plus H through the tunnel and GEI cables were 70.5 volts ( $67 + 3.5$ ) and 23.5 volts ( $22.3 + 1.18$ ), respectively. Common mode voltage, by definition, is the voltage developed across the total length of a cable core bundle. If the bundle is shorted to chassis ground on one end and connected through a high impedance on the other end (the test conditions), the voltage measured across the high impedance is equal to the common mode voltage. In the analysis of the prior test coupling data, the differential mode voltage was taken to be 10 percent of the common mode voltage. In chapter 6 and appendix B of this report, a model was developed which allows for a much more accurate computation of the differential mode voltages. The differential mode voltage, by definition, is the voltage developed between conductors within the cable bundle and is the voltage impressed across electronic circuits connected to the cable core conductors. The amount of differential mode voltage developed at the end of a shielded cable is highly dependent on how the circuit grounds are connected to chassis ground and how much capacitance there is between the printed circuit boards and chassis ground. Fortunately, the SRB electronic systems were designed with single point grounds and with high isolation impedances between the electronic circuits and chassis grounds within the electronic black boxes. The differential mode coupling model was applied to several conditions of printed circuit board capacitances and input circuit impedances. In general, the higher capacitances and higher impedances produce higher differential mode voltages. The size of the printed circuit boards in the SRB integrated electronic assemblies produces the highest parasitic capacitance between the boards and chassis ground of 22.5 picofarads (pf). For the highest estimate of circuit input impedance of  $10^5$  ohms, the differential mode voltages due to coupling through the tunnel and GEI cables are 144.8 millivolts on the forward cables and 45.9 millivolts ( $22.3 + 23.6$  from table 6-9) on the aft cables. The common mode voltages are reduced by a factor much larger than the previously used factor of ten because the cable conductors and printed circuit board input impedance and capacitance to chassis ground act much like a band pass filter which greatly attenuates frequencies higher and lower than the resonant frequency of the cables.



The low differential mode voltages suggests that the "new design" of the tunnel bond straps can be relaxed from the tested configuration and still provide adequate safety margins. A relaxed design (relative to the tested design) which prevents the debonding of the tunnel bond straps can be chosen from among several alternatives, some of which do not use any conductive epoxy. An optimized design could be developed after approval by NASA of a preliminary engineering change proposal (PECP).

The tests and analyses described in this report apply only to the design of the systems tunnel and the tunnel bond straps. There are other locations on the SRB which require hardware design changes to comply with NSTS 07636F. These other locations include the following:

1. Change to a conductive gasket at the nose cap/frustum interface.
2. Improve the electrical bonding between the separation ring and the forward skirt.
3. Improve the electrical bonding between the strut attachment brackets (H-bracket) and the motor case.
4. Improve the protection of the aft BSM ordnance cables from the direct effects of lightning.

## **Chapter 10 Recommendations**

If NASA decides that the STS should meet the lightning protection requirements of NSTS 07636F, the results of the tests and analyses described in this report should be used in the preparation of a detailed redesign of the SRB systems tunnel electrical bonding straps and in the determination of the actions required to bring the SRB into full compliance.

At this time, NASA has approved several hardware exceptions to the lightning protection requirements for the orbiter, external tank, and solid rocket boosters. The rationale for these exceptions is that the launch commit criteria and the return to landing restrictions preclude lightning strikes to the STS during flight, the rollout criteria and contingencies for protection preclude lightning strikes to the STS during rollout to the launch pad, and the overhead catenary wire system adequately protects the STS while it is on the launch pad.

## **Appendix A Calculated Differential Mode Voltages**

In chapter 6, the translation from common mode to differential mode voltages is discussed. Appendix B shows how in general, the translation acts much like a band pass filter. An automated circuit analysis code, PSpice, was applied to the circuit model of figure A-1 to calculate the VDM waveforms for input waveforms calculated in Chapter 6 with normalized amplitudes of 100, 20, or 10 volts as listed in table A-1. For reference and comparison, frequency responses were also calculated for conditions as identified in table A-1.

These calculations were made with the cable parameters of chapter 6, C2B equal to 22.5 pf, with two values of RG1 (0 ohms and 10 ohms) and with five values of RL1 (10,  $10^2$ ,  $10^3$ ,  $10^4$ ,  $10^5$  ohms). This value of C2B is the worst case parasitic capacitance between the SRB printed circuit boards and chassis ground. To illustrate the effects on VDM of larger values of RG1 and larger values of C2B, the frequency responses and VDM waveform responses were also calculated for RG1 = 100 ohms and C2B = 45, 90, 180, and 360 pf.

The present configuration of the SRB has no electronic circuits which match these excursion conditions. These conditions are included only for reference in future related studies and design changes. The following tables provide lists of all of the conditions for which PSpice calculations were made and indices to the figures which contain the results.

The peak values of the transient waveforms in this appendix were scaled to the appropriate peak values of VCM calculated in chapter 6 to result in the entries of tables 6-3 through 6-9.

### **Conditions:**

VCM, RL1, RG1 as defined in tables A-1 and A-2.

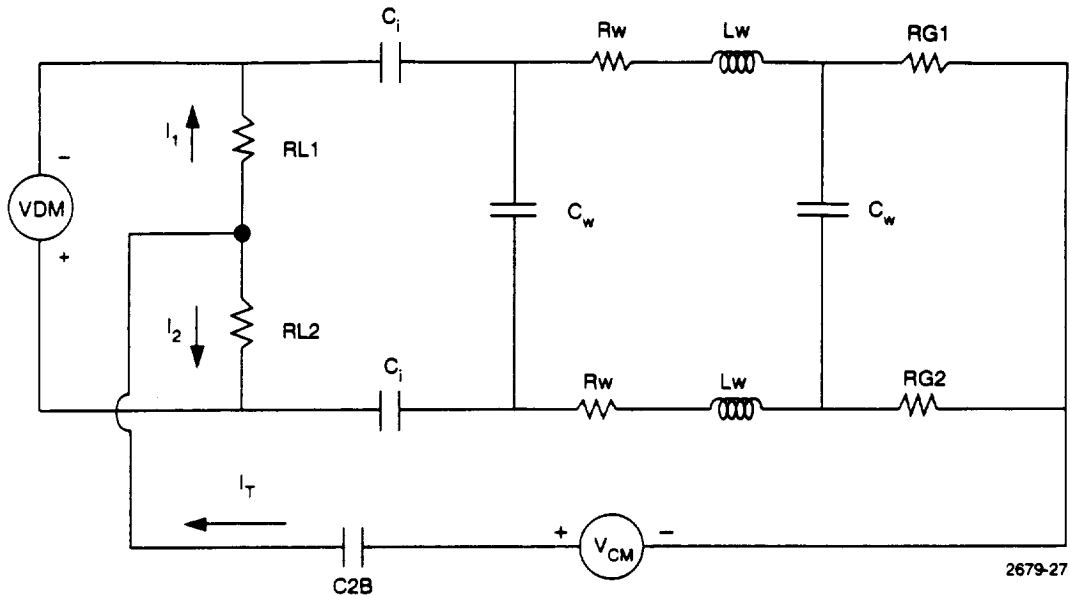
C2B = 22.5 pf for table A-1.

C2B as defined in table A-2.

Ci = 0, RG2 = 0, RL2 = 0 (see appendix B)

Cw, Lw, Rw (see Chapter 6)

V(9) = VDM in figures A-2 to A-76.



2679-27

**Figure A-1 Circuit used to Calculate VDM Responses to Calculated VCM Inputs (Chapter 6)**

**Table A-1 Index to Figures in this Appendix, Baseline Cases, C2B=22.5pf**

	VCM Volts	RL1 (ohms)									
		10		10 <sup>2</sup>		10 <sup>3</sup>		10 <sup>4</sup>		10 <sup>5</sup>	
RG1 (ohms)		0	10	0	10	0	10	0	10	0	10
Forward Cables Frequency Response Component A		A-2	A-4	A-6	A-8	A-10	A-12	A-14	A-16	A-18	A-20
	100	A-3	A-5	A-7	A-9	A-11	A-13	A-15	A-17	A-19	A-21
Aft Cables Frequency Response Component A		A-22	A-24	A-26	A-28	A-30	A-32	A-34	A-36	A-38	A-40
	100	A-23	A-25	A-27	A-29	A-31	A-33	A-35	A-37	A-39	A-41
Narrow Pulse A	20	—	A-42	—	A-43	—	A-44	—	A-45	—	A-46
Component H	10	—	A-47	—	A-48	—	A-49	—	A-50	—	A-51
Narrow Pulse H	10	—	A-52	—	A-53	—	A-54	—	A-55	—	A-56

2679-25

A – Refers to the component A waveform of the NSTS 07636 Lightning Specification—see Chapter 6.

H – Refers to the component H waveform of the NSTS 07636 Lightning Specification—see Chapter 6.

VCM – Is the peak value of the common mode voltage used as in input to the P-Spice model of the translation from common mode to differential mode voltage.

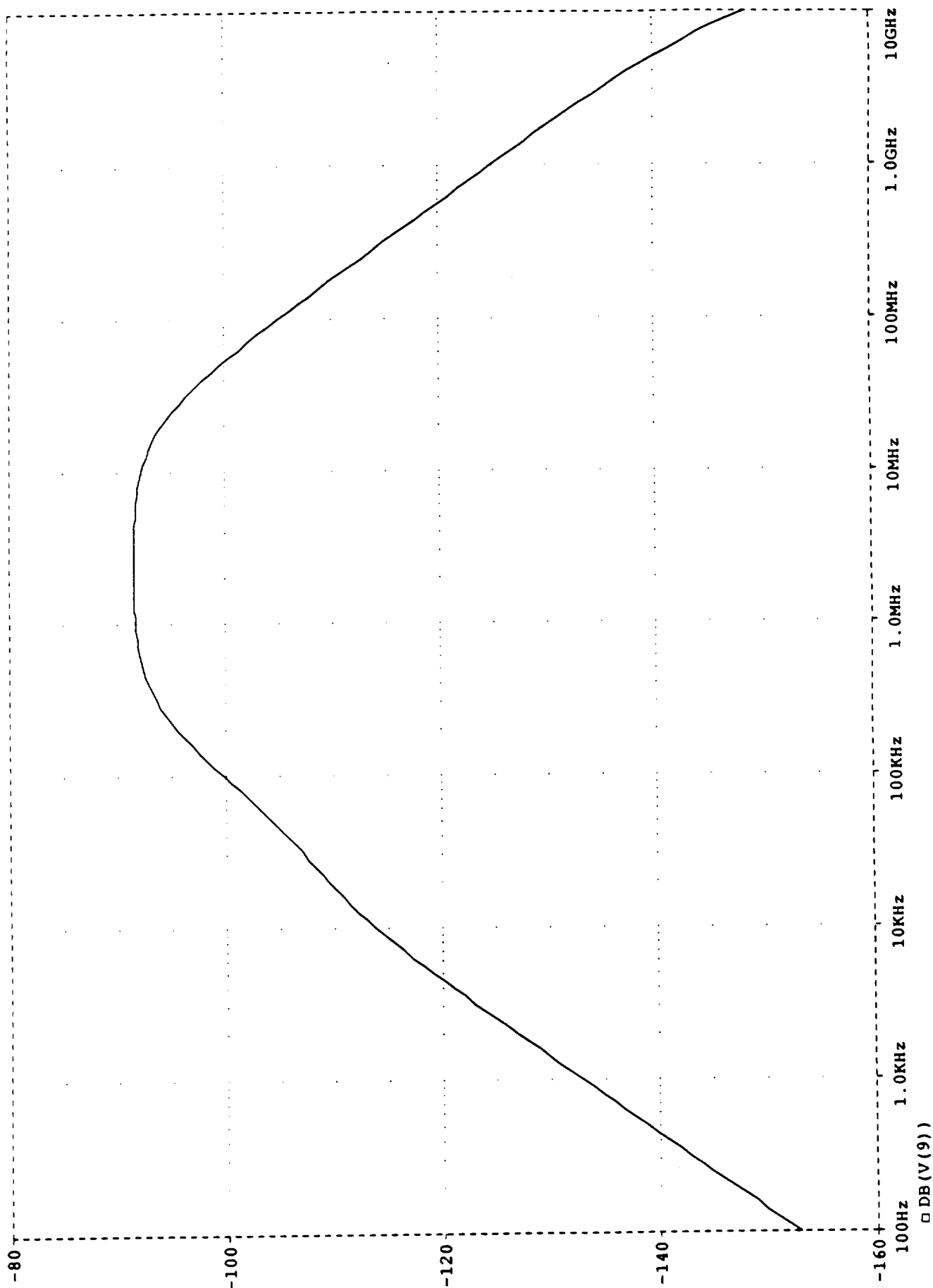
**Table A-2 Conditions applicable to circuit parameters used in calculation of differential mode voltage responses contained in Figures A-57 through A-76**

	Frequency Response RG1 = 100 ohms		Component (A) VCM = 100 RG1 = 100 ohms	
	RL1 (ohms)		RL1 (ohms)	
	10 <sup>3</sup>	10 <sup>5</sup>	10 <sup>3</sup>	10 <sup>5</sup>
<b>C2B (pf)</b>				
22.5	A-57	A-59	A-58	A-60
45	A-61	A-63	A-62	A-64
90	A-65	A-67	A-66	A-68
180	A-69	A-71	A-70	A-72
360	A-73	A-75	A-74	A-76

CALCULATED DIFFERENTIAL MODE VOLTAGE (SEE FIGURE A1 AND TABLES A1 AND A2 FOR CONDITIONS)

Temperature: 27.0

Date/Time run: 06/06/91 12:52:11



Frequency

Figure A-2

CALCULATED DIFFERENTIAL MODE VOLTAGE (SEE FIGURE A1 AND TABLES A1 AND A2 FOR CONDITIONS)

Temperature: 27.0

Date/Time run: 06/06/91 12:52:11

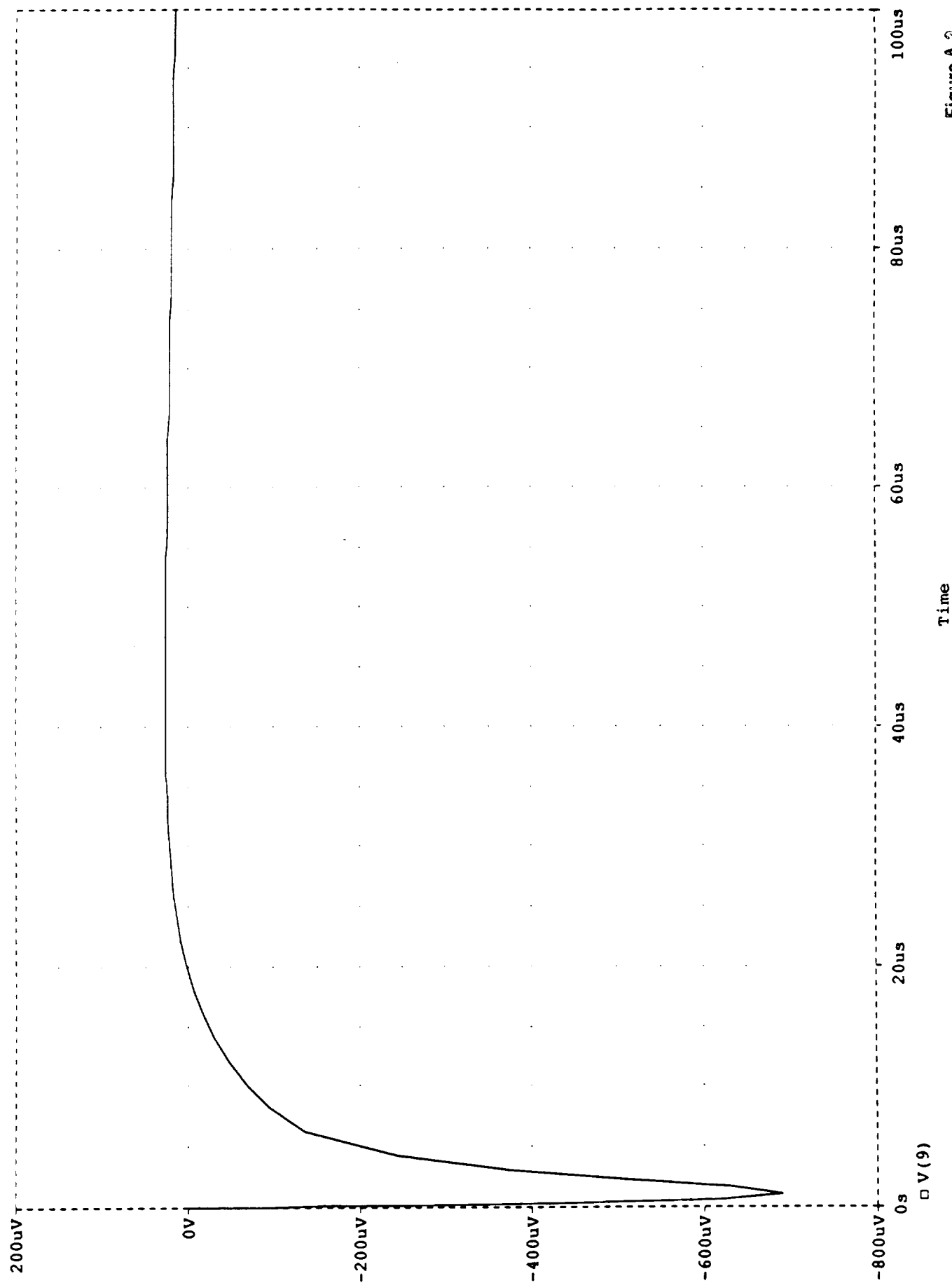


Figure A-3

CALCULATED DIFFERENTIAL MODE VOLTAGE (SEE FIGURE A1 AND TABLES A1 AND A2 FOR CONDITIONS)

Temperature: 27.0

Date/Time run: 06/06/91 14:10:06

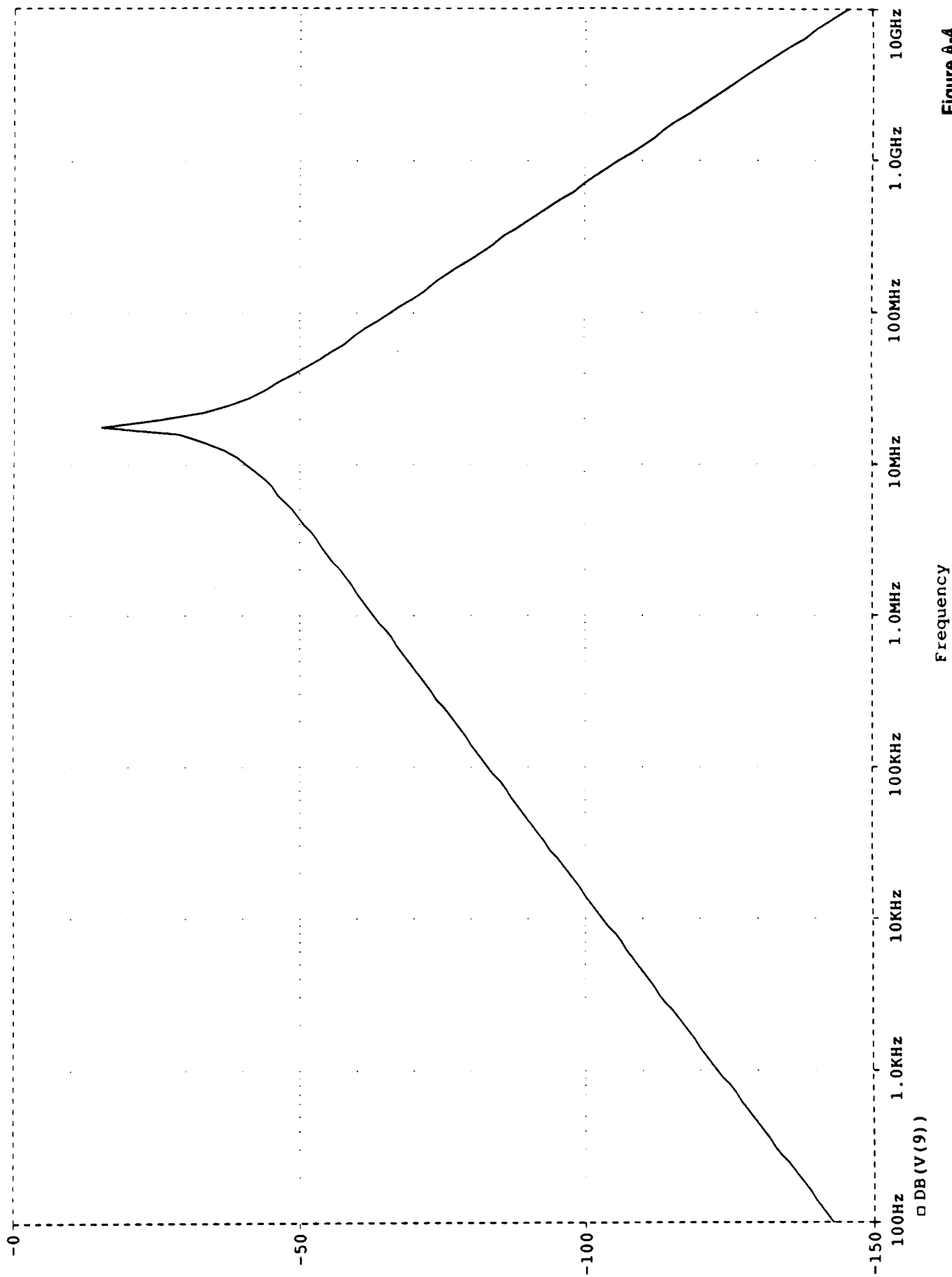


Figure A-4



CALCULATED DIFFERENTIAL MODE VOLTAGE (SEE FIGURE A1 AND TABLES A1 AND A2 FOR CONDITIONS)

Temperature: 27.0

Date/Time run: 06/06/91 14:10:06

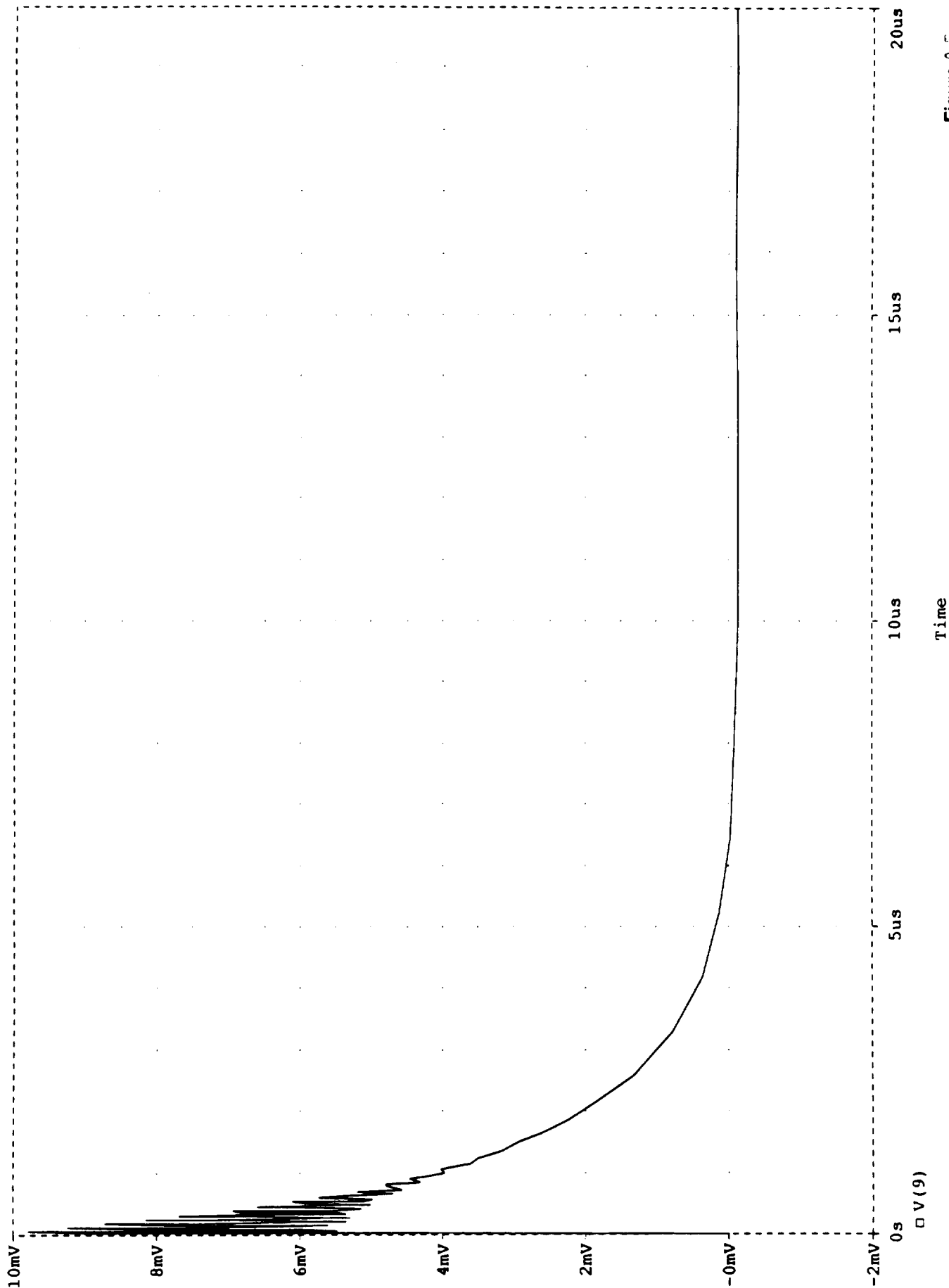
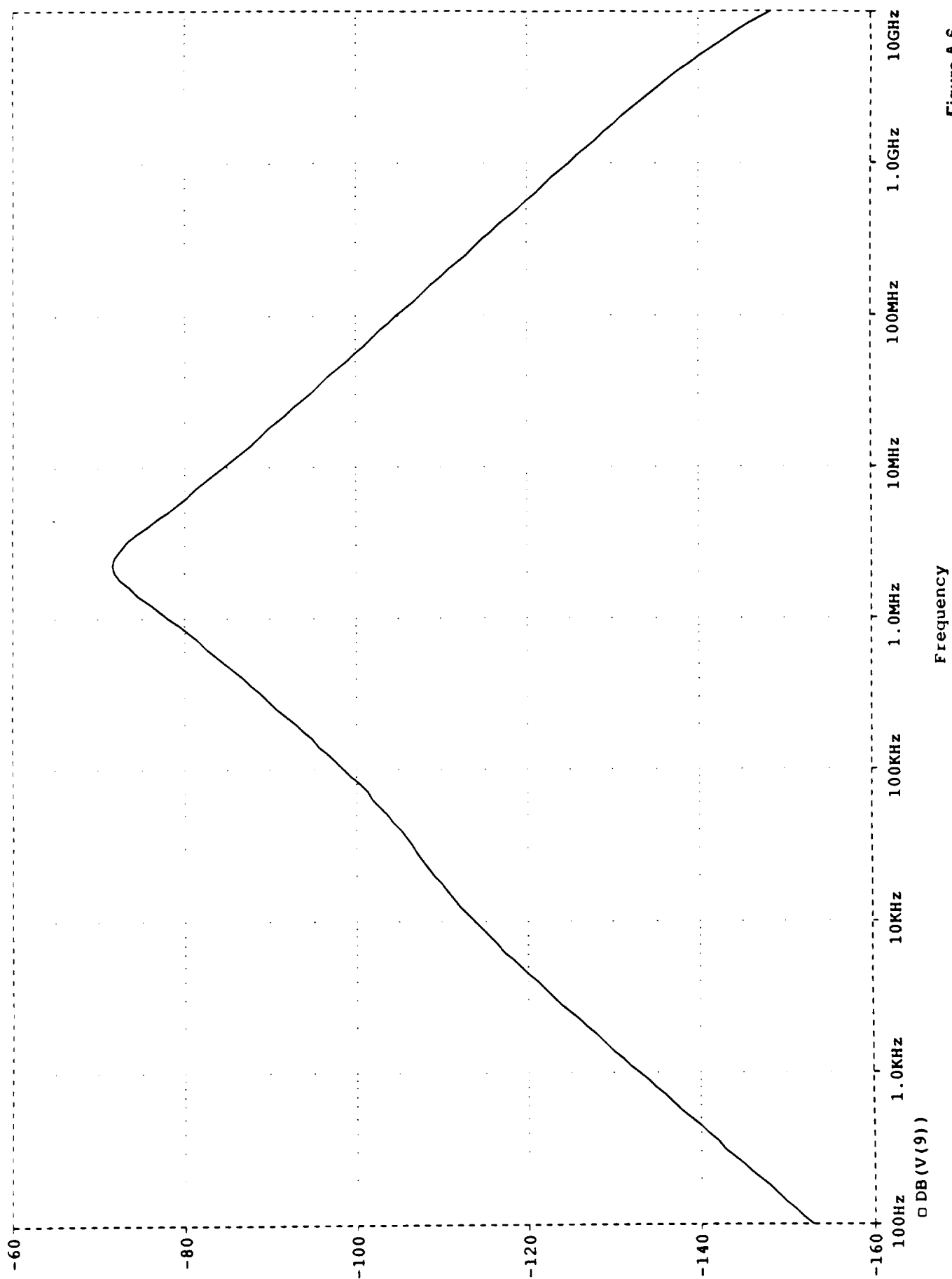


Figure A-5

# CALCULATED DIFFERENTIAL MODE VOLTAGE (SEE FIGURE A1 AND TABLES A1 AND A2 FOR CONDITIONS)

Temperature: 27.0

Date/Time run: 06/06/91 12:47:44



Frequency

Figure A-6

CALCULATED DIFFERENTIAL MODE VOLTAGE (SEE FIGURE A1 AND TABLES A1 AND A2 FOR CONDITIONS)

Temperature: 27.0

Date/Time run: 06/06/91 12:47:44

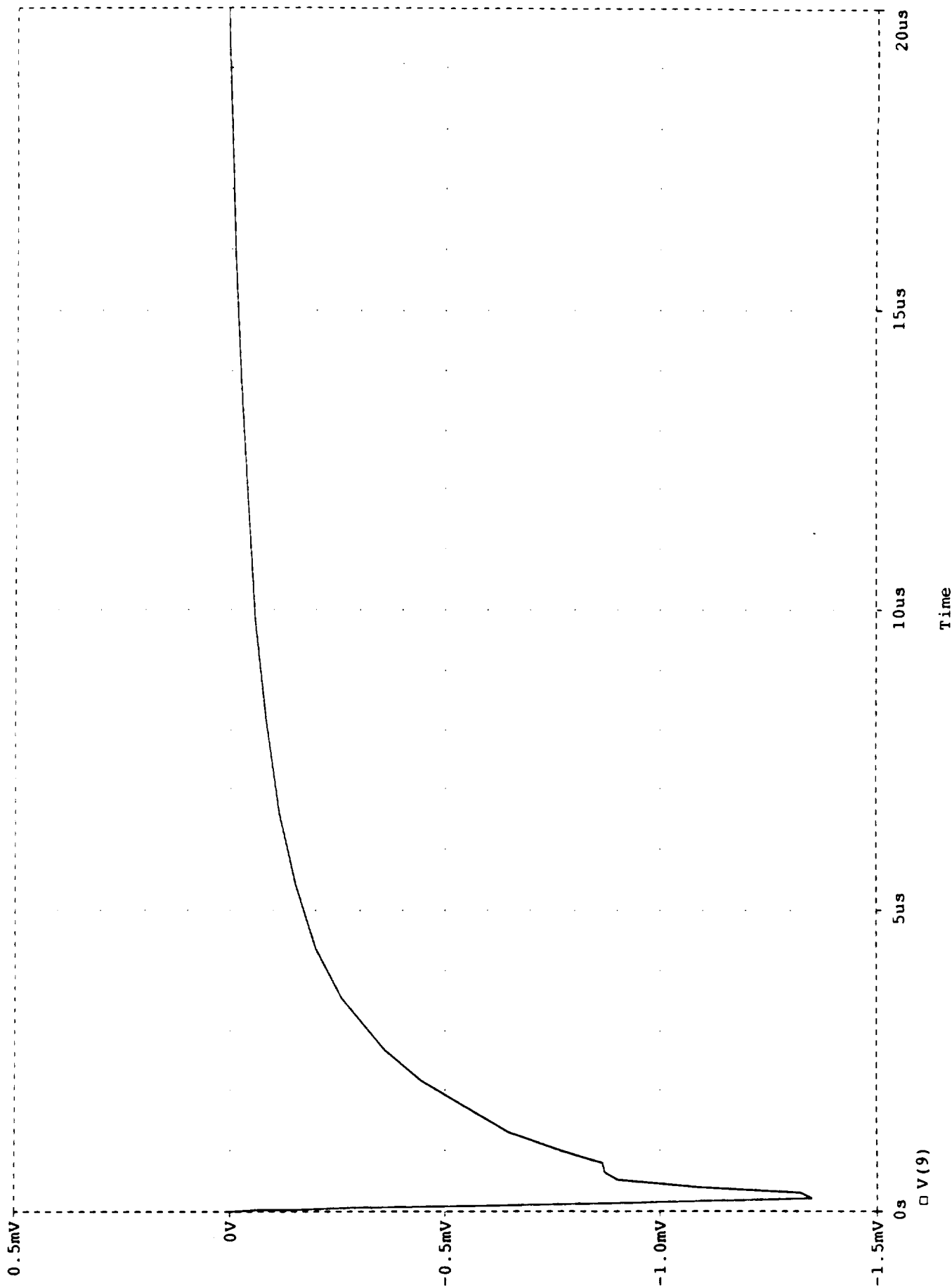


Figure A-7

CALCULATED DIFFERENTIAL MODE VOLTAGE (SEE FIGURE A1 AND TABLES A1 AND A2 FOR CONDITIONS)  
Date/Time run: 06/06/91 14:57:17

Temperature: 27.0

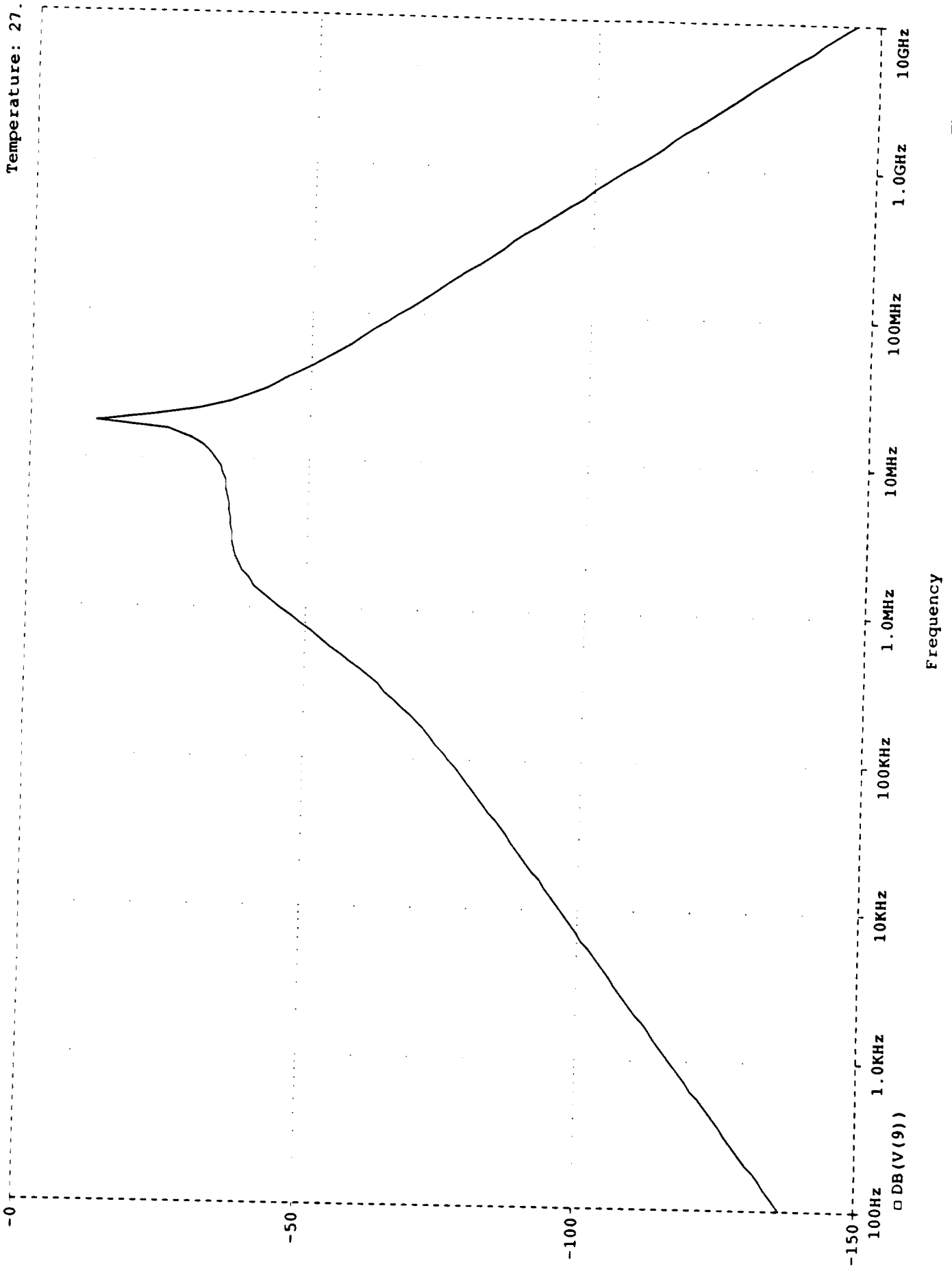


Figure A-8

CALCULATED DIFFERENTIAL MODE VOLTAGE (SEE FIGURE A1 AND TABLES A1 AND A2 FOR CONDITIONS)

Temperature: 27.0

Date/Time run: 06/06/91 14:57:17

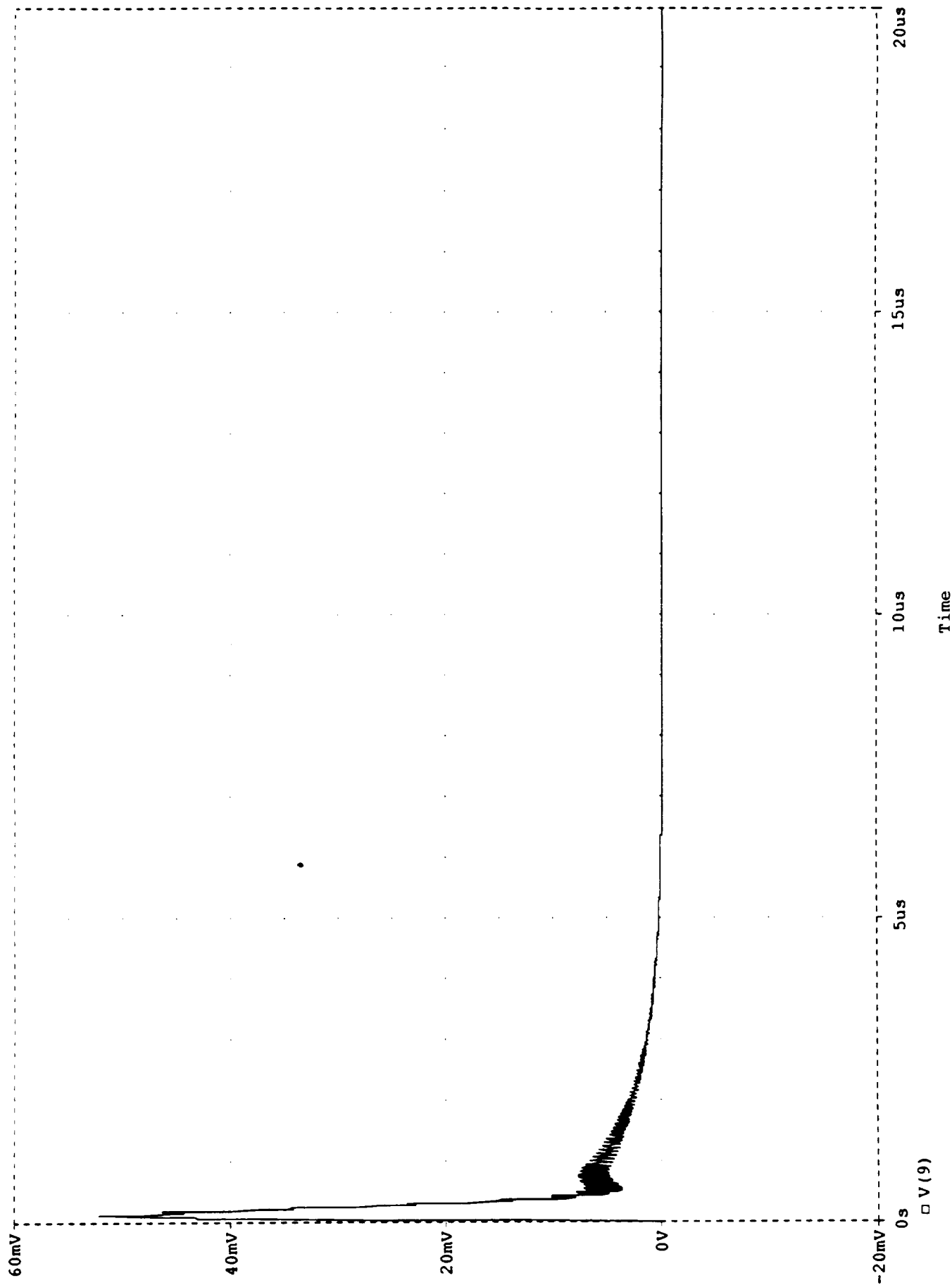


Figure A-9

CALCULATED DIFFERENTIAL MODE VOLTAGE (SEE FIGURE A1 AND TABLES A1 AND A2 FOR CONDITIONS)

Temperature: 27.0

Date/Time run: 06/06/91 13:00:39

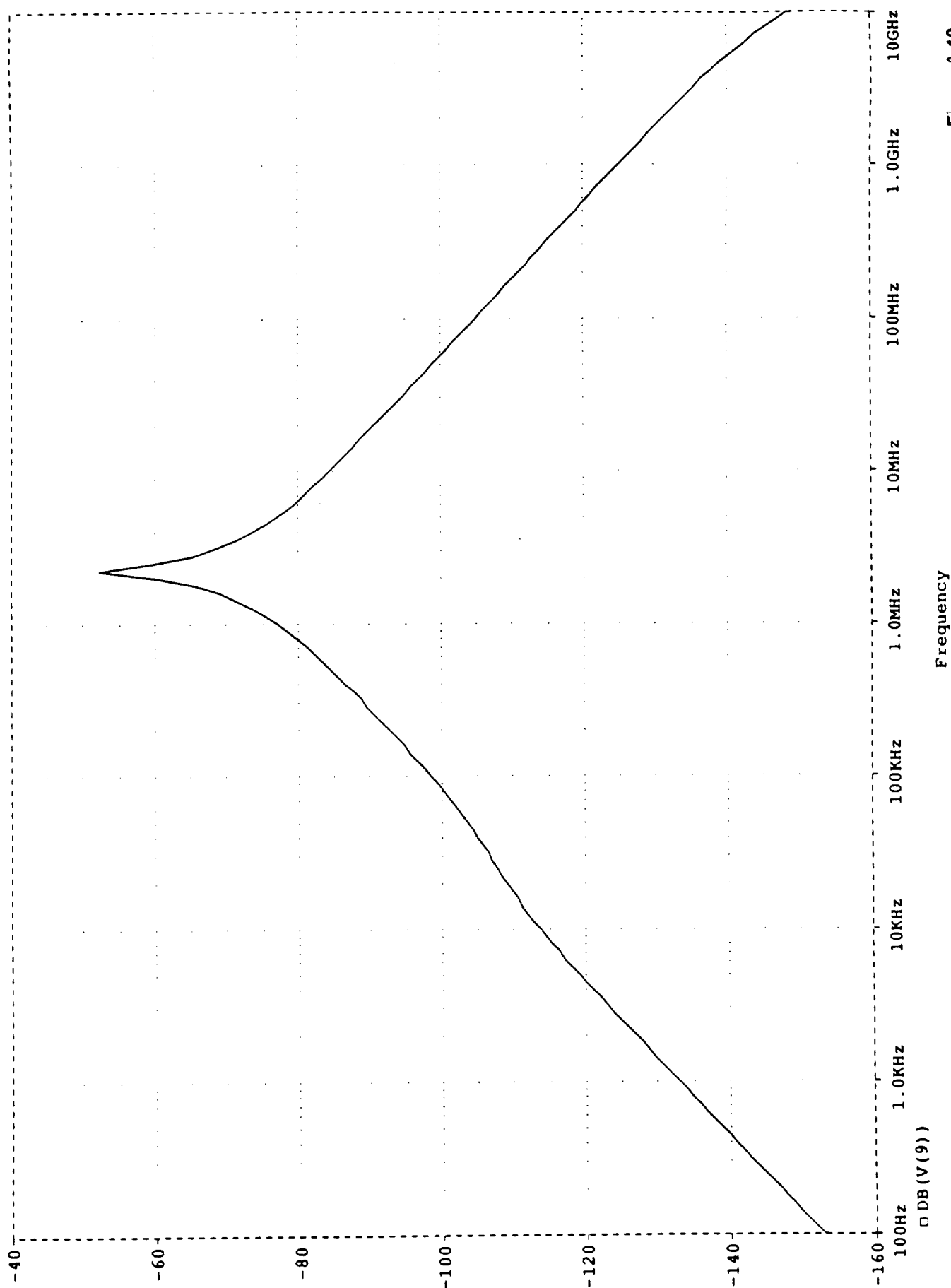


Figure A-10

CALCULATED DIFFERENTIAL MODE VOLTAGE (SEE FIGURE A1 AND TABLES A1 AND A2 FOR CONDITIONS)

Temperature: 27.0

Date/Time run: 06/06/91 13:00:39

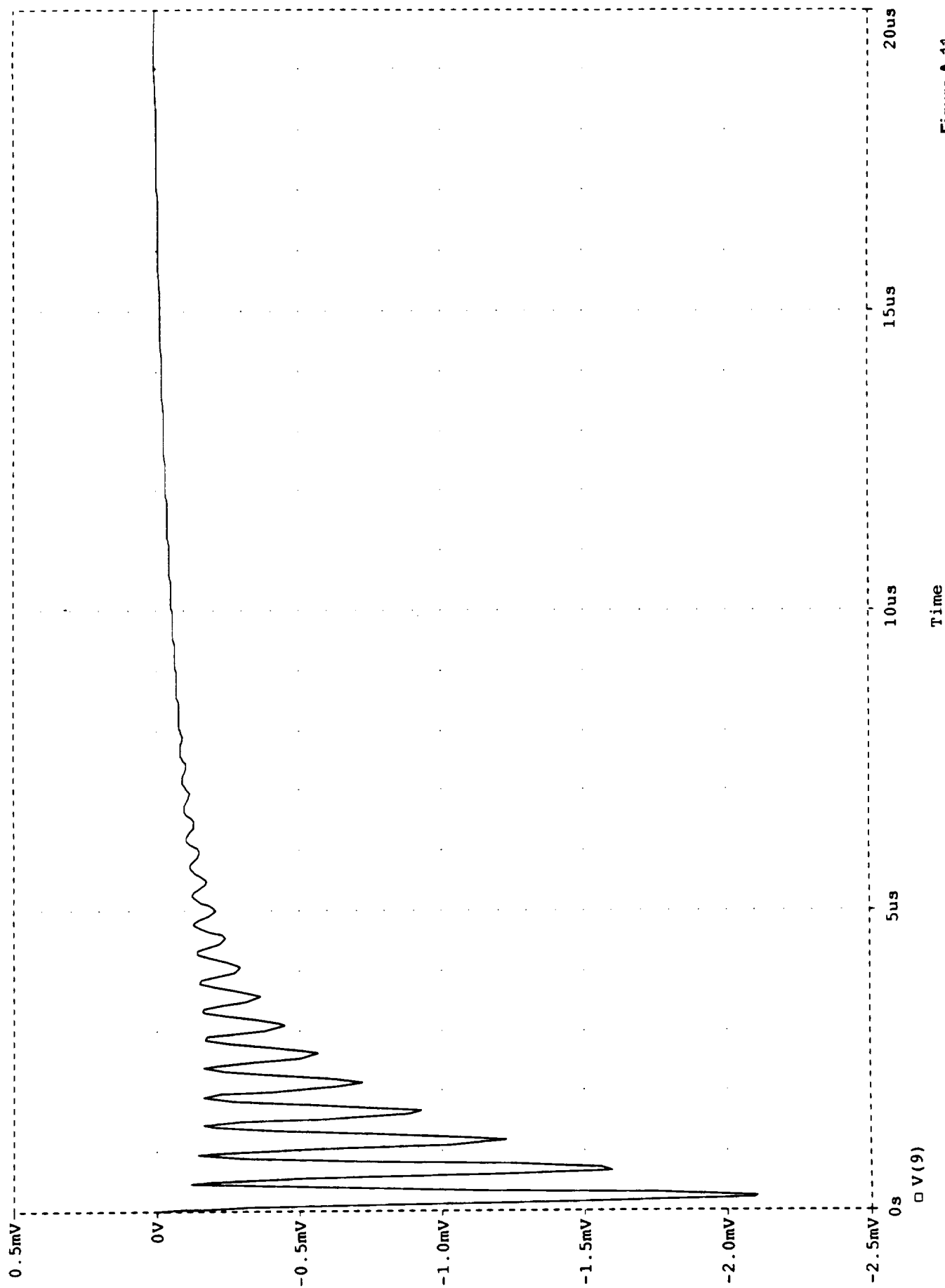


Figure A-11

CALCULATED DIFFERENTIAL MODE VOLTAGE (SEE FIGURE A1 AND TABLES A1 AND A2 FOR CONDITIONS)

Date/Time run: 06/07/91 08:03:57

Temperature: 27.0

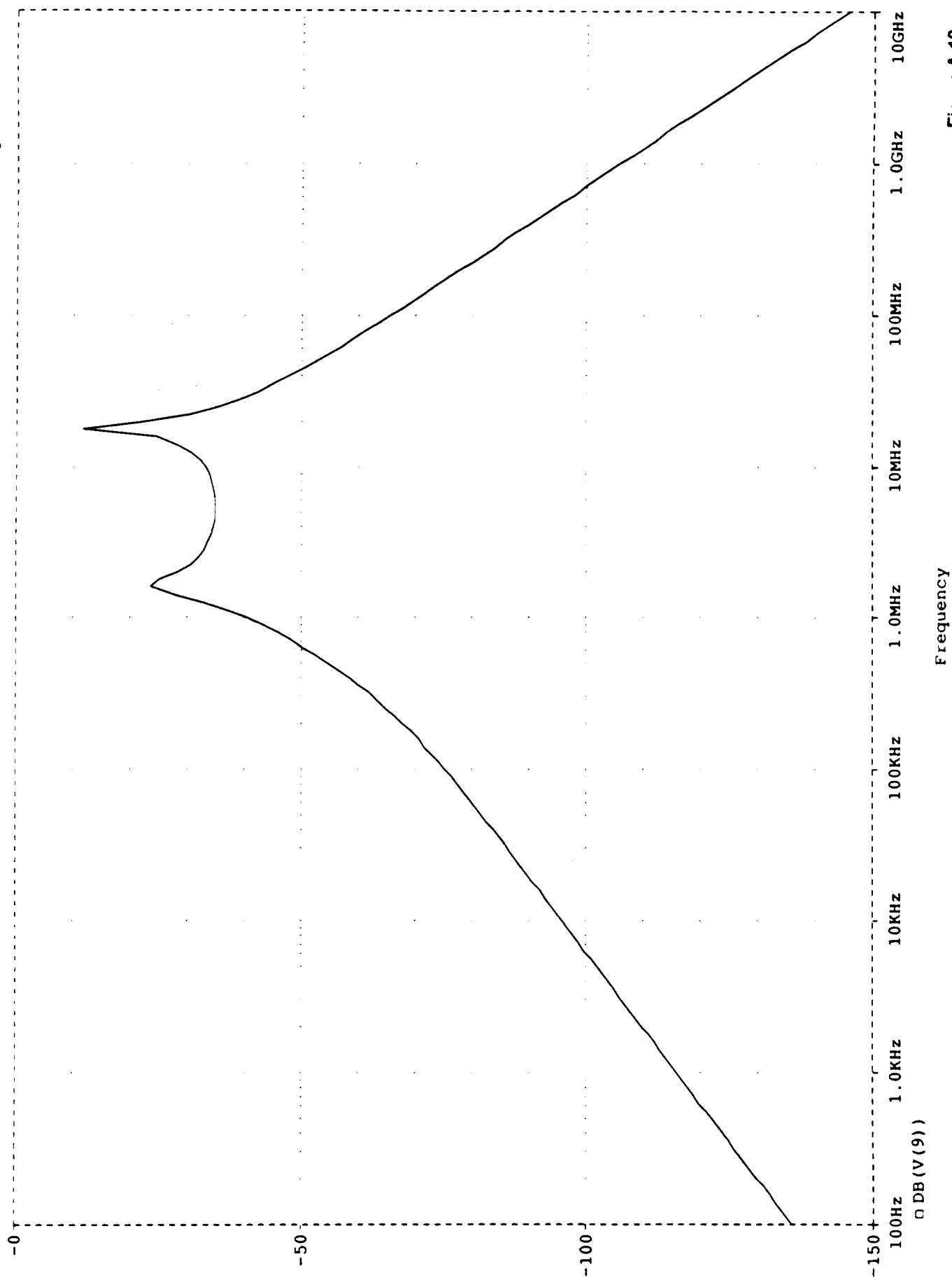


Figure A-12



CALCULATED DIFFERENTIAL MODE VOLTAGE (SEE FIGURE A1 AND TABLES A1 AND A2 FOR CONDITIONS)

Date/Time run: 06/07/91 08:03:57

Temperature: 27.0

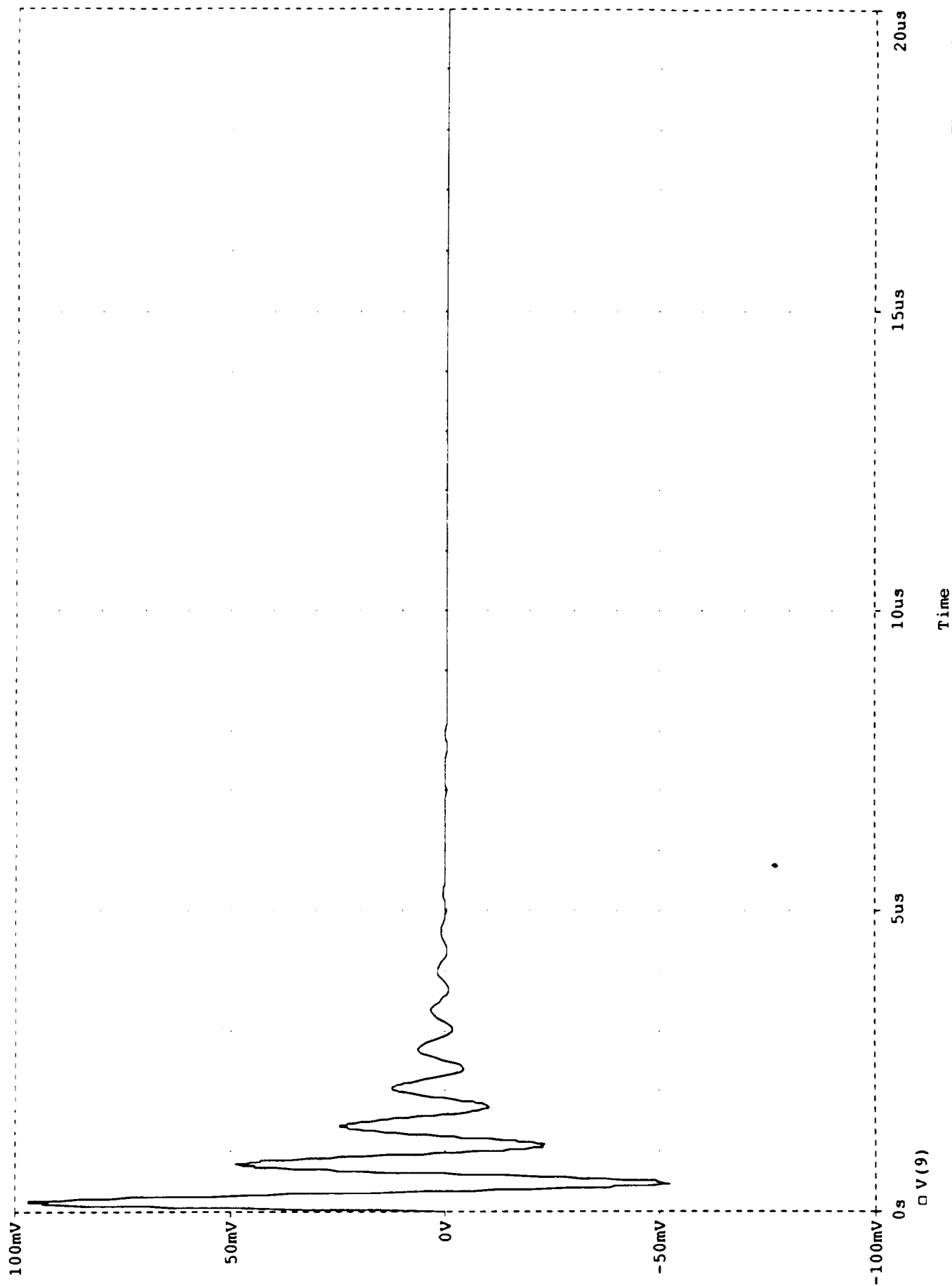
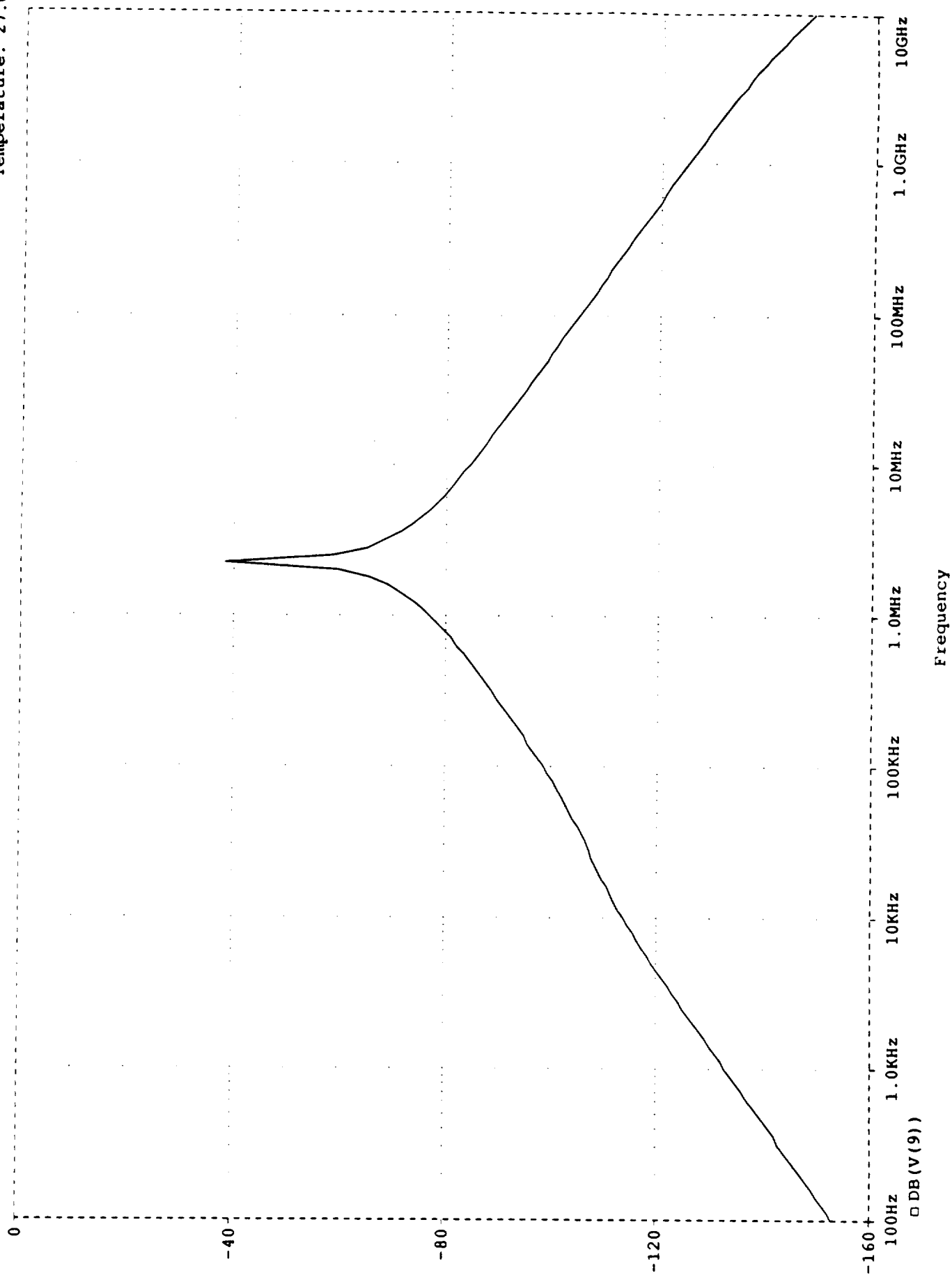


Figure A-13

CALCULATED DIFFERENTIAL MODE VOLTAGE (SEE FIGURE A1 AND TABLES A1 AND A2 FOR CONDITIONS)

Date/Time run: 06/06/91 13:23:08

Temperature: 27.0



Frequency

Figure A-14

CALCULATED DIFFERENTIAL MODE VOLTAGE (SEE FIGURE A1 AND TABLES A1 AND A2 FOR CONDITIONS)

Temperature: 27.0

Date/Time run: 06/06/91 13:23:08

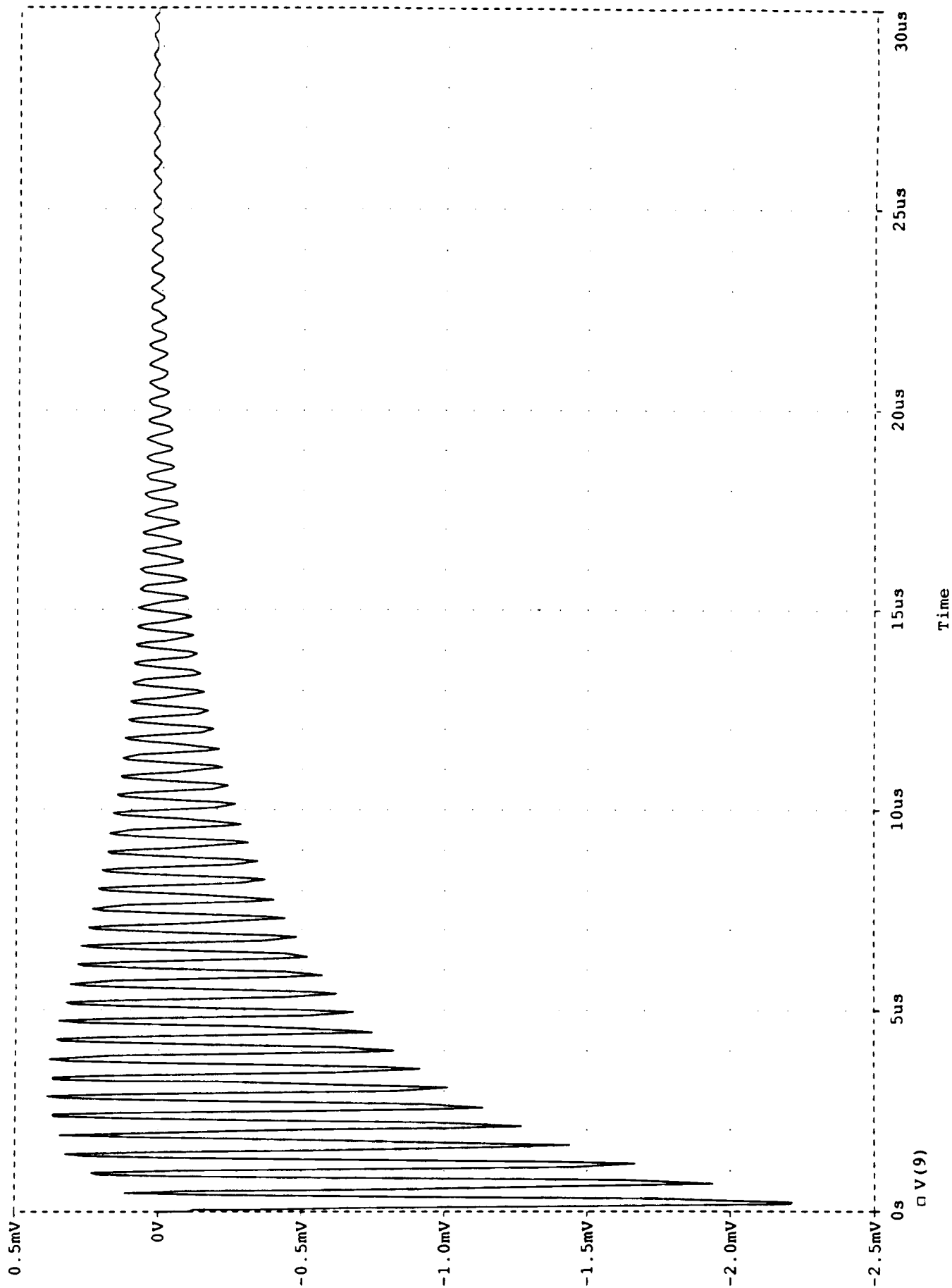


Figure A-15

CALCULATED DIFFERENTIAL MODE VOLTAGE (SEE FIGURE A1 AND TABLES A1 AND A2 FOR CONDITIONS)

Temperature: 27.0

Date/Time run: 06/07/91 08:18:06

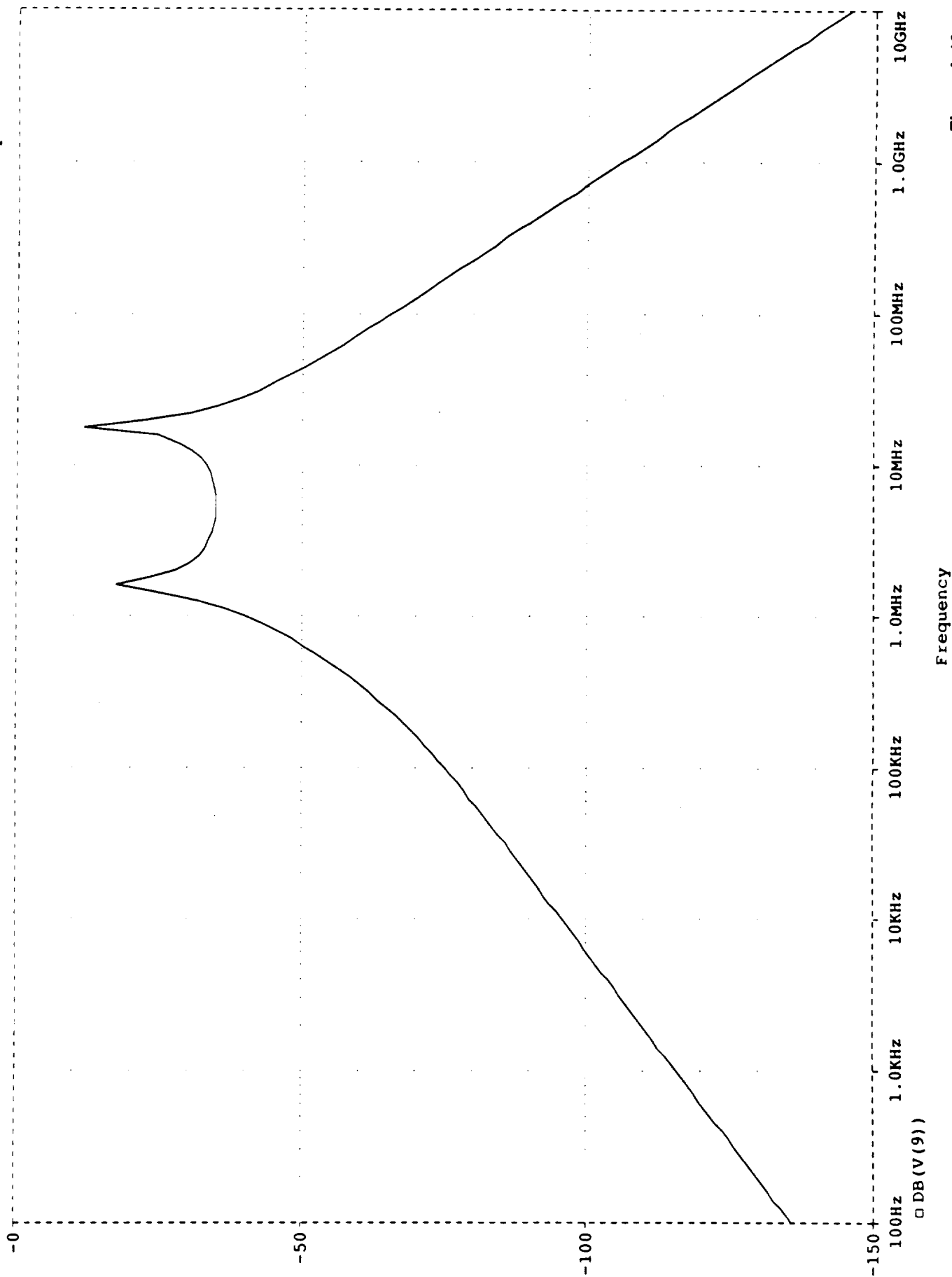


Figure A-16

CALCULATED DIFFERENTIAL MODE VOLTAGE (SEE FIGURE A1 AND TABLES A1 AND A2 FOR CONDITIONS)

Temperature: 27.0

Date/Time run: 06/07/91 08:18:06

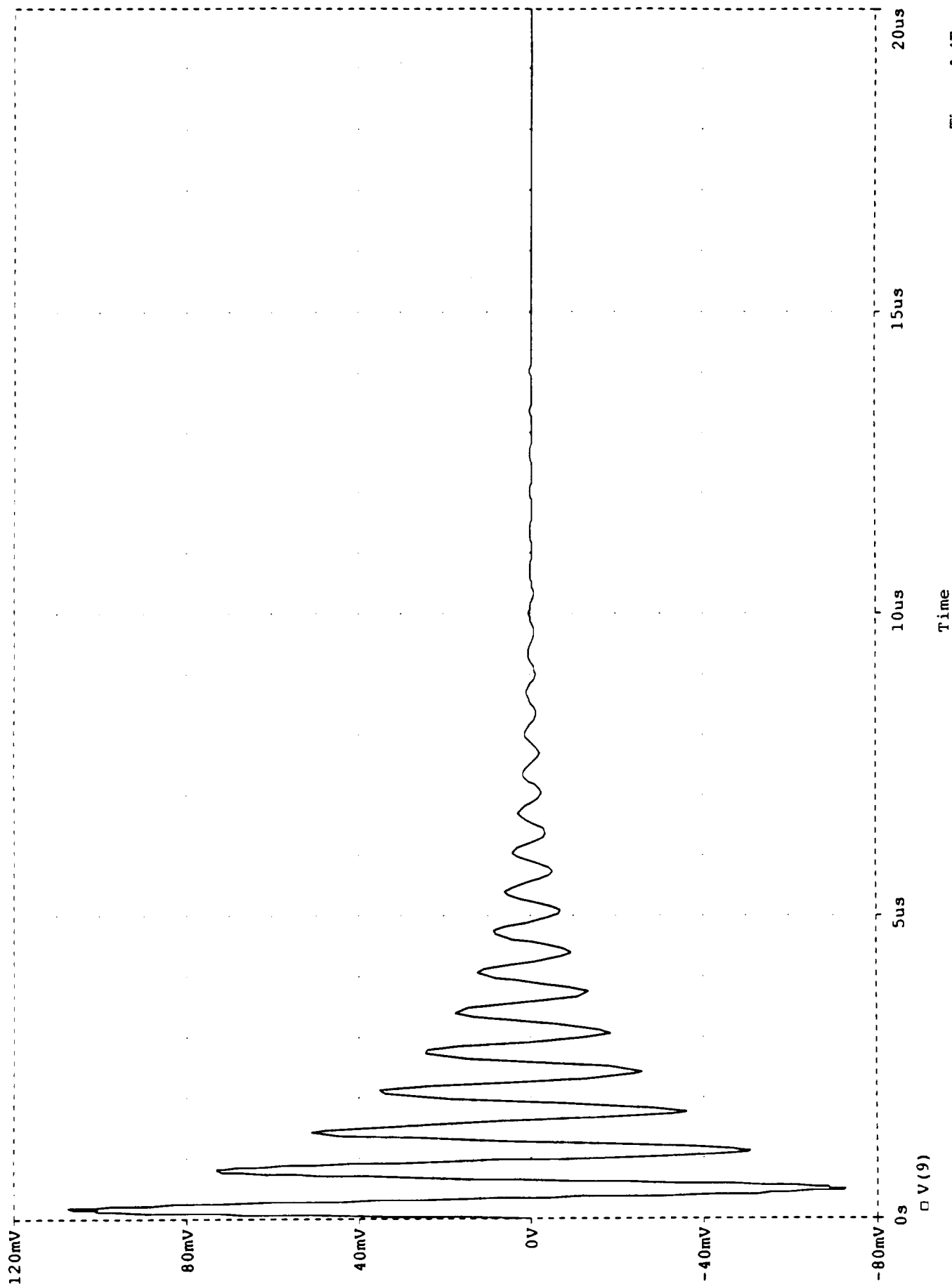


Figure A-17

CALCULATED DIFFERENTIAL MODE VOLTAGE (SEE FIGURE A1 AND TABLES A1 AND A2 FOR CONDITIONS)

Temperature: 27.0

Date/Time run: 06/06/91 13:40:57

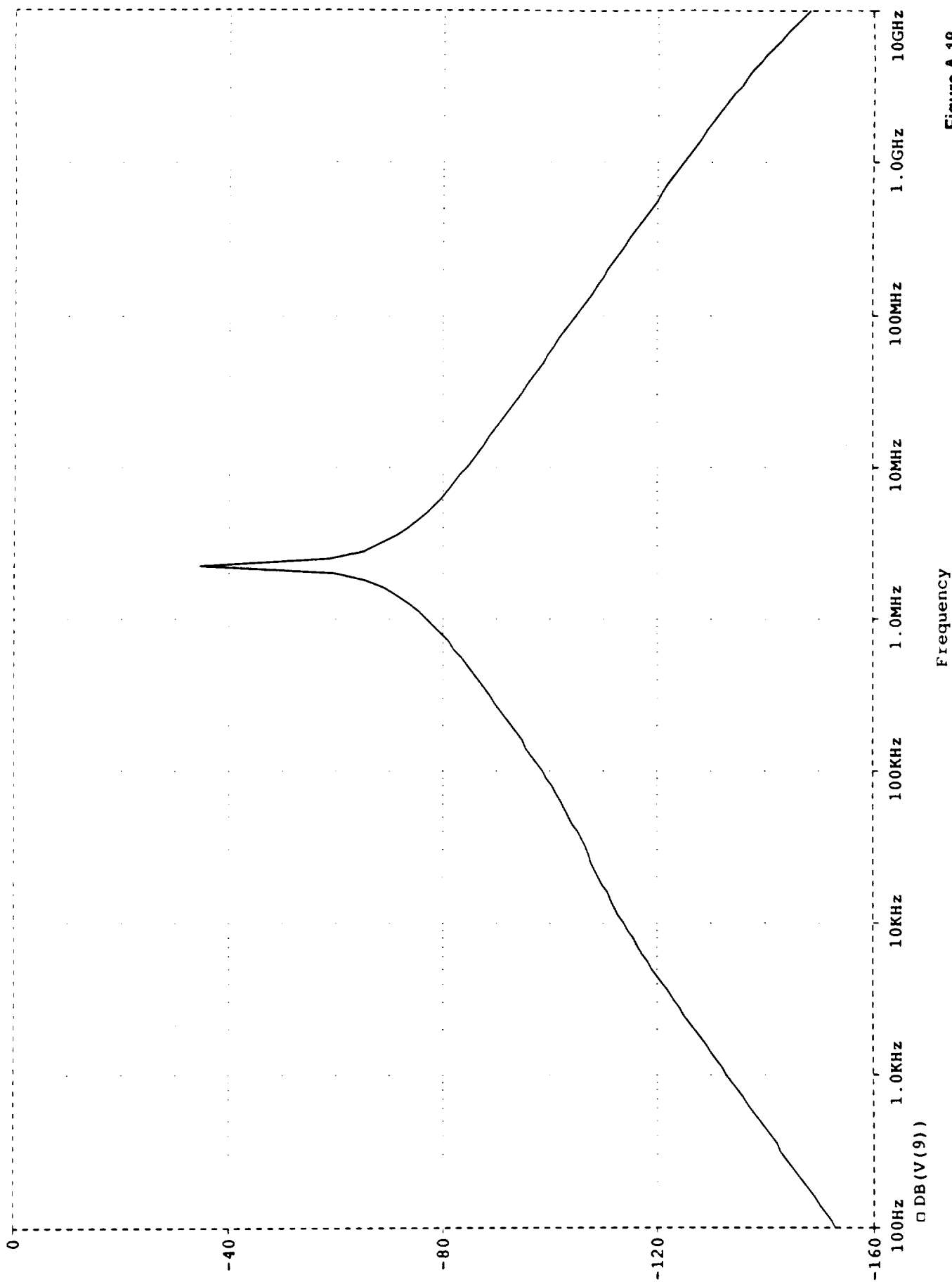


Figure A-18

CALCULATED DIFFERENTIAL MODE VOLTAGE (SEE FIGURE A1 AND TABLES A1 AND A2 FOR CONDITIONS)

Date/Time run: 06/06/91 13:40:57

Temperature: 27.0

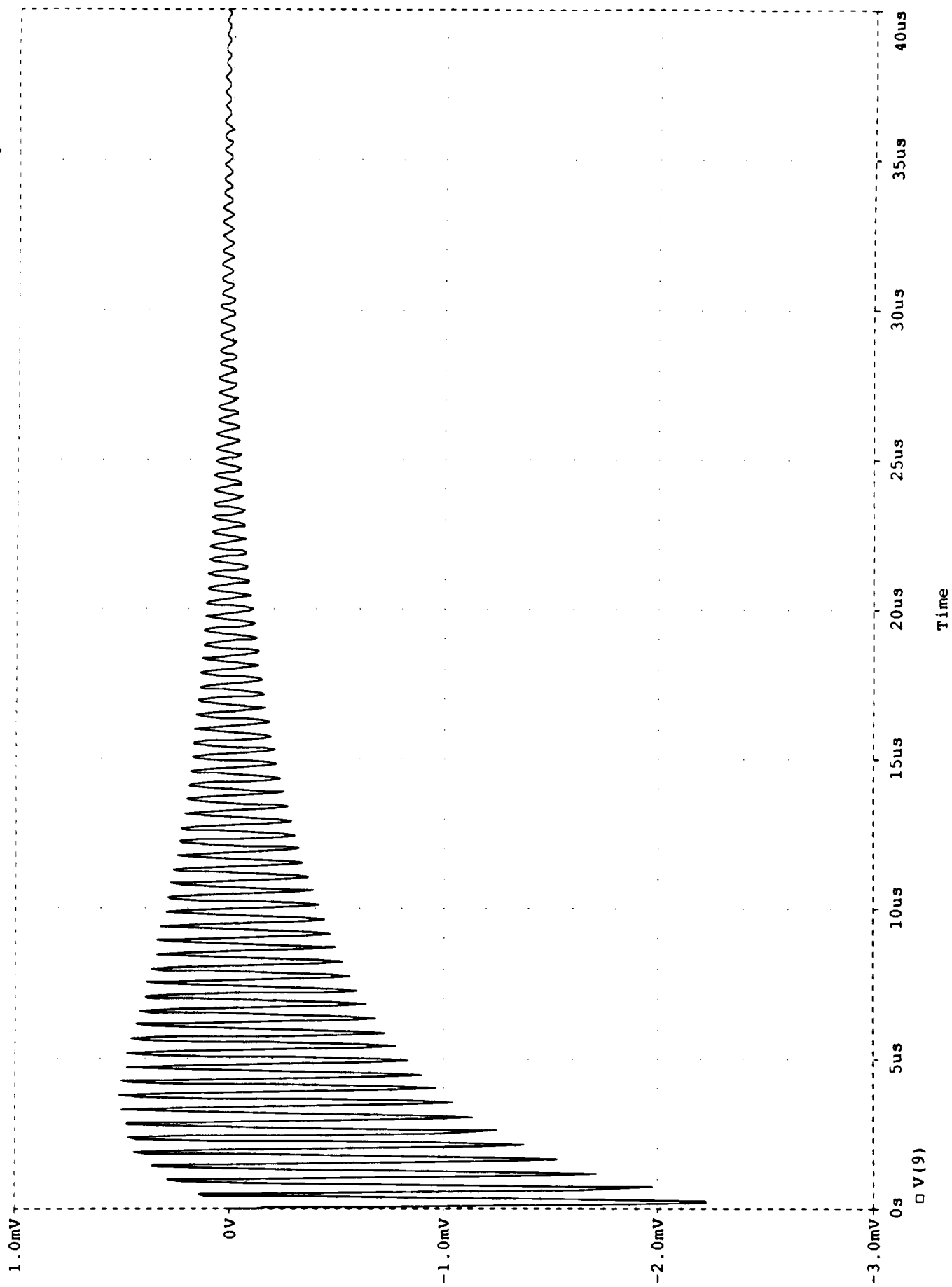


Figure A-19

CALCULATED DIFFERENTIAL MODE VOLTAGE (SEE FIGURE A1 AND TABLES A1 AND A2 FOR CONDITIONS)

Temperature: 27.0

Date/Time run: 06/07/91 08:29:34

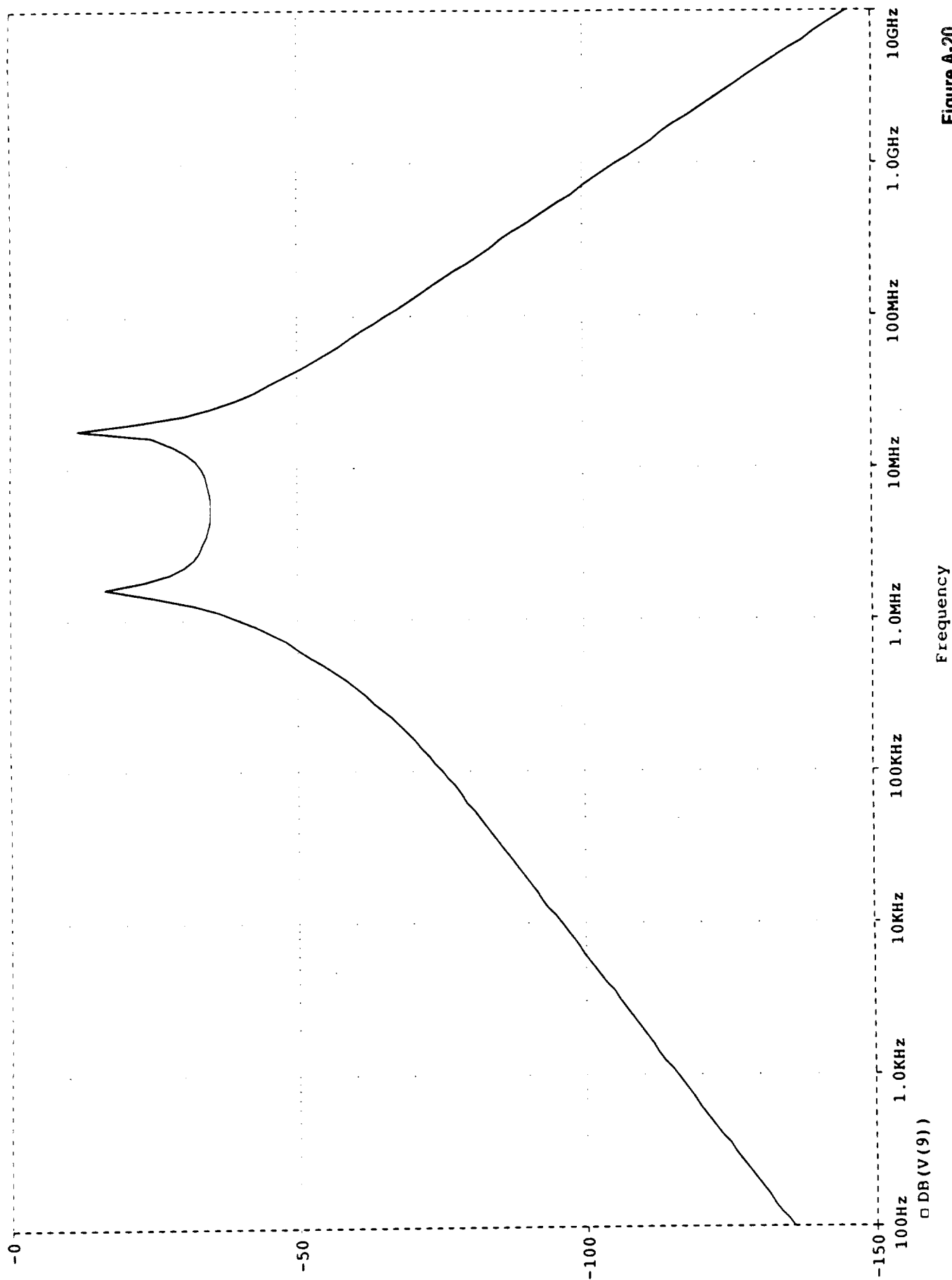


Figure A-20



CALCULATED DIFFERENTIAL MODE VOLTAGE (SEE FIGURE A1 AND TABLES A1 AND A2 FOR CONDITIONS)

Date/Time run: 06/07/91 08:29:34

Temperature: 27.0

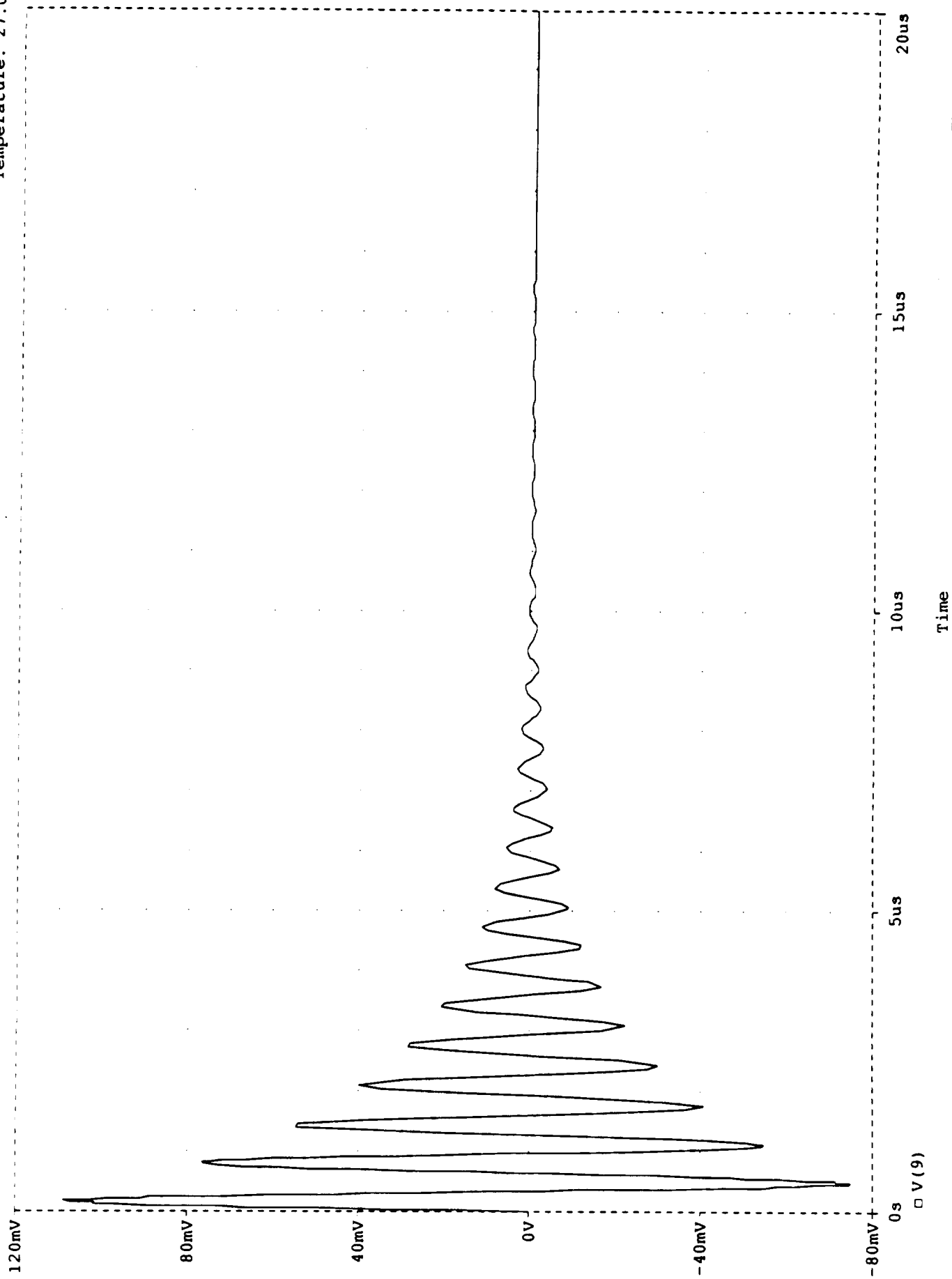
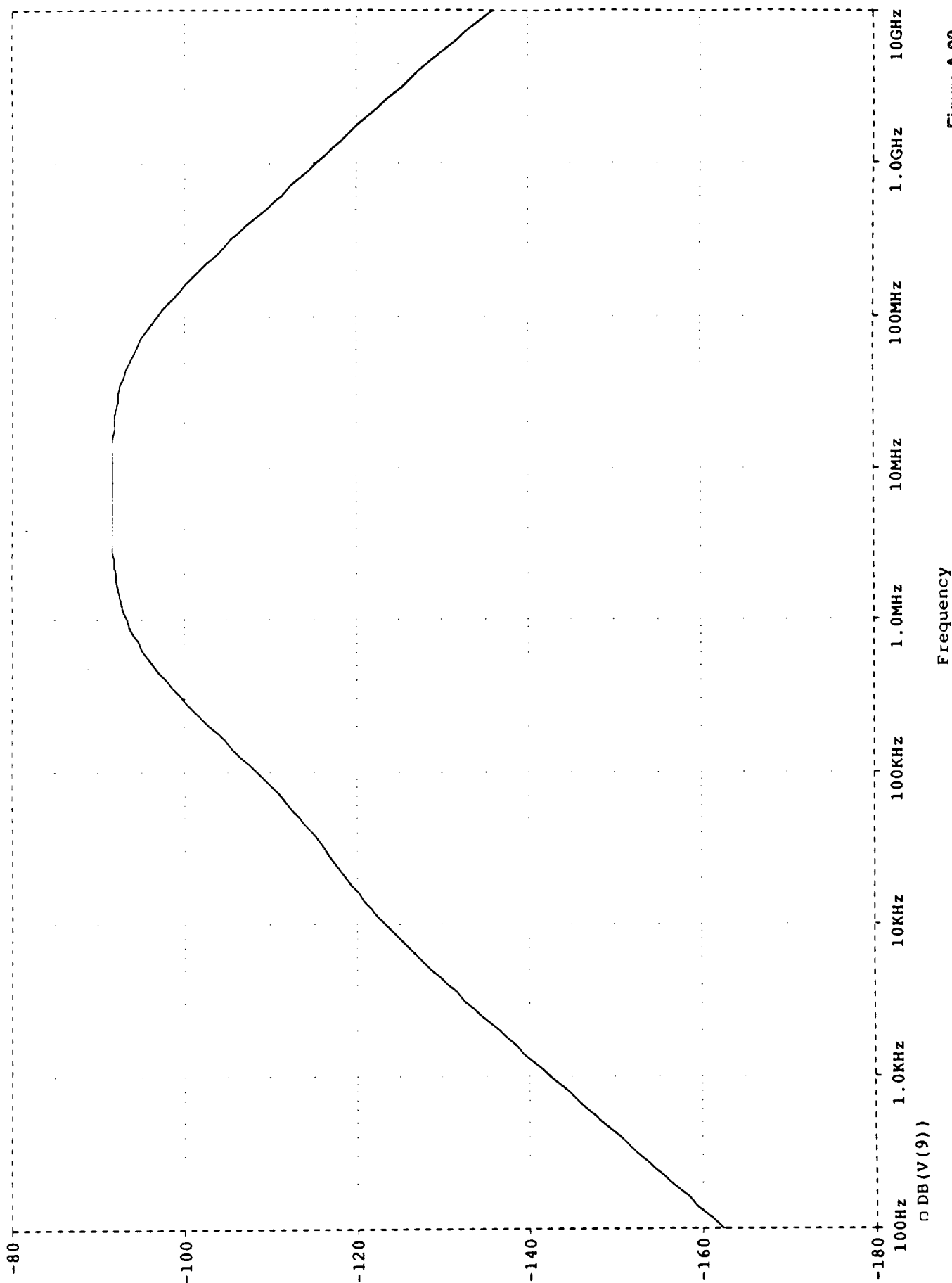


Figure A-2

CALCULATED DIFFERENTIAL MODE VOLTAGE (SEE FIGURE A1 AND TABLES A1 AND A2 FOR CONDITIONS)

Temperature: 27.0

Date/Time run: 06/07/91 09:36:28



Frequency

Figure A-22

CALCULATED DIFFERENTIAL MODE VOLTAGE (SEE FIGURE A1 AND TABLES A1 AND A2 FOR CONDITIONS)

Temperature: 27.0

Date/Time run: 06/07/91 09:36:28

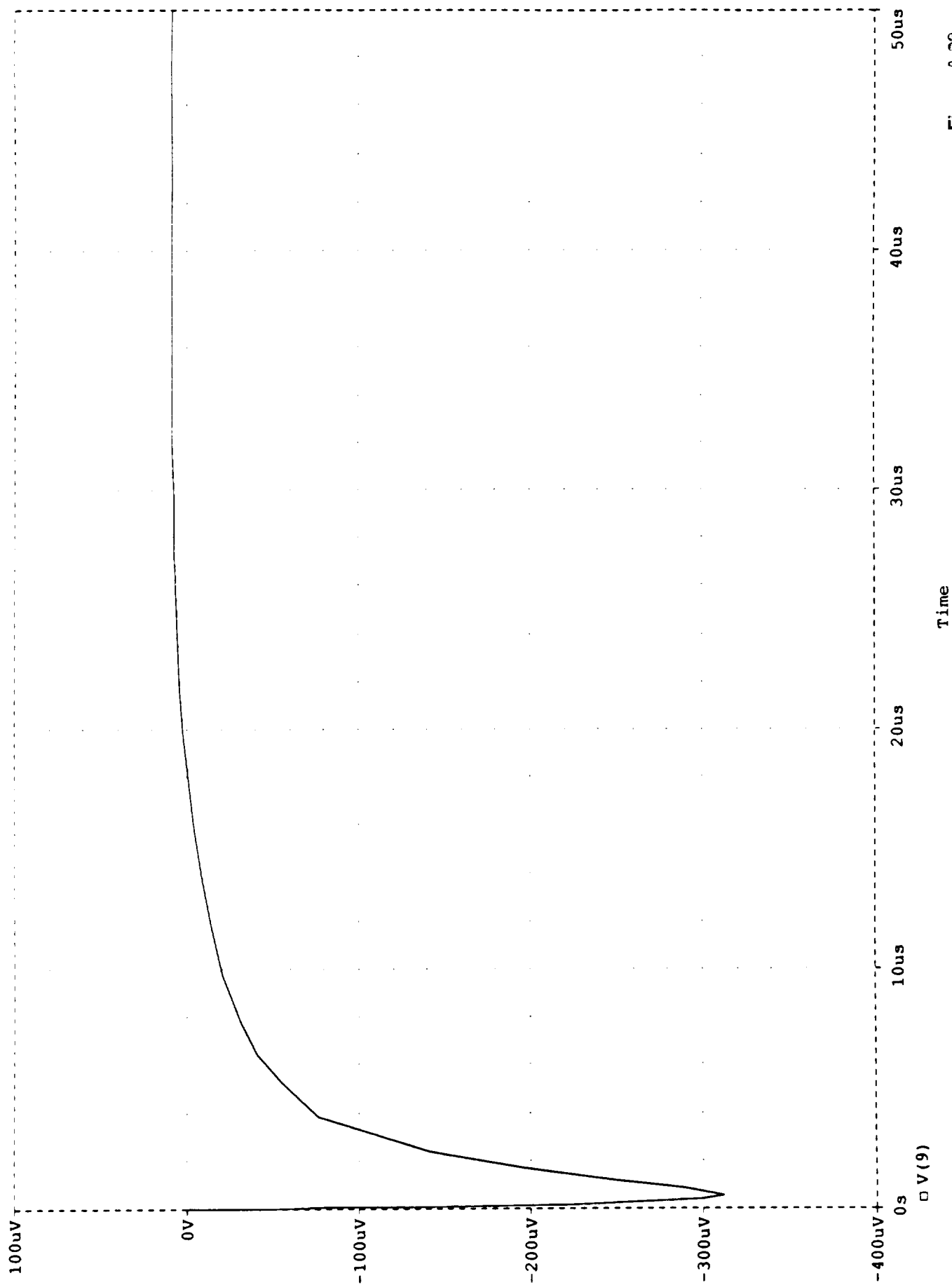
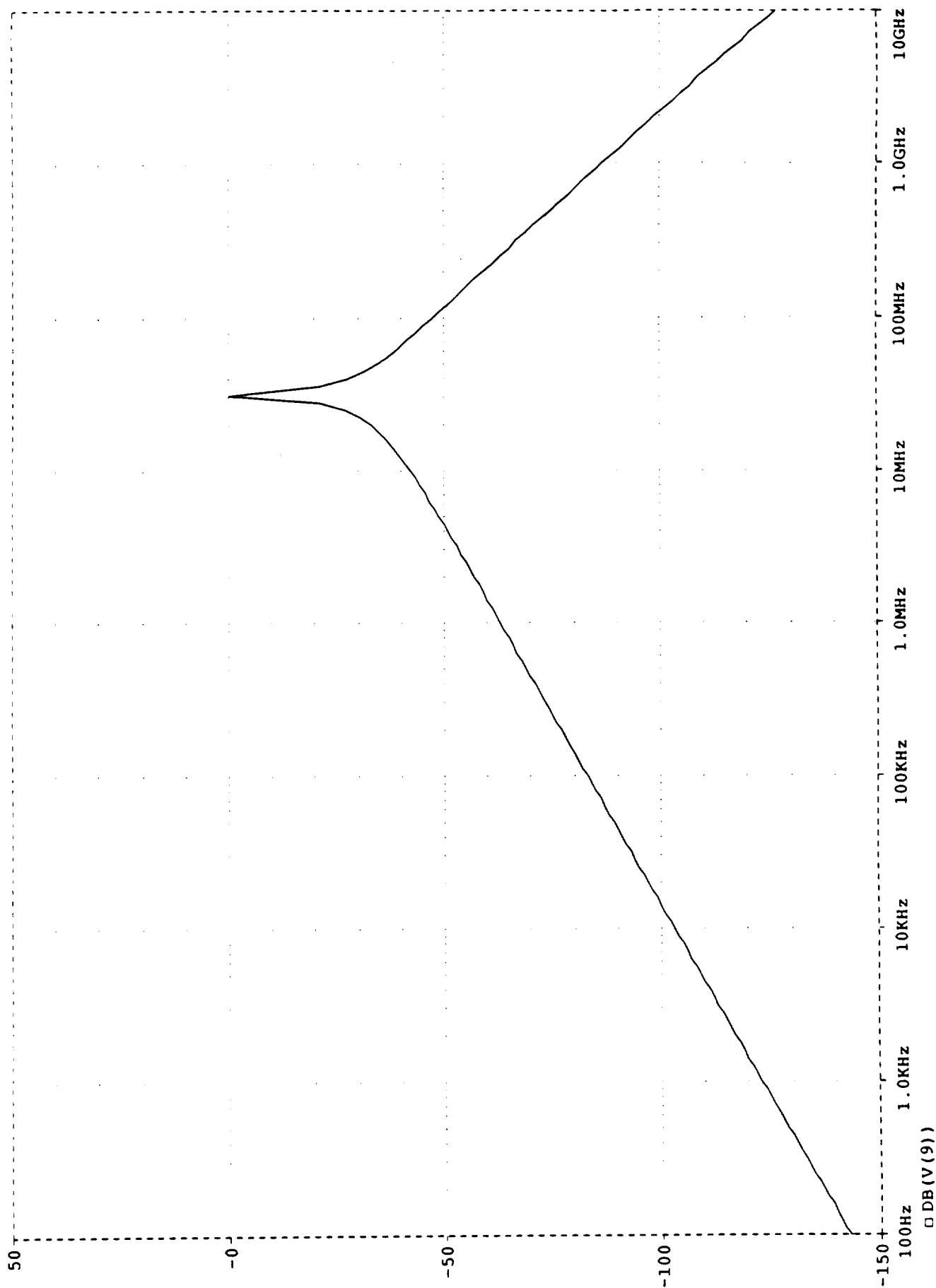


Figure A-23

CALCULATED DIFFERENTIAL MODE VOLTAGE (SEE FIGURE A1 AND TABLES A1 AND A2 FOR CONDITIONS)

Temperature: 27.0

Date/Time run: 06/07/91 11:06:16



Frequency

DB(V(9))

Figure A-24

CALCULATED DIFFERENTIAL MODE VOLTAGE (SEE FIGURE A1 AND TABLES A1 AND A2 FOR CONDITIONS)

Temperature: 27.0

Date/Time run: 06/07/91 11:06:16

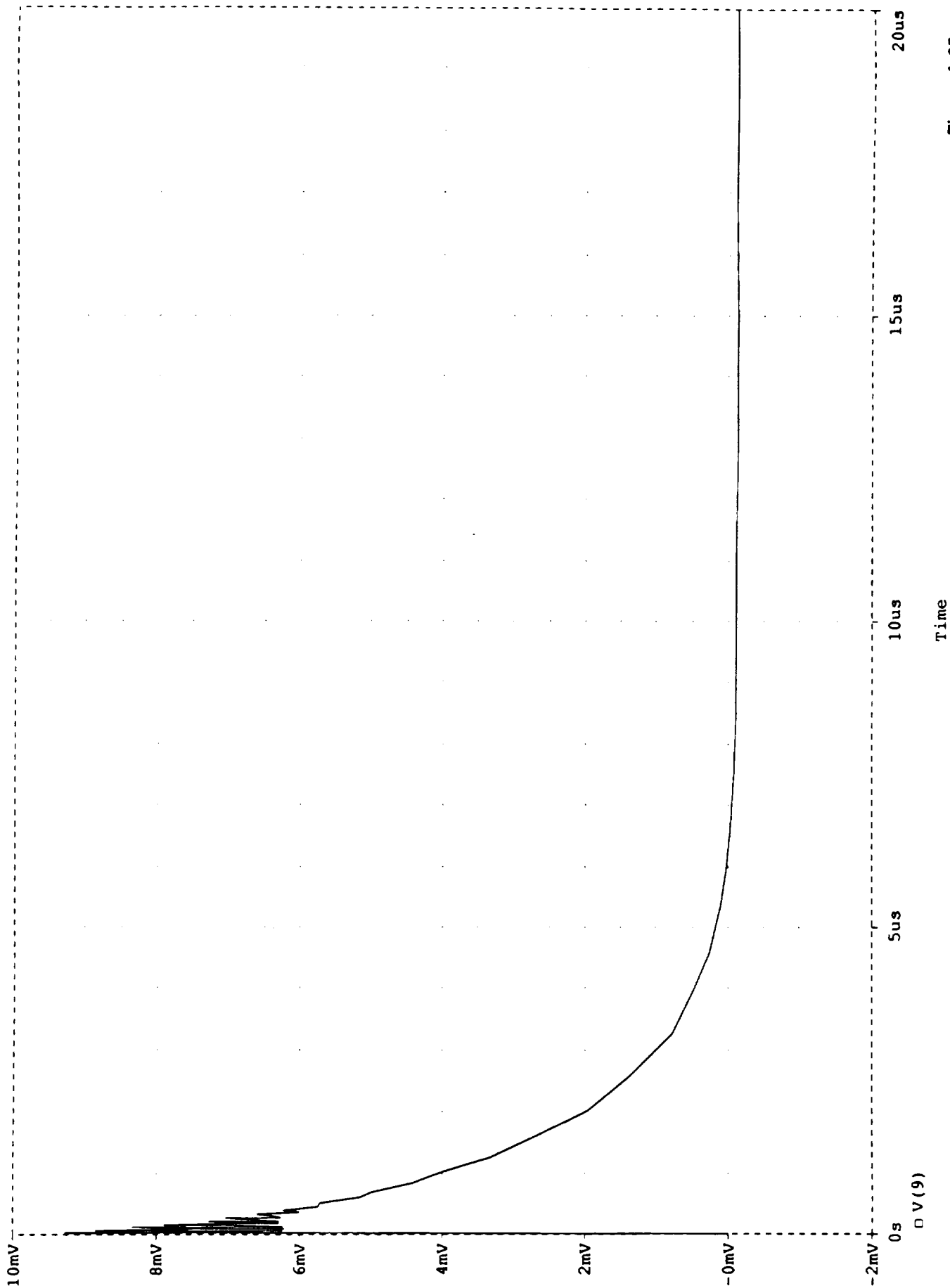


Figure A-25

CALCULATED DIFFERENTIAL MODE VOLTAGE (SEE FIGURE A1 AND TABLES A1 AND A2 FOR CONDITIONS)

Temperature: 27.0

Date/Time run: 06/07/91 09:47:39



Frequency

□ DB (V (9) )

Figure A-26

CALCULATED DIFFERENTIAL MODE VOLTAGE (SEE FIGURE A1 AND TABLES A1 AND A2 FOR CONDITIONS)

Temperature: 27.0

Date/Time run: 06/07/91 09:47:39

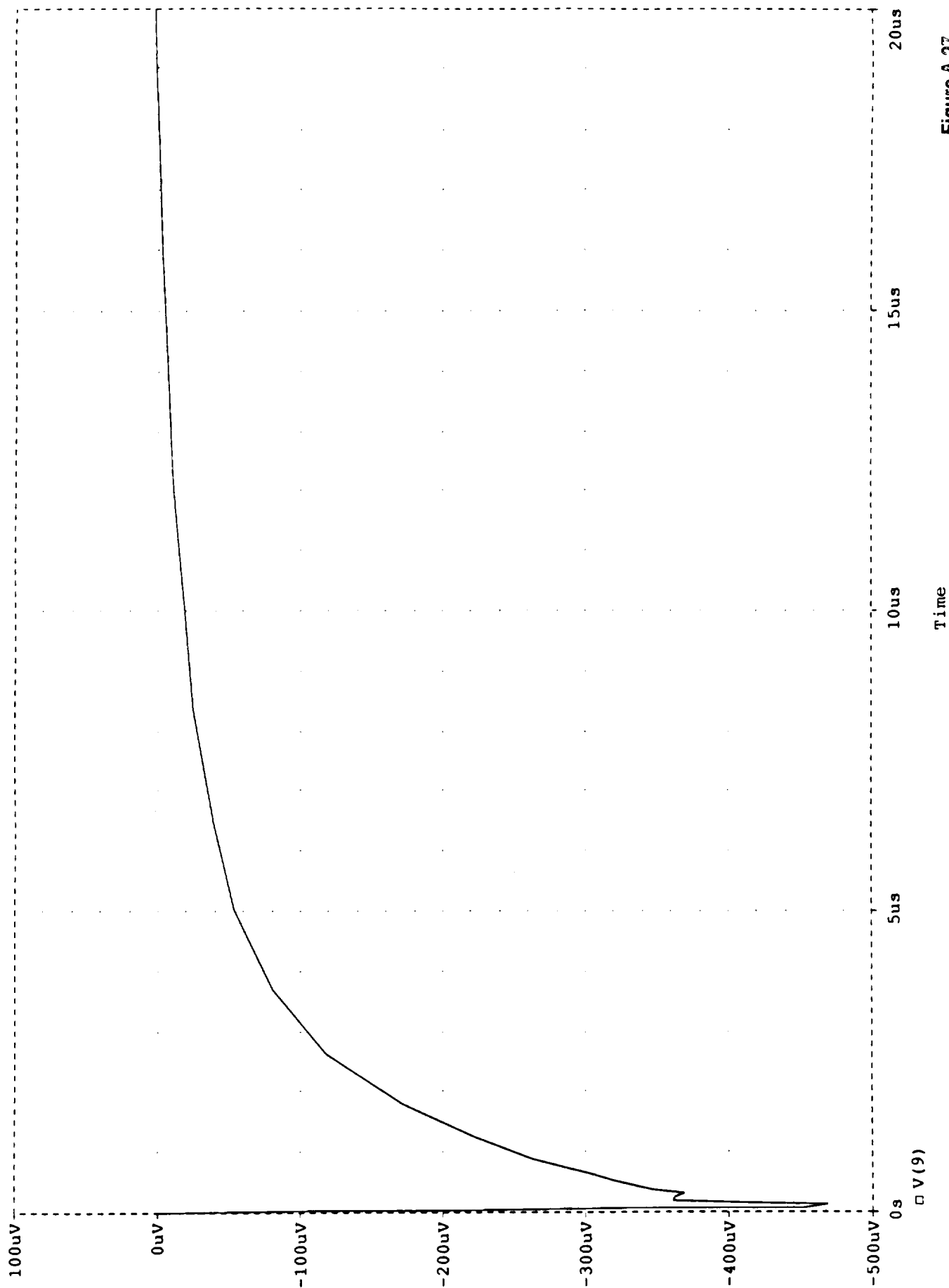


Figure A-27

CALCULATED DIFFERENTIAL MODE VOLTAGE (SEE FIGURE A1 AND TABLES A1 AND A2 FOR CONDITIONS)

Date/Time run: 06/07/91 12:17:44

Temperature: 27.0

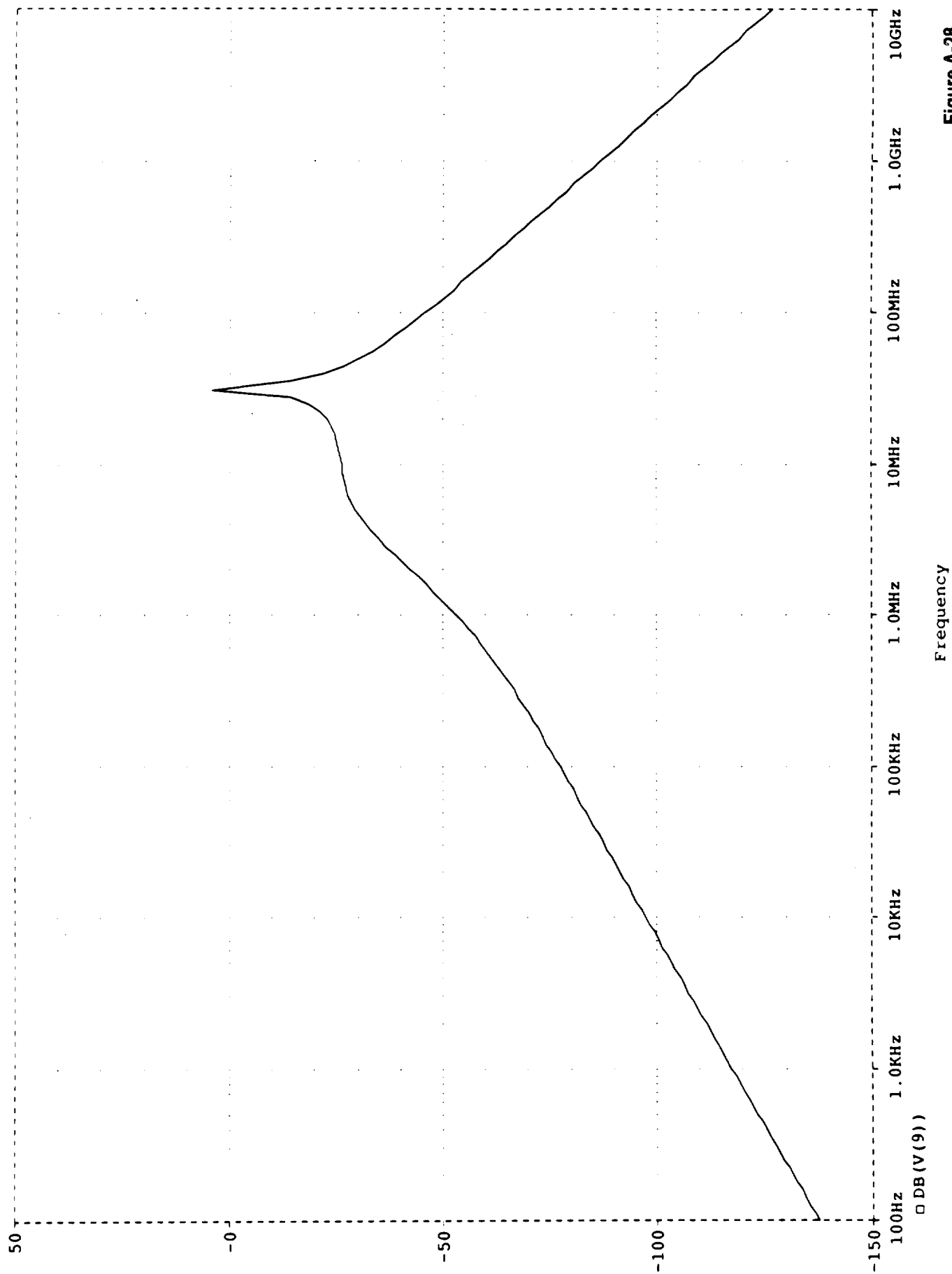


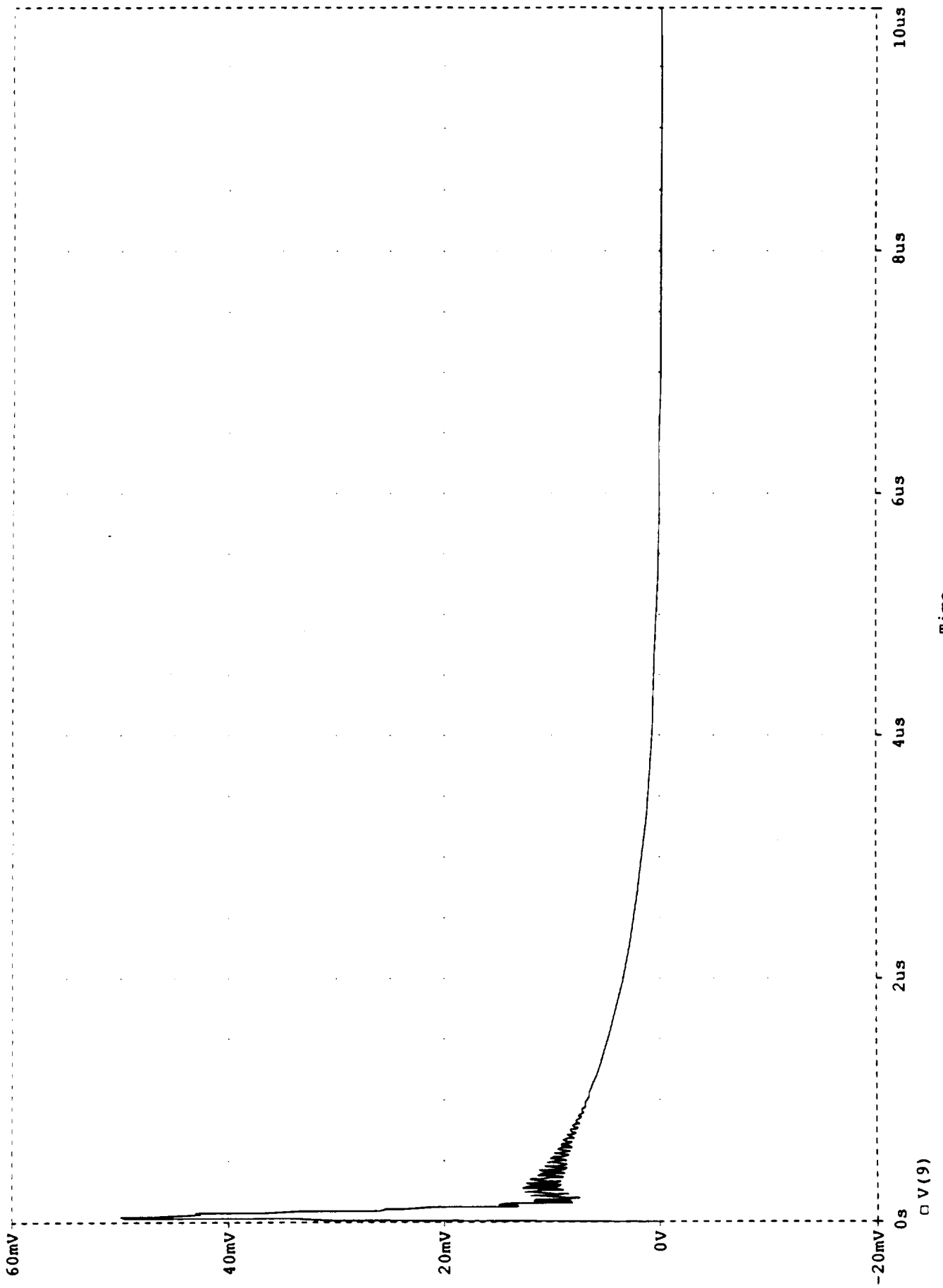
Figure A-28



CALCULATED DIFFERENTIAL MODE VOLTAGE (SEE FIGURE A1 AND TABLES A1 AND A2 FOR CONDITIONS)

Temperature: 27.0

Date/Time run: 06/07/91 12:17:44



Time

Figure A-29

CALCULATED DIFFERENTIAL MODE VOLTAGE (SEE FIGURE A1 AND TABLES A1 AND A2 FOR CONDITIONS)

Date/Time run: 06/07/91 10:10:20

Temperature: 27.0

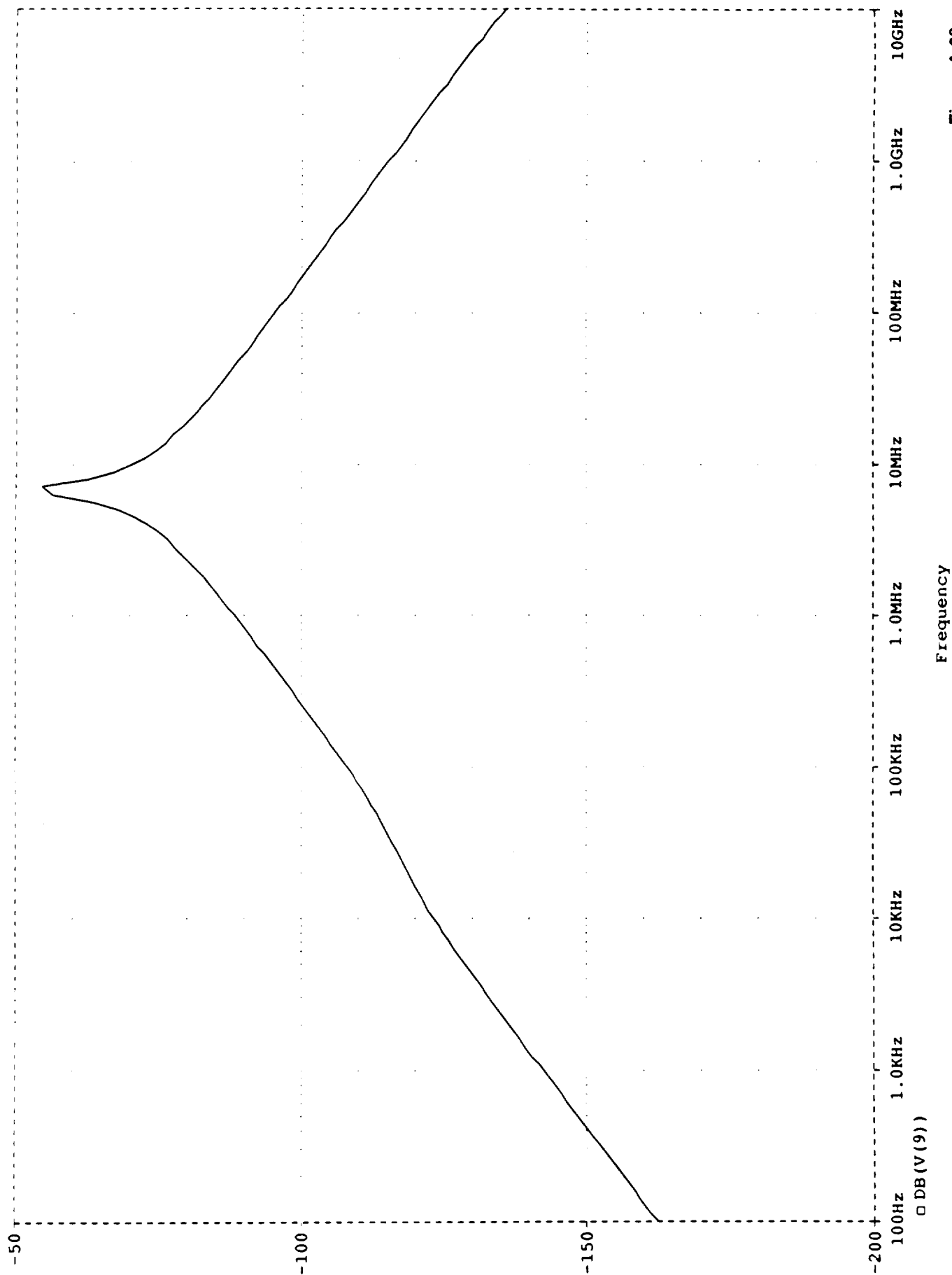


Figure A-30

CALCULATED DIFFERENTIAL MODE VOLTAGE (SEE FIGURE A1 AND TABLES A1 AND A2 FOR CONDITIONS)

Date/Time run: 06/07/91 10:10:20

Temperature: 27.0

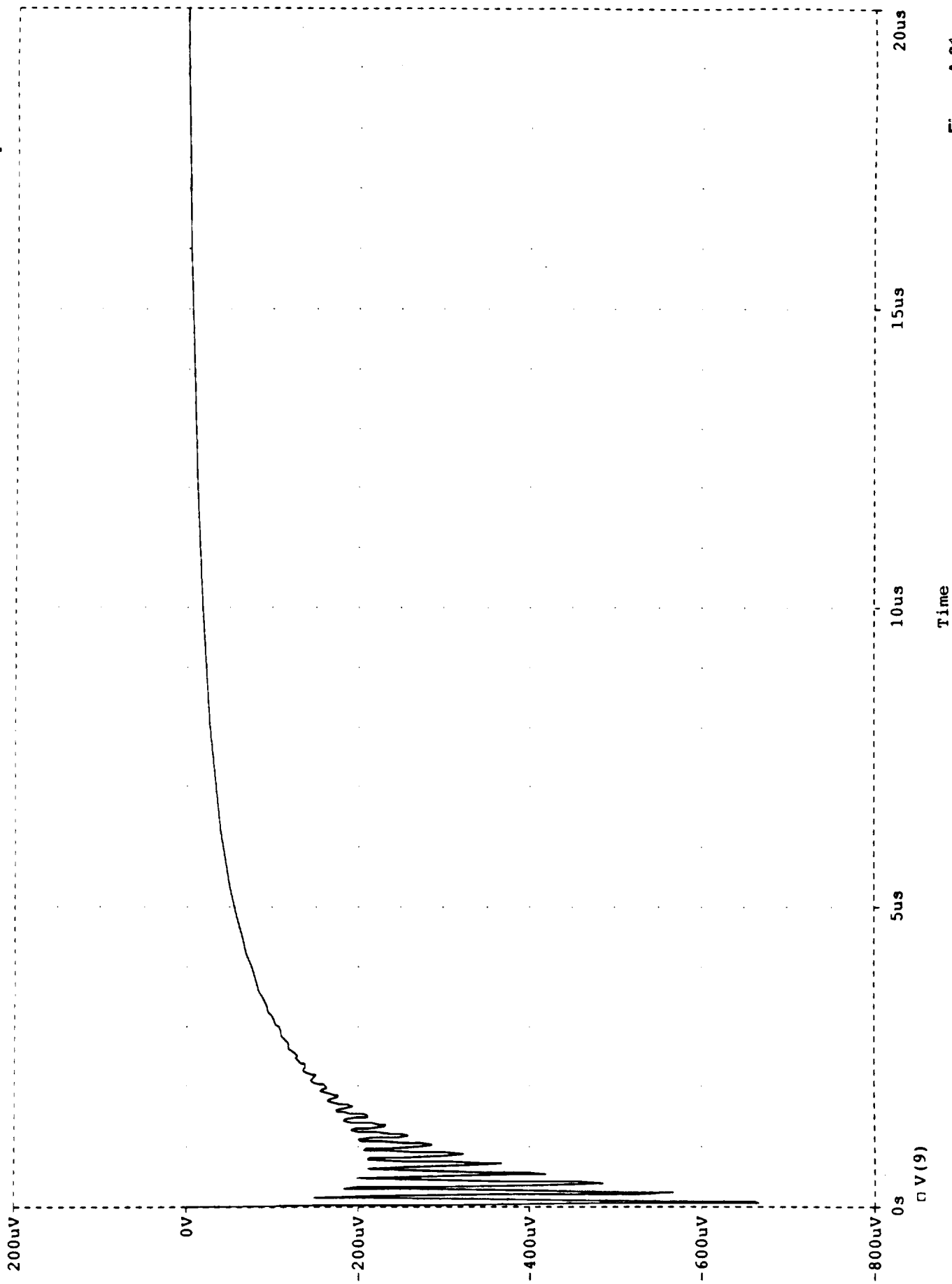
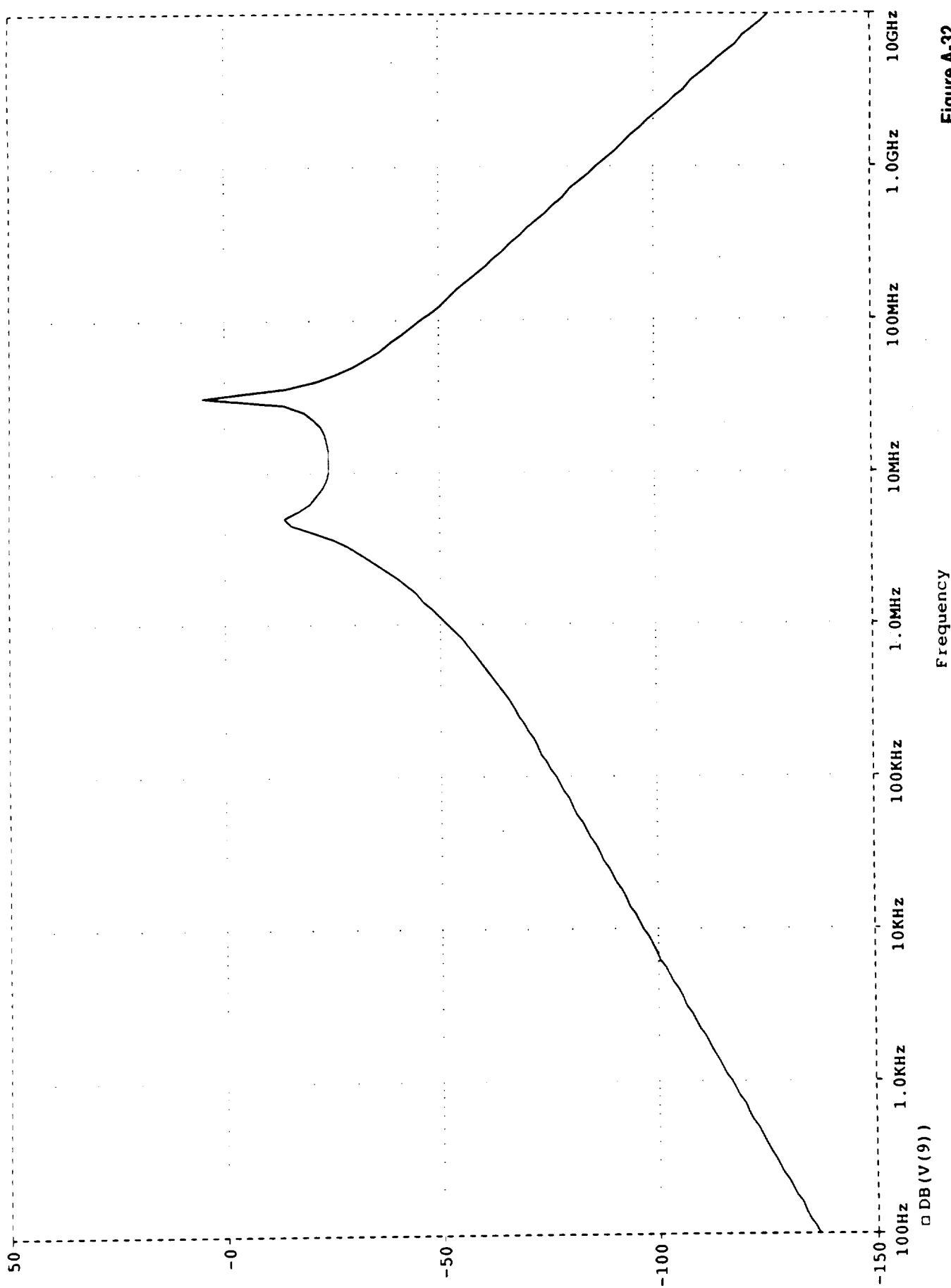


Figure A-31

# CALCULATED DIFFERENTIAL MODE VOLTAGE (SEE FIGURE A1 AND TABLES A1 AND A2 FOR CONDITIONS)

Temperature: 27.0

Date/Time run: 06/07/91 12:29:37



Frequency

Figure A-32

CALCULATED DIFFERENTIAL MODE VOLTAGE (SEE FIGURE A1 AND TABLES A1 AND A2 FOR CONDITIONS)

Temperature: 27.0

Date/Time run: 06/07/91 12:29:37

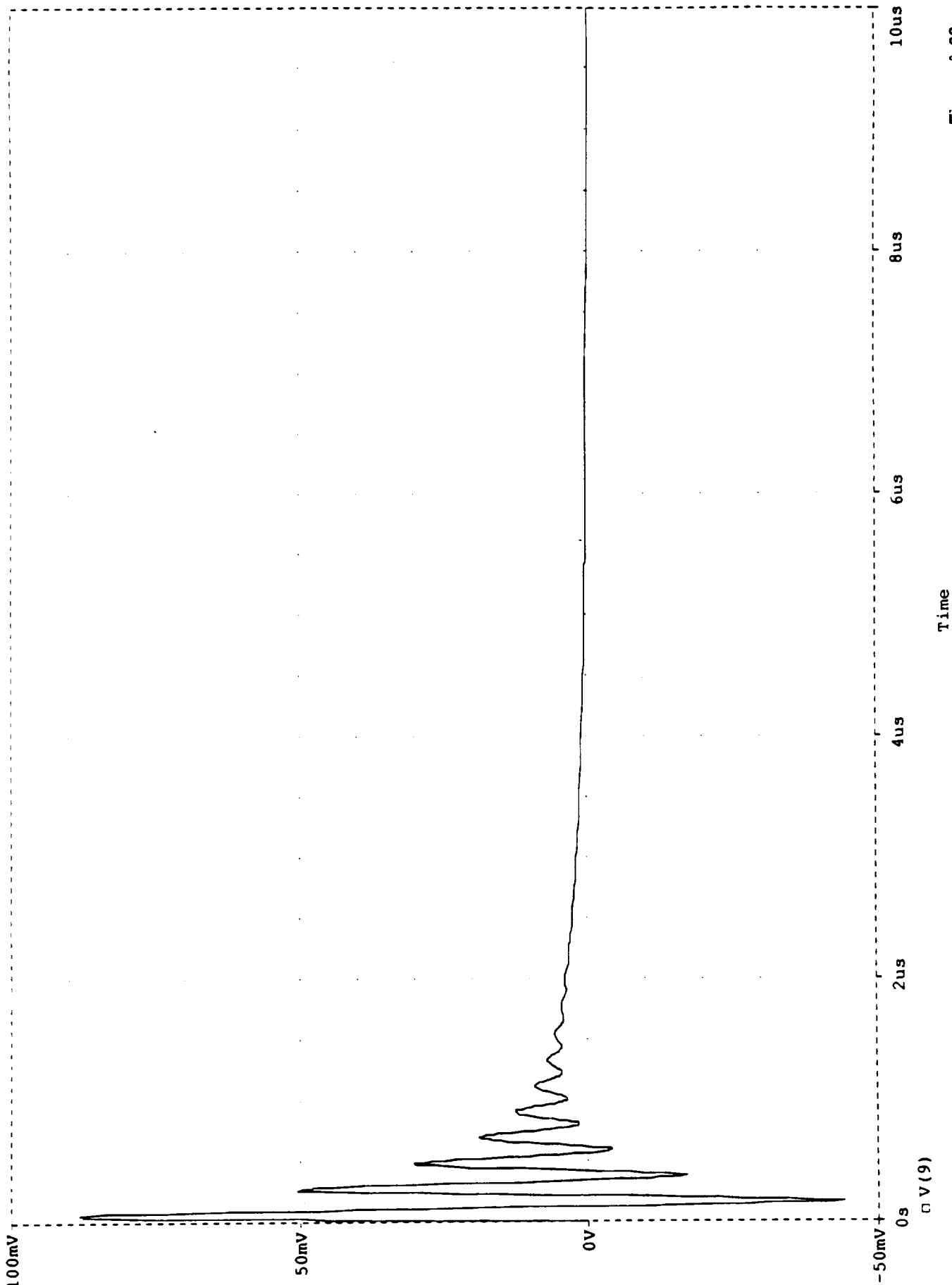
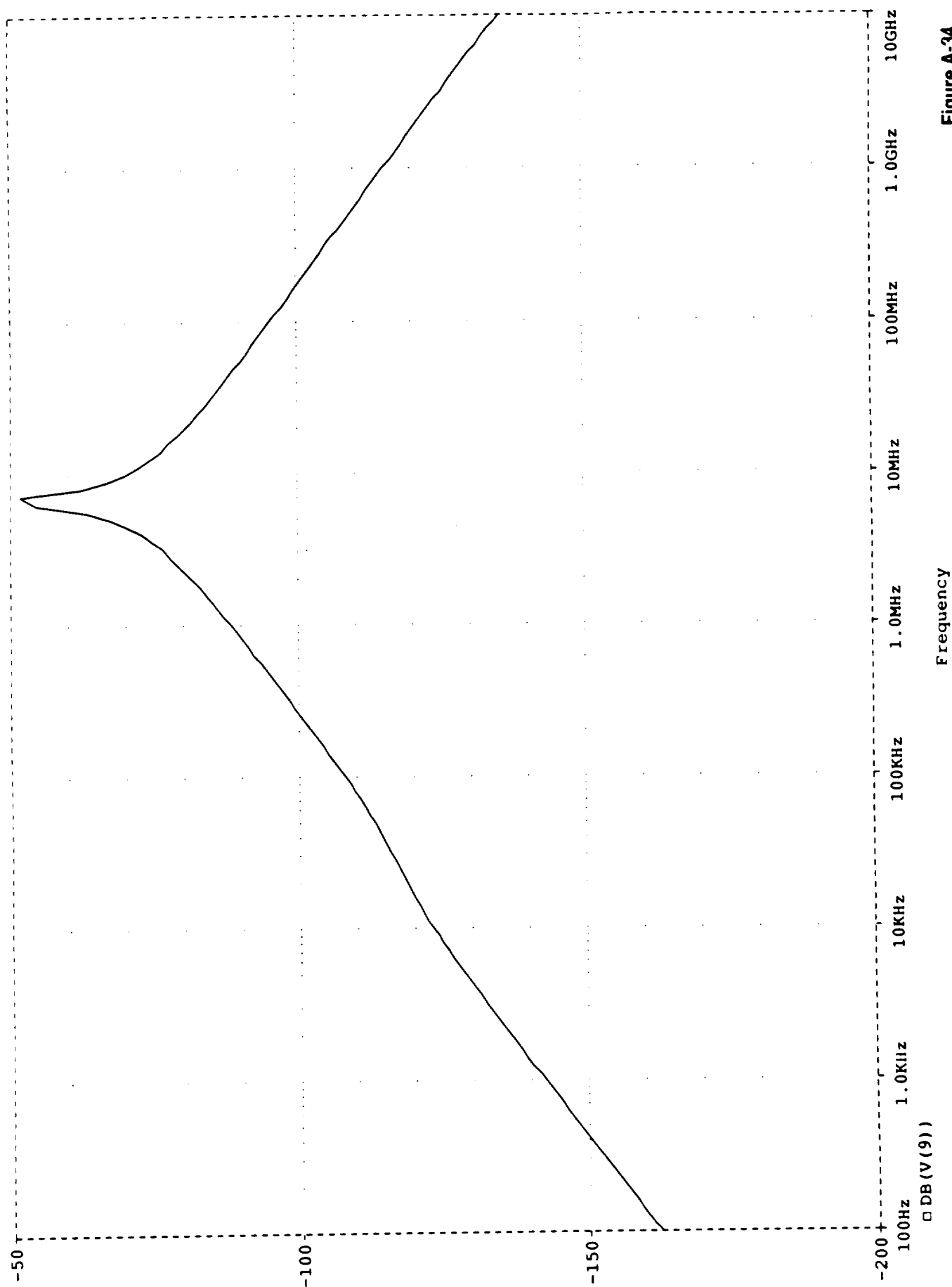


Figure A-33

# CALCULATED DIFFERENTIAL MODE VOLTAGE (SEE FIGURE A1 AND TABLES A1 AND A2 FOR CONDITIONS)

Temperature: 27.0

Date/Time run: 06/07/91 10:29:25



Frequency

DB(V(9))

Figure A-34

CALCULATED DIFFERENTIAL MODE VOLTAGE (SEE FIGURE A1 AND TABLES A1 AND A2 FOR CONDITIONS)

Temperature: 27.0

Date/Time run: 06/07/91 10:29:25

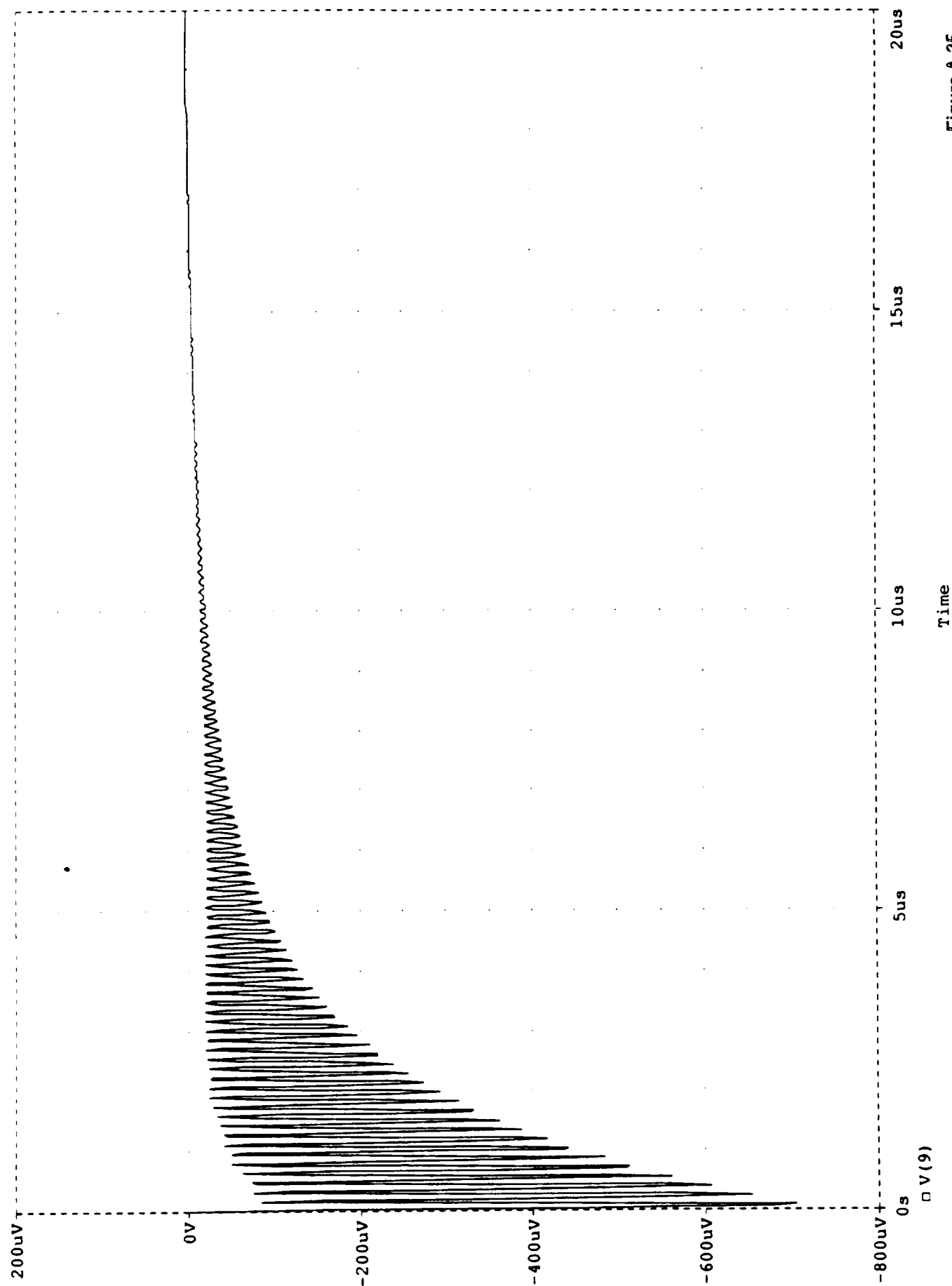


Figure A-35

CALCULATED DIFFERENTIAL MODE VOLTAGE (SEE FIGURE A1 AND TABLES A1 AND A2 FOR CONDITIONS)

Date/Time run: 06/07/91 12:39:14 Temperature: 27.0

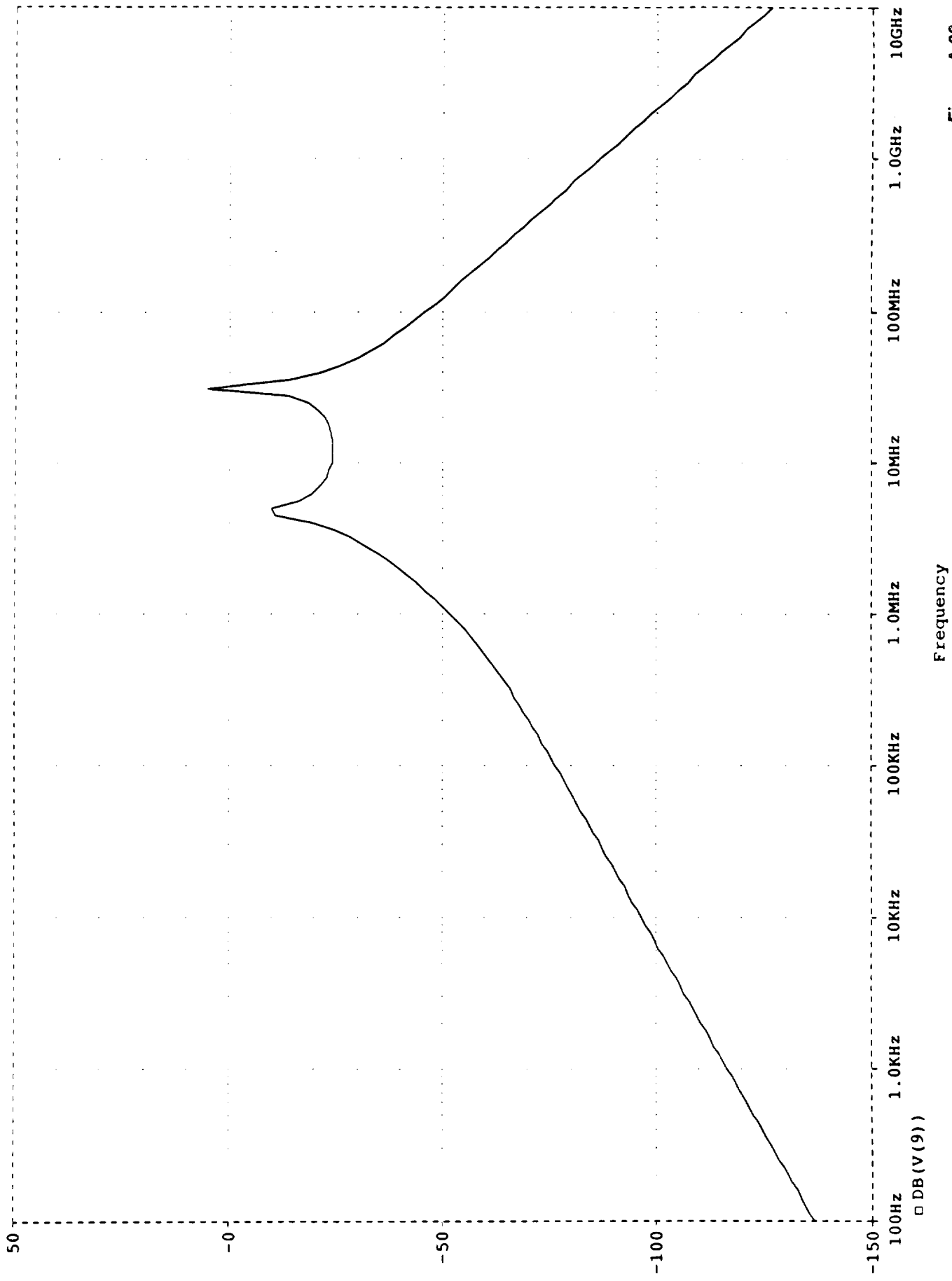


Figure A-36



CALCULATED DIFFERENTIAL MODE VOLTAGE (SEE FIGURE A1 AND TABLES A1 AND A2 FOR CONDITIONS)  
Temperature: 27.0

Date/Time run: 06/07/91 12:39:14

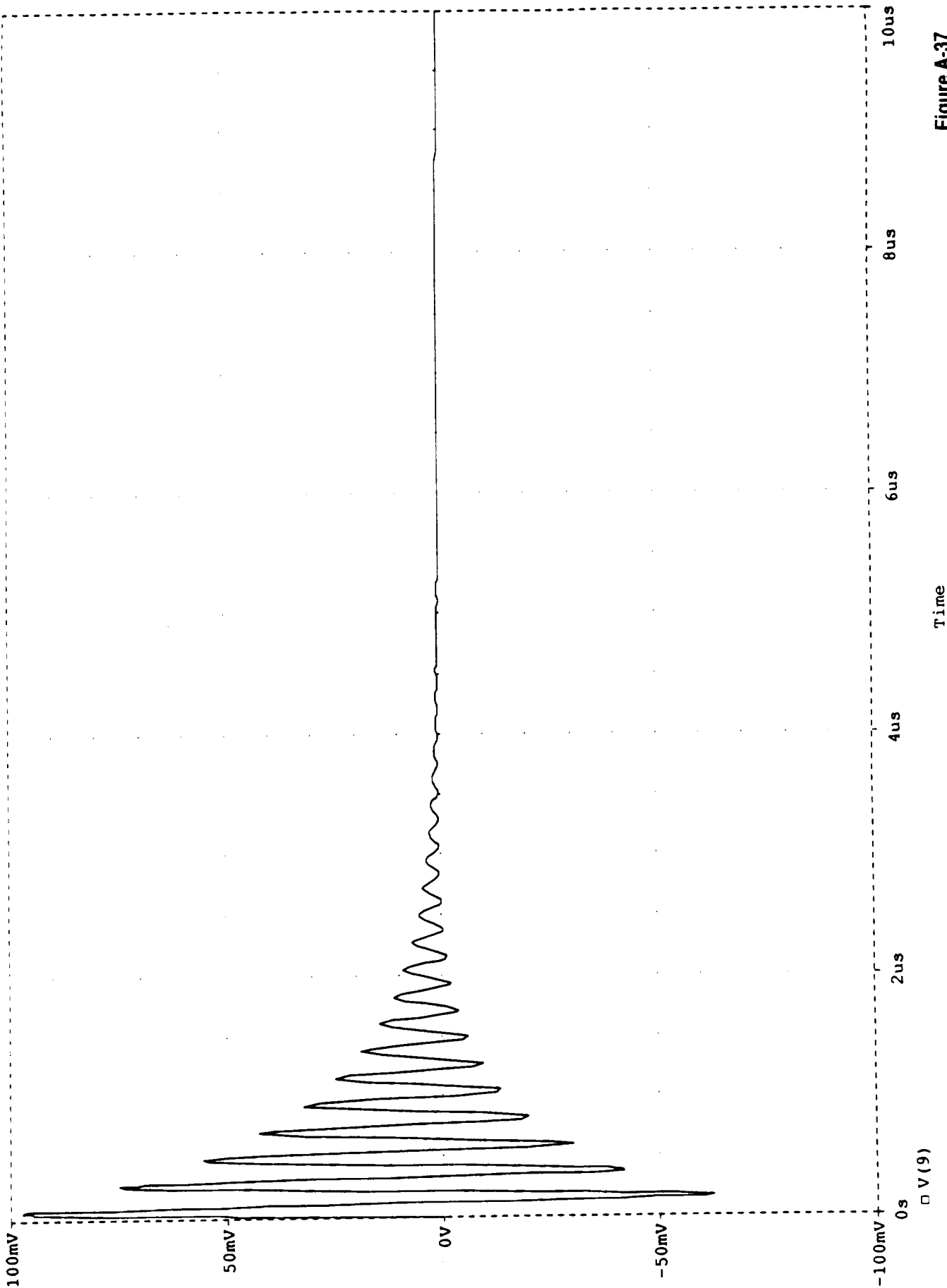


Figure A-37

CALCULATED DIFFERENTIAL MODE VOLTAGE (SEE FIGURE A1 AND TABLES A1 AND A2 FOR CONDITIONS)

Date/Time run: 06/07/91 10:48:47

Temperature: 27.0

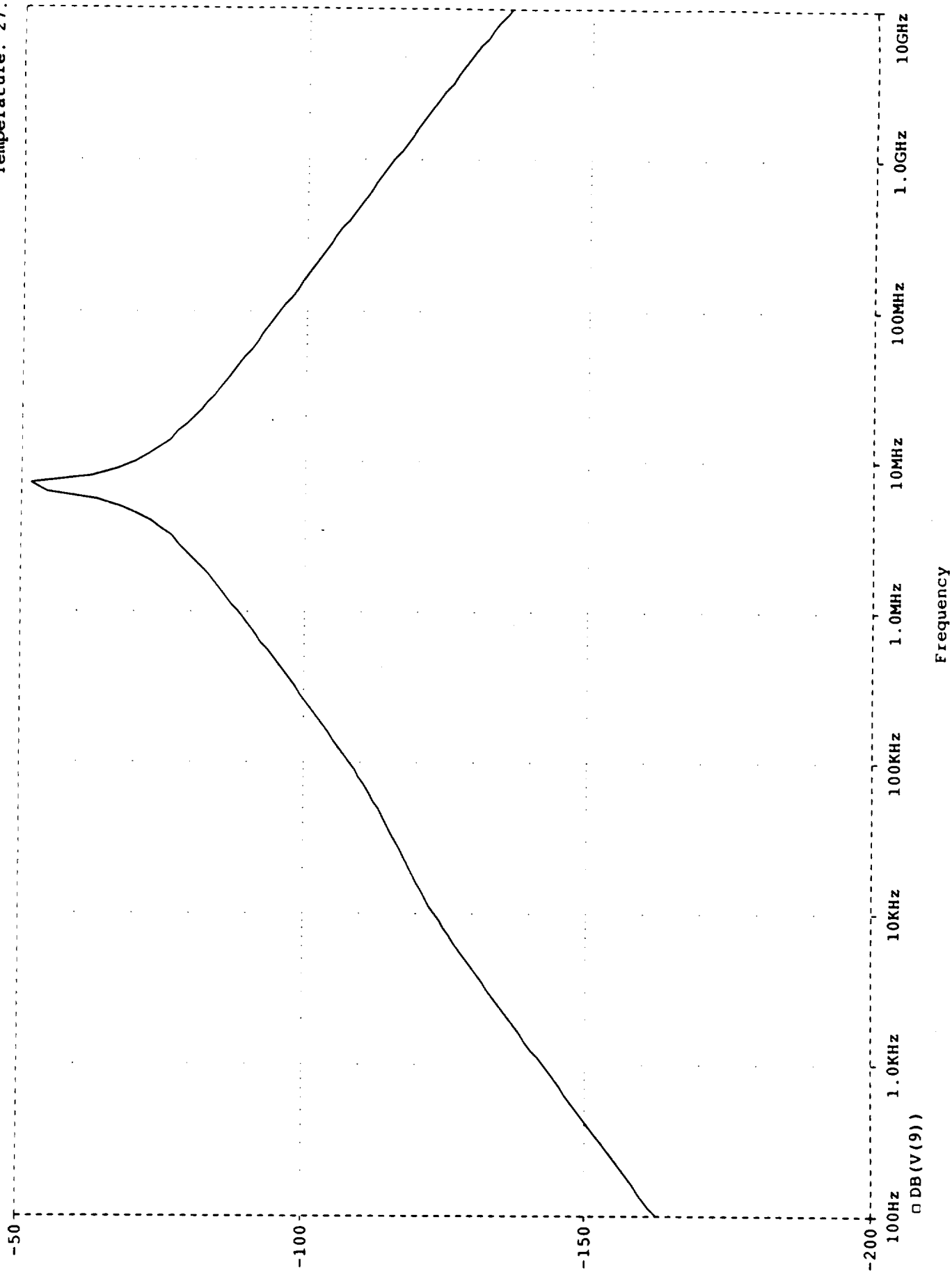


Figure A-38

CALCULATED DIFFERENTIAL MODE VOLTAGE (SEE FIGURE A1 AND TABLES A1 AND A2 FOR CONDITIONS)

Temperature: 27.0

Date/Time run: 06/07/91 10:48:47

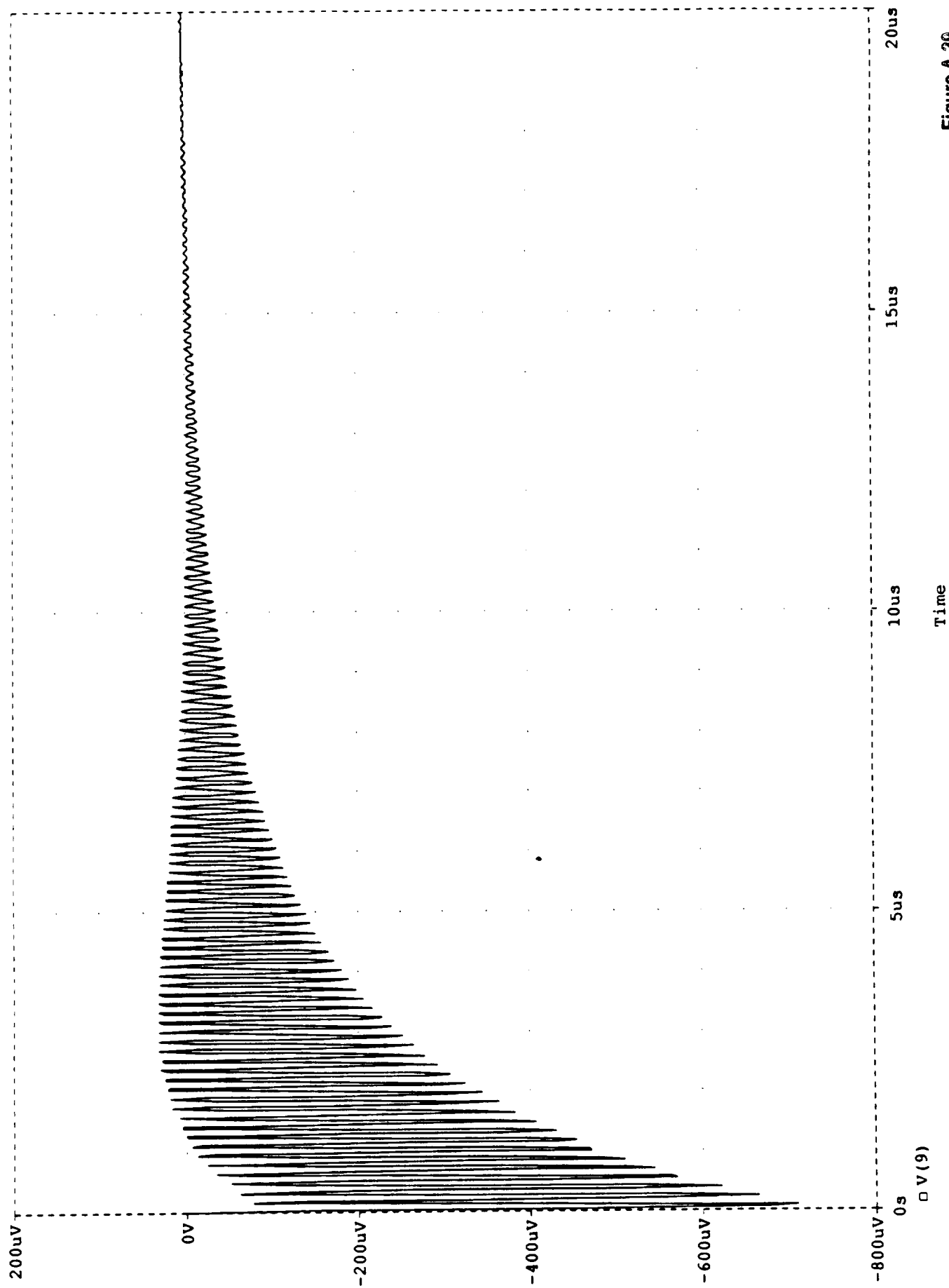


Figure A-39

CALCULATED DIFFERENTIAL MODE VOLTAGE (SEE FIGURE A1 AND TABLES A1 AND A2 FOR CONDITIONS)

Date/Time run: 06/07/91 12:50:03

Temperature: 27.0

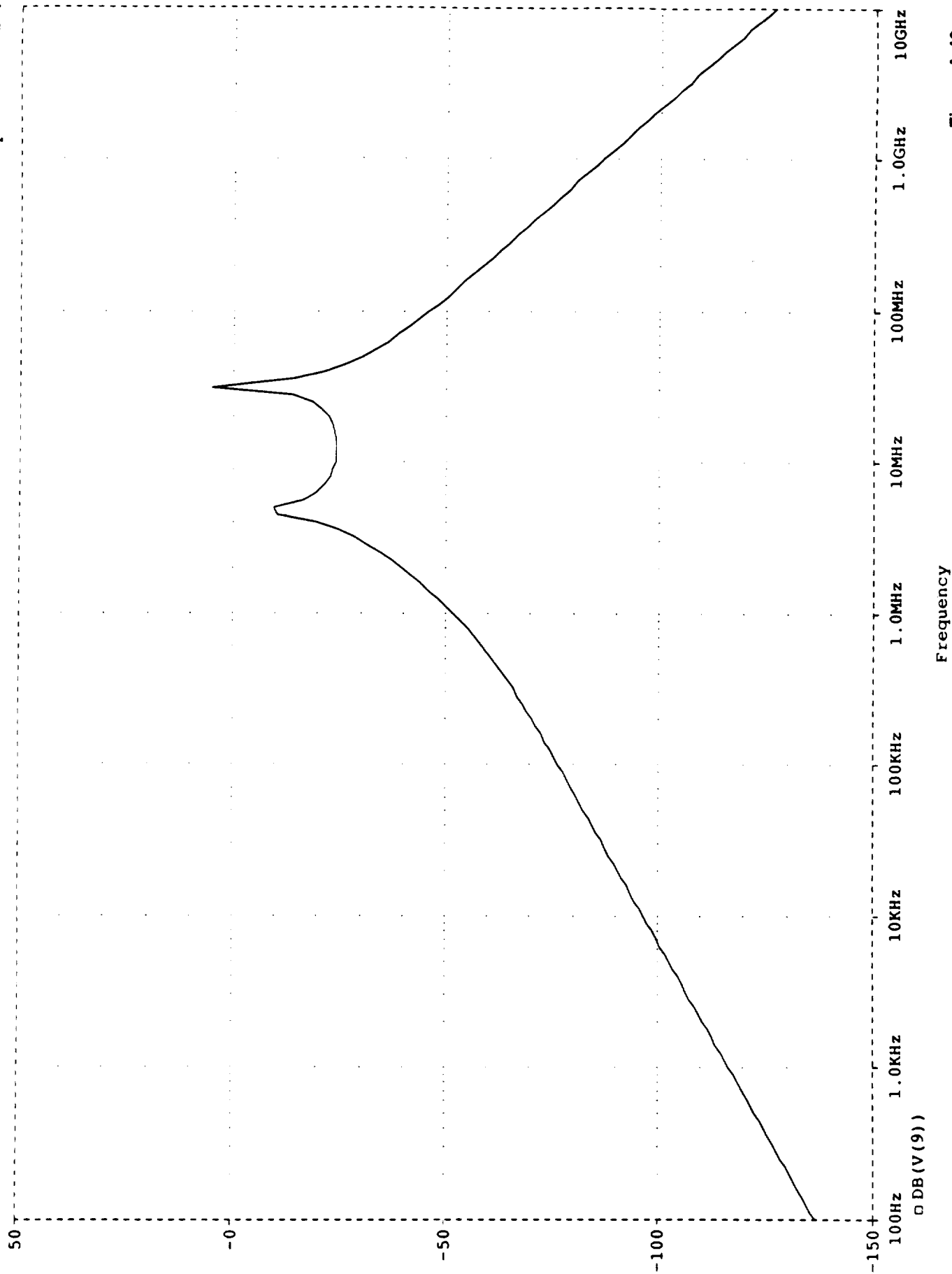


Figure A-40

CALCULATED DIFFERENTIAL MODE VOLTAGE (SEE FIGURE A1 AND TABLES A1 AND A2 FOR CONDITIONS)

Temperature: 27.0

Date/Time run: 06/07/91 12:50:03

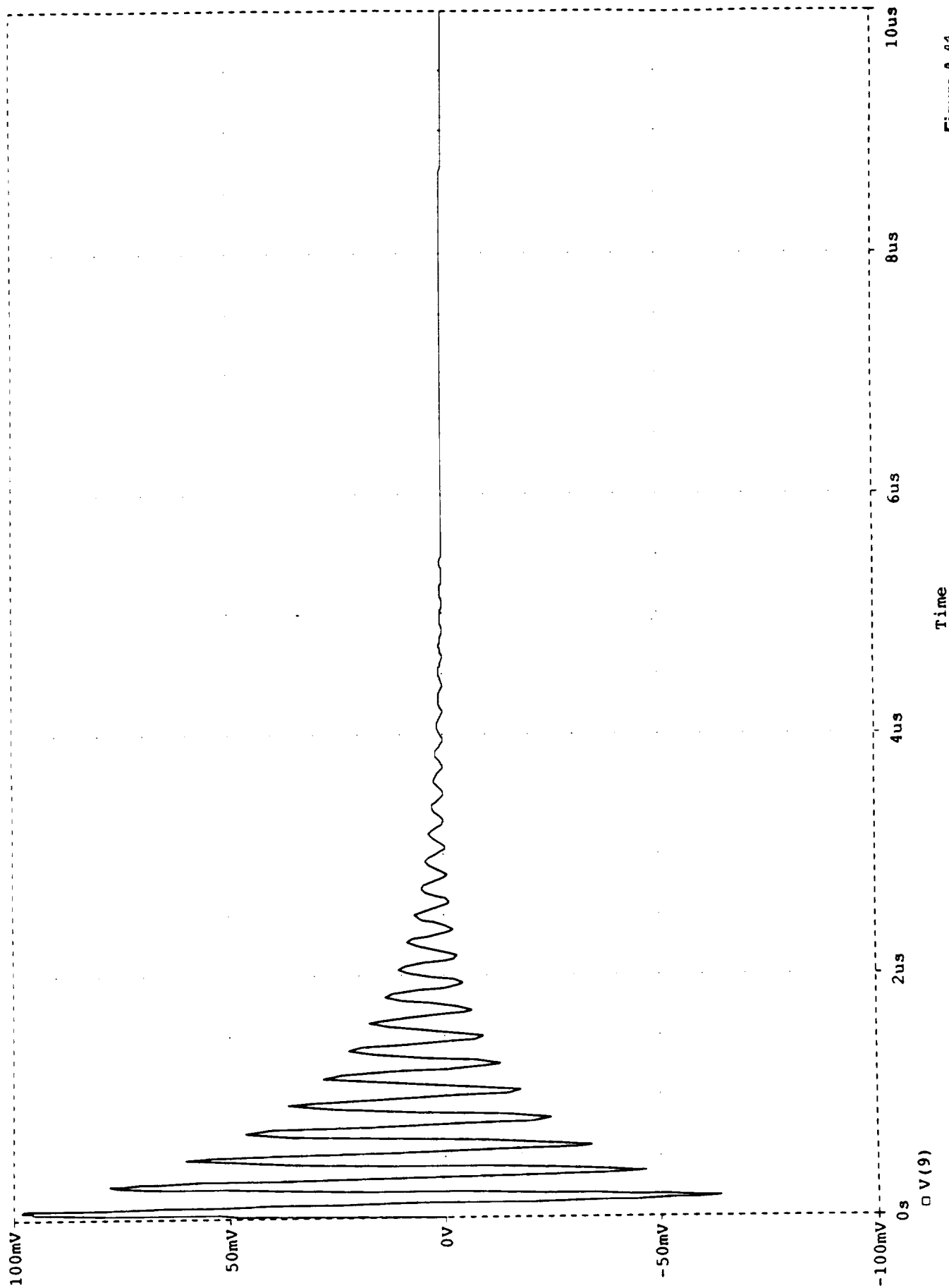


Figure A-41

CALCULATED DIFFERENTIAL MODE VOLTAGE (SEE FIGURE A1 AND TABLES A1 AND A2 FOR CONDITIONS)

Temperature: 27.0

Date/Time run: 09/30/91 07:44:59

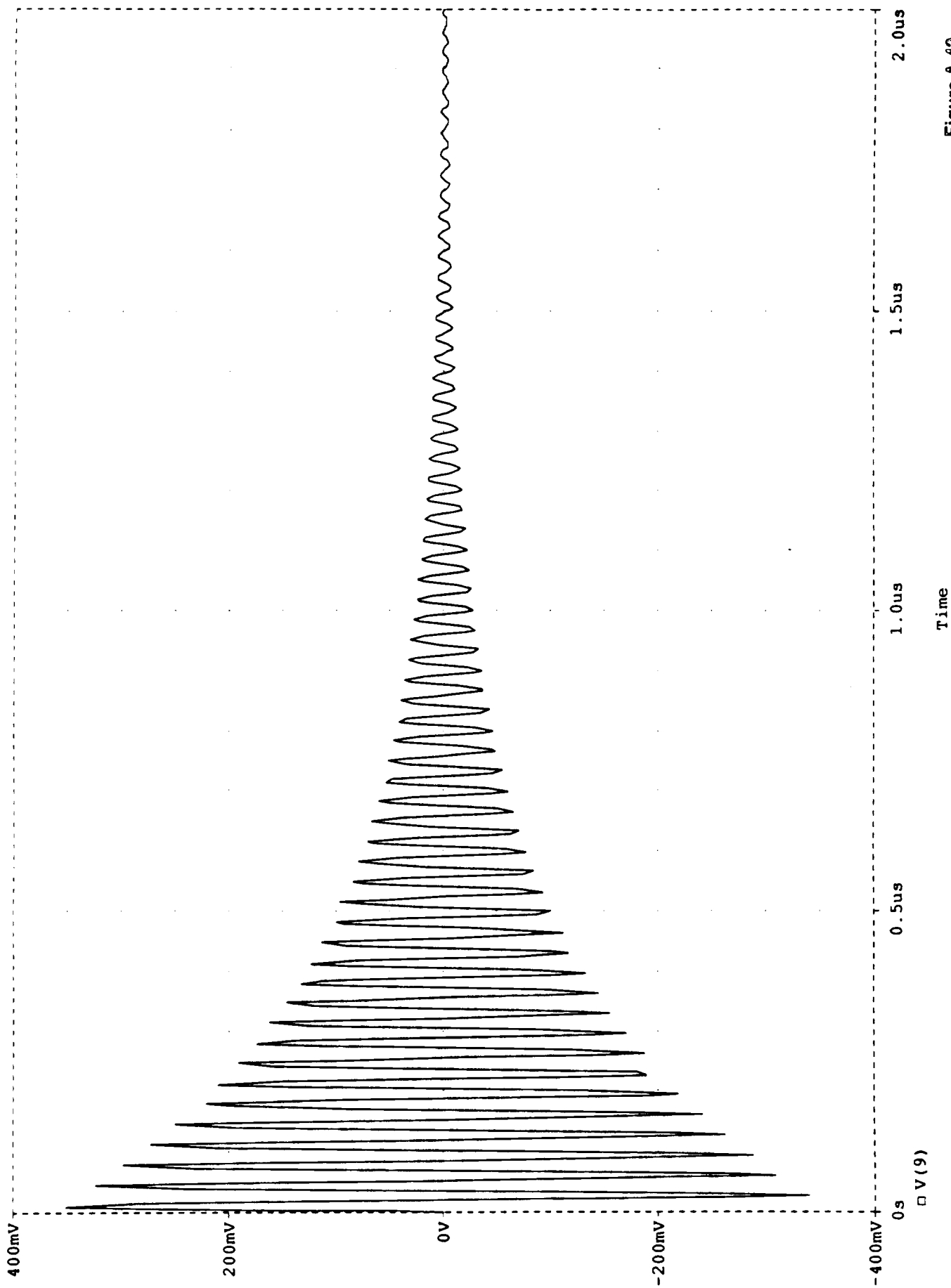


Figure A-42

CALCULATED DIFFERENTIAL MODE VOLTAGE (SEE FIGURE A1 AND TABLES A1 AND A2 FOR CONDITIONS)

Temperature: 27.0

Date/Time run: 09/27/91 09:45:41

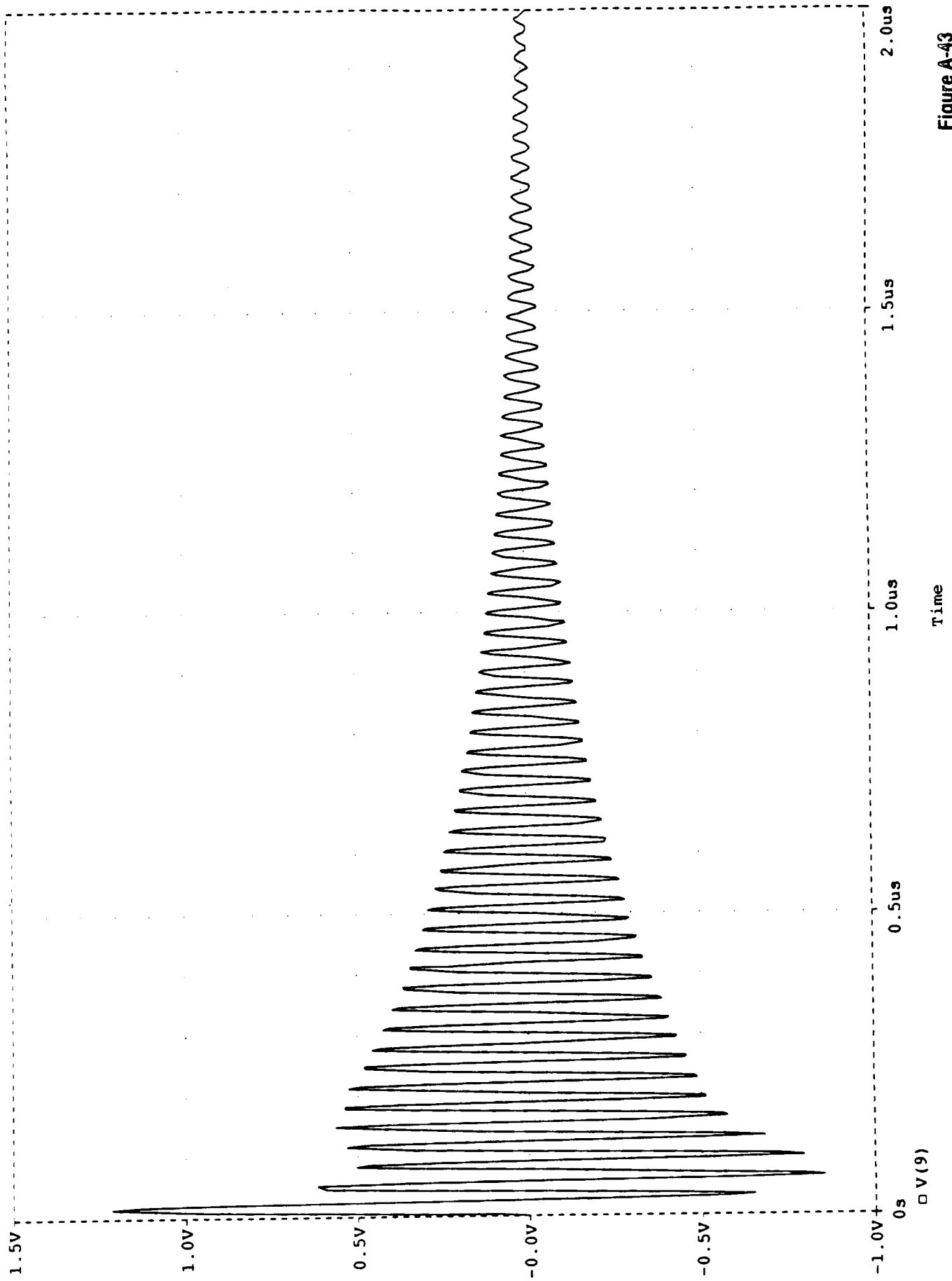
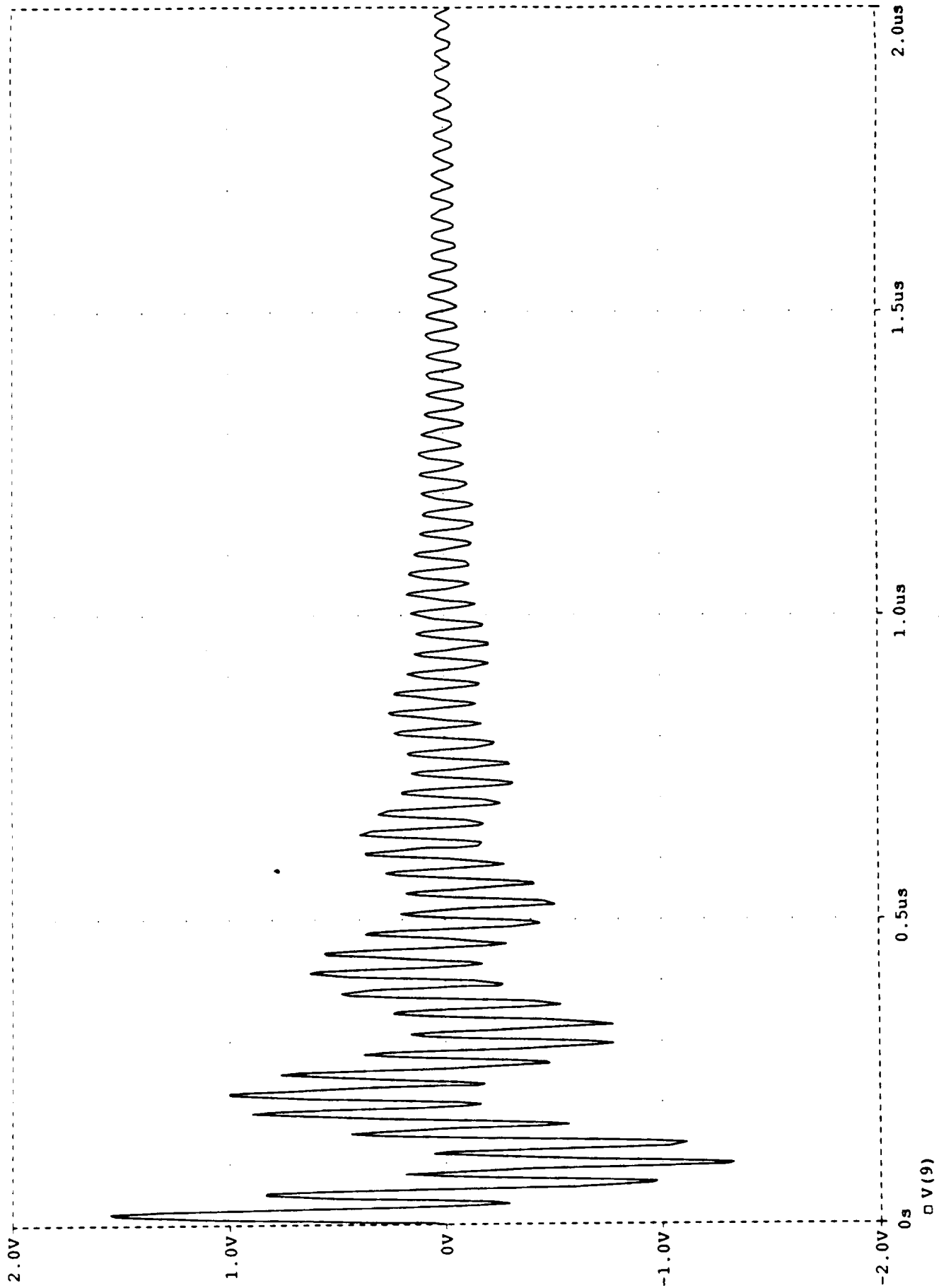


Figure A-43

CALCULATED DIFFERENTIAL MODE VOLTAGE (SEE FIGURE A1 AND TABLES A1 AND A2 FOR CONDITIONS)

Temperature: 27.0

Date/Time run: 09/27/91 09:59:36



Time

Figure A-44



CALCULATED DIFFERENTIAL MODE VOLTAGE (SEE FIGURE A1 AND TABLES A1 AND A2 FOR CONDITIONS)

Date/Time run: 09/27/91 10:29:31

Temperature: 27.0

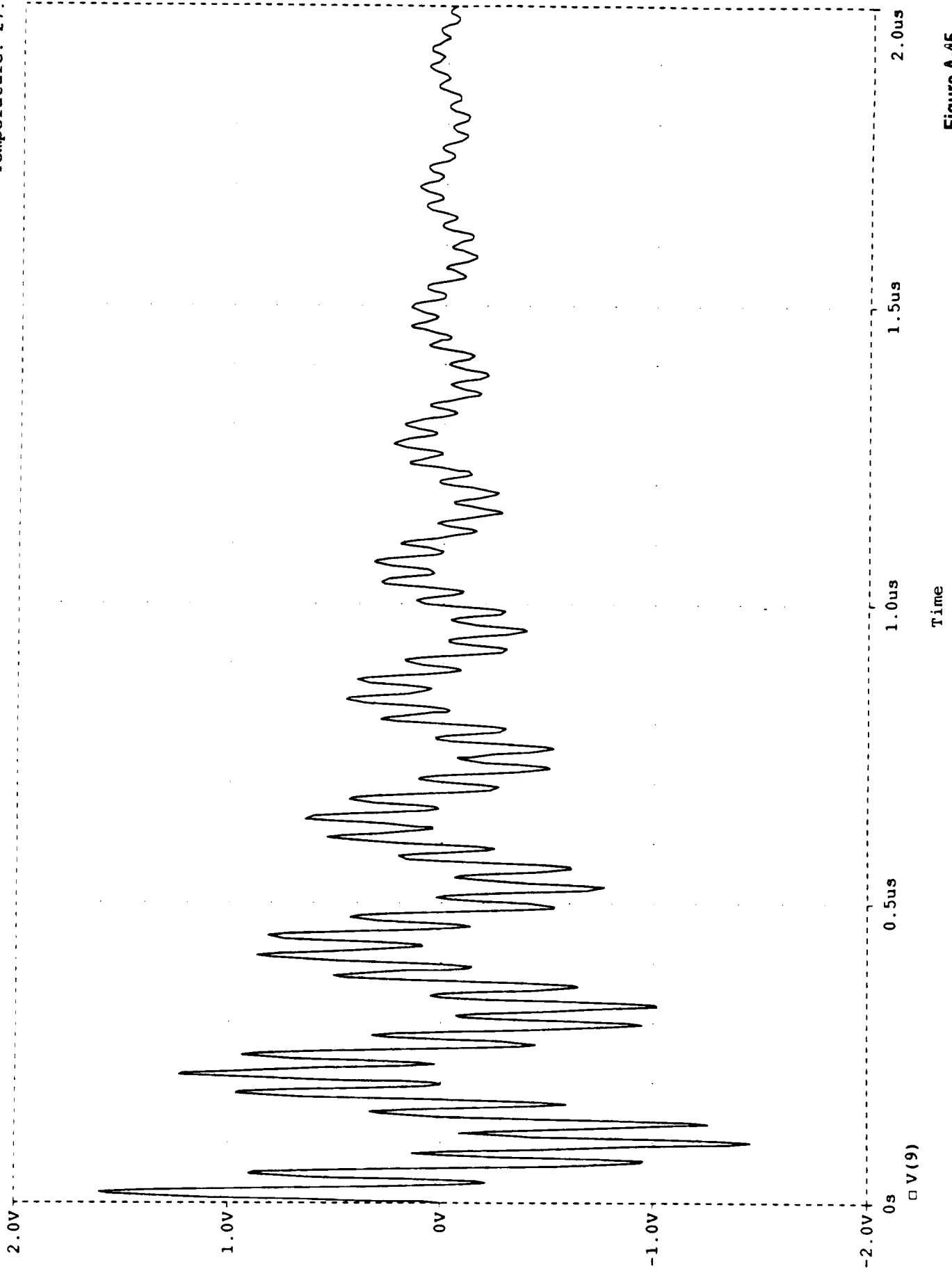


Figure A-45

CALCULATED DIFFERENTIAL MODE VOLTAGE (SEE FIGURE A1 AND TABLES A1 AND A2 FOR CONDITIONS)

Temperature: 27.0

Date/Time run: 09/27/91 10:37:51

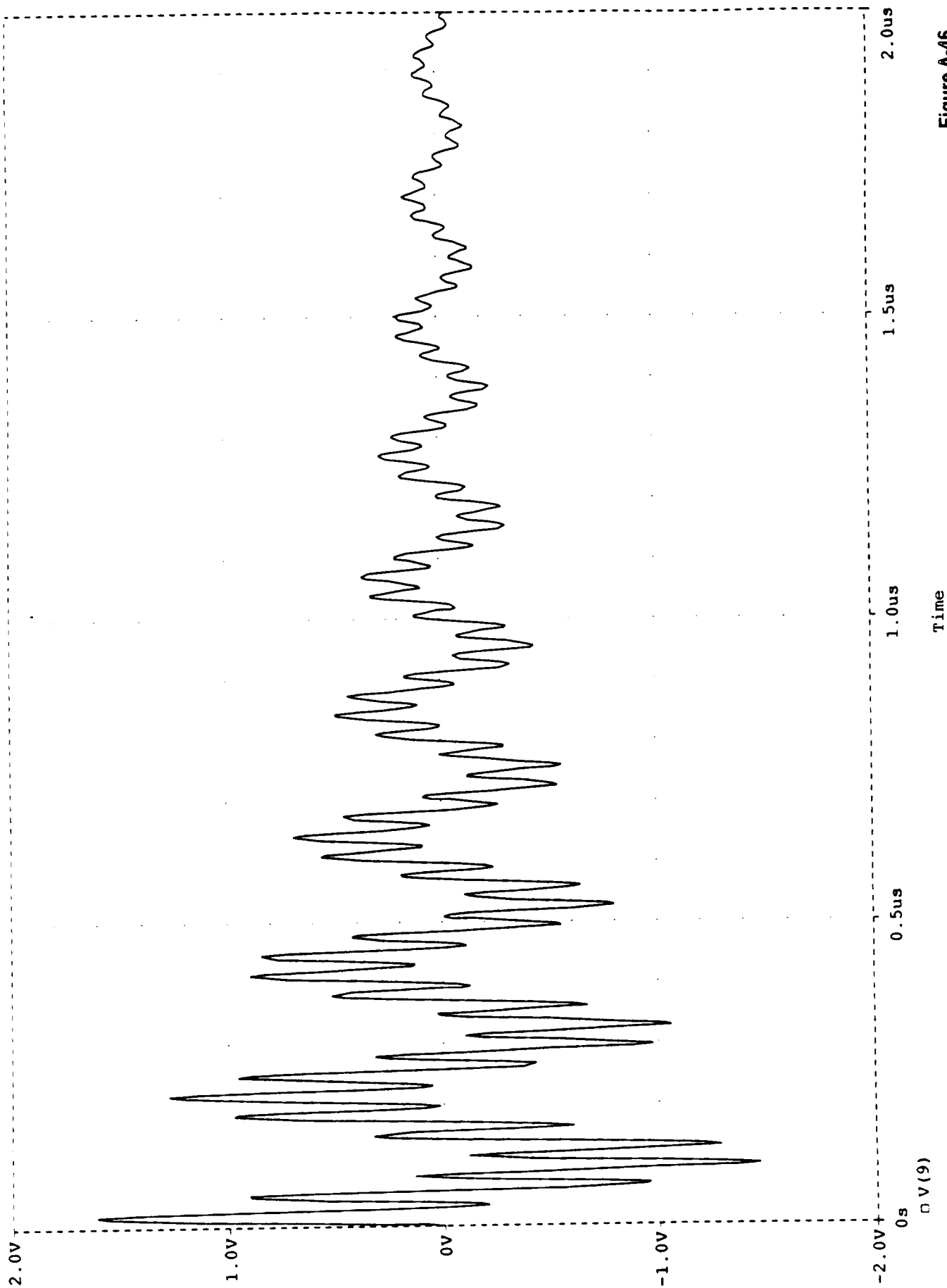


Figure A-46

CALCULATED DIFFERENTIAL MODE VOLTAGE (SEE FIGURE A1 AND TABLES A1 AND A2 FOR CONDITIONS)

Temperature: 27.0

Date/Time run: 10/01/91 15:54:37

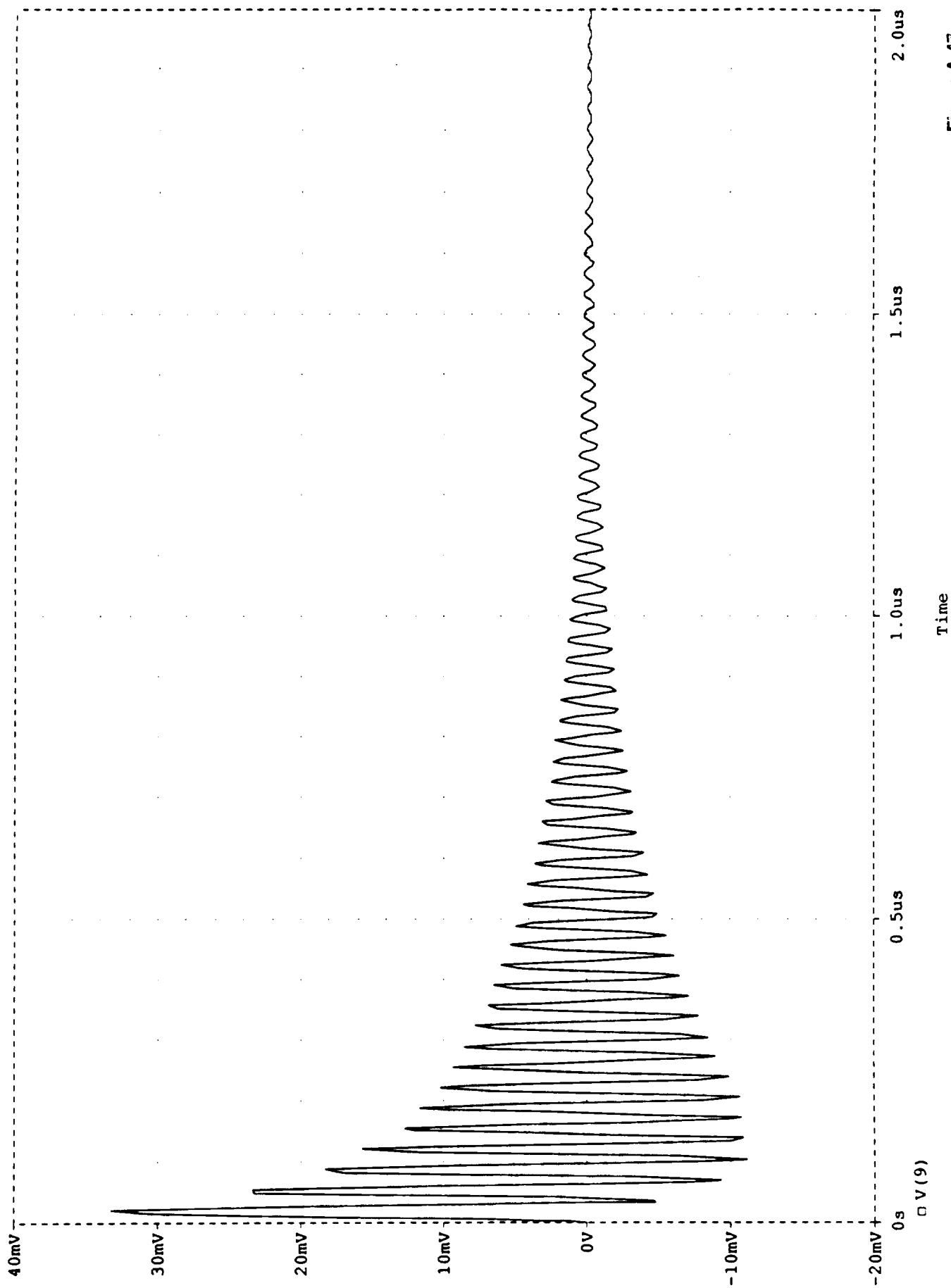


Figure A-47

CALCULATED DIFFERENTIAL MODE VOLTAGE (SEE FIGURE A1 AND TABLES A1 AND A2 FOR CONDITIONS)

Temperature: 27.0

Date/Time run: 10/01/91 16:06:36

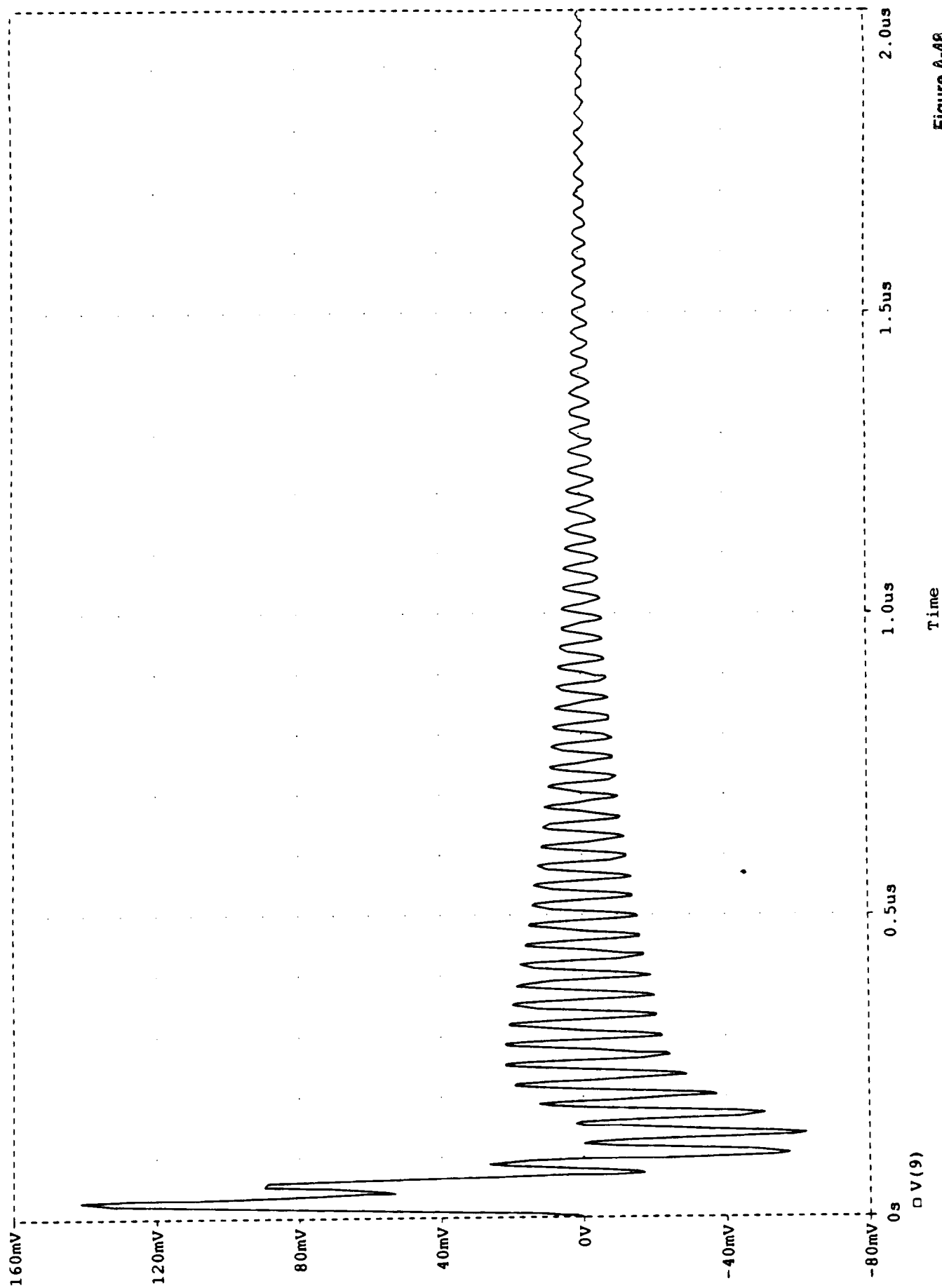


Figure A-48

CALCULATED DIFFERENTIAL MODE VOLTAGE (SEE FIGURE A1 AND TABLES A1 AND A2 FOR CONDITIONS)

Temperature: 27.0

Date/Time run: 10/02/91 07:38:40

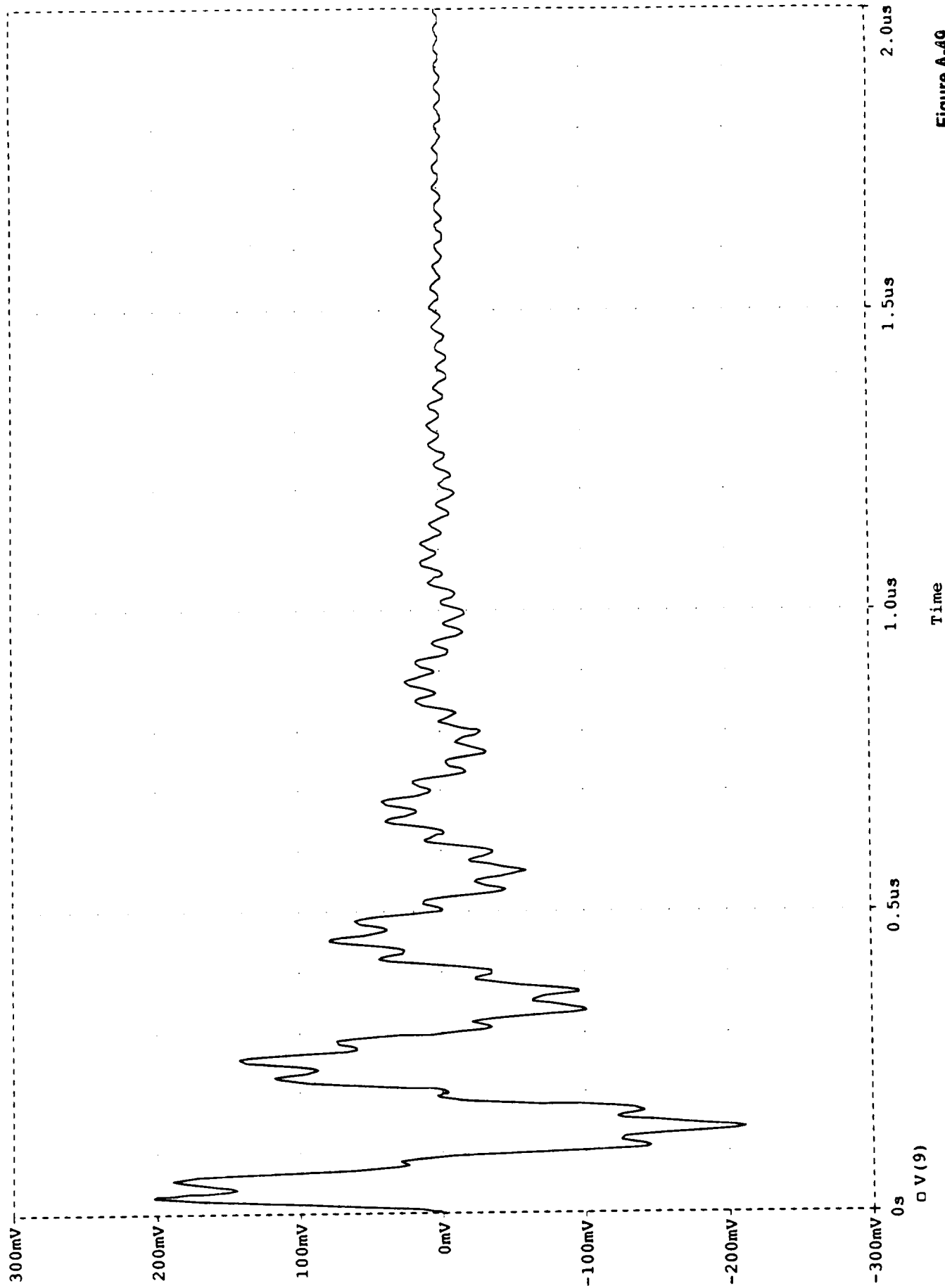


Figure A-49

CALCULATED DIFFERENTIAL MODE VOLTAGE (SEE FIGURE A1 AND TABLES A1 AND A2 FOR CONDITIONS)

Date/Time run: 10/02/91 08:11:19

Temperature: 27.0

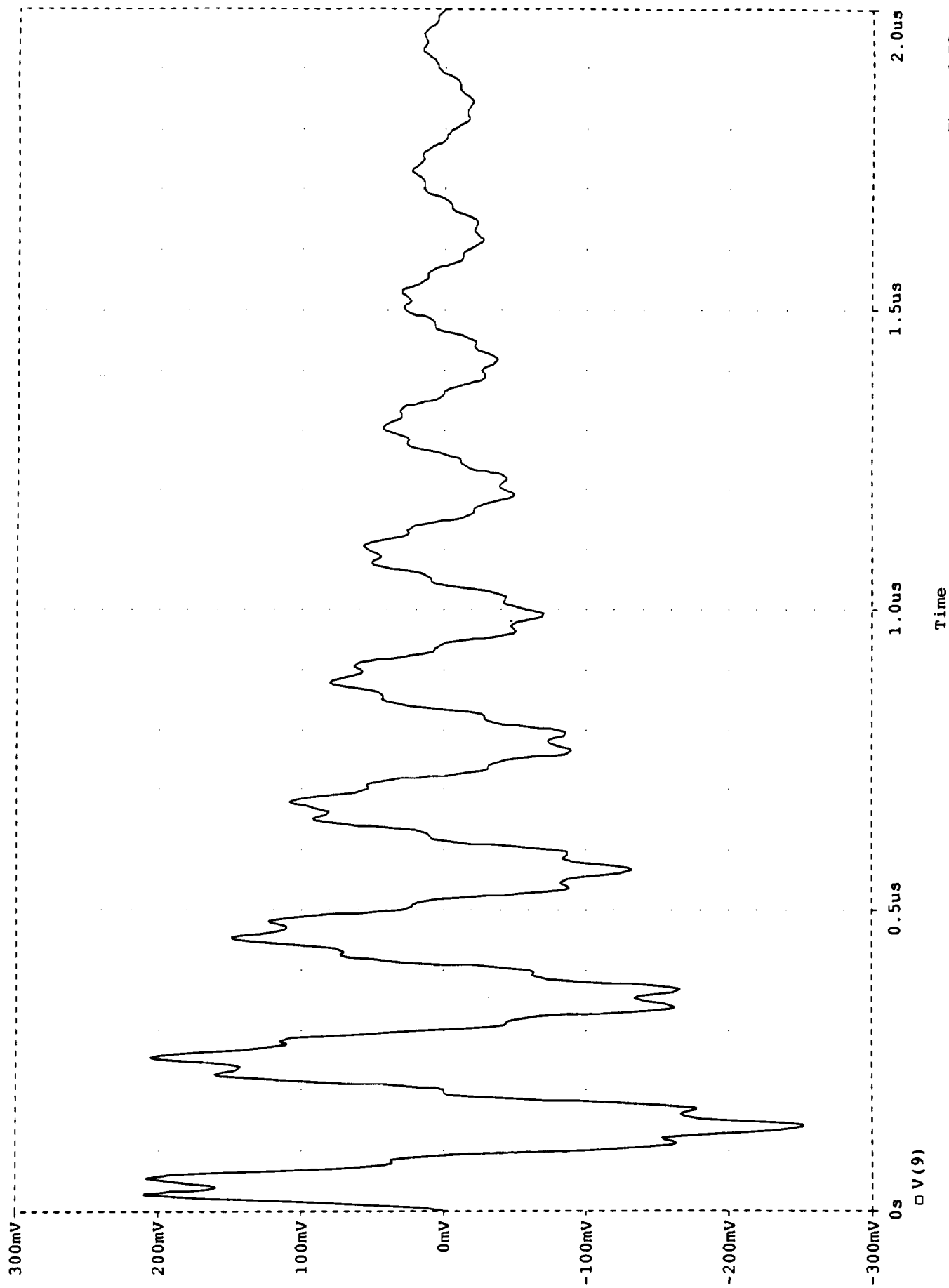


Figure A-50

CALCULATED DIFFERENTIAL MODE VOLTAGE (SEE FIGURE A1 AND TABLES A1 AND A2 FOR CONDITIONS)

Temperature: 27.0

Date/Time run: 10/02/91 08:29:39

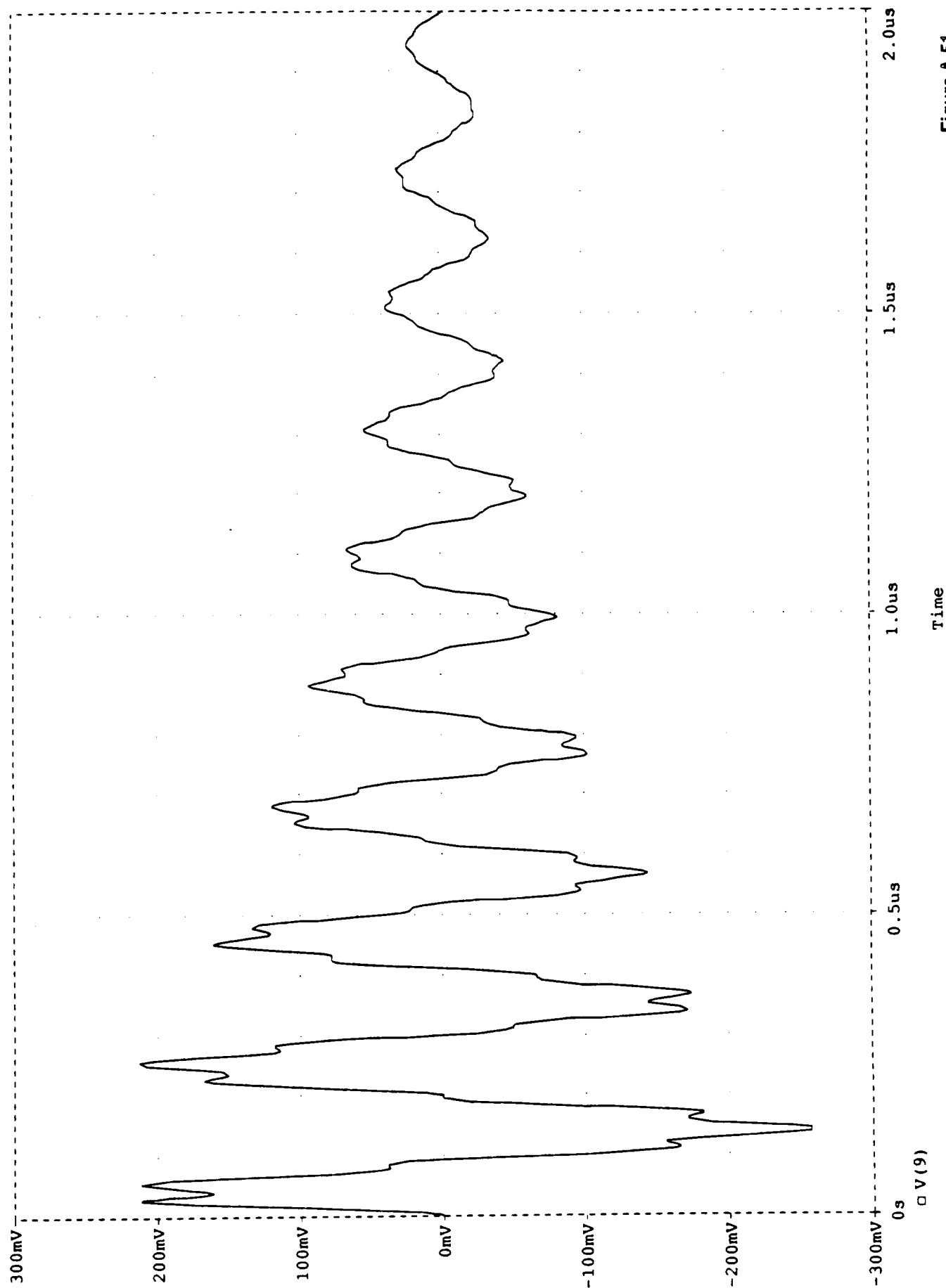


Figure A-51

CALCULATED DIFFERENTIAL MODE VOLTAGE (SEE FIGURE A1 AND TABLES A1 AND A2 FOR CONDITIONS)

Temperature: 27.0

Date/Time run: 10/02/91 09:30:12

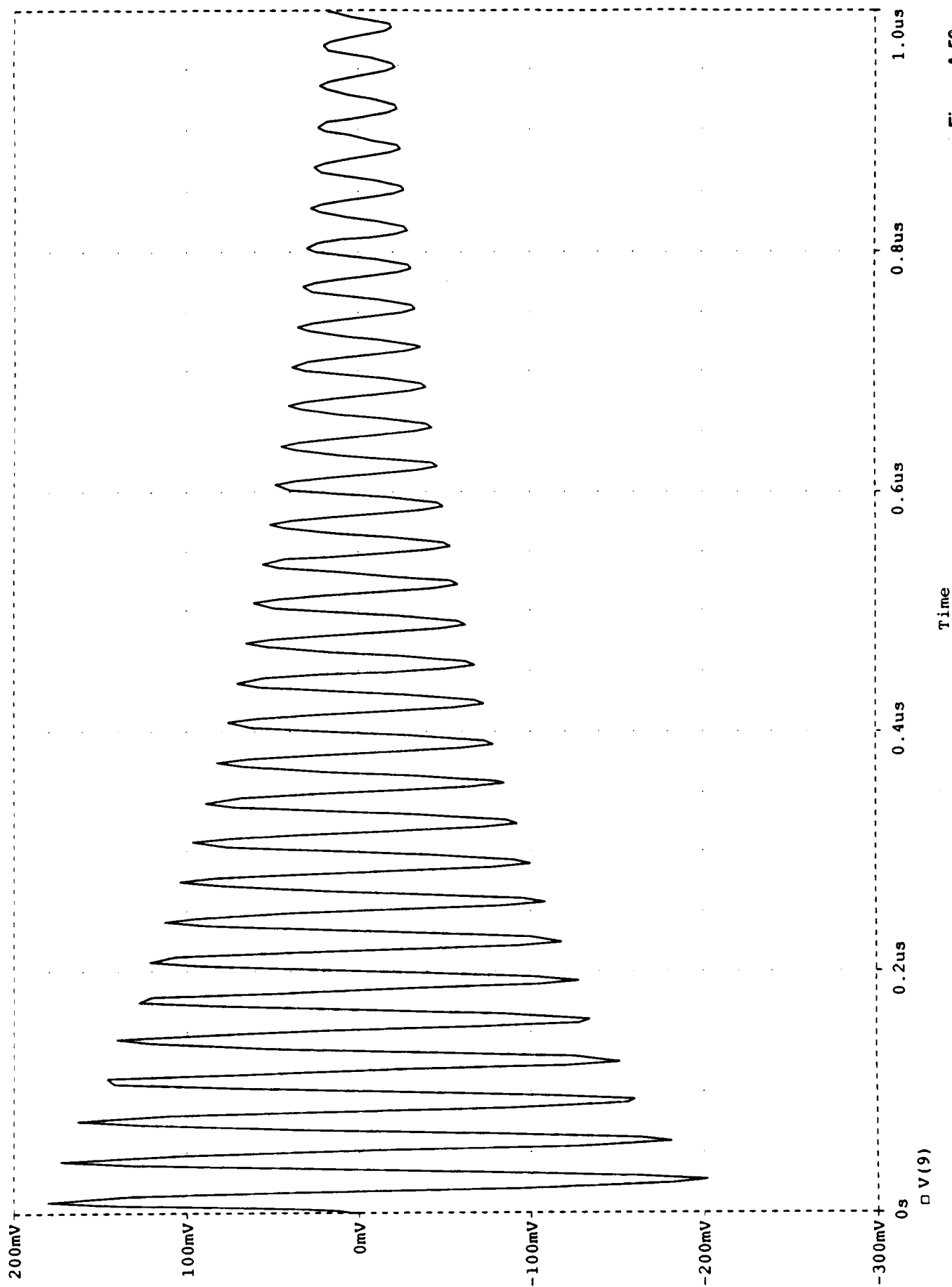


Figure A-52



CALCULATED DIFFERENTIAL MODE VOLTAGE (SEE FIGURE A1 AND TABLES A1 AND A2 FOR CONDITIONS)

Temperature: 27.0

Date/Time run: 10/02/91 10:58:43

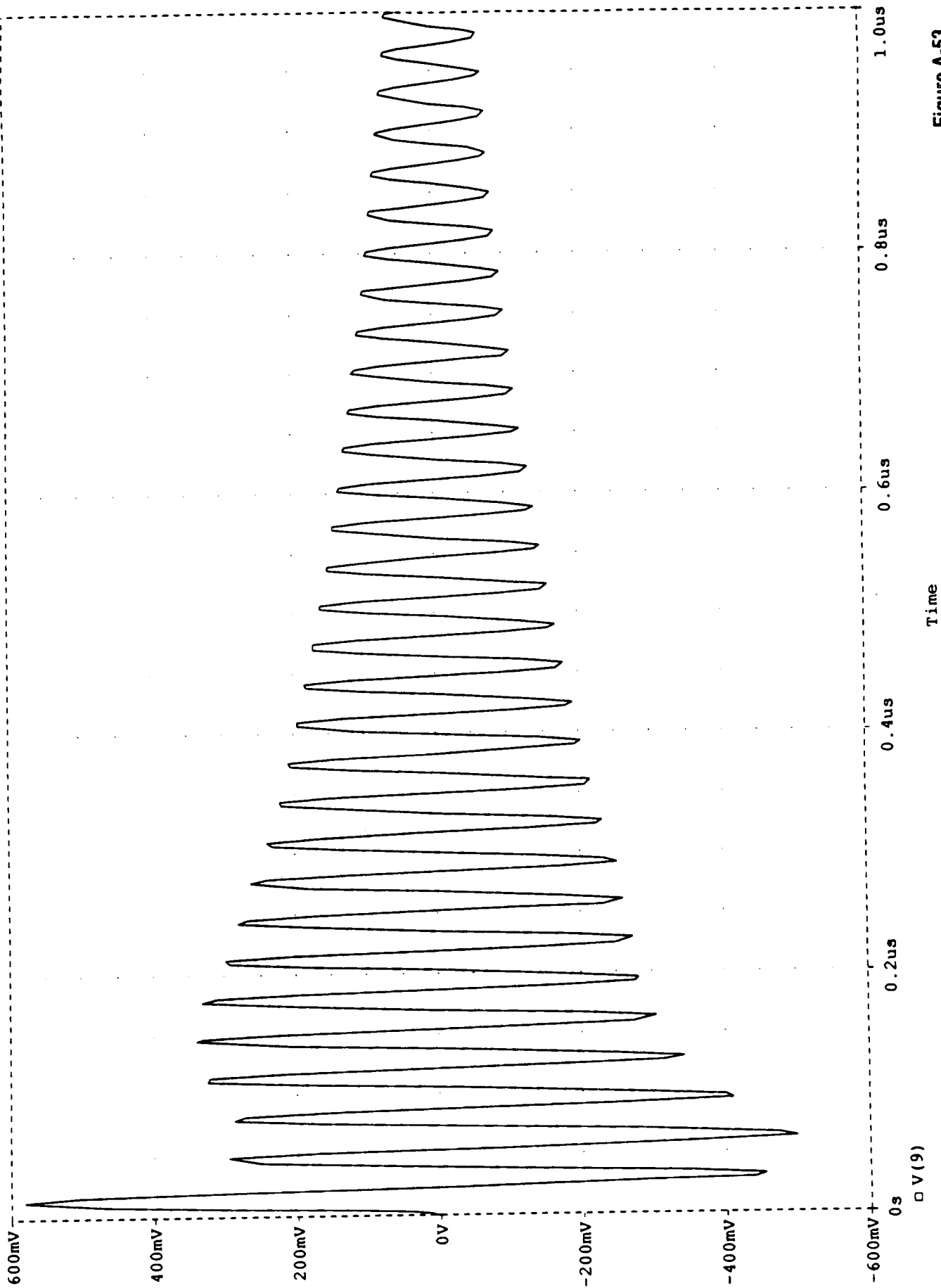


Figure A-53

CALCULATED DIFFERENTIAL MODE VOLTAGE (SEE FIGURE A1 AND TABLES A1 AND A2 FOR CONDITIONS)

Temperature: 27.0

Date/Time run: 10/02/91 11:02:47

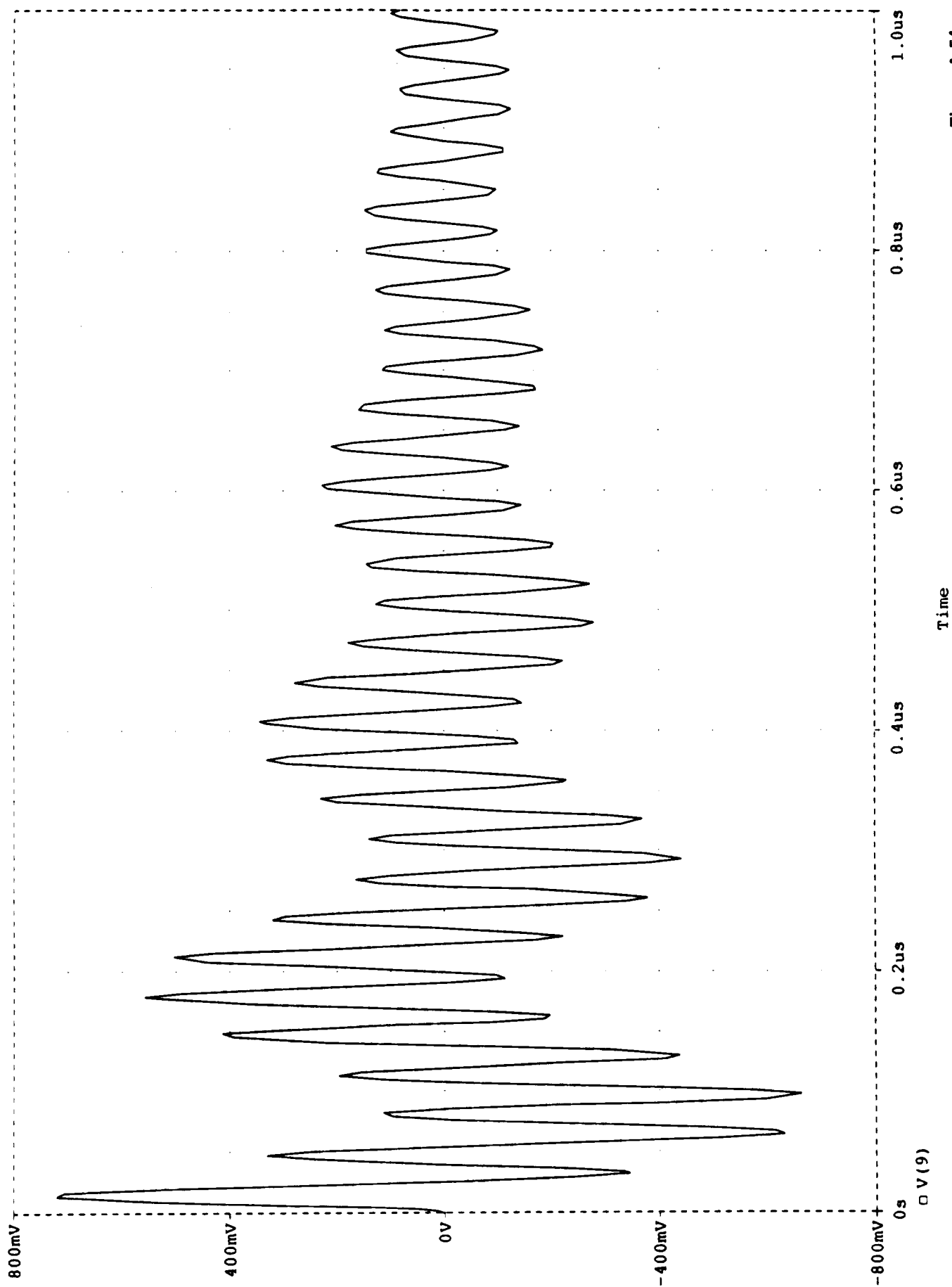


Figure A-54

CALCULATED DIFFERENTIAL MODE VOLTAGE (SEE FIGURE A1 AND TABLES A1 AND A2 FOR CONDITIONS)

Temperature: 27.0

Date/Time run: 10/02/91 11:06:50

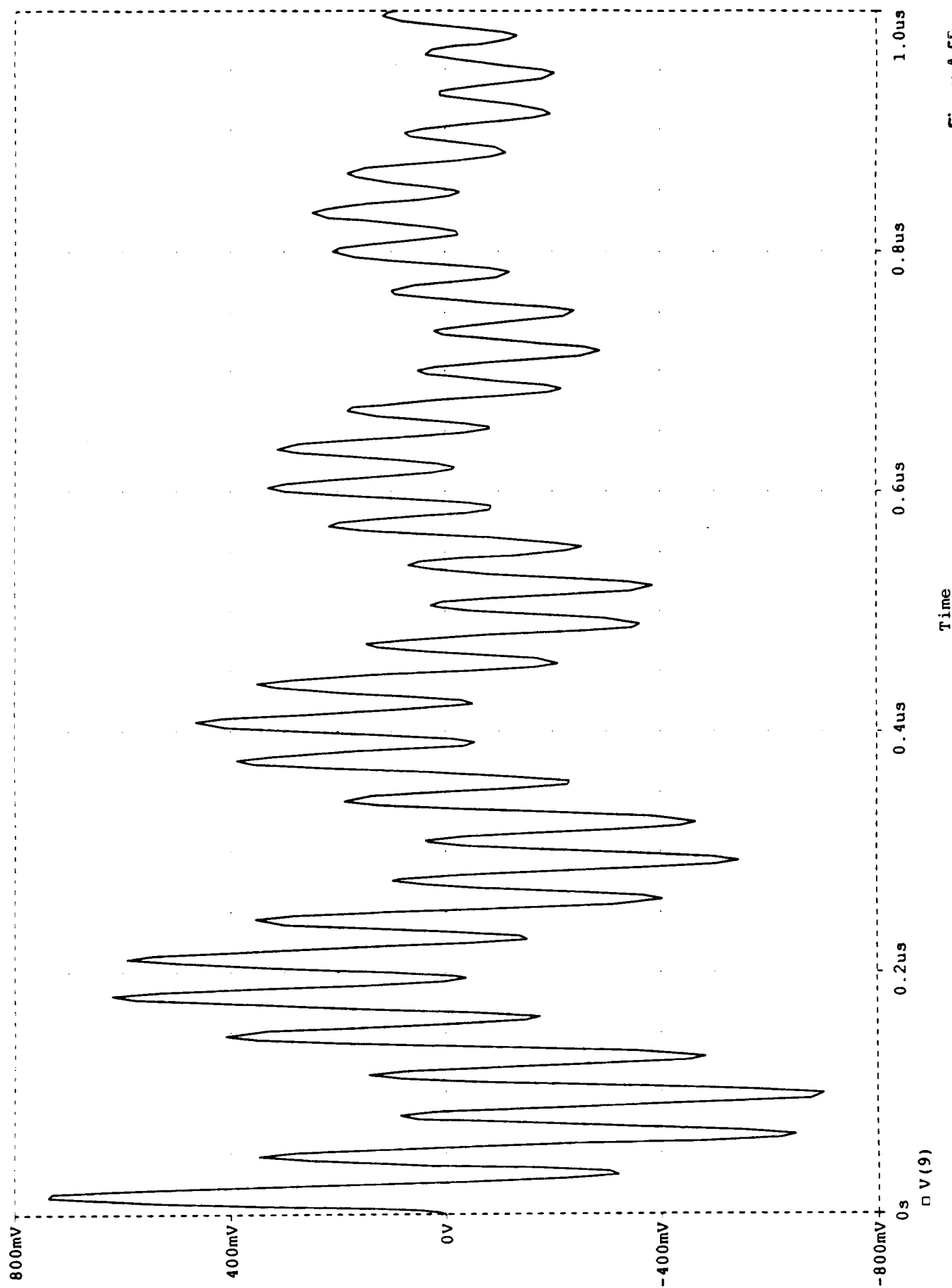


Figure A-55

CALCULATED DIFFERENTIAL MODE VOLTAGE (SEE FIGURE A1 AND TABLES A1 AND A2 FOR CONDITIONS)

Temperature: 27.0

Date/Time run: 10/02/91 11:11:05

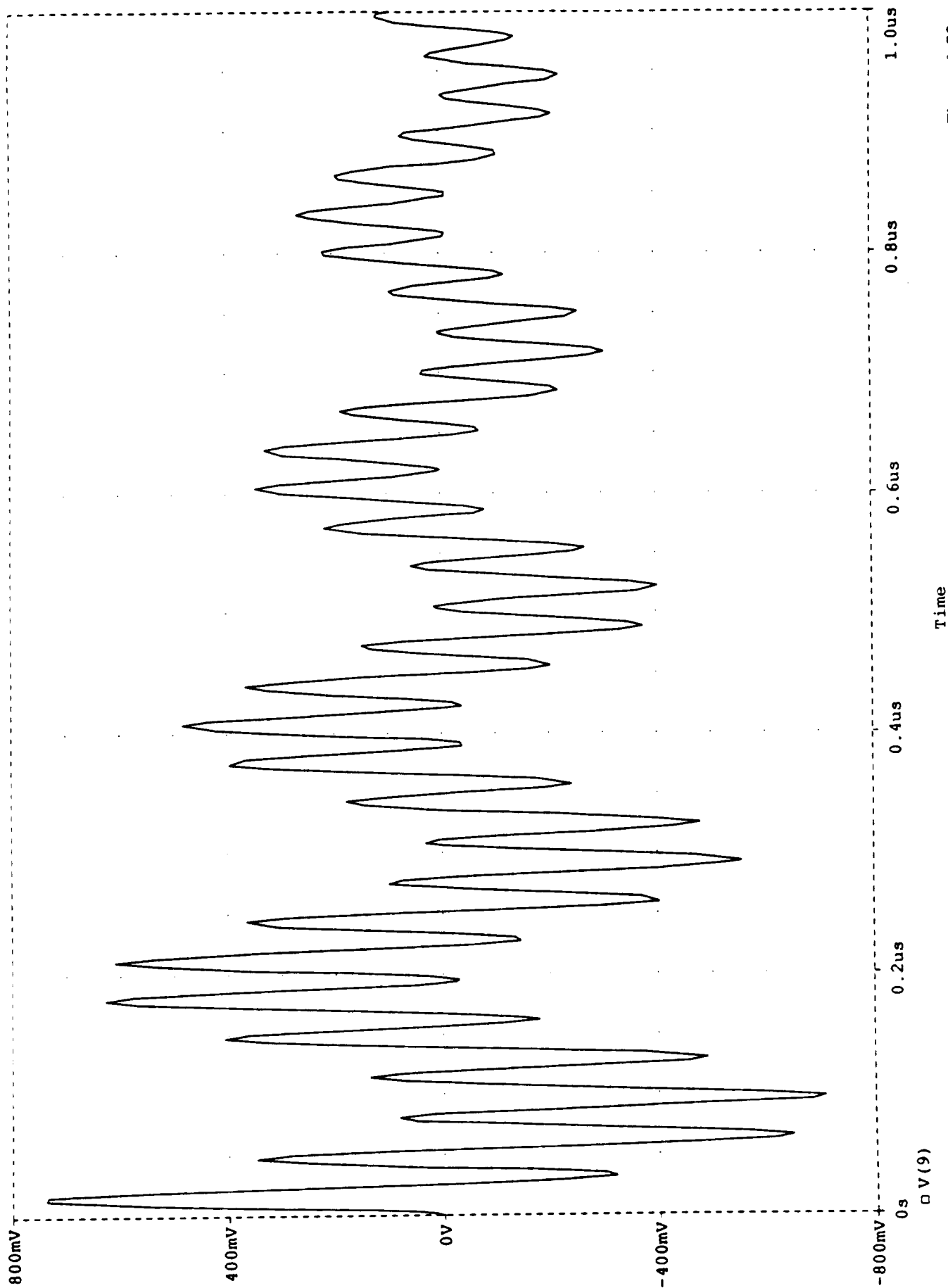
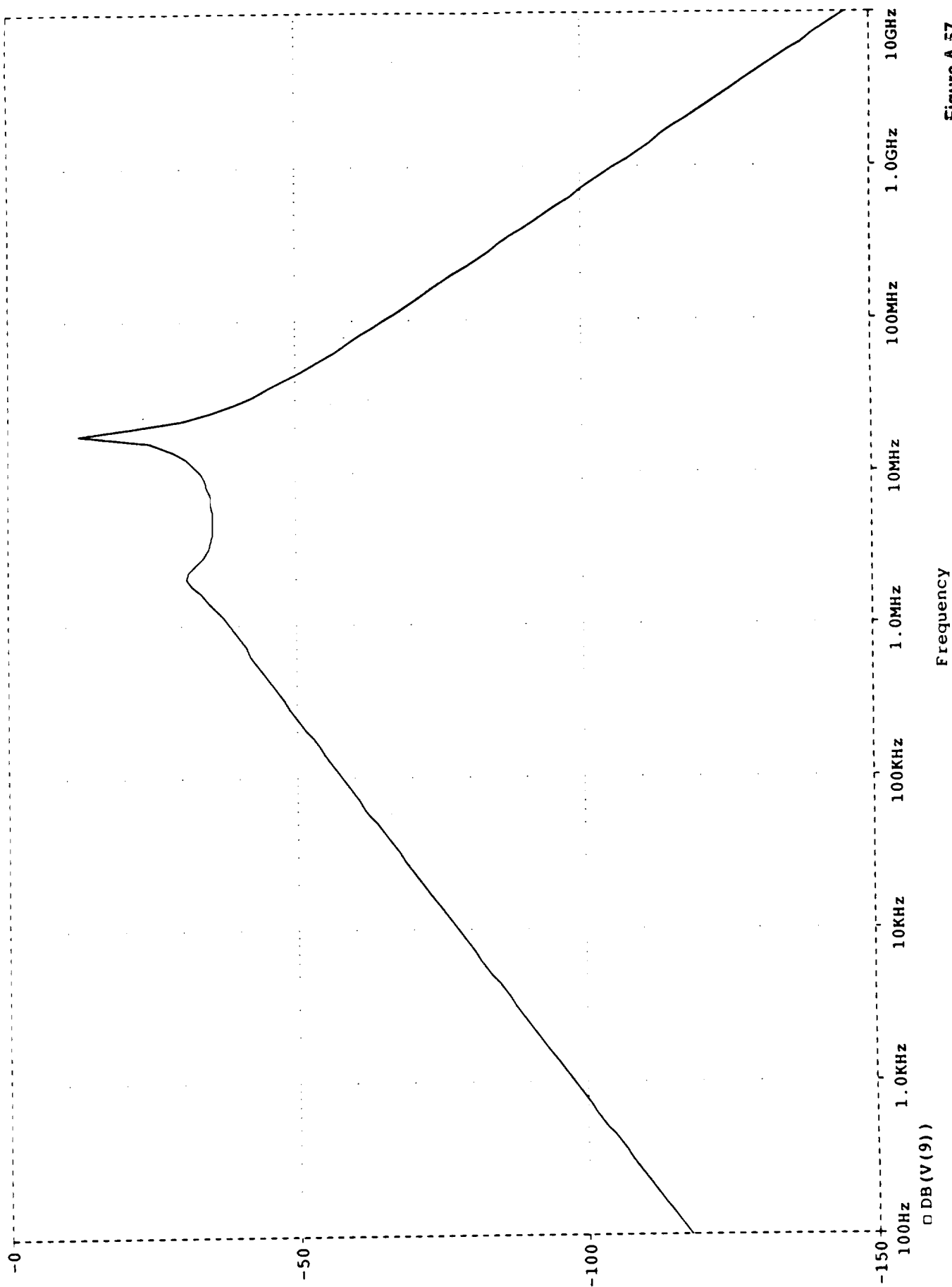


Figure A-56

CALCULATED DIFFERENTIAL MODE VOLTAGE (SEE FIGURE A1 AND TABLES A1 AND A2 FOR CONDITIONS)

Temperature: 27.0

Date/Time run: 06/07/91 14:21:19



Frequency

Figure A-57

CALCULATED DIFFERENTIAL MODE VOLTAGE (SEE FIGURE A1 AND TABLES A1 AND A2 FOR CONDITIONS)

Temperature: 27.0

Date/Time run: 06/07/91 14:21:19

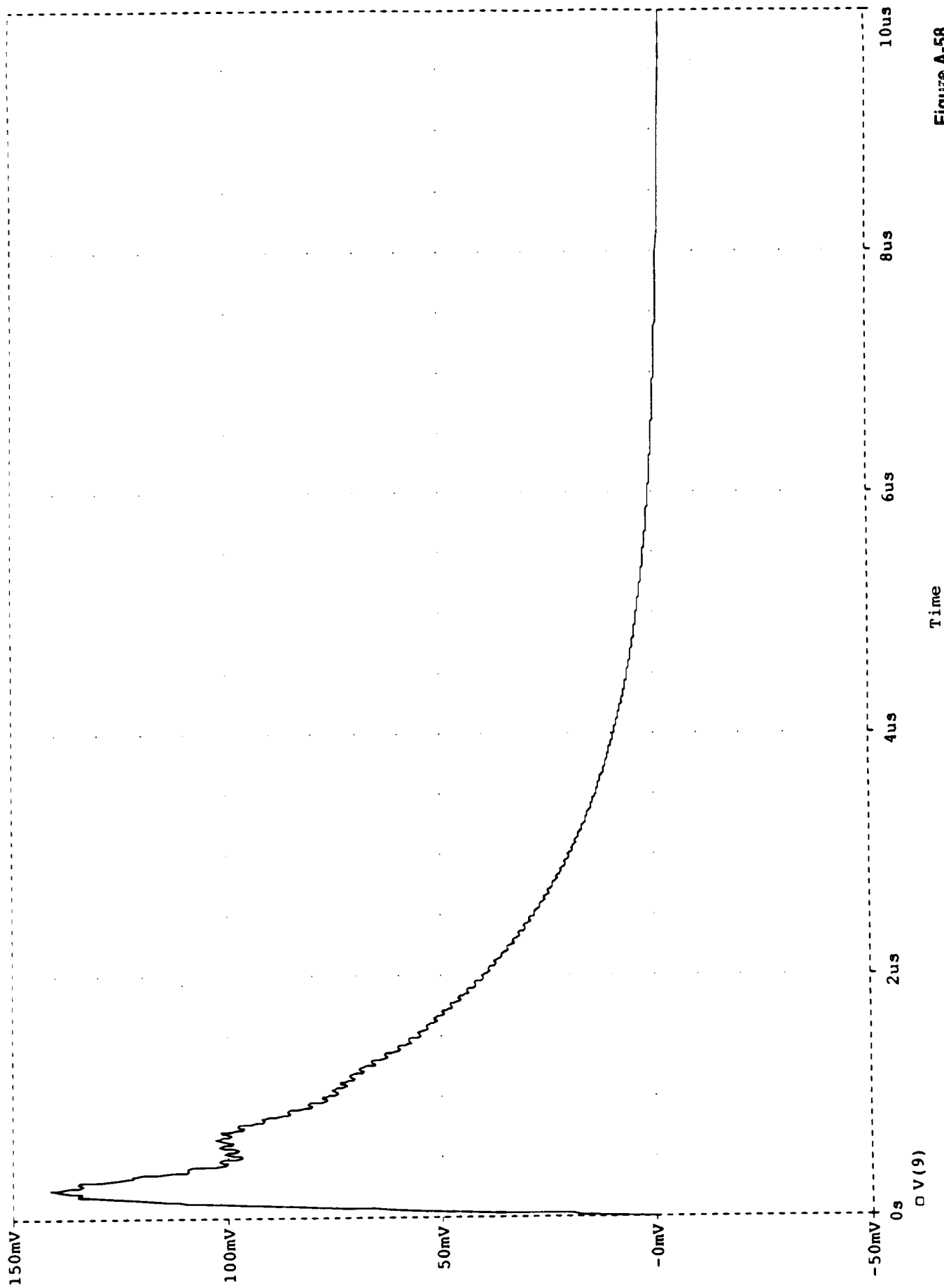
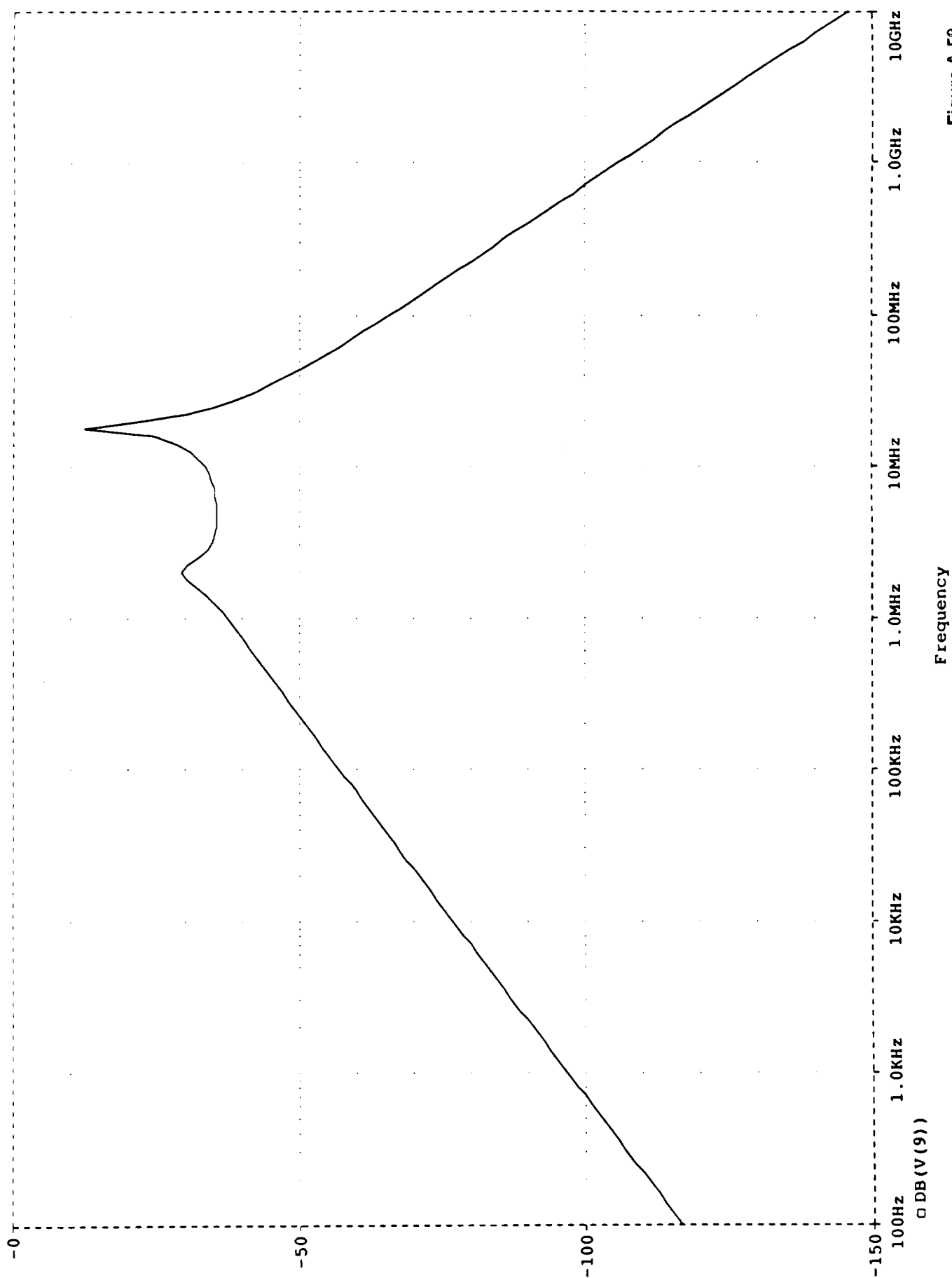


Figure A-58

CALCULATED DIFFERENTIAL MODE VOLTAGE (SEE FIGURE A1 AND TABLES A1 AND A2 FOR CONDITIONS)

Temperature: 27.0

Date/Time run: 06/07/91 14:38:20



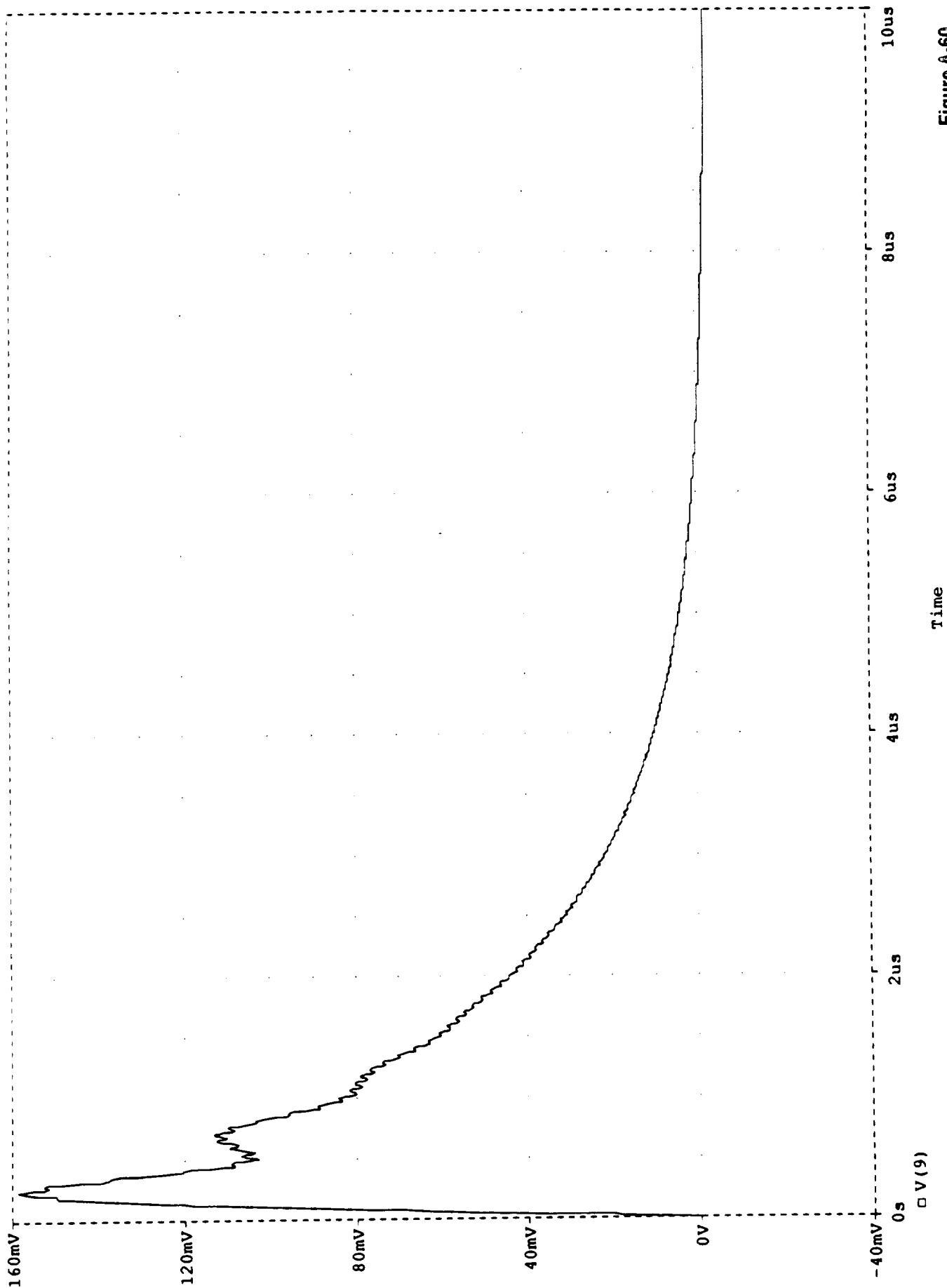
Frequency

Figure A-59

CALCULATED DIFFERENTIAL MODE VOLTAGE (SEE FIGURE A1 AND TABLES A1 AND A2 FOR CONDITIONS)

Temperature: 27.0

Date/Time run: 06/07/91 14:38:20



Time

□ V(9)

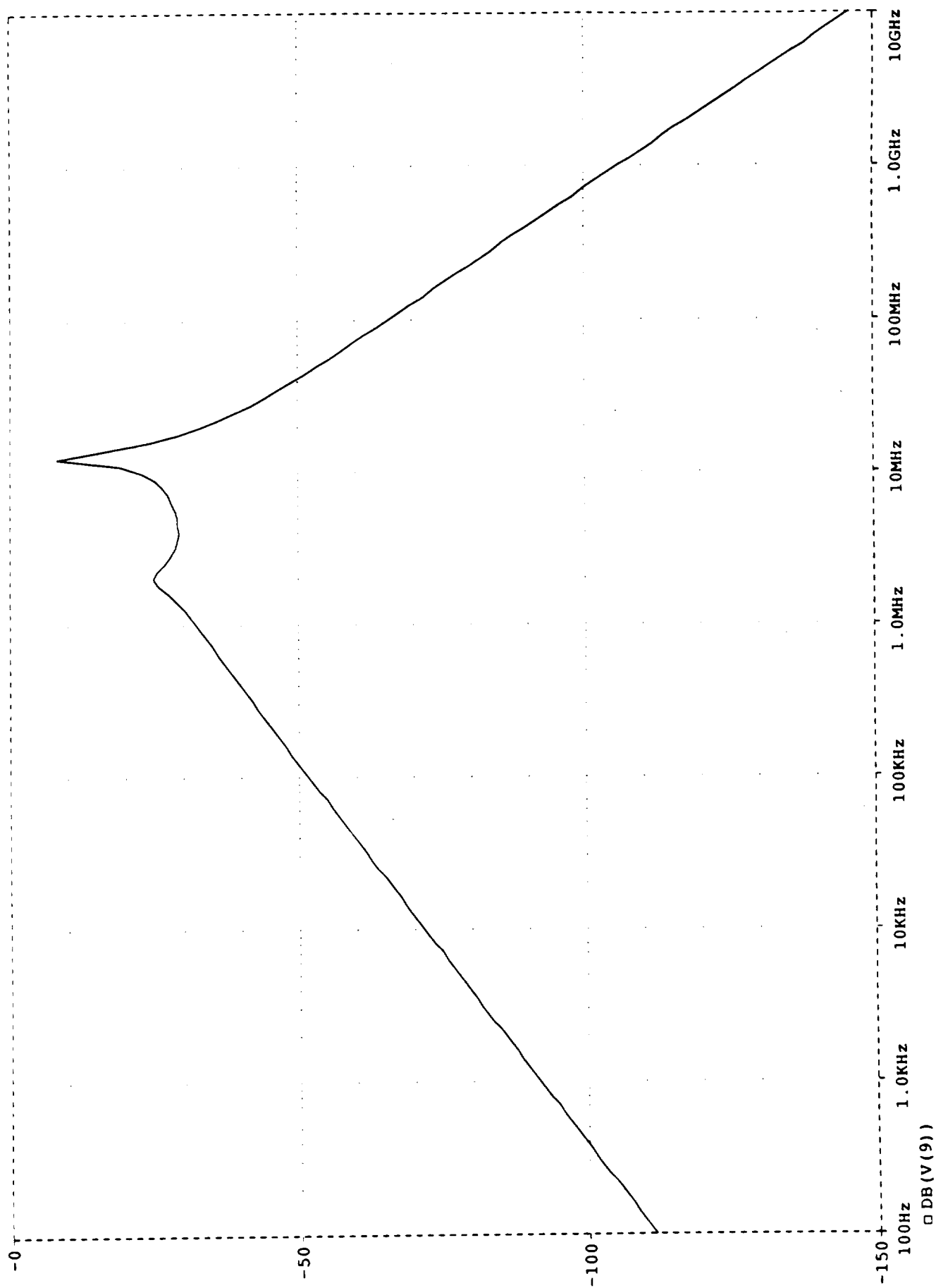
Figure A-60



CALCULATED DIFFERENTIAL MODE VOLTAGE (SEE FIGURE A1 AND TABLES A1 AND A2 FOR CONDITIONS)

Temperature: 27.0

Date/Time run: 06/07/91 14:45:50



Frequency

DB(V(9))

Figure A-61

CALCULATED DIFFERENTIAL MODE VOLTAGE (SEE FIGURE A1 AND TABLES A1 AND A2 FOR CONDITIONS)

Temperature: 27.0

Date/Time run: 06/07/91 14:45:50

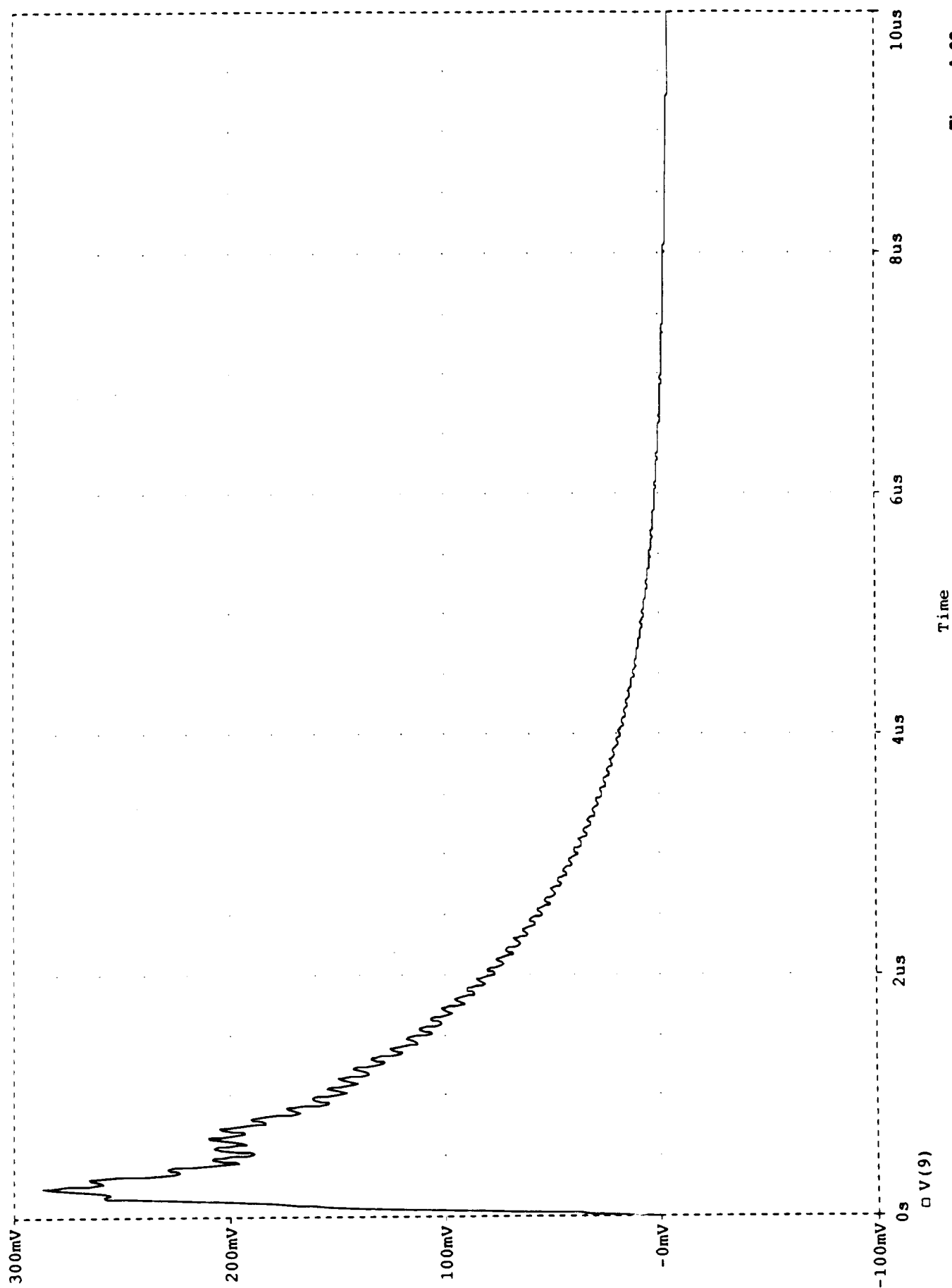
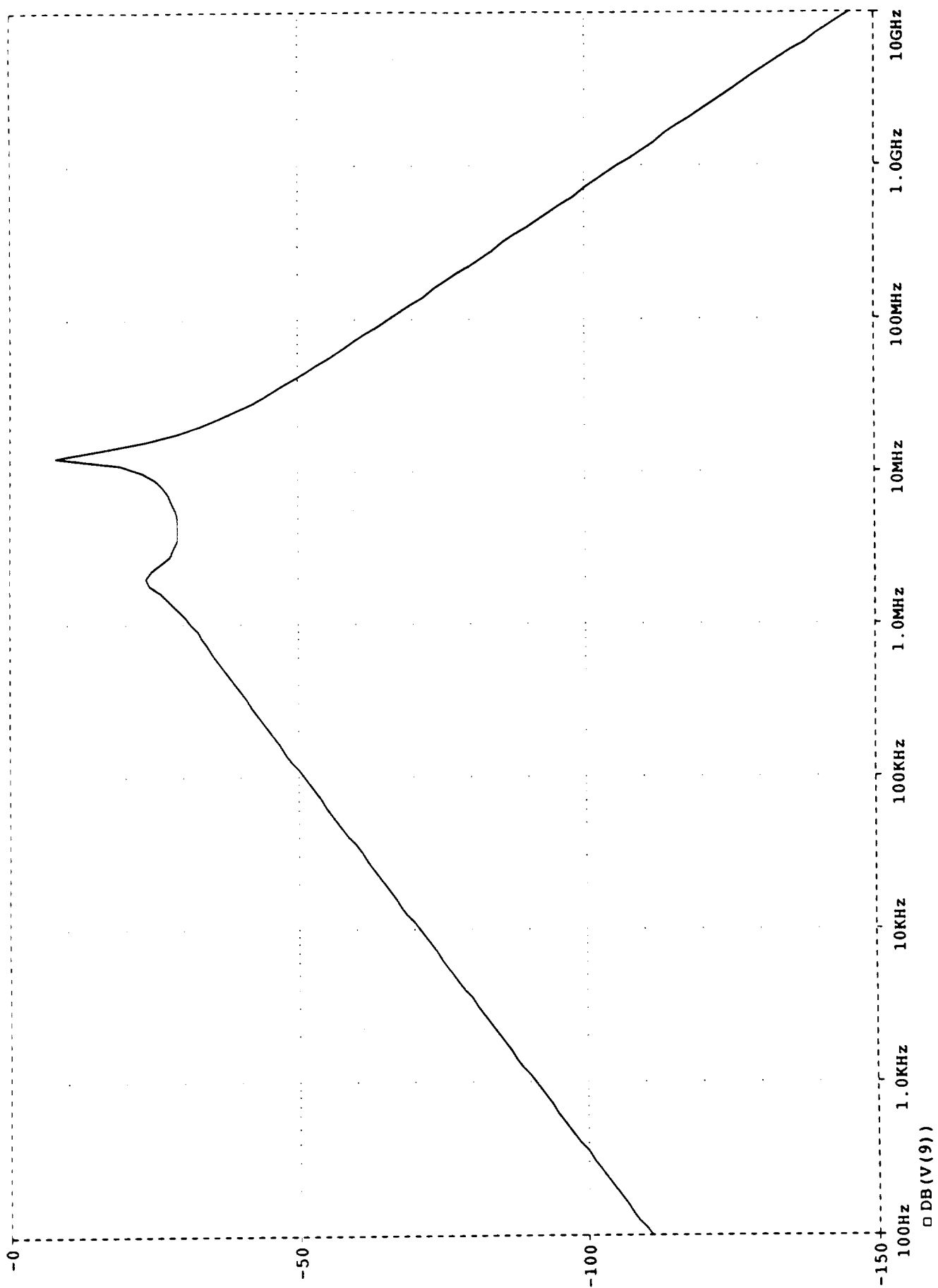


Figure A-62

CALCULATED DIFFERENTIAL MODE VOLTAGE (SEE FIGURE A1 AND TABLES A1 AND A2 FOR CONDITIONS)

Temperature: 27.0

Date/Time run: 06/07/91 14:52:46



Frequency

Figure A-63

CALCULATED DIFFERENTIAL MODE VOLTAGE (SEE FIGURE A1 AND TABLES A1 AND A2 FOR CONDITIONS)

Temperature: 27.0

Date/Time run: 06/07/91 14:52:46

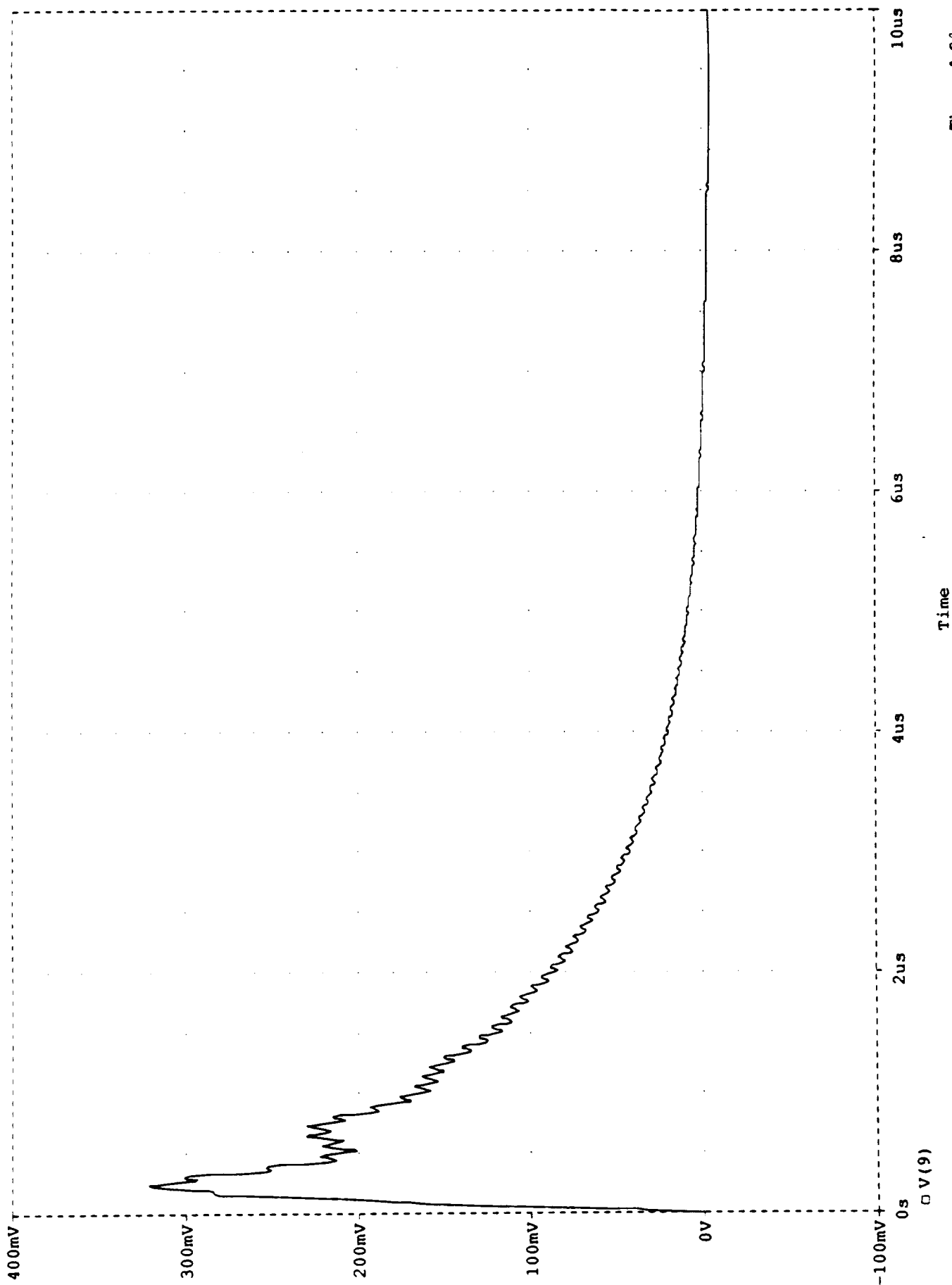


Figure A-6A

CALCULATED DIFFERENTIAL MODE VOLTAGE (SEE FIGURE A1 AND TABLES A1 AND A2 FOR CONDITIONS)

Temperature: 27.0

Date/Time run: 06/07/91 16:05:33

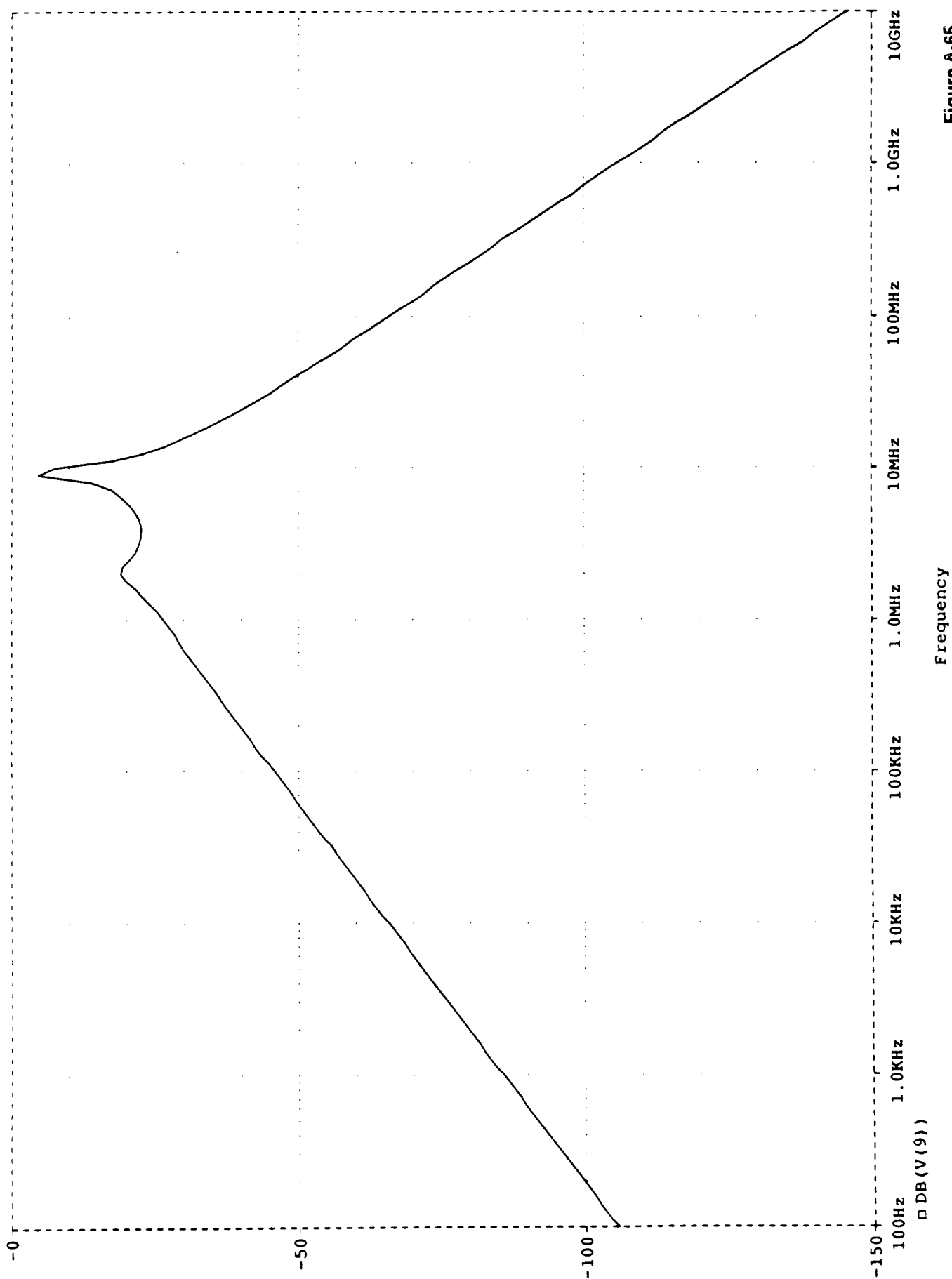


Figure A-65

CALCULATED DIFFERENTIAL MODE VOLTAGE (SEE FIGURE A1 AND TABLES A1 AND A2 FOR CONDITIONS)

Temperature: 27.0

Date/Time run: 06/07/91 16:05:33

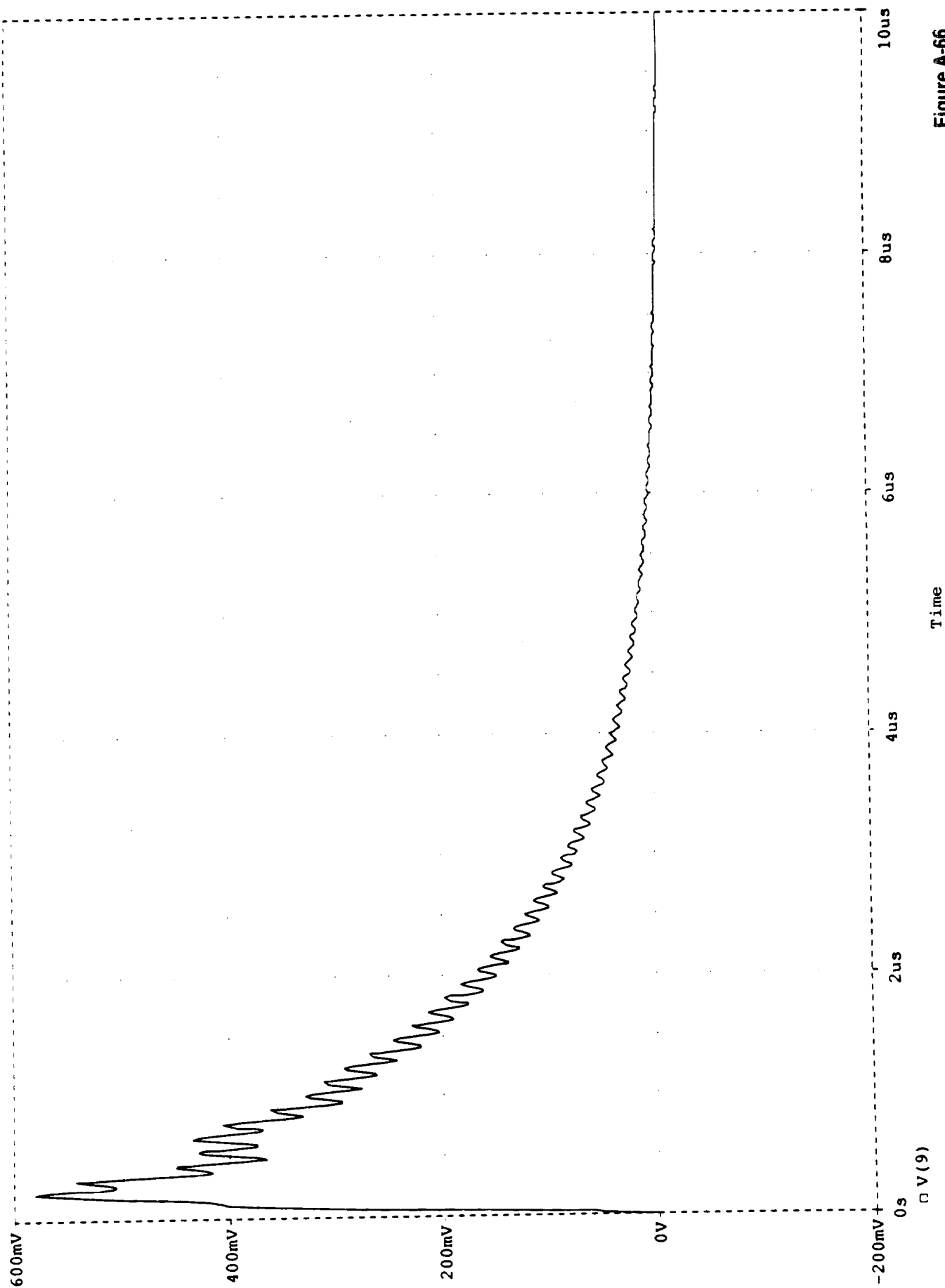
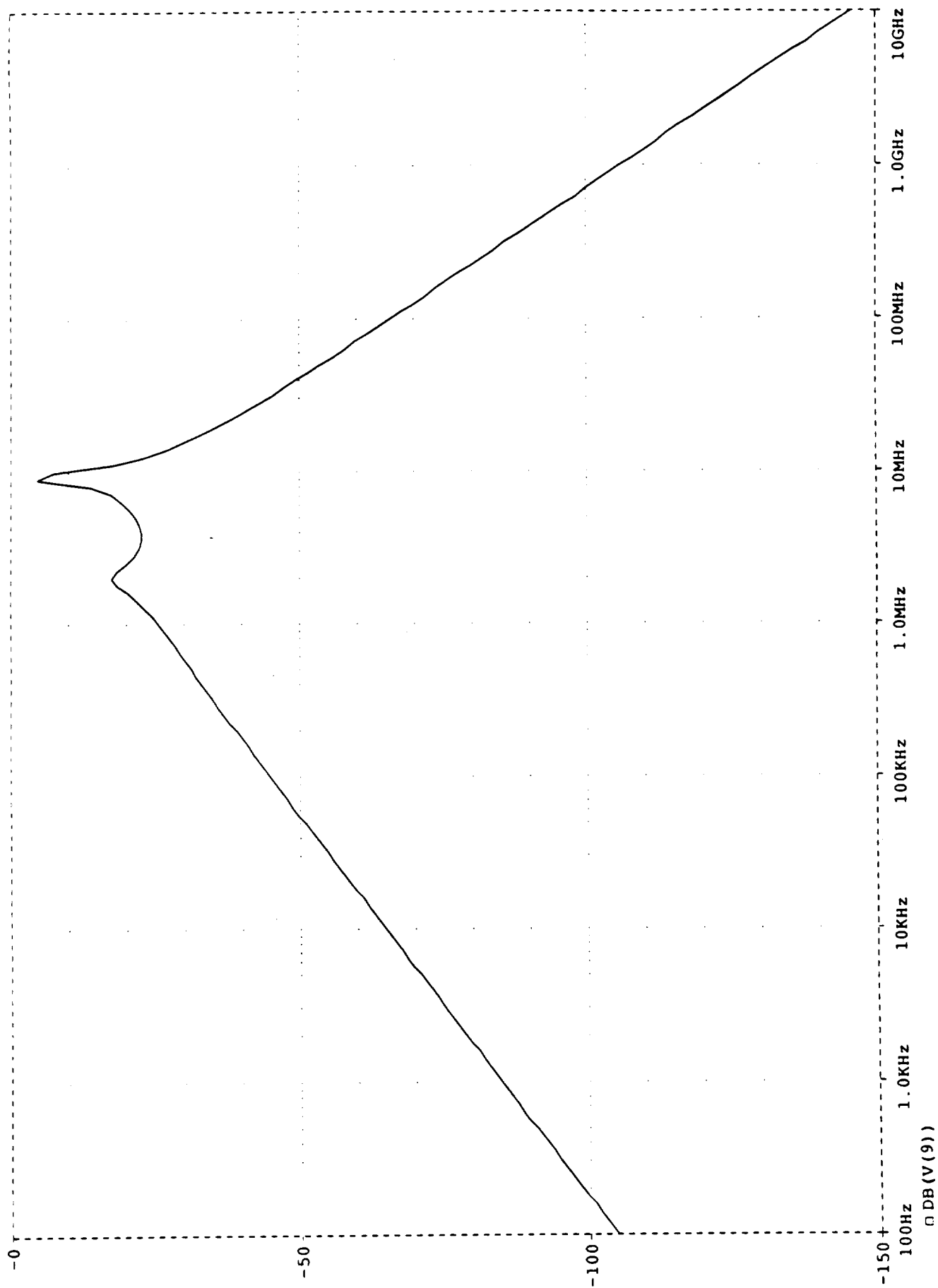


Figure A-66

CALCULATED DIFFERENTIAL MODE VOLTAGE (SEE FIGURE A1 AND TABLES A1 AND A2 FOR CONDITIONS)

Date/Time run: 06/10/91 13:11:18

Temperature: 27.0



Frequency

Figure A-57

CALCULATED DIFFERENTIAL MODE VOLTAGE (SEE FIGURE A1 AND TABLES A1 AND A2 FOR CONDITIONS)

Temperature: 27.0

Date/Time run: 06/10/91 13:11:18

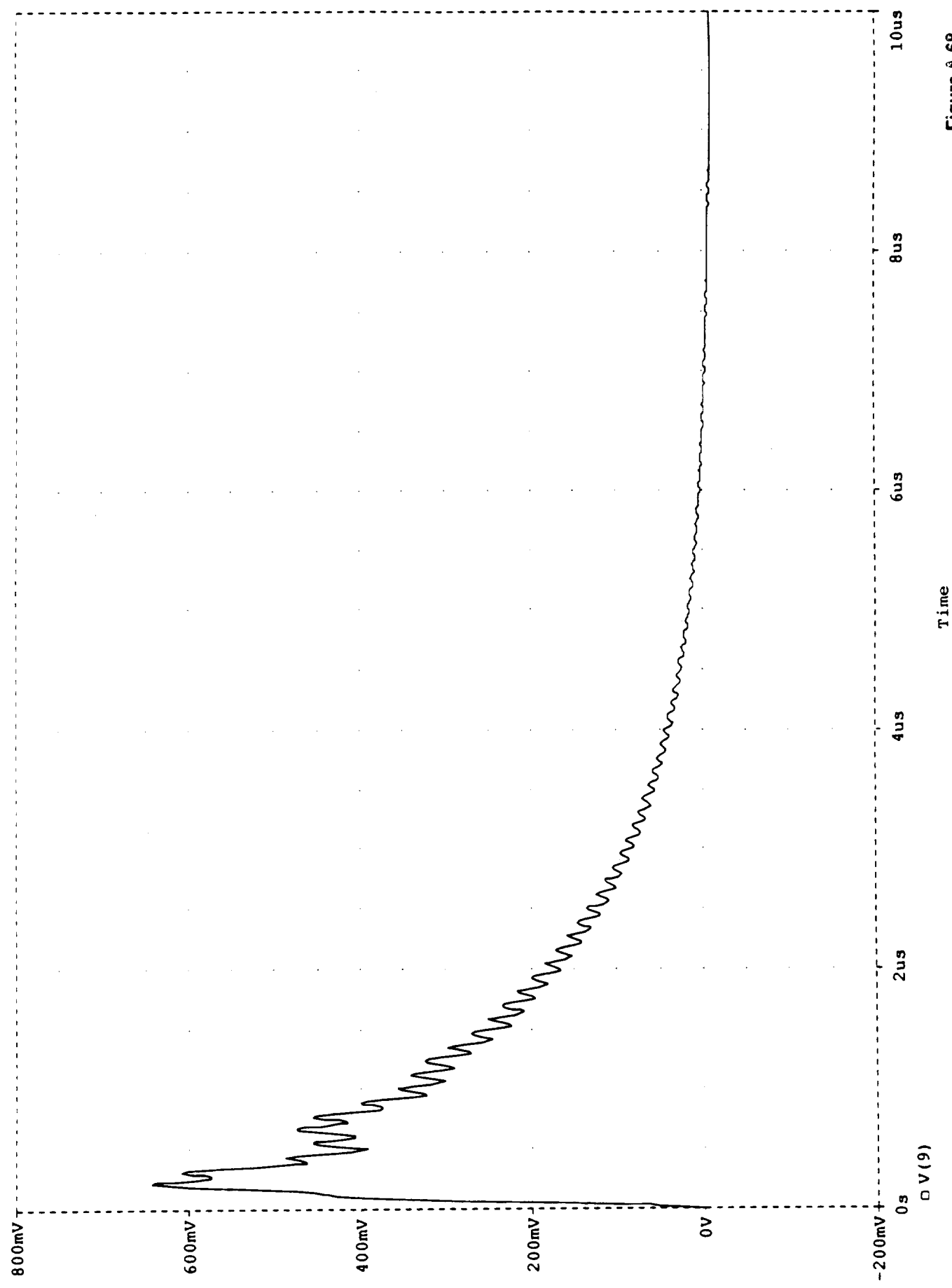


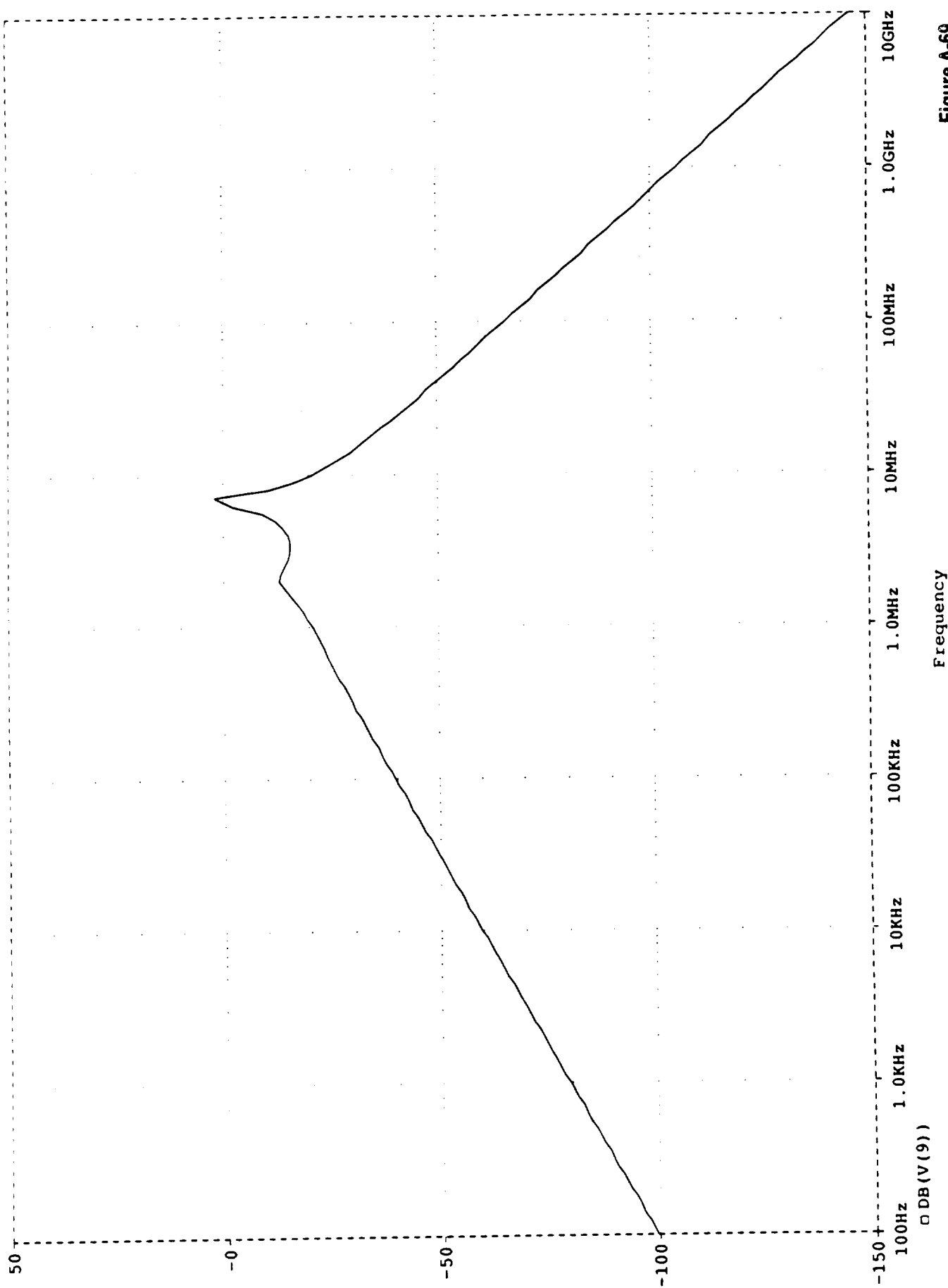
Figure A-68



CALCULATED DIFFERENTIAL MODE VOLTAGE (SEE FIGURE A1 AND TABLES A1 AND A2 FOR CONDITIONS)

Temperature: 27.0

Date/Time run: 06/10/91 13:18:45



Frequency

Figure A-69

CALCULATED DIFFERENTIAL MODE VOLTAGE (SEE FIGURE A1 AND TABLES A1 AND A2 FOR CONDITIONS)

Temperature: 27.0

Date/Time run: 06/10/91 13:18:45

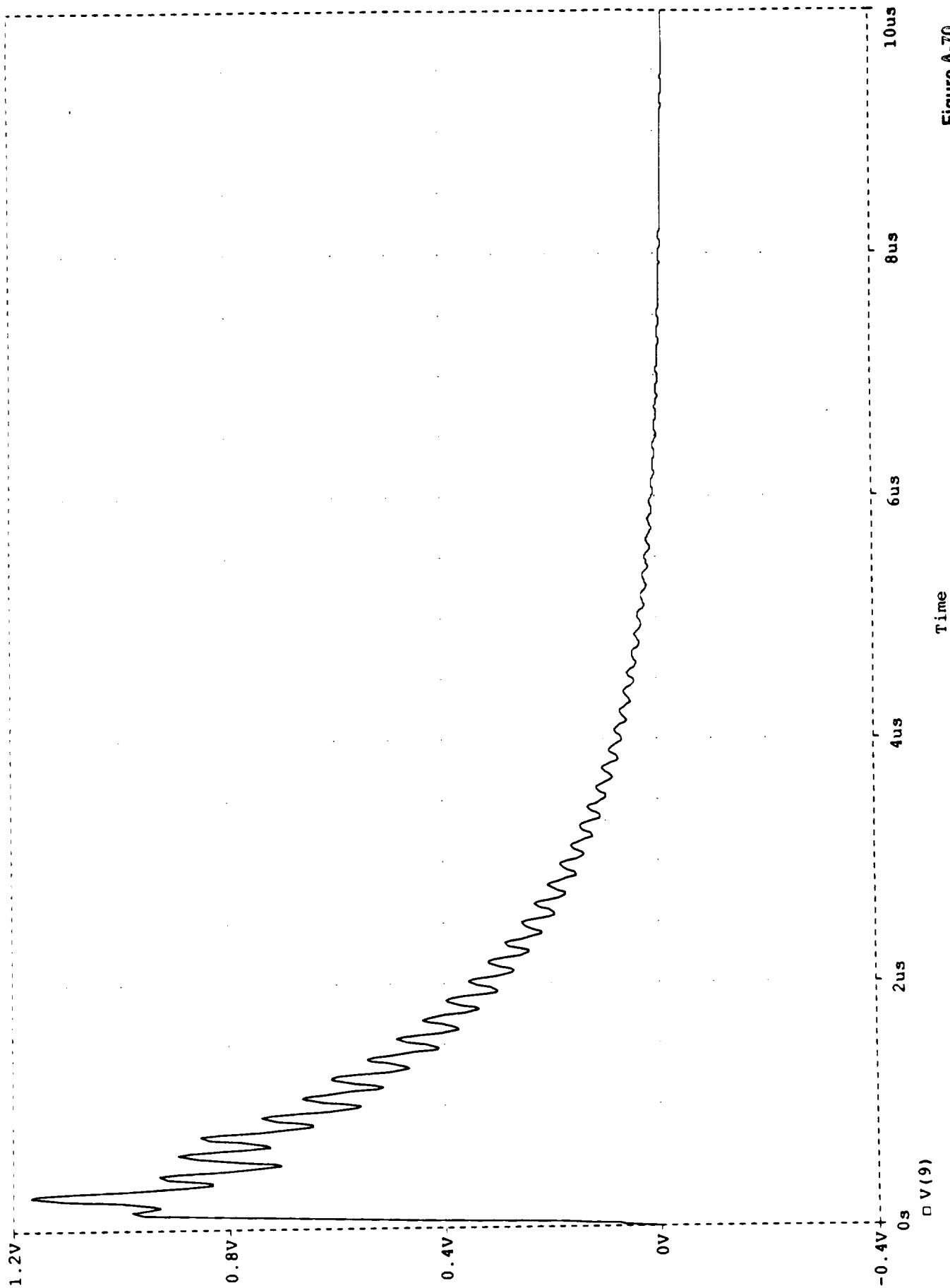


Figure A-70

CALCULATED DIFFERENTIAL MODE VOLTAGE (SEE FIGURE A1 AND TABLES A1 AND A2 FOR CONDITIONS)

Temperature: 27.0

Date/Time run: 06/10/91 13:24:23

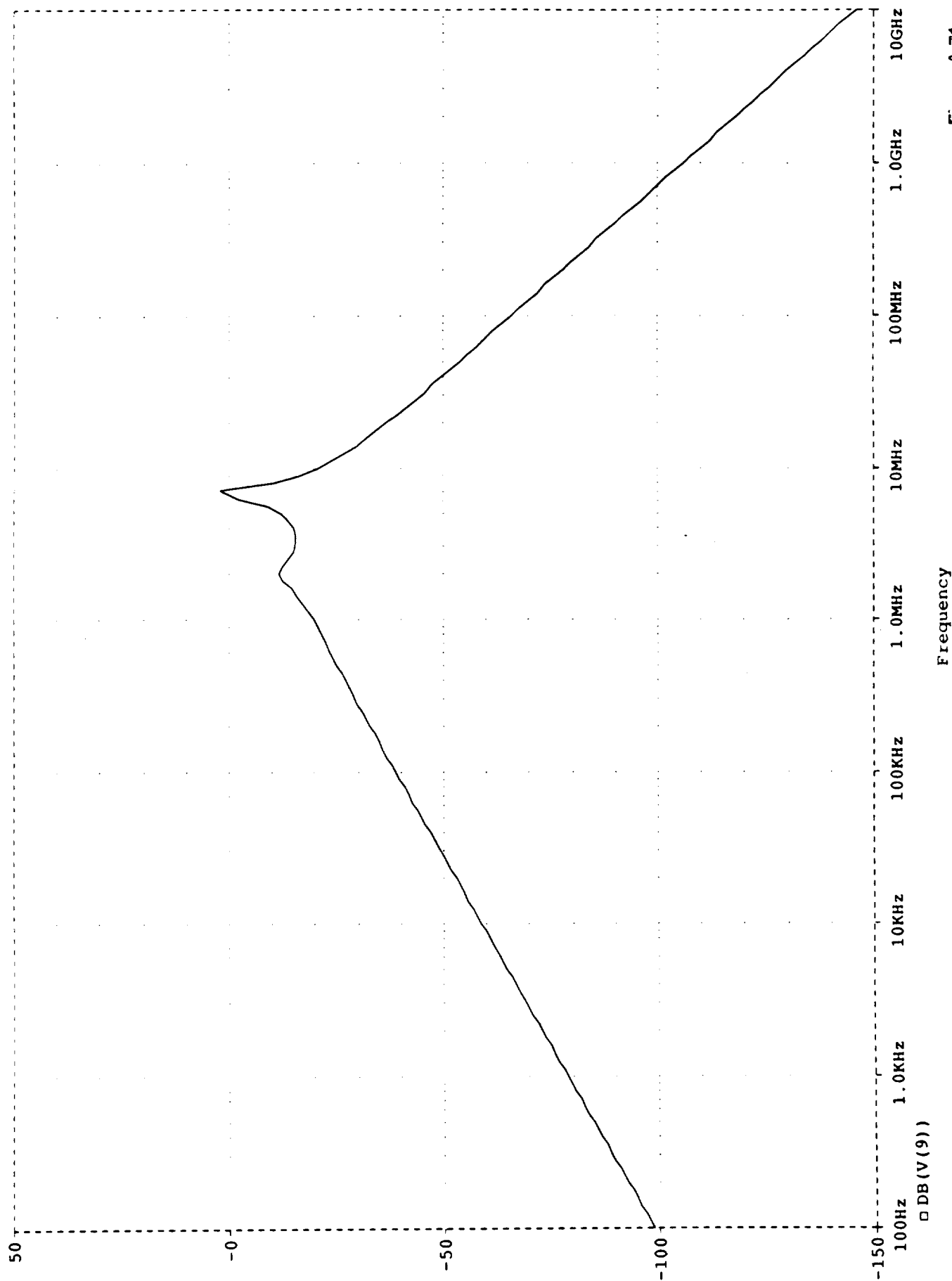


Figure A-71

CALCULATED DIFFERENTIAL MODE VOLTAGE (SEE FIGURE A1 AND TABLES A1 AND A2 FOR CONDITIONS)

Temperature: 27.0

Date/Time run: 06/10/91 13:24:23

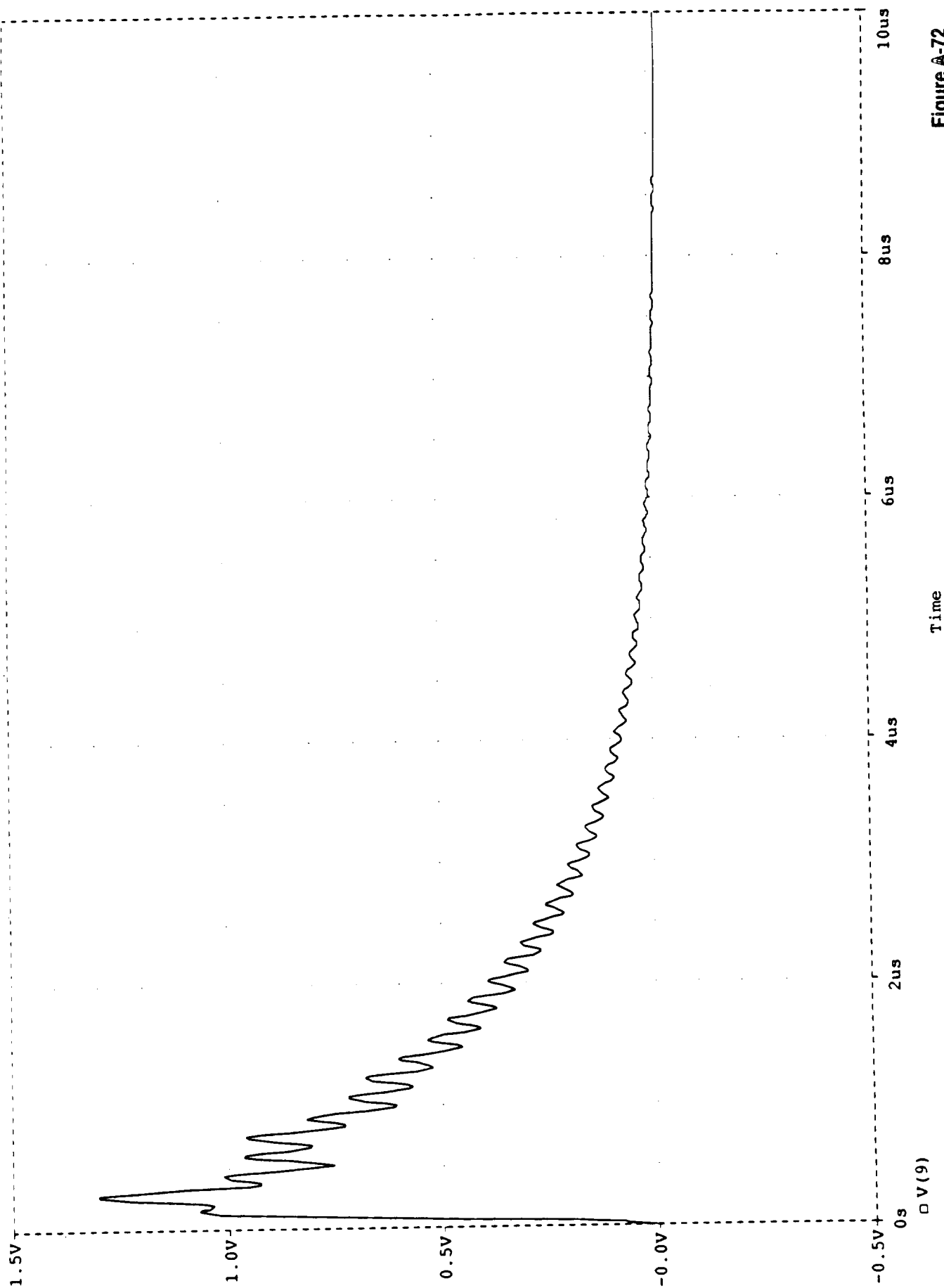
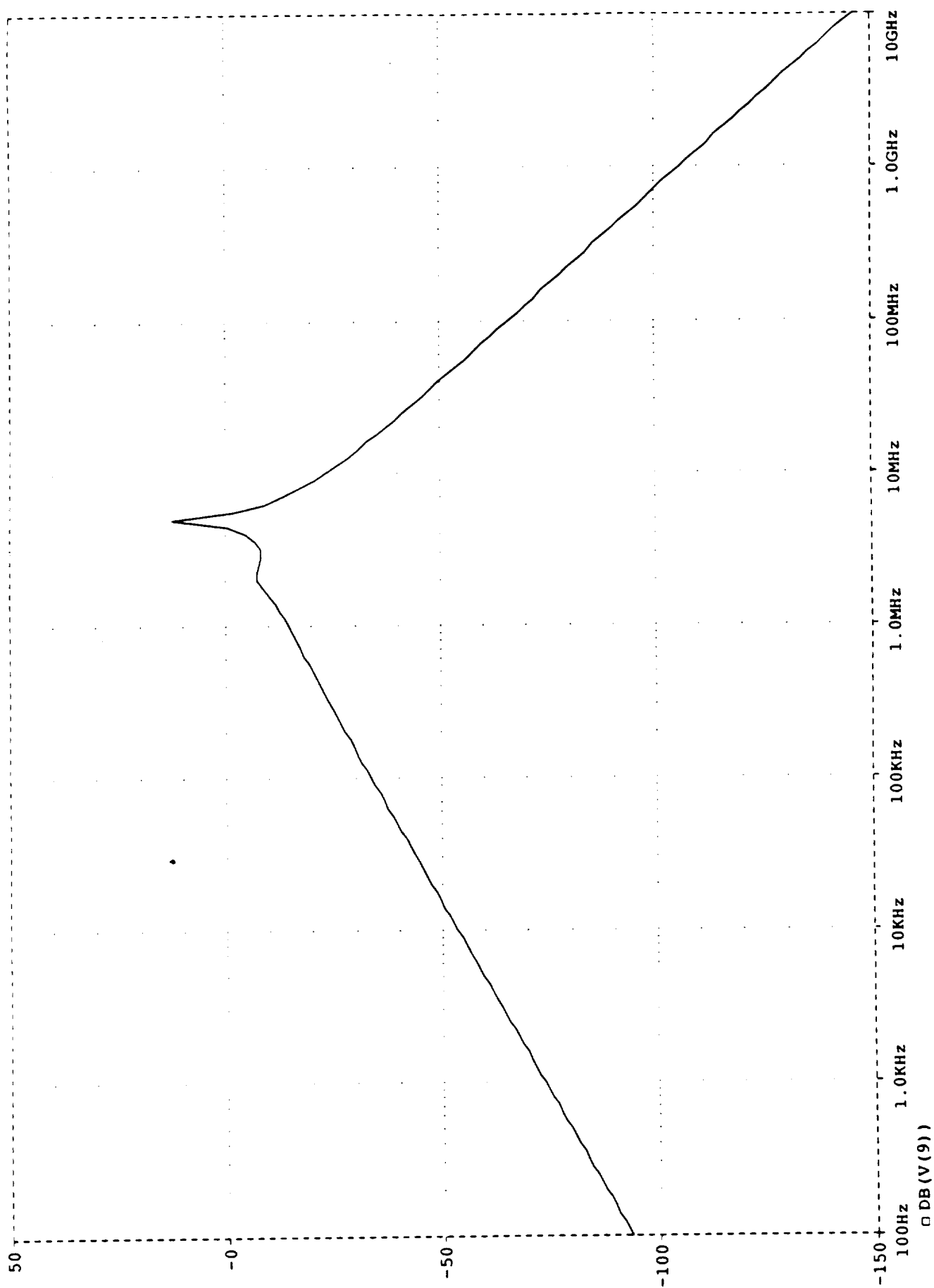


Figure A-72

CALCULATED DIFFERENTIAL MODE VOLTAGE (SEE FIGURE A1 AND TABLES A1 AND A2 FOR CONDITIONS)

Temperature: 27.0

Date/Time run: 06/10/91 13:30:34



Frequency

Figure A-73

LED DIFFERENTIAL MODE VOLTAGE (SEE FIGURE A1 AND TABLES A1 AND A2 FOR CONDITIONS)

Temperature: 27.0

10/91 13:30:34

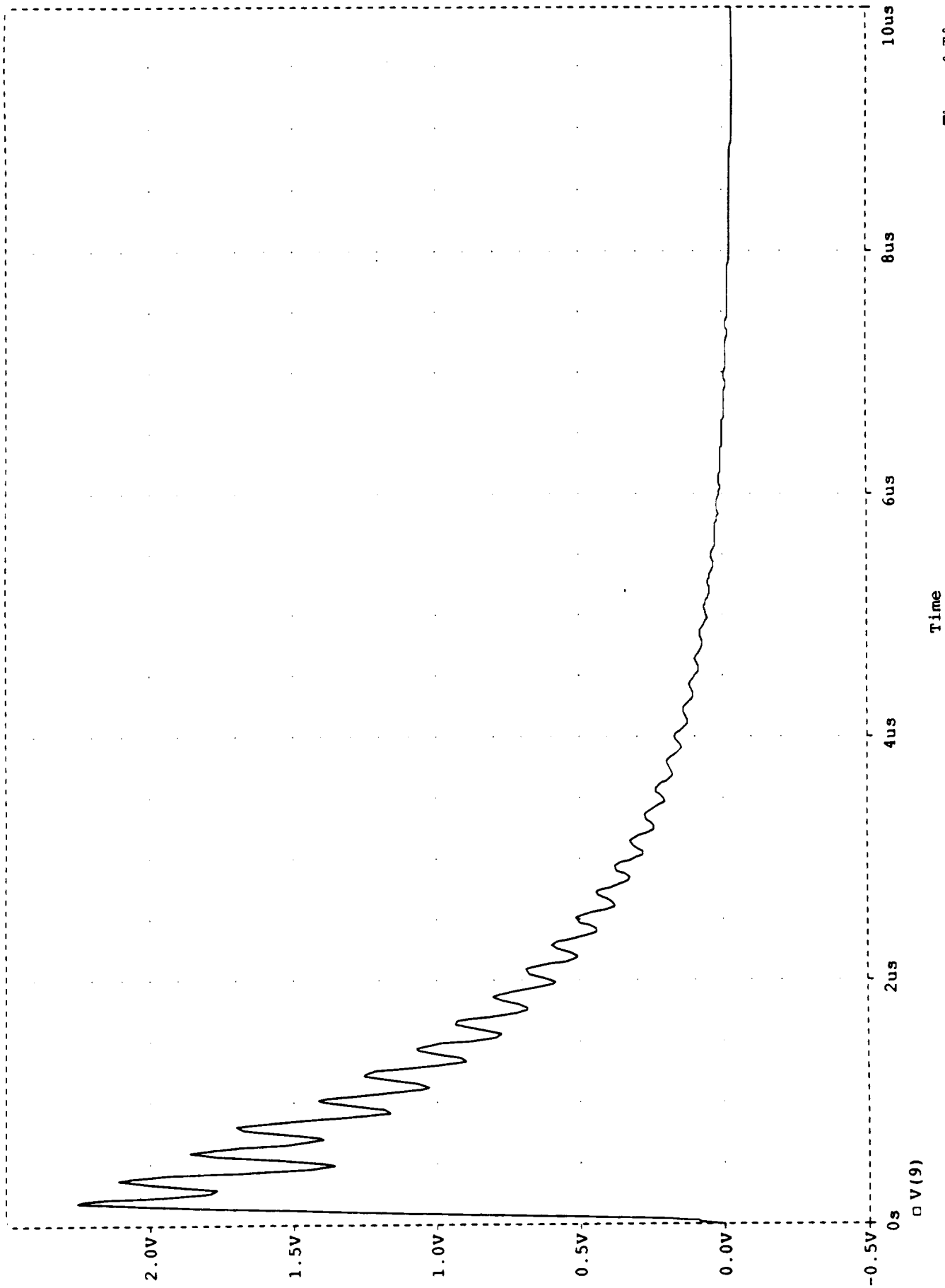


Figure A-74

CALCULATED DIFFERENTIAL MODE VOLTAGE (SEE FIGURE A1 AND TABLES A1 AND A2 FOR CONDITIONS)

Temperature: 27.0

Date/Time run: 06/10/91 13:36:40

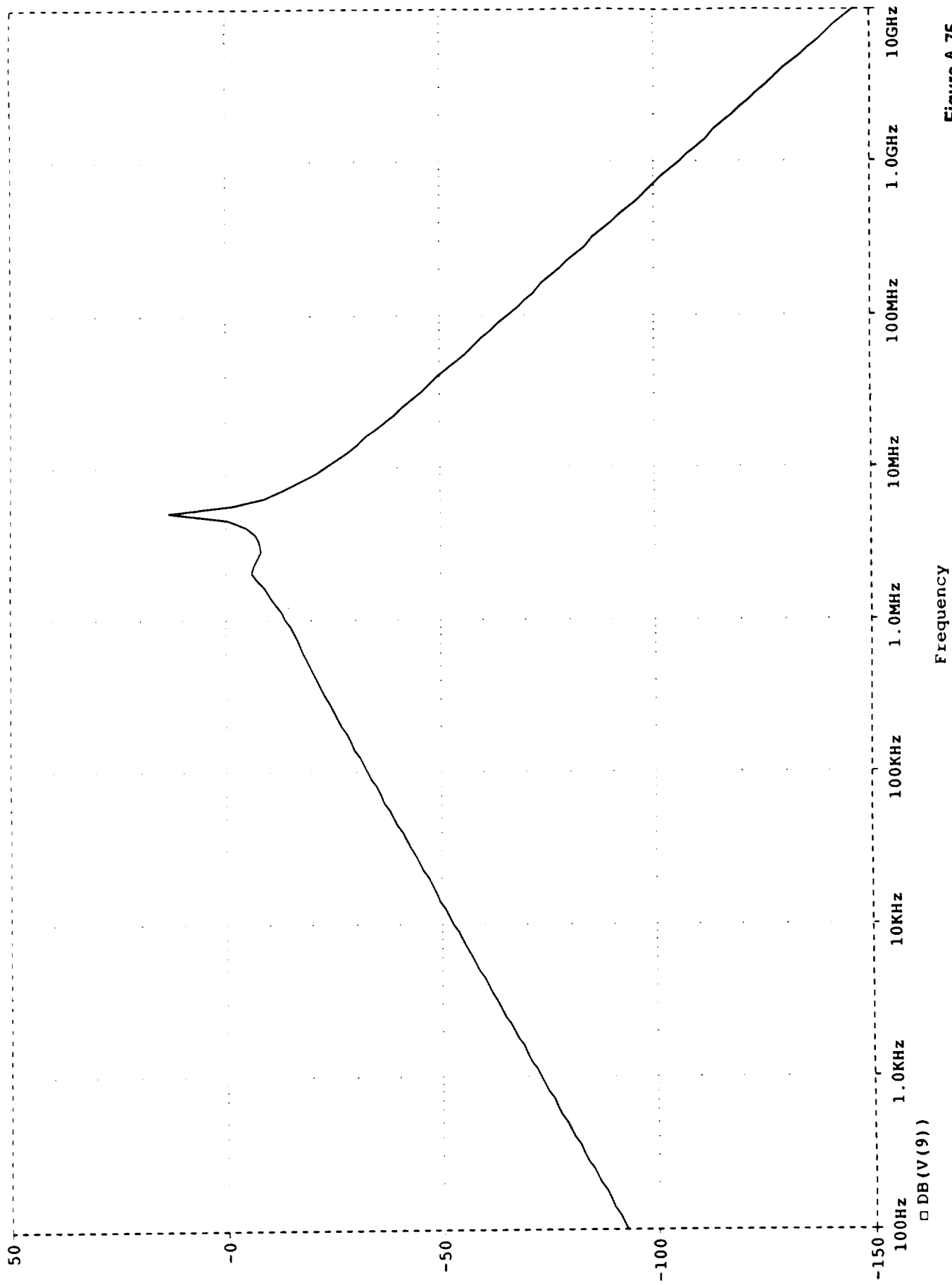


Figure A-75

CALCULATED DIFFERENTIAL MODE VOLTAGE (SEE FIGURE A1 AND TABLES A1 AND A2 FOR CONDITIONS)

Date/Time run: 06/10/91 13:36:40

Temperature: 27.0

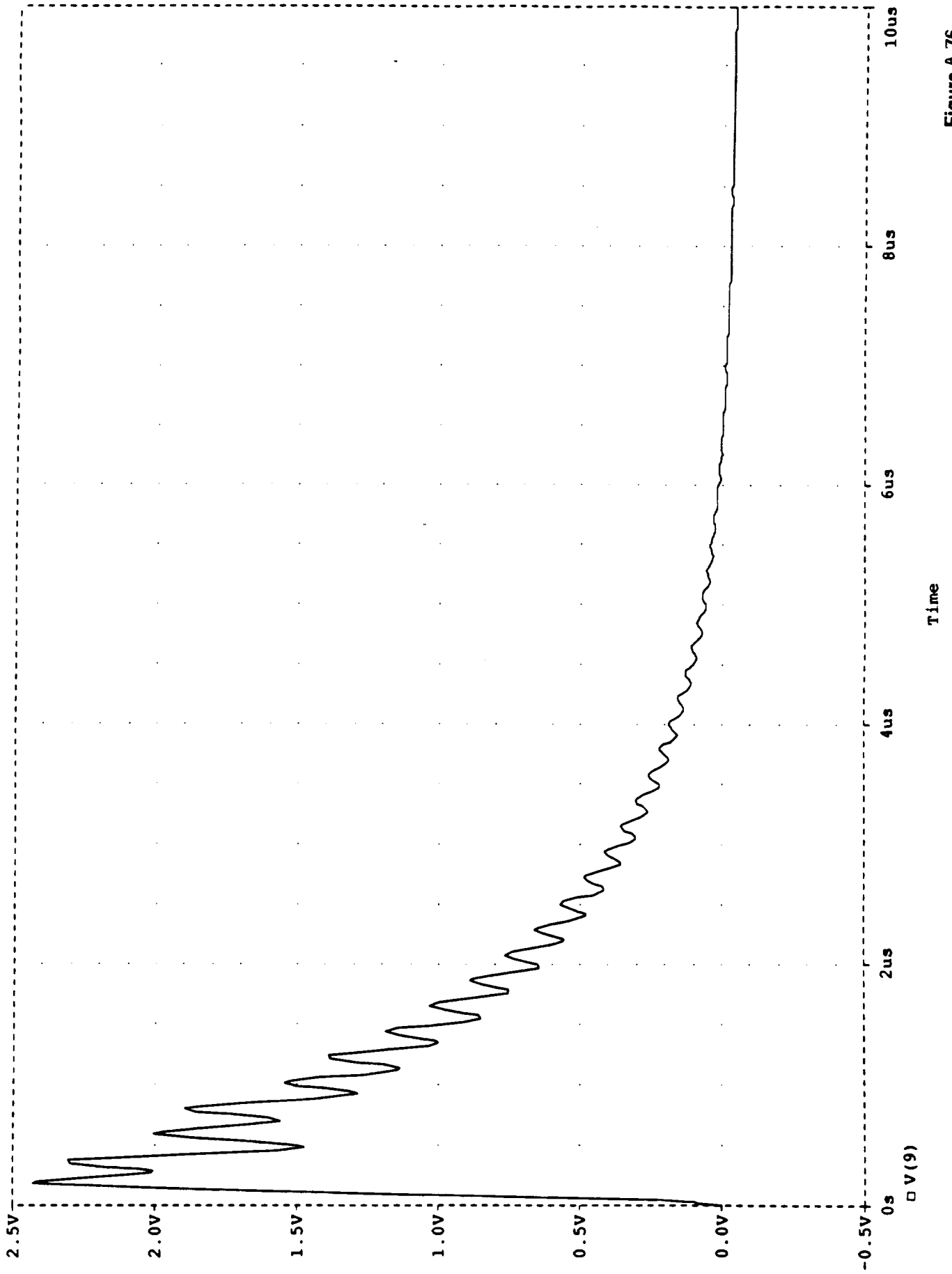


Figure A-76



## Appendix B Common Mode to Differential Voltage as a Band Pass Filter

The circuit model in figure 6-9 may be redrawn as shown in figure B-1. From this figure it can be seen that VDM is produced as a voltage division of VCM between the impedance of C2B and the effective impedance of the remaining elements of the circuit.

$$VDM = I_1 RL1 - I_2 RL2$$

$$I_T = I_1 + I_2$$

From inspection of figure B-1, we see that if the impedances of the two legs of the circuit are exactly equal,  $I_1 = I_2$ , and if  $RL1 = RL2$ , VDM will be zero. In general, the impedances of the two legs are not equal. In most cases, one leg will be a circuit ground return and  $RL2$  and  $RG2$  will both be zero. In this case  $RL1$  may be viewed as the receiving circuit input impedance and  $RG1$  may be viewed as the sending circuit output impedance. A review of the SRB Criticality 1 circuits indicates that the receiving circuit input impedances can be viewed as a resistance of value between 10 ohms and 10,000 ohms and that there are no input circuit capacitances equivalent to  $C_i$ .

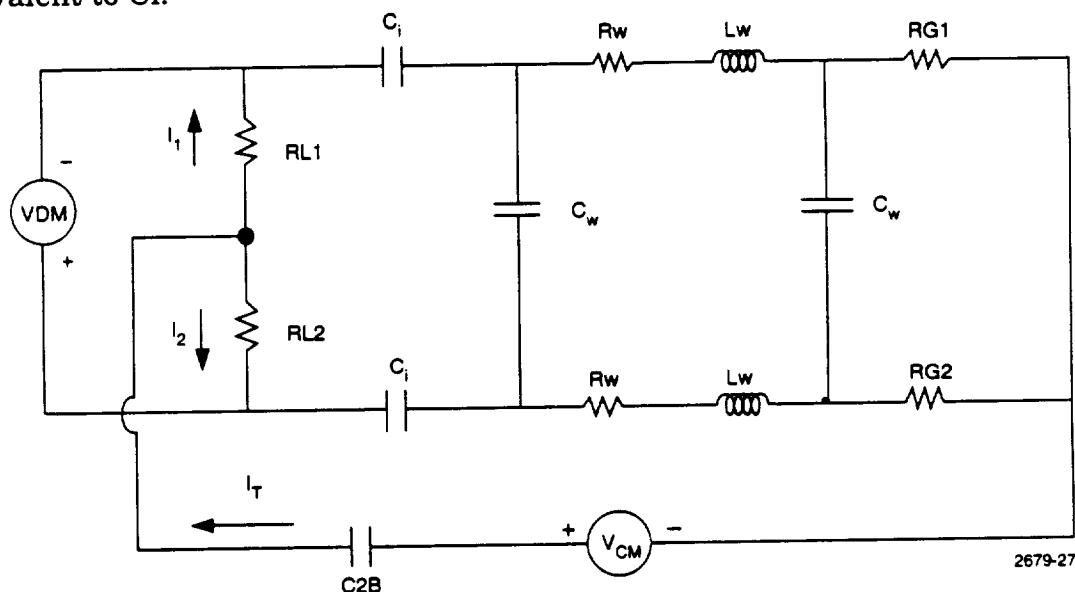


**Figure B-1 Circuit Model to Calculate Differential Mode Voltages**

At low frequencies, the circuit model becomes figure B-2 because the capacitive reactances of  $C_w$  are high and the inductive reactances of  $L_w$  are low. Under these conditions and  $RL1 \gg R_w$ ,  $RL1 \gg RG1$ ,  $RL2 = RG2 = 0$ :

$$\frac{VDM}{VCM} = (j\omega C_{2B}) \frac{(RG1)(R_w)}{RL1 + RG1 + 2R_w}$$

and the ratio increases linearly with frequency.

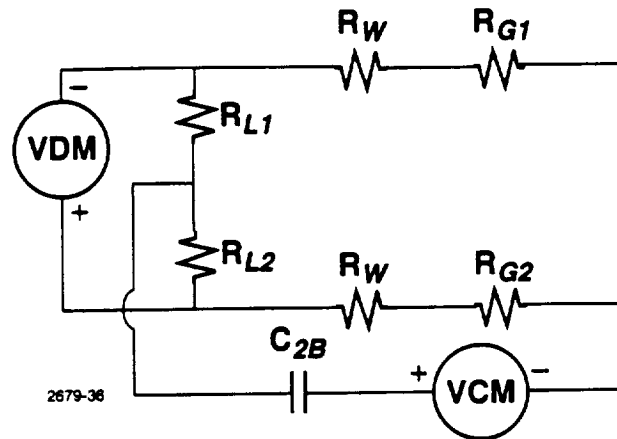


**Figure B-2 Low Frequency Model of Figure B-1**

When the frequency is increased to the point where the inductive reactance,  $\omega L_w$  approaches  $R_w$ ,

$$\frac{VDM}{VCM} = (j\omega C_{2B})(R_w + j\omega L_w)$$

and the ratio increases at a steeper rate than linear. When the frequency increases further to where the capacitive reactances of  $C_w$  are not large, a first resonance condition is reached where the ratio  $VDM/VCM$  is a maximum. The first resonance frequency is reached approximately when:

$$\omega_1 = 2\pi f_1 = \frac{1}{\sqrt{L_w C_w}}$$

A second resonance frequency is reached when the effective capacitance of  $C_{2B}$  and  $C_w$  are resonant with  $L_w$ . This frequency is approximately:

$$\omega_2 = 2\pi f_2 = \frac{1}{\sqrt{0.5 L_w C_{eff}}}$$

$$C_{eff} = \frac{(C_{2B})(2C_w)}{C_{2B} + 2C_w}$$

When the frequency is increased beyond resonance the inductive reactances of  $L_w$  become large enough that they tend to equalize the impedances of the two legs of the circuit and the currents become more equal which causes the ratio of  $VDM/VCM$  to decrease with increasing frequency. The overall shape of the total plot of  $VDM/VCM$  therefore causes high attenuation of frequencies much lower and much

higher than the resonant frequencies. The circuit behaves much like a bandpass filter.

It should be noted that at low frequency, the ratio  $VDM/VCM$  is directly proportional to  $C2B$ .  $C2B$  is determined by the size and spacing from the chassis of the printed circuit board. In chapter 6 of this report, we have let  $C2B$  be 22.5 pf which represents printed circuit boards in the SRB IEA. Larger values of  $C2B$  would increase the  $VDM/VCM$  ratio at low frequencies which would translate into larger peak values of  $VDM$ . Also longer cables, which are resonant at lower frequencies, would receive more of the pulse energy from the injected current waveform. Also, it should be noted that, at resonance, the maximum value of  $VDM/VCM$  is obtained when the circuit input impedance,  $RL1$ , is high. Higher values of this ratio produce higher differential mode voltages at the input to circuits connected to the wires in the cables.

To demonstrate the effects of higher values of parasitic capacitances,  $C2B$ , and larger values of  $RG1$ , we have plotted the ratio of  $VDM/VCM$  as a function of frequency for the actual SRB circuit conditions and for some conditions that would produce higher ratios (appendix A).

### **Appendix C References**

1. C.O. (Change Order) 191 Lightning Test, USBI-SYS-10RPT-010, December 1989.
2. NSTS 07636F, Space Shuttle Lightning Protection, Test, and Analysis Requirements, November 13, 1991.
3. Follow-on Cable Coupling Lightning Test, Final Test Report, Volumes 1, 2, and 3, Thiokol Corporation Report TWR-60187, 31 October 1990.
4. USBI Drawing number 10400-0520, sheet 8.
5. EMI Control Methodology and Procedures, Fourth Edition, 1985, by D. White and M. Mardiguan, Interference Control Technologies, Inc., Gainesville, VA.
6. Lightning Protection of Aircraft by F.A. Fisher, J.A. Plumer, and R.A. Perala, 1990, Published by Lightning Technologies, Inc., Pittsfield, MA.
7. Coupling to Shielded Cables, by Edward F. Vance, John Wiley & Sons, Inc., 1978.
8. Final Report, Support of Lightning Analysis and Testing on the Solid Rocket Booster (SRB) Vehicle, Mission Research Corporation, AMRC-R-122, March 1978.
9. Measured Electromagnetic Shielding Performance of Commonly Used Cables and Connectors, by L.O. Hoeft and J.S. Hofstra, IEEE Transactions on Electromagnetic Compatibility, Volume 30, number 3, August 1988.
10. 10CEI-0001, Contract End Item Specification, Part I, Integrated Solid Rocket Booster (ISRB).
11. Coupon Test Summary, Thiokol Corporation, Memo L622-FY-90-M092, by P. St. Jean, 20 Feb. 1990.
12. 40M39513. Wire, Electrical, Hook up, General Specification
13. Personal Communication with Mr. Joe Godfrey, Thiokol Corporation.
14. Evaluation and Mitigation of Lightning and Microwave Hazards to the SRB Propellant, EMA-87-R-63, June, 1987.

